1992

Improving scale-up procedures for the design of pneumatic conveying systems

Renhu Pan
University of Wollongong

IMPROVING SCALE-UP PROCEDURES FOR THE DESIGN OF PNEUMATIC CONVEYING SYSTEMS

A thesis submitted in fulfilment of the requirements

for the award of the degree of

DOCTOR OF PHILOSOPHY

from

UNIVERSITY OF WOLLONGONG

by

RENHU PAN

B.Sc. (USTB), M.Sc. (USTB)

Department of Mechanical Engineering

1992

DECLARATION

This is to certify that the work presented in this thesis was carried out by the author in the Department of Mechanical Engineering at the University of Wollongong and has not been submitted for a degree to any other university or institution

Renhu Pan

ACKNOWLEDGMENTS

I would like to thank my supervisor, Dr P. W. Wypych, Senior Lecturer in the Department of Mechanical Engineering at the University of Wollongong, for his supervision and generous assistance and encouragement during the period of this study. I also wish to thank my former supervisor, Professor P. C. Arnold, for his invaluable guidance and help during my first two years of PhD candidature.

I am very grateful to the University of Wollongong for providing me with a Postgraduate Research Award and paying my Overseas Student Charge for this study.

Acknowledgment is also made of the assistance given by other staff of the department, especially that of Mrs M. Wall and Mrs R. Hamlet. My thanks are extended to the technical staff in the Workshop and Bulk Solids Handling Laboratory with whose help and expertise the experimental apparatuses were constructed. In particular, I would like to express my gratitude to Mr D. Cook, Mr I. Frew, Mr K. Maywald, Mr F. Escribano, Mrs W. Halford and Mr I. McColm.

Finally, special acknowledgment is made to my dear wife Wei Lu and my parents for their unfailing help and encouragement.

SUMMARY

An accurate estimation of the total pipeline air pressure drop is considered widely to be one of the most important aspects of pneumatic conveying system design. Since there are numerous influential parameters, such as velocity, particle properties, pipe length, diameter and material, the determination of the total pipeline air pressure drop in pipelines of different length, diameter, step and bend number is based largely on the scale-up of test rig data.

In many systems, the air-only component of pressure drop is significant (e.g. dilute-phase, long-distance conveying). This thesis modifies initially the correlations for predicting pressure drop caused by an incompressible fluid flowing through bends and straight sections of pipe. These correlations are sufficiently accurate as long as mean conditions (based on average air density) for each straight pipe and conditions at the outlet of each bend are used in the analysis.

Based on detailed mathematical and dimensional analyses, semi-empirical correlations then are set up for predicting the pressure drop due to the presence of solids in bends and straight pipes. Fly ash is used as the test material. By using the data from any constant diameter pipeline with one bend and two long straight pipes, the exponents in the semi-empirical correlations are determined. These correlations then are used to predict the total pipeline air pressure drop in pipelines of different length, diameter and bend number. A close agreement between predicted and experimental results is obtained as long as there are no short straight pipes in the pipeline.

However, in industry, short straight pipes are in common use. It is found that the previously 'determined' values of exponents underpredict significantly the total pipeline air pressure drop in pipelines that contain short straight pipes. Therefore, the semi-empirical correlation for bend pressure drop is modified by determining the exponents from data obtained on a simple configuration of constant diameter pipeline, which comprises two bends and three sections of pipe, two long and one short. The operating conditions of several pipeline having different lengths and diameters are predicted accurately and this demonstrates the good reliability and stability of this new scale-up procedure.

Finally, the results from two other test materials with significantly different particle properties (viz. pulverised coal and plastic pellets) demonstrate further the high accuracy and reliability of the scale-up procedure developed in this thesis.

TABLE OF CONTENTS

List of Figures

List of Tables

NOMENCLATURE

A	Cross-sectional area of pipe (m^2), $A = 0.25\ \pi\ D^{-2}$
A_p	Average projected area of a particle in Equation (2.10)
a, b, c, e, f, h, i	Exponents in dimensional analysis Equations (4.2), (4.13), (5.7) and (6.5)
a_b, a_c, a_s	Constant in Equation (2.7)
B	Coefficient in Equation (2.5)
C_d	Drag coefficient
C_m	Relevant air resistance coefficient in Equation (2.10)
D	Internal diameter of pipe (m)
d_p	Mean particle diameter (m)
dp_b	Pressure drop over elemental section R $d\phi$ in bend (Pa)
dp_s	Pressure drop over length dx (Pa)
dv	Velocity increment over length dx (m s^{-1})
dx	Differential length of straight pipe section (m)
$d\phi$	Angle increment in bend
$\hat{e}_i$	Relative deviation
e	Average relative deviation
$\|e\|$	Average absolute deviation
F_1, F_2, F_3	Coefficients in Equations (2.2) and (7.3a)
F_c	Centrifugal force acting on sliding solids (N)
F_{cs}	Frictional force due to centrifugal force (N), $F_{cs}=F_c\ \upsilon$
F_d	Drag force acting on solids from conveying air (N)
F_f	Frictional force between pipe wall and conveying air (N)
F_g	Gravity force of solids over length dx (N)

F_r	Froude number, $F_r=V_f\ (g\ D)^{-0.5}$
F_{rs}	Particle Froude number, $F_{rs}=v_\infty\ (g\ D)^{-0.5}$
F_s	Frictional force between pipe wall and particles (N)
g	Acceleration due to gravity, $g \approx 9.81$ (m s^{-2})
k	Coefficient in dimensional analysis Equations (4.2), (4.13), (5.7) and (6.5)
k_b	Coefficient in Equation (2.13)
k_r	Coefficient in Equation (2.4)
L	Total effective length [68] of pipeline (m)
L'	Value of L modified to allow for bends (m)
m_f	Air mass flow rate (kg s^{-1})
m_p	Average weight of a particle in Equation (2.10) (kg)
m_s	Product mass flow rate (kg s^{-1})
m*	Product to air mass flow rate ratio, $m^*=m_s\ m_f^{-1}$
n	Number of particle rebounds around bend in Equation (2.11) or exponent in Equation (5.14)
N	Number of experimental data
n_s	Exponent in Equation (2.14)
N_b	Number of bends in a pipeline
p	Static air pressure (Pag)
p_b	Pressure in bend (Pag)
Pw	Wetted perimeter (m)
Q	Fluid flow rate ($m^3\ s^{-1}$)
R	Centreline bend radius (m)
R_a	Gas constant for air (N m kg^{-1} K^{-1}), $R_a=287.1$
R_e	Reynold's number, $R_e=\rho_f\ V_f\ D\ \mu^{-1}$
R_{ep}	Particle Reynold's number, $R_{ep}=\rho_f\ v_\infty\ d_p\ \mu^{-1}$

R_{es}	Reynold's number defined as $R_{es}=\rho_f (v_f - v_s) d_p \mu^{-1}$ in Equations (2.18) and (2.19)
r_o	Internal radius of pipe (m)
r_1	Distance from the pipe centreline to a particular point on the pipe cross section (m)
s	Distance between two points in Table 6.1 (m)
S1	Length of a short straight pipe connecting two long radius bends in Figure 7.32 (m)
S2	Length of a short straight pipe connecting two short radius bends in Figure 7.32 (m)
T	Absolute air temperature (K)
v	Axial fluid velocity on the cross section of straight pipe (m s^{-1})
V_{fav}	Average superficial air velocity in pipeline (m s^{-1})
$v_{b\infty}$	Free-settling velocity of a solid particle in the bend in Equation (2.8) (m s^{-1})
v_f	Actual air velocity (m s^{-1})
V_f	Superficial air velocity(m s^{-1})
v_s	Particle velocity (m s^{-1})
v_∞	Terminal velocity or free setting velocity of particle (m s^{-1})
x1, ..., x11	Exponents in Equations (2.3), (4.18) to (4.22), (5.9) and (5.12)
y1, ..., y4	Exponents in Equations (6.7), (6.8) and (7.4)
z	Particle shape factor
α	Coefficient in Equation (4.16) or angle in Equation (2.11)
β	Constant, $\beta=0$ in horizontal straight pipe, $\beta=1$ in vertical lift section, $\beta=-1$ in vertical drop section.
β_a	Angle of bend deflection in Equation (2.6)
ε	Porosity in pipe

ε	Pipe roughness (m)
γ	Constant in Equation (5.13)
η	Particle to air velocity ratio, $\eta = v_s\, v_f^{-1}$
μ	Dynamic viscosity (Pa s)
θ	Constant in Equation (5.14)
ρ_{fav}	Air density based on average superficial air velocity (kg m^{-3}), $\rho_{fav}=m_f\,(V_{fav}\,A)^{-1}$
ρ_b	Bulk density of bulk solid (kg m^{-3})
ρ_d	Dispersed density (kg m^{-3}), $\rho_d= (1-\varepsilon)\,\rho_s$
ρ_f	Fluid or air density (kg m^{-3})
ρ_s	Particle density (kg m^{-3})
ρ_{sd}	Suspension density (kg m^{-3}), $\rho_{sd}=m_s\,(V_{fe}\,A)^{-1}$
λ_f	Air-alone friction factor in straight pipe
λ_s'	Solid friction factor in straight pipe (between particles and pipe wall)
λ_s	Total solid friction factor in straight pipe (between solids-air mixture and pipe wall)
λ_t	Total friction factor in straight pipe, $\lambda_t = \lambda_f + \lambda_s$
ζ_{bs}	Bend friction factor due to collisions between the particles and bend wall in Equation (2.8)
ζ_f	Air-alone friction factor in bend
ζ_s	Friction factor due to solids in bend
ζ_t	Total friction factor in bend, $\zeta_t = \zeta_f + \zeta_s$
ϕ	Angle along bend, starting from the bend inlet
Φ, $\Phi 1$, $\Phi 2$	Functions
σ	Standard deviation
σ_m	Average flight coefficient of a single particle in Equation (2.9)

ω	Coefficient in Equation (5.14)
τ	Wall friction stress (N m^{-2})
υ	Friction coefficient between pipe wall and particles
ξ	$\xi = Pwf\ (\pi\ D)^{-1}$
ΔL	Length of straight pipe section (m)
Δp	Air pressure drop (Pa)
Δp_b	Pressure drop due to solids-air mixture through bend (Pa), $\Delta p_b = \Delta p_{bf} + \Delta p_{bs}$
Δp_{b1}	Pressure drop located in bend itself (Pa)
Δp_{b2}	Pressure drop occurring in straight pipe downstream from bend for the re-acceleration of particles (Pa)
Δp_s	Pressure drop due to solids-air mixture over ΔL (Pa), $\Delta p_s = \Delta p_{sf} + \Delta p_{ss}$
Δp_{sc}	Calculated pressure drop in straight pipe in Equation (5.15) (Pa)
Δp_{se}	Measured pressure drop in straight pipe in Equation (5.15) (Pa)
Δp_t	Total pipeline air pressure drop (Pa)
Δp_{ta}	Total pipeline air pressure drop due to the acceleration of particles from rest (Pa)
Δp_{tb}	Total pipeline air pressure drop caused by all bends (Pa)
Δp_{ts}	Total pipeline air pressure drop due to the friction between the particles and the pipe wall along the pipeline (Pa)
Δp_{tv}	Total pipeline air pressure drop due to particle gravity (Pa)
δp_s	Solids-air mixture pressure gradient in straight pipe (Pa m^{-1}), $\delta p_s = \delta p_{sf} + \delta p_{ss}$
δp_{sd}	Pressure gradient in straight section downstream of bend (Pa m^{-1})
δp_{su}	Pressure gradient in straight section upstream of bend (Pa m^{-1})

Subscripts

1	Experimental data pertaining to a test rig
2	Scale-up data pertaining to an actual or proposed system
e	Final value at end of pipeline or section of pipe
f	Fluid or air
h	Horizontal
i	Initial value at start of pipeline or inlet of bend
m	Mean value for pipeline or section of pipe (based on average air density)
o	Value at outlet of bend
s	Solids or particles
v	Vertical

CHAPTER 1

INTRODUCTION

The pneumatic transportation of bulk solids through pipelines is gaining popularity for a wide range of applications, especially as more effective hardware and techniques are introduced onto the market. The main features that make this method of transport attractive to the designers of materials handling plants are listed below.

a) The relative ease of routing the conveying pipeline (e.g. verticals, bends, inclines) adds flexibility to the design or uprating of a plant.

b) The physical size of a pneumatic conveying pipeline is small compared to an equivalent conveyor-belt/bucket-elevator system (especially for the dense-phase mode of transport which usually requires smaller sizes of pipe).

c) Atmospheric contamination is avoided due to the completely enclosed nature of the transport system (e.g. dusty, hygroscopic and even toxic products can be conveyed safely and hygienically).

d) New technology allows friable products to be transported at low-velocity and with either extremely low or undetectable levels of product degradation or damage [69]. As a consequence, air consumption and hence running costs are reduced significantly. Also, erosion of the system (e.g. bends, conveying pipeline) is minimised.

e) The use of a pipeline can offer increased security as opposed to an open-belt conveyor system (e.g. for diamond recovery plants).

f) With improved hardware (e.g. blow tanks) and techniques (e.g. solids metering [11], air injection [15], stepped-diameter pipelines [30, 49]), several materials such as pulverised coal, cement and fly ash are able to be transported efficiently at large conveying rates (e.g. 100 to 200 t h^{-1}) and/or over long distances (e.g. 1 to 3 km).

To attract more users of such equipment, it is extremely important to estimate accurately the total pipeline air pressure drop, which is considered widely to be one of the most important aspects of pneumatic conveying system design.

In the literature, there is no lack of theoretical and empirical studies on the determination of the total pipeline air pressure drop and/or the pressure drop caused by bends and straight sections of pipe [2, 3, 6, 7, 8, 9, 14, 16, 18, 22, 28, 31, 32, 34, 35, 39, 42, 45, 52, 58, 61, 66, 67, 68, 71, 72, 75, 76, 78]. However, the theoretical analysis is based usually on the assumptions that the particles are coarse, rigid and of uniform size and conveyed in very dilute-phase. Also, the knowledge of particle velocity and its variation along the pipeline must be known. The majority of pneumatic conveying systems in industry transport particles of different size, size distribution, density, shape and surface roughness [70]. The possible values of product to air mass flow rate ratio also are considerable. Therefore, it is difficult to quantify theoretically the total pipeline air pressure drop (or the pressure drop caused by bends and straight pipes). As a result, empiricism has been used widely.

Pneumatic conveying systems in industry include numerous configurations of pipeline (e.g. different length, diameter, bend number and step). Therefore, it is almost impossible to carry out laboratory experiments on an identical pneumatic conveying system. Usually, a pilot-scale test rig is built and operated with a sample

of the product to be conveyed in the proposed system(s). The data obtained then are scaled to predict total pipeline air pressure drop in other pipelines. Hence, scaling-up of test rig data to full-scale installations is a subject of considerable practical interest.

Over recent decades, many scale-up procedures have been developed and used quite extensively [6, 7, 8, 14, 34, 39, 58, 68, 71]. However, most of these have not taken into account:

- the geometry, number and/or location of bends,
- the number and/or location of straight pipes,
- the influences of the conveyed material(s),
- relatively short pipe lengths (e.g. between bends), and/or
- a variable pressure gradient along the straight sections of pipe.

These disadvantages may preclude the reliable and accurate scale-up of the test rig data to full-scale installations.

The work described in this thesis, which generally aims to develop accurate procedures to scale-up test rig data to full-scale installations, focuses on the following aspects.

i) Establishing a technique for accurately calibrating the pressure transducers that are used to measure pressure along the test rig pipelines (Chapter 3).

ii) Obtaining correlations for predicting the air-only component of pressure drop through bends and straight pipes (Chapter 4).

iii) Establishing semi-empirical correlations to predict the pressure drop due to solids-air mixture through bends and straight sections of pipe, which are applicable to both coarse and fine particles (Chapter 5 and 6).

iv) Evaluating the existing correlations of predicting total pipeline air pressure drop or pressure drop caused by bends and straight pipes (Chapter 5, 6 and 7).

v) Scaling up test rig data to different full-scale installations containing short straight pipes and for materials having significantly different particle properties (Chapter 7 and 8).

Finally, concluding remarks and suggestions for further work based on the investigations and results presented in this thesis are contained in Chapter 9.

CHAPTER 2

LITERATURE SURVEY

Since the accurate estimation of total pipeline air pressure drop is one of the most important aspects of pneumatic conveying system design, much work has been done on its determination since early this century. Most of this work has been carried out empirically. With more understanding of the motion of particles in the pipe from numerous experimental works, many attempts have been made to predict the pressure drop caused by bends and straight sections of pipe using theoretical models (i.e. the total pipeline air pressure drop is the sum of pressure drops caused by all bends and straight pipes). However, the established theoretical correlations are used only with restricted conditions (e.g. the particles are coarse, rigid, of uniform size and/or conveyed in very dilute phase). The research reported in the literature on total pipeline air pressure drop can be summarised in two different categories: scaling-up of test rig data of total pipeline air pressure drop, and dealing separately with bends and straight sections of pipe.

2.1 Scaling-Up of Test Rig Data

Mills et al. [39] and Mason et al. [34] proposed a very simple scale-up procedure. That is, for constant solids pressure drop and $m_f D^{-2}$:

$$m_{s2} = m_{s1} \frac{L1}{L2} \left(\frac{D2}{D1}\right)^{2.0} \qquad (2.1)$$

where: subscript 1 refers to the test rig and 2 to the actual or proposed plant.

Since it is simple and has good physical relevance, this scale-up procedure has been used quite extensively.

Wypych and Arnold [68] in 1987 transported three products (fly ash/cement mix, PVC powder, screened coke) in four test rigs. These four test rigs had different total effective lengths, pipe diameters, bend numbers or locations, as listed below:

Test Rig 1:	L=162 m	D=0.060 m	Five 1 m radius 90° bends.
Test Rig 2:	L=162 m	D=0.105 m	Five 1 m radius 90° bends.
Test Rig 3:	L=25 m	D=0.052 m	Five 1 m radius 90° bends.
Test Rig 4:	L=71 m	D=0.052 m	Eleven 1 m radius 90° bends and two 90° blinded-tee bends.

Based on the steady-state pipeline conveying characteristics, Equation (2.1) was found [68] to be inadequate, and the following improved scale-up procedure was developed:

$$m_{s2} = m_{s1} \frac{L1'}{L2'} \left(\frac{D2}{D1}\right)^{2.8}$$

where L1' and L2' represent adjusted values of L1 and L2 to allow for any differences between the number (and type) of bends used on the test rig and actual plant.

The Engineering Equipment Users Association (EEUA) [14] divided total pipeline air pressure drop into three components:

- Acceleration of particles from rest, Δp_{ta}.
- Pipeline friction, Δp_{ts}.
- Changes of direction (bend pressure drop), Δp_{tb}.

For each component, a similar equation with different constants was used, as given below:

$$\Delta p_{ta} = F_1 (1 + m^*) \frac{\rho_{fav} V_{fav}^2}{2}$$

$$\Delta p_{ts} = F_2 (1 + m^*) \frac{L}{D} \frac{\rho_{fav} V_{fav}^2}{2}$$

$$\Delta p_{tb} = F_3 (1 + m^*) N_b \frac{\rho_{fav} V_{fav}^2}{2} \qquad (2.2)$$

where: V_{fav} is the average superficial air velocity in the pipeline.

$$\rho_{fav} = \frac{m_f}{V_{fav} A}$$

The determination of constants F_1, F_2 and F_3 was based on the experimental data from many researchers who conveyed different products (e.g. limestone, salt, sand, wheat and coal) in different configurations of pipeline. Because of their convenience of calculation and good physical relevance, these equations have been used quite extensively in various applications (e.g. feasibility studies, troubleshooting, system uprating and general design).

Chambers et al. [9] in 1986 collected numerous existing empirical correlations and experimental data of total pipeline air pressure drop in pipelines of different length, diameter, bend number and step. By using the collected correlations, the total pipeline air pressure drop was calculated for different configurations of pipeline.

Then the comparison between the predicted and experimental values of total pipeline air pressure drop was carried out for a range of particle size (16 μm to 3 mm), product to air mass flow ratio (2 to 530) and pipe length (25 to 1600 m). The equations selected and used by Chambers et al. [9] are listed below:

$$\Delta p_{ta} = (1 + 2\, m^* \frac{v_s}{V_{fm}}) \frac{\rho_{fi}\, V_{fi}^2}{2}$$

$$\Delta p_{tv} = m^*\, g \frac{\rho_{fm}\, V_{fm}}{v_s} L_v$$

$$\Delta p_{ts} = (\lambda_f + m^*\, \lambda_s) \frac{\rho_{fm}\, V_{fm}^2}{2\, D} L$$

$$\Delta p_{tb} = F_3\, (1 + m^*)\, N_b \frac{\rho_{fm}\, V_{fm}^2}{2}$$

$$\Delta p_t = \Delta p_{ta} + \Delta p_{tv} + \Delta p_{ts} + \Delta p_{tb}$$

$$\frac{v_s}{V_{fm}} = (1 - 0.008\, d_p^{0.3}\, \rho_b^{0.5}) \qquad d_p \text{ in mm}$$

$$\lambda_f = \frac{1.325}{\{\ln[\frac{\varepsilon}{3.7D} + \frac{5.74}{Re^{0.9}}]\}^2}$$

$$\lambda_s = \frac{2.1\, F_{rs}^{0.25}\, (\frac{D}{d_p})^{0.1}}{m^{*0.3}\, F_{rm}} \qquad d_p < 0.5 \text{ mm}$$

$$\lambda_s = \frac{0.082\, F_{rs}^{0.25}\, (\frac{D}{d_p})^{0.1}}{m^{*0.3}\, F_{rm}^{0.86}} \qquad d_p > 0.5 \text{ mm}$$

$$F_{rs} = \frac{v_\infty}{\sqrt{g\ D}}$$

$$v_\infty = [\frac{4\ g\ d_p\ (\rho_b - \rho_{fm})}{3\ C_d\ \rho_{fm}}]^{0.5}$$

$$C_d = \frac{24}{R_{ep}}(1 + \frac{3\ R_{ep}}{16}) \qquad R_{ep} < 1$$

$$C_d = 0.4 + \frac{26}{R_{ep}^{0.8}} \qquad 1 < R_{ep} < 1000$$

$$C_d = 0.4 \qquad R_{ep} > 1000$$

$$R_{ep} = \frac{v_\infty\ \rho_f\ d_p}{\mu}$$

$$R_e = \frac{V_f\ \rho_f\ D}{\mu}$$

Generally, the selected empirical correlations were able to predict total pipeline air pressure drop to better than a factor of 2. However, it was suggested [9] that conveying tests still are necessary to prove the feasibility of economically attractive options and to confirm that products can be conveyed at the selected values of mass flow ratio and air velocity.

It has been shown clearly [13, 33, 41, 62, 63, 64] that conveyed materials have numerous influences on total pipeline air pressure drop. Also, it is believed that the predictions of Chambers et al. [9] to within a factor of 2 are too inaccurate, especially when the operating pressures are significant (e.g. in excess of 300 kPag). Therefore,

recently Wypych and Arnold [71] developed a new test-design procedure. The total pipeline air pressure drop is determined by using the following correlations:

$$\Delta p_t = (\lambda_f + m^* \lambda_s) \frac{\rho_{fm} V_{fm}^2}{2\ D} L$$

$$\lambda_f = \frac{1.325}{\{\ln[\frac{\varepsilon}{3.7D} + \frac{5.74}{Re^{0.9}}]\}^2}$$

$$\lambda_s = x1\ m^{*x2}\ F_{rm}^{x3}\ \rho_{fm}^{x4} \qquad (2.3)$$

The exponents x1, ..., x4 are determined empirically and only valid for a given product. After the exponents x1, ..., x4 are determined by the experimental data of total pipeline air pressure drop from a test rig, the correlations can be used to predict total pipeline air pressure drops in other configurations of pipeline (i.e. of different length, diameter, bend number and step).

2.2 Dealing Separately with Bends and Straight Sections of Pipe

Due to the compressibility of conveying air, conveying conditions (e.g. air velocity, density, particle velocity and concentration) vary along the pipeline. However, the pressure drop caused by bends and straight sections of pipe is a function of the conveying conditions. Hence, a potentially accurate way of estimating total pipeline air pressure drop is to deal separately with bends and straight sections of pipe. To date, numerous empirical and theoretical correlations have been set up [6, 8, 16, 28, 45, 52, 66] for this purpose.

Generally, the correlations were developed using experimental values of bend pressure drop and pressure gradient in straight sections of pipe. The so-called 'traditional' method used for this purpose is depicted in Figure 2.1.

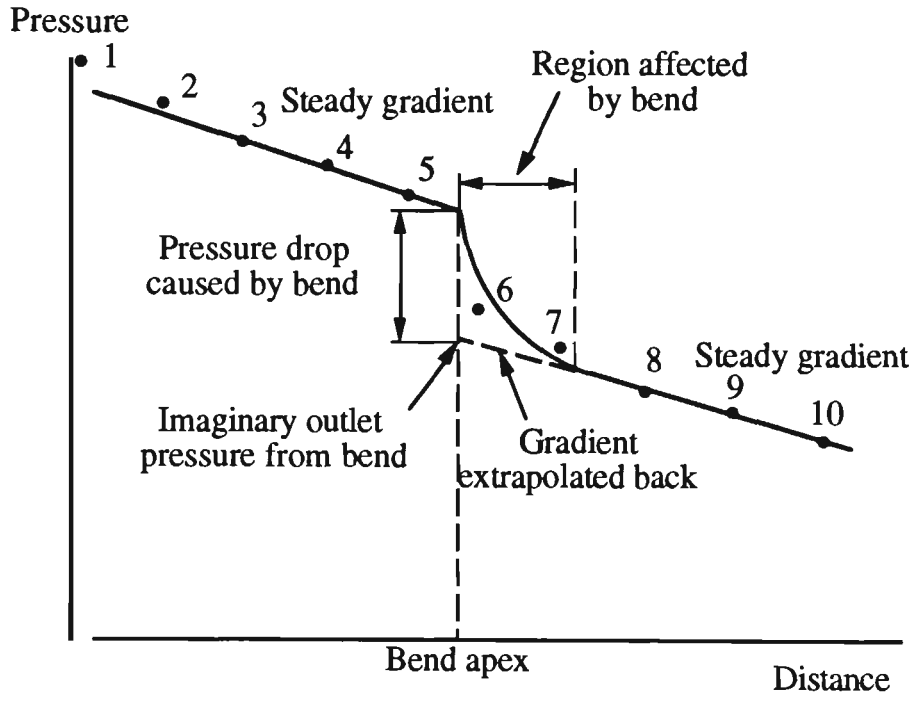

Figure 2.1 Traditional method used to determine pressure drop caused by bend and pressure gradient in straight section of pipe.

2.2.1 Empirical Correlations

2.2.1.1 Straight Section of Pipe

Two vertical straight sections of pipe with length of 13 ft. (4.12 m) and diameters of 0.473 and 1.023 in. were used by Belden et al. [2] in 1949 to transport spherical catalyst. The properties of the catalyst are as follows:

Material	Shape	d_p (μm)	ρ_s (kg m^{-3})	ρ_b (kg m^{-3})
Small catalyst	Spherical	963	860	492
Large catalyst	Spherical	1941	976	594

The total pressure drop in the vertical pipe was measured by a water manometer. The product to air mass flow rate ratios ranged from 0 to 11.43. Based on the experimental values of pressure drop, a correlation for the frictional pressure drop was developed, where:

$$\Delta p_{sv} = (1+m^*)\left(0.049+0.22\frac{m^*}{(1+m^*)^2}\right) Re^{-0.2}\frac{\rho_{fm} V_{fm}^2}{2}$$

which is independent of particle diameter and density.

Numerous products were tested through a one-inch horizontal pipe by Richardson et al. [47] in 1960. The materials conveyed are listed as follows:

Material	Shape	d_p (μm)	ρ_s (kg m^{-3})	v_∞ (m s^{-1})
Coal A	Rounded	762	1402	2.81
Coal B	Rounded	635	1402	2.44
Coal C	Rounded	508	1402	2.14
Coal D	Rounded	1016	1402	3.26
Coal E	Rounded	2032	1402	3.72
Perspex A	Angular	1524	1186	3.74
Perspex B	Angular	3810	1186	5.00
Perspex C	Spherical	762	1186	2.35

Polystyrene	Spherical	356	1081	1.62
Lead	Spherical	305	11086	8.17
Brass	Porous	381	8443	4.09
Aluminium	Rounded	229	2836	3.02
Rape seed	Spherical	1905	1081	5.92
Radish seed	Spherical	2540	1065	6.48
Sand	Nearly spherical	1270	2611	4.67
Manganese dioxide	Rounded	762	4005	5.28

The conveying line included a brass horizontal straight pipe, 114 ft (34.8 m) in length. Twelve pressure tappings connected to a water manometer were brazed at intervals of 10 ft (3.05 m) along the pipe. By injecting an air pulse into the system, the velocity of particles was measured over a wide range of conveying conditions. Hence, a relationship between particle velocity and superficial air velocity was obtained:

$$V_f - v_s = \frac{v_\infty}{0.468 + \sqrt{\frac{v_\infty}{\rho_s}}}$$

Also, based on the measured parameters (e.g. m_s, m_f, v_s and pressure along the pipe), an empirical correlation of calculating the pressure drop attributable to the presence of the solids in horizontal straight pipes was set up, that is:

$$\frac{\Delta p_{ss}}{\Delta p_{sf}} \frac{v_s^2}{m_s} = \frac{k_r}{v_\infty} \qquad (2.4)$$

where $k_r = 219618$ for one-inch brass pipe.

Compared with the results obtained by Segler [53] for the conveying of wheat in pipes ranging from 2 to 16 in. diameter, k_r was found to be a function of pipe diameter.

Extensive experimental investigations were carried out by Dogin et al. [12] in 1962 to determine a universal and generalised relationship between the flow resistance and the parameters governing the flow of solids-gas suspensions. Six granular solids were conveyed through a horizontal straight section of pipe with a diameter of 124.8 mm. The test materials are listed below.

Material	d_p (μm)	ρ_s (kg m^{-3})
Millet	1900	1332
Peas	5760	1310
Turnip seed	1280	1160
Wheat	4000	1220
Pine kernels	8400	880
Sunflower seeds	5850	740

The pressure drop was measured by an alcohol differential micromanometer. During conveyance, it was believed that all the particles were suspended. By maintaining all the other parameters constant, the effect of each parameter (e.g. m_s, V_f, d_p, ρ_s) on friction factor, λ_s, was analysed. Based on the subsequent analysis, a generalised correlation for the calculation of λ_s was obtained:

$$\lambda_t = \lambda_f + \lambda_s$$

$$\lambda_s = B \frac{m_s \left(\frac{d_p}{D}\right)0.1\ Re^{0.4}}{F_{rm}} \frac{\rho_s}{\rho_{fm}} \qquad (2.5)$$

The coefficient B is a function of pipe diameter but constant for a given pipe diameter (e.g. $B=1.65\times10^{-6}$ for D=124.8 mm). However, Equation (2.5) is valid only for the following range of conditions:

$$110\times10^3 \le R_e \le 321\times10^3,\ m^* \le 15,\ 178 \le F_r \le 1300,$$

$$9\times10^{-3} \le \frac{d_p}{D} \le 37\times10^{-3}, \text{ and } 573 \le \frac{\rho_s}{\rho_f} \le 1150.$$

By using a large quantity of pressure drop data in vertical risers, Richards and Wiersma [46] in 1973 reviewed several models and finally developed a correlation:

$$\frac{\Delta p_s}{\Delta L} = \frac{1+m^*}{\Delta L} \rho_{fm} V_{fm}^2 + (1+m^*)\, g\, \rho_{fm} \left(1+17.5 \sqrt{\frac{D}{\Delta L}}\right)$$

to predict the pressure drop in vertical straight sections of pipe. The equation does not include the particle properties and pipe material properties. However, the large quantity of data used by Richards and Wiersma [46] was based on 18 products (d_p = 40 to 600 μm and ρ_s = 1450 to 2660 kg m^{-3}) and on pipelines ranging in diameter from 51 to 300 mm and length from 4 to 25 m.

Shimizu et al. [54] in 1978 used two commercial vacuum cleaners as blowers to transport spherical copper particles in a vertical straight pipe with an internal diameter of 28 mm. The mean diameter of copper particles ranged from 45 to 170 μm. Also, the values of Reynolds number and solid loading ratio were varied up to 50,000 and 5, respectively. The pressure drop in the section beyond the acceleration zone was measured by a water manometer. Based on experimental results, a simple correlation for the calculation of the total pressure drop due to solids-air mixture was set up:

$$\frac{\Delta p_s}{\Delta p_{sf}} = 1 + 0.379\ m^*$$

Michaelides [37] in 1987 collected nine sets of experimental data from different investigators, totalling 1450 data points. These nine sets of data covered different products (e.g. rape seed, sand, coal, lucite powder) transported in vertical and/or horizontal straight pipes of different length and diameter over a wide range of conveying conditions. Based on all these data, the constant λ_s in the correlation:

$$\Delta p_s = (\lambda_f + \lambda_s \frac{m^*}{\sqrt{F_{rm}}}) \frac{\rho_{fm} V_{fm}^2}{2\ D} \Delta L$$

proposed by Michaelides was determined by using the least squares method. The determined value of λ_s was 0.076. This equation was proposed by Michaelides [38] as the best correlation and can be used for pneumatic conveying system design.

2.2.1.2 Bend

Cornish and Charity [10] in 1966 used dimensional analysis in organising and conducting their study. First, they listed all the important factors (e.g. bend radius, particle density) which affected elbow loss. For a given pipe material and product, some of these parameters (e.g. particle shape factor, friction between particles and pipe wall) were considered constant. Therefore, the number of variables with significant influence on elbow loss was reduced to nine. These nine variables then were expressed by six terms, as given below:

$$\frac{\Delta p_{bs}}{\rho_{fo}\, V_{fo}^2} = \Phi\left(\frac{R}{D}, \frac{m_s}{\rho_{fo}\, V_{fo}\, D^2}, \frac{D}{d_p}, \frac{\rho_s}{\rho_{fo}}, \frac{\rho_{fo}\, V_{fo}\, D}{\mu}\right)$$

Numerous experiments were conducted with spherical pellets, such as Alaska peas, grain sorghum and rape seed which had different values of d_p. The pipe diameter was 2 in. and the bend to pipe radius ratios ranged from 1.25 to 36. From these experimental results, it was demonstrated [10] that:

- pressure losses are higher for short radius elbows and little can be gained in terms of reducing pressure loss by increasing the 2R/D ratio beyond six;

- elbow pressure loss is a linear function of solid loading;

- the terms D/d_p and ρ_s/ρ_f might have a significant influence on elbow pressure loss.

Schuchart [52] in 1968 completed a comprehensive study of the pressure loss caused by bends. The pipe diameter was 34.35 mm and the conveyed materials were:

Material	d_p (μm)	ρ_s (kg m^{-3})
Quartz beads	1490	2610
	1850	2610
	2350	2610
	2960	2610
Polyamide plastic	2180	1140

Solids loadings were generally in the range between 0 and 20. Schuchart [52] explored a wide range of bend diameters from 3.5D to 21.5D and developed a final correlation given as:

$$\frac{\Delta p_{bs}}{\Delta p_{ss}} = 210 \left(\frac{2R}{D}\right) - 1.15$$

This correlation was expressed as a ratio of solids pressure loss attributable to the bend and a straight section of pipe of equivalent length. The formulae yielded by Ito [23] were used for the prediction of the air-only component of bend pressure loss.

Singh and Wolf [55] in 1972 also used dimensional analysis and listed all the important variables. For their test pipeline (D=5.91 in., R=15, 30, 48 in.) and product (granular chopped forage), the number of significant variables was reduced to seven and the variables were expressed in the following dimensionless ratios:

$$\frac{\Delta p_{bs}}{\rho_{fo} V_{fo}^2} = \Phi\left(\frac{R}{D}, \frac{m_s}{\rho_{fo} V_{fo} D^2}, \beta_a\right) \qquad (2.6)$$

where: β_a is the angle of bend deflection (i.e. change in flow direction).

It was assumed that a generalised power law was valid and from 108 test results, a linear relationship was developed between $\frac{\Delta p_{bs}}{\rho_{fo} V_{fo}^2}$ and $\frac{m_s}{\rho_{fo} V_{fo} D^2}$, resulting in the following model for bend pressure drop:

$$\Delta p_b = a_c + a_s \frac{m_s V_{fo}}{D^2} \left(\frac{R}{D}\right)^{ab} \qquad (2.7)$$

where: a_c represents the bend pressure loss under air-only conditions.

Using the least squares method, Singh and Wolf [55] found that:

$$\Delta p_b = 0.13 + a_s \frac{m_s V_{fo}}{D^2} \left(\frac{R}{D}\right) - 0.18$$

For deflection angles equal to:

45°, $a_s = 0.00334$

90°, $a_s = 0.00537$

Ikemori and Munakata [22] in 1973 developed the concept of a bend friction factor associated with Δp_{bs}:

$$\Delta p_{bs} = \zeta_s \frac{\pi R}{2 D} m^* \frac{\rho_{fo} V_{fo}^2}{2}$$

where: $$\zeta_s = \frac{\zeta_{bs}\, v_{b\infty}}{V_{fo}} + \frac{2\, v_\infty\, v_{b\infty}\, D}{V_{fo}^2\, R}$$

$$\zeta_{bs} = 2\, \frac{(1 - \frac{v_{b\infty}}{V_{fo}})^2}{\frac{v_\infty^2}{g\, D}\, \frac{v_{b\infty}}{V_{fo}}} \qquad (2.8)$$

ζ_{bs} is the bend friction factor due to collisions between the particles and bend wall,

and $v_{b\infty}$ is the free-settling velocity of a solid particle in the bend.

This relationship takes into account [22] the energy relationship between particles undergoing centrifugal settling motion in a 'theoretical' bend and the additional pressure drop due to solids in the actual bend. However, the calculation of Δp_{bs} relies on an experimentally determined constant depending on the size and properties of the particles and pipe. Also, the solids loading is not included in the equation of ζ_s.

Work performed by Mason and Smith [35] in 1973 suggested an expression for a bend resistance number based on solids loading, and for which pressure loss due to air flow is nearly constant, giving:

$$\zeta_s = 0.027\ m^* - 0.0025\ m^{*2}$$

The data were acquired using a bend of 2R/D ≈ 20, $R_e \approx 10^5$, solids loading from 0.4 to 4.8, and pipe diameter of 51 mm. The test material was alumina particles with diameters of 15-70 μm and a particle density of 3990 kg m^{-3}. The final bend loss equation was:

$$\Delta p_b = (0.025 + \zeta_s) \frac{\rho_{fo} V_{fo}^2}{2}$$

Rossetti [50] in 1983, working with bends with 2R/D = 2 to 8.4, reported the relation:

$$\Delta p_b = (\zeta_f + \zeta_s) \frac{\rho_{fo} V_{fo}^2}{2}$$

in which ζ_f accounts for the pressure drop due to the air while ζ_s accounts for the pressure drop due to solids. A value of 0.35 for ζ_f was claimed, and ζ_s was influenced primarily by the particle terminal velocity. Rossetti [50] also observed that fine particles tend to slide around bends, thereby incurring a frictional pressure loss for which they must be compensated by the kinetic energy of the air. Coarse materials tend to lose energy through wall collisions, incurring less re-acceleration energy loss.

A 50 mm bore horizontal pipeline of 50 m including eleven bends was employed by Mills and Mason [40] in 1985 to convey pulverised fuel ash. The central group of seven identical bends positioned in the corners of the double loop was changed for each test program. There was a reasonable length of straight pipe before each test bend to ensure that the particles would be accelerated. Tests were carried out with

long radius bends (2R/D=24), short radius bends (2R/D=6), tight elbows (2R/D=2) and blinded tees over a wide range of conveying conditions (V_f = 4 ~ 45 m s^{-1}, m* = 0 ~ 120). A comparison then was made, based on the total pipeline air pressure drop required to achieve a certain product mass flow rate for a given air mass flow rate. It was demonstrated that: the short radius bends (2R/D=6) provided the best performance and the blinded tees the worst performance over the widest range of conveying conditions. The long radius bends (2R/D=24) were marginally better than short radius bends at the high values of flow rates but probably not sufficiently better to recommend their use, since they are likely to be more expensive both to purchase and install.

Westman et al. [66] in 1987 used a vacuum pneumatic conveying system to convey four products, which are listed as follows:

Material	Shape	d_p (μm)	ρ_s (kg m^{-3})	ρ_b (kg m^{-3})
Alanthon polyethylene L5005	Cylindrical	3410	877	572
Alanthon polyethylene M6450	Cylindrical	3382	924	636
Yellow polyester 6936F	Cylindrical	3398	1298	800
White polyester 1933F	Ellipsoidal	3517	1320	824

Pipe diameter was 4 in. and solids loadings were generally in the range of 0 to 7.5. Three interchangeable bend components with bend-to-pipe radius ratios of 24, 10

and 3 were employed. Based on all the experimental data of bend pressure drop, the following correlations were obtained:

$$\zeta_f = 0.167\ [1 + 17.062\ (\frac{2\ R}{D})^{-1.219}]\ R_e^{-0.17}\ (\frac{2\ R}{D})^{0.84}$$

$$\zeta_s = \frac{5.4\ m^*\ 1.293}{F_{ro}^{0.84}\ (\frac{2\ R}{D})^{0.39}}$$

$$\Delta p_b = (\zeta_f + \zeta_s)\frac{\rho_{fo}\ V_{fo}^2}{2}$$

It is interesting to note from the ζ_s equation that longer radius bends produce a lower pressure drop (i.e. with respect to short radius bends).

Seven different types of bends with varying radius and design, fitted by two different means into a pneumatic conveying pipeline with diameter of 2 in., were tested by Bradley [7] for conveying white wheat flour over a wide range of conveying conditions (V_f = 4 ~ 45 m s^{-1}, m^* = 0 ~ 130). The properties of the white wheat flour were: ρ_s=1470 kg m^{-3}, d_p=78 μm, and ρ_b=510 kg m^{-3}. Based on the experimental data of each type of bend, it was found [7] that there was little to choose between the various radius bends. Therefore, the short radius bends would appear [7] to be the best choice for a situation where wear or attrition are not a severe problem. That is, the short radius bends are cheaper to buy and install and less bulky than longer radius bends whilst offering similar values of pressure drop. Due to their high pressure drop, blinded tees should be restricted to situations where wear is a serious problem (i.e. high velocities with abrasive products). However, the blinded tees should not be used where suspension densities are high and velocities low (in which

case wear is unlikely to be a problem) because that is where their performance is worst of all.

2.2.1.3 Bend and Straight Section of Pipe

Segler [53] in 1951 conveyed granular products (e.g. wheat, oats, rye and barley) in dilute-phase along pipelines of different diameter (e.g. D=1.81, 4.44, 11.6 and 16.5 in.). In the horizontal straight section beyond the acceleration region, the friction factor, λ_{sh}, was expressed as:

$$\lambda_{sh} = \frac{4\, m_s}{\pi\, D\, V_f} \frac{(1-\eta)^3}{\sigma_m\, \eta} \tag{2.9}$$

where: η is the ratio of the mean solids velocity to air velocity, which is constant for any given material

$$\eta = \frac{v_s}{v_f}$$

σ_m is the average flight coefficient of a single particle

$$\sigma_m = \frac{m_p}{C_m\, A_p} \tag{2.10}$$

m_p represents the average weight of a particle

A_p is the average projected area of a particle

C_m is the relevant air resistance coefficient

It was found that the pressure drop for conveying wheat was somewhat higher. Hence, because of the difficulty of calculating λ_{sh} , many diagrams for conveying wheat were presented to express the relationship between λ_{th} and D, m_s, V_f. The values of λ_{th} from these diagrams could be used in design calculations of other granular particles. For vertical sections,

$$\frac{\lambda_{tv}}{\lambda_{th}} = \frac{1.09\times10^{-2}\, m_s + 17}{3.46\times10^{-3}\, m_s + 17}$$

For the work on bends, an equivalent length was used. This length was a function of m_s, V_f, ρ_f and R/D and given by diagrams. Also, the bend radius was expressed as:

$$R = \frac{D}{2\,(\frac{1}{\cos\alpha} - 1)} \qquad (2.11)$$

where: $\alpha = \frac{90^\circ}{n+1}$

n is the number of particle rebounds around the bend.

For a given number of rebounds, there is only one value of bend radius. A consideration of possible solutions shows a curve where R=6D is preferred. The bend of radius 1.2D can be rejected as it is too sharp and would give a high resistance to flow and the bend of radius 14.0D is inconveniently large.

Sproson et al. [56] in 1973 transported large coal particles (d_p=1020 ~ 1280 μm) in two full-scale horizontal pipelines with a diameter of 127 mm. In the test section of the first pipeline, there were two long straight sections of pipe and one 180° bend

with R=3D. In the test section of the second pipeline, there were three long straight sections of pipe and two 90° bends with radii of 3D and 12D respectively. The loading ratios ranged from 2.5 to 9.8. Based on the experimental results of pressure along the straight sections of pipe, the correlation for calculating the friction factor due to solids was set up, as given below:

$$\lambda_{th} = \lambda_{fh} + \lambda_{sh}$$

$$\lambda_{sh} = 0.00374\ m^* - 0.0012$$

The experimental data of bend pressure drop were used to evaluate the Schuchart [52] correlation. A good agreement was obtained.

Also in 1976, Sproson et al. [57] conveyed the same product in a full-scale pipeline of 127 mm. In the test section, there were two long horizontal sections and one vertical straight section of pipe and two bends, one bend with a radius of 12D located from horizontal to vertical and another bend with a radius of 3D from vertical to horizontal. Based on test results, the following correlations for vertical pipe and bend were determined:

$$\lambda_{tv} = \lambda_{fv} + \lambda_{sv} = 0.0265\ m^* - 0.006$$

$$\zeta_t = \zeta_f + \zeta_s = 0.0241\ m^* + 0.031 \qquad (2.12)$$

Equation (2.12) shows that bend location and radius have no effect on ζ_t.

Morikawa et al. [42] in 1978 studied pressure losses in both circular and elliptical bends, relying on Ito's single-phase correlation for air-only losses. They used a vacuum pneumatic conveying system and the pipe diameter was 40 mm. Experimenting with nearly spherical polyethylene pellets with a mean diameter of 1100 μm and particle density of 923 kg m^{-3}, they explored bends with 2R/D = 12.3 to 36.1 and mean air velocity = 18 to 29 m s^{-1}. The solids loading ratio varied up to 8. For losses due to solids, they employed an empirical approach, using the Froude number, F_r, as a parameter along with 2R/D. In an approach similar to Schuchart [52], they arranged their expression for Δp_{bs} in terms of a non-dimensional quantity based on pressure loss due to solids per unit length of straight pipe:

$$\lambda_s = \frac{\Delta p_{ss}}{\Delta L} \frac{2\ D}{\rho_f\ V_f^2}$$

which, being independent of air velocities larger than 20 m s^{-1}, was seen to vary linearly with solids loading:

$$\lambda_s = (1.51 + 1.69\ m^*)\times 10^{-3} \qquad \text{upstream}$$

$$\lambda_s = (2.06 + 1.75\ m^*)\times 10^{-3} \qquad \text{downstream}$$

Defining the coefficient of pressure drop due to solids as:

$$\zeta_s = \frac{\Delta p_{bs}}{\frac{1}{2}\rho_f\ V_f^2}$$

Morikawa et al. [42] arrived at a correlation for pressure loss attributable to the bend due to the presence of solids:

$$\frac{\zeta_s}{\lambda_s} = \frac{1.5\times10^4}{F_r\,(\frac{2\,R}{D})\,0.5} \qquad F_r > 30$$

Bradley [6, 8] and Bradley and Reed [45] pointed out that the method currently employed widely for the prediction of total pipeline air pressure drop was fundamentally inaccurate. The employed method was to build a pilot-scale test rig, operate it with a sample of the product to be conveyed in the proposed systems, measure the total pipeline air pressure drop, air and product mass flow rates and then scale the results to the proposed system(s). It also was found that there were no correlations available to predict accurately the pressure drop caused by bends or straight sections of pipe for conveying products with significantly different particle properties. Therefore, the following method was proposed.

- Testing the product to be conveyed in a rig designed to obtain data on the effects of individual pipeline features (straight lengths, bends, etc.);

- Entry of the results into a specially developed data storage system designed to be quick and easy to use;

- Retrieval of the data from the storage system and synthesising the performance characteristics of the proposed pipelines.

In the data storage system, the equation:

$$\Delta p_b = \frac{1}{2} k_b \rho_{sd} V_f^2 \qquad (2.13)$$

where: ρ_{sd} is suspension density, $\rho_{sd} = \frac{m_s}{V_{fe} A}$

k_b is a coefficient

was used to predict the bend pressure drop. However, k_b was also a function of the variables in the equation and was represented on a single graph for each bend and product type against either air velocity or suspension density. For straight pipes:

$$\Delta p_s = \Delta p_{sf} + \Delta p_{ss}$$

Δp_{sf} was calculated from appropriate single phase flow methods. Δp_{ss} had different correlations for different types of product. For instance,

$$\frac{\Delta p_{ss}}{\Delta L} = 6.5\times10^{-3} \left(\frac{\rho_{sd}}{100}\right)^{n_s} \qquad \text{for wheat flour} \qquad (2.14)$$

$$n_s = \frac{V_{fe}}{8}$$

$$\frac{\Delta p_{ss}}{\Delta L} = 4.4\times10^{-3} \rho_{sd} V_{fe} \qquad \text{for polyethylene pellets}$$

2.2.2 Theoretical Correlations

2.2.2.1 Straight Section of Pipe

By using material and force balances in a differential section of pipe length, Yang [73, 74] in 1973 obtained theoretical correlations to calculate the particle velocity in the straight section of pipe beyond the acceleration region.

$$\varepsilon = 1 - \frac{4\, m_s}{(\rho_s - \rho_f)\, \pi\, D^2\, v_s} \tag{2.15}$$

$$v_s = V_f - v_\infty \sqrt{(1 + \frac{\lambda_s\, v_s^2}{2\, g\, D})\, \varepsilon^{4.7}} \tag{2.16}$$

vertical conveying

$$v_s = V_f - v_\infty \sqrt{\frac{\lambda_s\, v_s^2}{2\, g\, D}\, \varepsilon^{4.7}} \tag{2.17}$$

horizontal conveying

where: $\varepsilon^{4.7}$ corrects the drag coefficient for a relatively dense solids-air mixture.

To solve for particle velocity from Equations (2.15), (2.16) and (2.17), a knowledge of solid friction factor, λ_s, is necessary. Based on data for vertical conveying by Hariu and Molstad [19] and for horizontal by Hinkle [20], Yang [75] in 1974 proposed two empirical equations for both vertical and horizontal pneumatic conveyings:

$$\lambda_s = 0.0206\, \frac{1-\varepsilon}{\varepsilon^3} \left[(1-\varepsilon) \frac{Re_p}{Re_s} \right]^{-0.869} \tag{2.18}$$

vertical conveying

$$\lambda_s = 0.117\, \frac{1-\varepsilon}{\varepsilon^3} \left[(1-\varepsilon) \frac{Re_p}{Re_s} \frac{V_f}{\sqrt{g\, D}} \right]^{-1.15} \tag{2.19}$$

horizontal conveying

The materials and conveying conditions employed by Hariu and Molstad [19] and Hinkle [20] are listed as follows:

By Hariu and Molstad [19]:

Material	d_p (μm)	ρ_s (kg m^{-3})	v_∞ (m s^{-1})	D (mm)	m*
Sand A	503	2650	3.9	6.78; 13.5	1.16 - 30.99
Sand B	357	2650	2.8	6.78; 13.5	0.46 - 33.19
Sand C	274	2650	2.2	6.78; 13.5	1.38 - 39.54
Sand D	213	2710	1.59	6.78; 13.5	1.55 - 47.07
Cracking catalyst	110	980	0.31	6.78; 13.5	1.12 - 12.82

By Hinkle [20]:

Material	Sphericity	d_p (μm)	ρ_s (kg m^{-3})	v_∞ (m s^{-1})	D (mm)	m*
Tenite	0.93	2270	1130	6.47	50.8	0.61 - 6.02
Catalin	1.00	6350	1120	13.57	50.8	0.47 - 1.65
Polystyrene	0.96	356	1050	2.64	50.8	0.36 - 2.11
Alundum	1.00	8390	1820	19.9	50.8	1.50 - 4.90

Since the variables v_S, ε and λ_S interact, a trial and error solution is required to solve Equations (2.15), (2.16) and (2.18) for vertical conveying and Equations (2.15), (2.17) and (2.19) for horizontal conveying. Hence, the total pressure drop in straight section of pipe where particles have been accelerated is:

$$\Delta p_S = \rho_S\, g\, (1-\varepsilon)\, \Delta L + \lambda_f \frac{\rho_f\, V_f^2}{2\, D} \Delta L + \lambda_S \frac{\rho_S\, (1-\varepsilon)\, v_S^2}{2\, D} \Delta L$$

For horizontal conveying, the first term should be omitted.

To evaluate the above equations, Yang [76] calculated the pressure drop in vertical conveying pipelines by Jones et al. [24]. The agreement between predicted and experimental pressure drop was better than ±30%, except for fused alumina particles with a sphericity around 0.4. The material and conveying conditions employed by Jones et al. [24] are listed below.

Material	Sphericity	d_p (μm)	ρ_s (kg m^{-3})	D (mm)	m*
Glass bead No. 106	0.887	570	2500	7.75; 10.2; 22.1	0.35 - 12.5
Glass bead No. 109	0.947	333	2530	7.75; 10.2	0.31 - 13.2
Fused alumina No. 36	0.403	732	3890	7.75; 10.2; 22.1	0.21 - 6.50
Fused alumina No. 60	0.429	438	3960	7.75; 10.2	0.47 - 7.69
Fused alumina No. 100	0.450	182	3890	775; 10.2	1.09 - 16.7
Zircon sllica No. 1	0.769	549	3480	7.75; 10.2	0.60 - 8.29
Zircon sllica No. 2	0.763	369	3330	7.75; 10.2	0.57 - 11.5
Steel shot A	0.785	482	7560	7.75; 10.2	0.54 - 11.6
Steel shot C1	0.964	269	7600	7.75; 10.2	0.94 - 22.2
Steel shot C2	0.895	310	7610	7.75; 10.2; 22.1	1.03 - 16.1
Steel shot D1	0.747	760	7260	7.75; 10.2	0.72 - 8.80
Steel shot D2	0.777	658	7240	10.2	0.78 - 7.57

Also, Yang [78] predicted the pressure drop in a 10-cm horizontal conveying pipeline. The agreement still was within ±30%. The material was crushed acrylic particle. Its sphericity was 0.9 and mean diameter 1100 μm. The product to air mass flow ratios were up to 8.

2.2.2.2 Bend

The first truly theoretical analysis on solids-air pressure drop caused radius bends was performed by Ghosh and Kalyanaraman [16] in 1970. In their analysis, the assumptions:

- the conveying particles are rigid, interacting and of uniform size;
- the frictional forces between the particles and air are negligible;
- the drag coefficient is constant over the region $30\times10^3 \leq R_e \leq 100\times10^3$.

were accepted and the various aspects of particle dynamics were considered to account for friction, impact and centrifugal resistances. By comparing the theoretical results with their experimental values, it was found that the agreement was very close. In their experiments, the pipe diameter was 25.4 mm, the conveying products were paddy, wheat and sand, the bend-to-pipe radius ratios ranged from 5.9 to 25 and the solid loadings from 0 to 5.3. The pressure along the pipeline was measured by manometers with mercury or colored water. However, in calculating the pressure drop across a bend using the theoretical equations, knowledge of the fractions of particles sliding and impacting against the bend wall, as well as particle velocities at the entrance and the exit of the bend, is required.

Kovacs [28] in 1971 considered that the pressure drop caused by a bend was the sum of two components. The first component was located in the bend itself and the second occurred in the straight section of pipe immediately downstream from the

bend for the re-acceleration of particles. By employing a sliding frictional term for particles moving around the bend (i.e. assuming that all particles slide along the outside wall of the bend), the equations for calculating the pressure drop in the bend itself were set up. The pressure losses for the re-acceleration of particles were predicted by using the impulse theorem. All the equations sounded simple and had appropriate physical relevance. However, no experiments were conducted to verify these equations.

2.2.2.3 Bend and Straight Section of Pipe

Based on the equation of particle motion in straight pipe and around bend, a method was proposed by Tsuji [61] in 1982 for predicting the pressure drop in dilute-phase systems. In this method, only a few empirical correlations for some parameters (e.g. solids friction factor, λ_S, wall friction, υ) were employed from other investigators. Since the solution of the equation has been re-arranged, designers can predict total pipeline air pressure drop easily by using an electronic hand-held calculator with some mathematical function keys. However, Tsuji claimed that the method is limited to dilute-phase conveying, high air velocities and coarse particles. Also, by using this method, it can be determined that the different radius bends located in horizontal-horizontal cause the same pressure drop.

CHAPTER 3

TEST FACILITY & PROCEDURES

3.1 Introduction

Pneumatic conveying systems have been used in industry for several decades. Several theoretical and empirical correlations have been developed already to predict the total pipeline air pressure drop [9, 14, 34, 39, 44, 54, 58, 68, 71, 72] and/or the pressure drop caused by bends and straight sections of pipe [2, 3, 6, 7, 8, 16, 22, 28, 31, 35, 42, 45, 47, 52, 61, 66, 67, 75, 76, 78]. Some of these correlations have been accepted by designers for a range of materials and conveying systems.

However, most of the theoretical equations are restricted to the dilute-phase conveying of coarse particles of relatively narrow size distribution. Also, the empirical correlations are based on given products, pipe materials and/or conveying conditions. In industry, the majority of pneumatic conveying systems are used to transport particles of different size, size distribution, density, shape, surface roughness and chemical property (e.g. blue metal, cement, coffee granules, dog food, fish, fly ash, milk powder, raw wool, crushed coal, walnuts, wheat, wheat flour). It has been shown [13, 33, 41, 62, 63, 64] that product properties have numerous influences on pressure drop. These influences are very complicated and only can be determined by experiment. Also, it has been demonstrated [63, 71] that no general correlation exists to predict accurately the pressure drop for conveying a wide range of materials, especially fine powders.

To evaluate the existing correlations, and/or develop new empirical correlations, it is necessary to conduct in a test rig of appropriate size a series of pneumatic conveying experiments on the actual material.

The main purpose of this chapter is to provide a description of the test rig, instrumentation and test materials. Where necessary, a brief explanation of some of the more important features also is provided. The pneumatic conveying test facility and instruments described in this chapter were used to obtain all the data necessary for the various aspects of this thesis project. Also, a technique used to obtain accurate values of pressure along a pipeline is described.

3.2 Pneumatic Conveying Test Facility

3.2.1 Conveying Plant

A diagrammatic layout of the blow tank feeder and receiving hopper is shown in Figure 3.1. Major components of the test facility are listed below.

- 0.425 m^3 capacity blow tank with a maximum safe working pressure (S.W.P.) of 350 kPag and fitted with a Figure 990 Keystone butterfly-type discharge valve with positioner. Note that this valve is bolted directly to the outlet flange of the blow tank.

- 0.5 m^3 receiving hopper with vibrating bin discharger.

- Electro-pneumatic control cabinet housing all the necessary control equipment for conveyor operation (e.g. pressure regulators).

- DCE vokes reverse-jet insertable filter mounted on top of the 0.5 m^3 receiving hopper and fitted with epitropic Goretex™ bags.

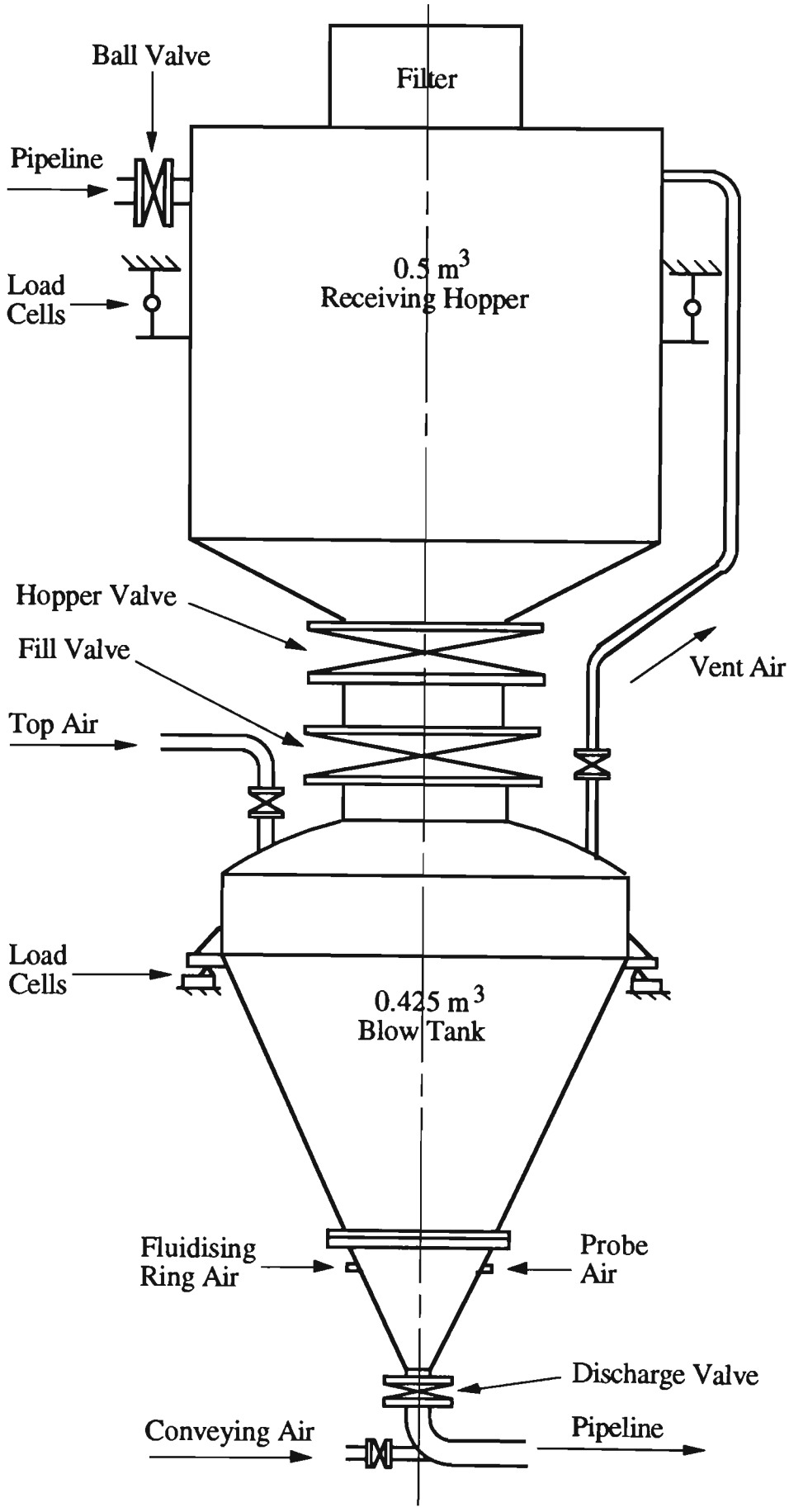

Figure 3.1 A diagrammatic layout of the test rig.

The test rig operates in batch mode. That is, product is conveyed from the bottom of the blow tank, through the conveying pipeline and back into the receiving hopper. For the purpose of this thesis project the product was recirculated. One concern was that change in conveying performance due to product degradation. However, for the two powders tested in this project (viz. fly ash, pulverised brown coal), the change in particle size, size distribution and density was found to be very small. Also, during later experiments on plastic pellets, there did not appear to be any change in particle properties (e.g. dust, streamers). In any case, by repeating the initial experiments on each test material (i.e. towards the end of the test program), the conveying performance (e.g. pressure drop for a given air flow and conveying rate) was found generally to be unchanged.

3.2.2 Pipelines and Bends

A total of four different loops of mild steel pipeline were employed for the test program. A general layout is shown in Figure 3.2 and the relevant details are listed in Table 3.1. Note that all pipelines utilised radius bends with R=254 mm (except for the test bend) and Pipeline IV also employed a 180° bend to increase the vertical lift (dashed line in Figure 3.2).

Table 3.1 Details of test rig pipelines (refer to Figure 3.2).

	Effective length of section (m)										
Pipeline	Sa	Sb	Sc	Sd	Se	Sf	Sg	Sh	Si	Sj	D (m)
I	1.9	5.9	21.3	21.1	6.5	20.7	17.0	3.0	2.5	2.0	0.0525
II	1.9	5.9	21.3	37.6	6.5	37.2	17.0	3.0	2.5	2.0	0.0525
III	2.1	5.9	21.9	37.7	7.4	36.5	17.3	3.4	2.5	2.6	0.0805
IV	1.9	8.0	20.8	21.1	6.5	20.7	17.0	3.0	2.5	2.0	0.0525

Four different radius bends and one blinded-tee bend, as shown in Figure 3.3, were tested on Pipeline I. These bends were connected by two horizontal straight sections of pipe with effective lengths of 21.3 and 21.1 m respectively (see Figure 3.2 and Table 3.1). Details on these bends are provided in Table 3.2.

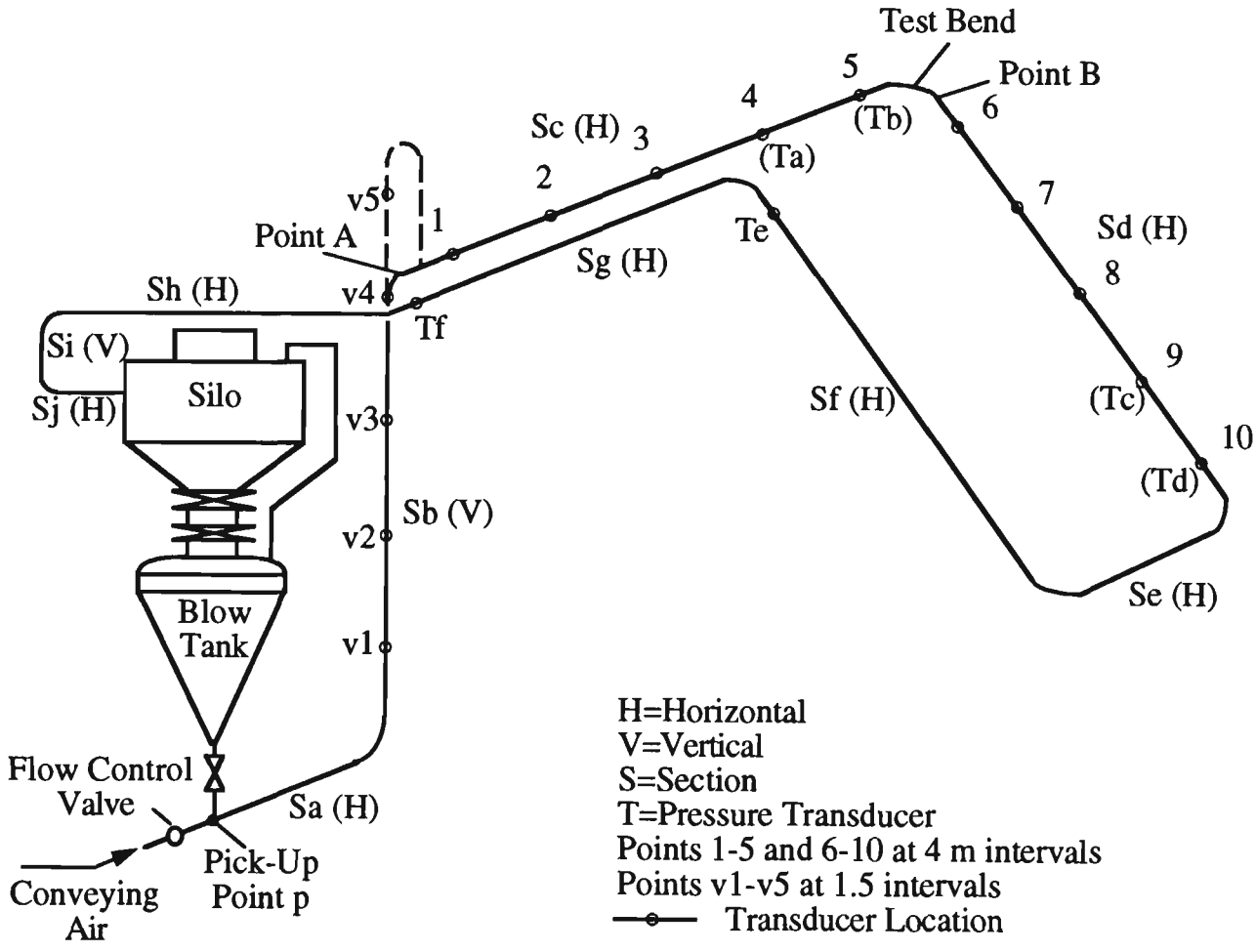

Figure 3.2 Schematic layout of test pipeline.

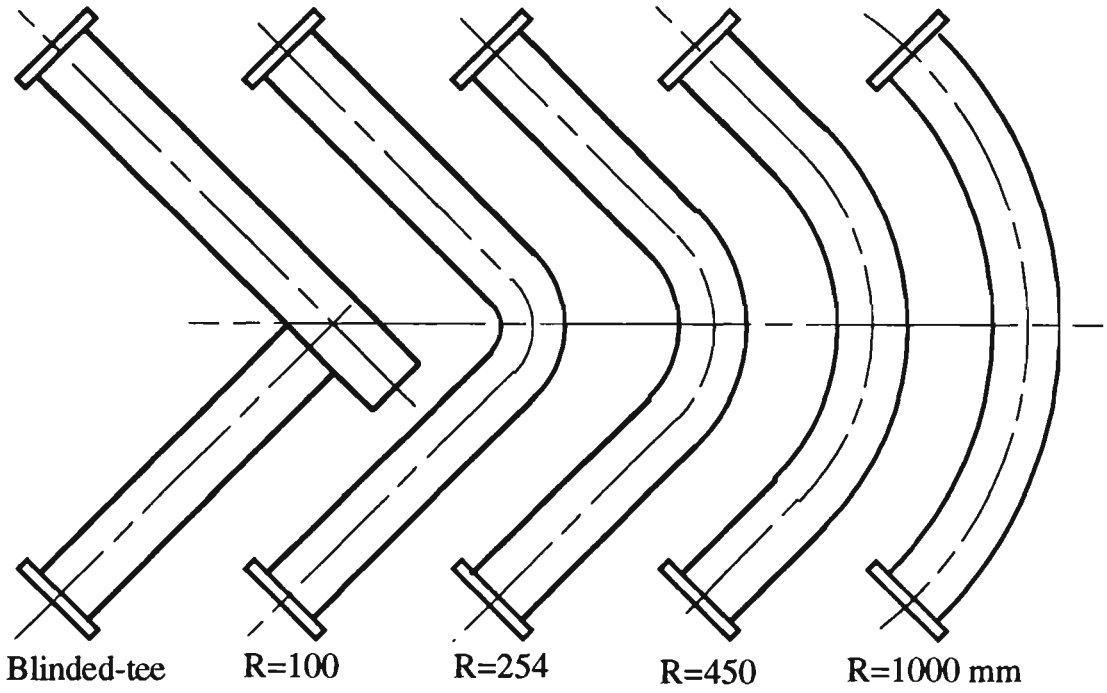

Figure 3.3 Test bends.

Table 3.2 Bend radius to pipe diameter ratio for test bends.

Bend	Blinded-tee	R=100	R=254	R=450	R=1000
$\frac{R}{D}$ (D=52.5 mm)	0.0	1.9	4.8	8.6	19.0

3.2.3 Air Supply

Air at a maximum pressure head of ≈800 kPag is supplied from any combination of the three following rotary screw compressors.

- Atlas Copco electric-powered Model GA-308, 3.1 m^3 min^{-1} free air delivery.
- Ingersoll Rand diesel-powered Model P375-WP, 10.6 m^3 min^{-1} free air delivery.
- Ingersoll Rand diesel-powered Model P850-WGM, 24.1 m^3 min^{-1} free air delivery.

The compressors are connected to an aftercooler, two refrigerated air dryers and two air receivers (1.75 and 6.0 m^3 capacity). Various filters and separators are installed in series with these compressors to ensure a dry and oil-free air supply. Figure 3.4 provides a general arrangement of the air supply system.

However, for this thesis project with 52.5 and 80.5 mm bore pipelines, the output of only one compressor (GA-308 or P375-WP) was required.

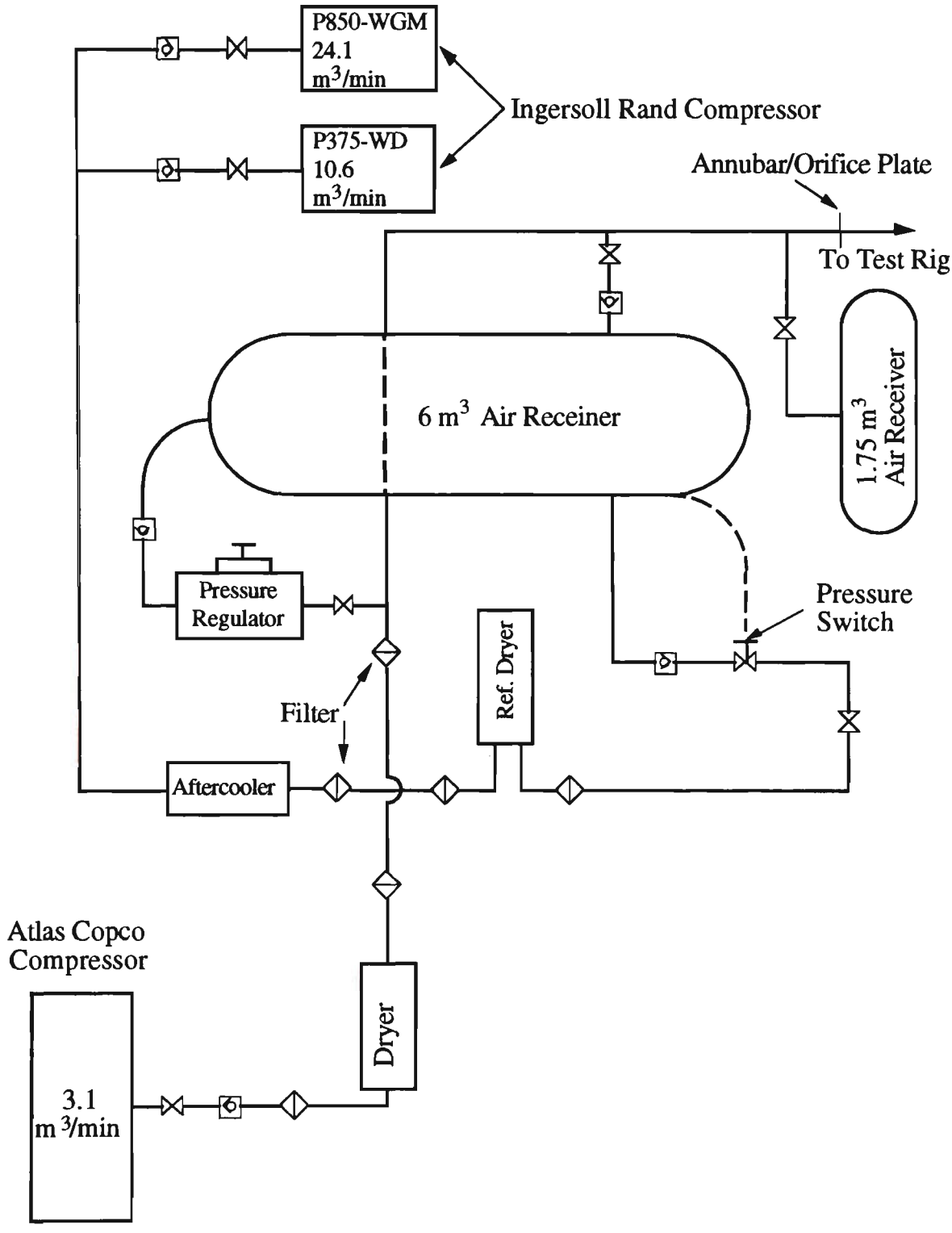

Figure 3.4 General arrangement of compressed air supply.

3.3 Instrumentation

Four shear-beam-type load cells are installed on the blow tank to measure the mass of solids leaving the blow tank. The 0.5 m^3 receiving hopper is supported by three tension load cells which monitor the mass entering the receiving hopper (see Figure 3.1). The combined electrical output signal from each set of load cells is fed to a recording instrument.

Air mass flow rates are measured by an annubar. After the upstream and differential air pressures in the annubar are obtained, the amount of air being used to convey the solids along the pipeline is calculated by the relevant equation.

Pressures at different locations such as the air supply, the blow tank and the pipeline are measured by pressure transducers (see Figure 3.2). Refer to Figure 3.5 for an exploded view of a typical tapping location. The differential air pressure of the annubar is recorded by a DP meter.

In order to record the electrical output signals from the load cells, the pressure transducers and DP meter, a portable Hewlett-Packard 3054A Data Acquisition System (which is used to capture the voltage of up to 20 analogue channels) with the necessary software has been developed at the University of Wollongong [70]. Major components of the system includes: a HP-85B desk-top computer, a HP-3497A scanning control unit and a transducer signal-conditioning unit, as shown in Figure 3.6. Typical channels, which are recorded with respect to cycle time, include: blow tank top-air pressure; pipeline air pressure; upstream pipeline and differential air pressures for the annubar; the mass of material entering the receiving hopper and/or

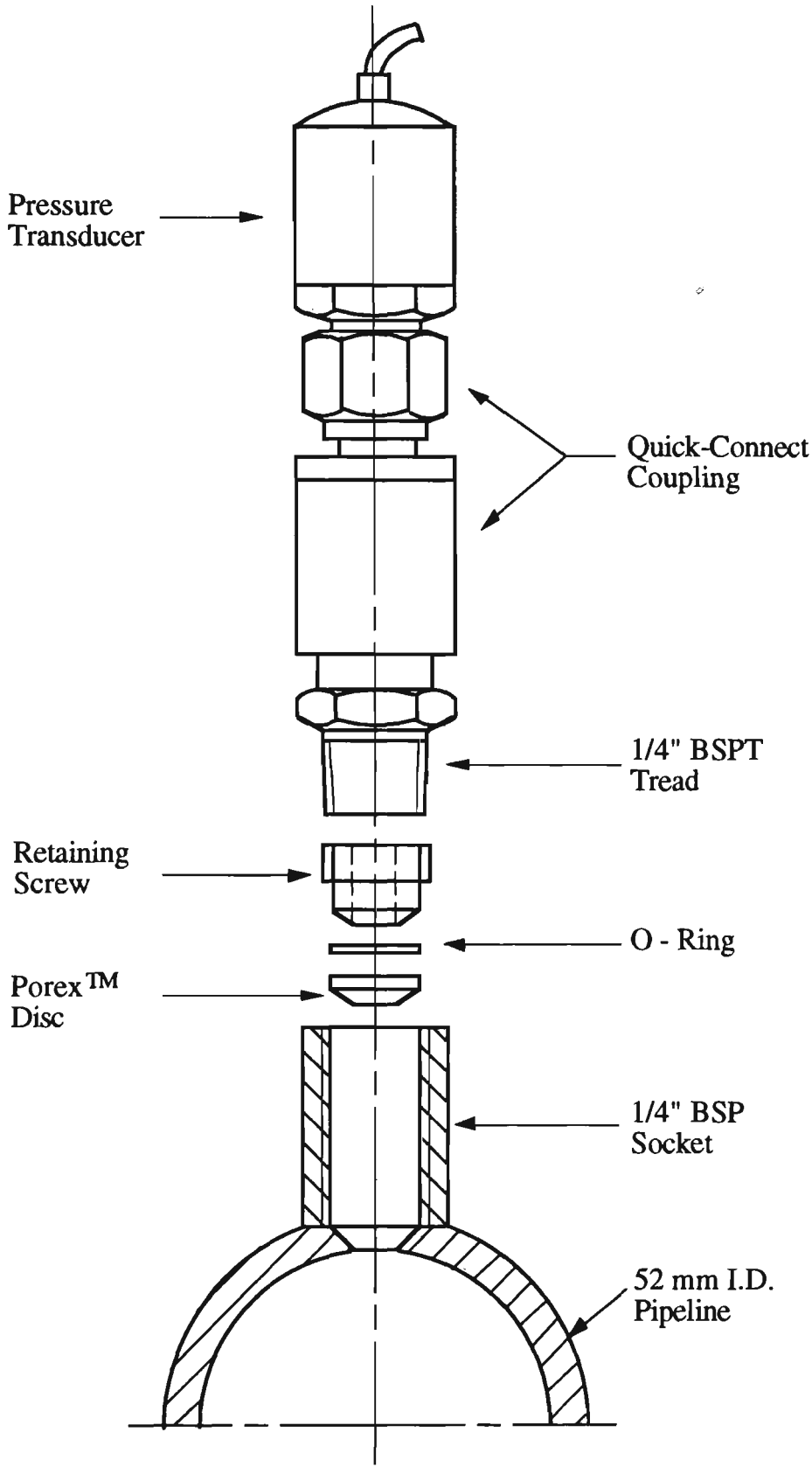

Figure 3.5 Exploded view of a typical pipeline air pressure tapping location.

leaving the blow tank. After storing these responses on either the HP-85B computer or a Tektronix 4923 digital tape recorder, the data are then transferred to an NEC APCIV PC for final processing and graphical output. From these measurements, the relevant parameters such as air mass flow rate, product mass flow rate, blow tank top-air pressure and pipeline air pressure are obtained. On-site graphics also are available on the HP-85B computer, so that plots of raw data also can be achieved easily after the completion of any experiment. An example of a typical pipeline air pressure response copied from the HP-85B CRT screen is presented in Figure 3.7.

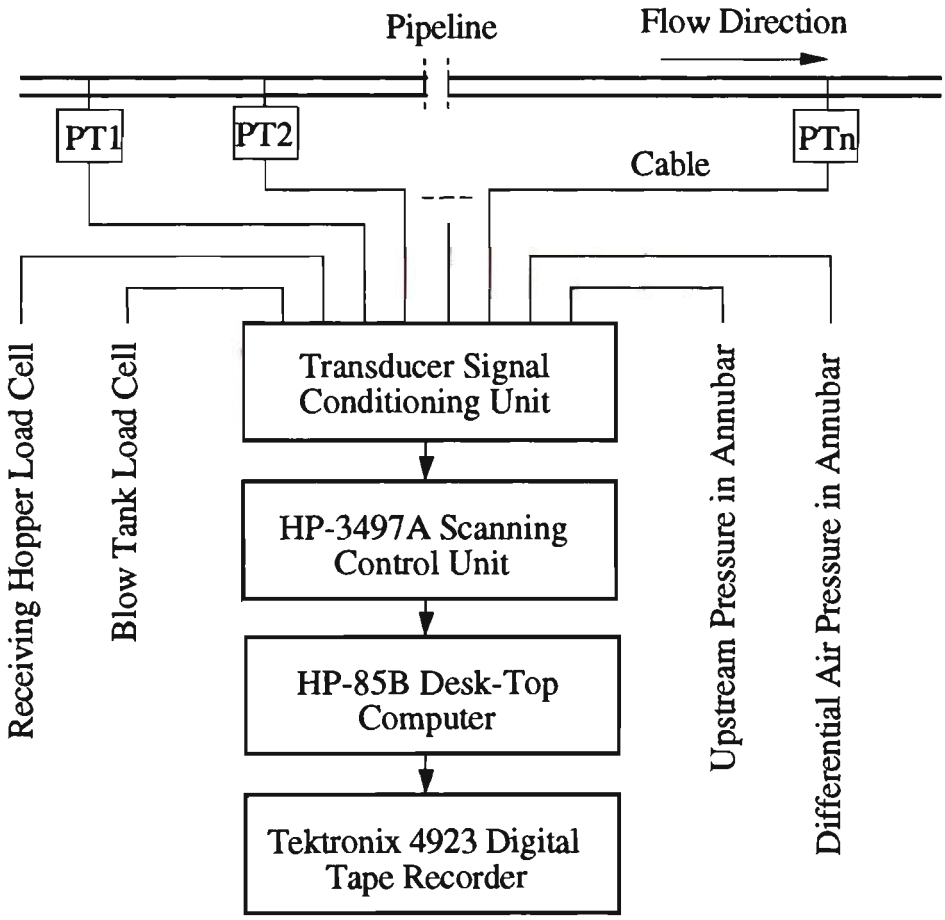

Figure 3.6 Schematic layout of Data Acquisition System (PT = Pressure transducer).

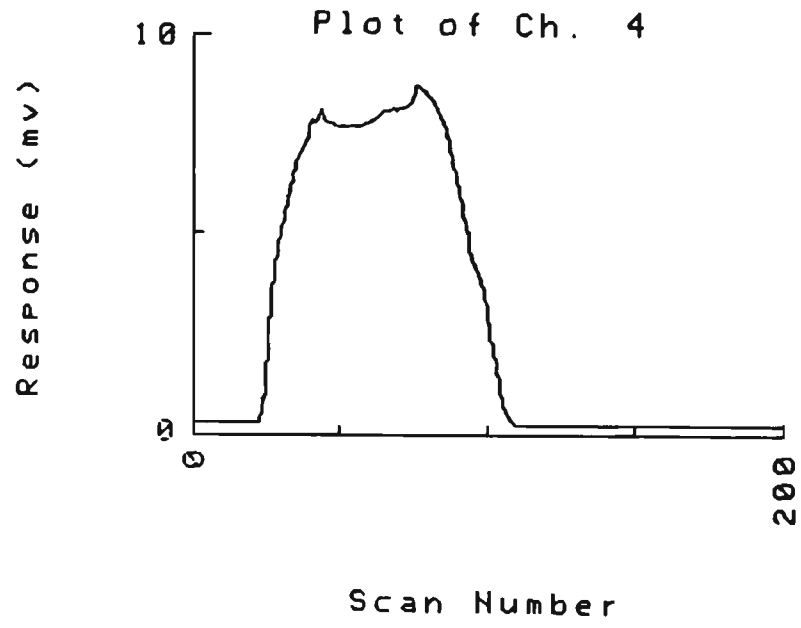

Figure 3.7 HP-85B plot of a typical uncalibrated pipeline air pressure transducer response.

3.4 Calibration

The mass of the solids leaving the blow tank or entering the receiving hopper and the pressure in the blow tank or along the pipeline are monitored by the load cells and the pressure transducers, respectively. However, actual values of mass or pressure cannot be measured directly by the load cells or pressure transducers. The load cells or the pressure transducers only can provide the electrical signals (i.e. voltages) due to changes in mass or pressure. To obtain the appropriate values accurately, it is very important to set up an accurate relationship between the mass or the pressure and the voltage (i.e. the calibration factor of the load cell and pressure transducer).

3.4.1 Load Cell Calibration

As a new pipeline is installed, usually some of the product is conveyed initially from the blow tank to the receiving hopper through the new pipeline. After many runs, the new pipeline is 'clean'. The 'dirty' product then is removed from the system and the blow tank is re-filled with fresh product. During this filling operation, the load cells supporting both the blow tank and the receiving hopper are calibrated. The load cell calibration procedure is as follows.

i) Firstly, fill the blow tank with a designated mass of product (e.g. 50 kg) and record the voltage output of the blow tank load cells.
ii) Convey the product from the blow tank to the receiving hopper and record the voltage output of the receiving hopper load cells.
iii) Open the hopper valve, the fill valve (see Figure 3.1) and allow all the material to drop into the blow tank (using the bin discharger to ensure no residual material in the receiving hopper). Then fill the blow tank with more product (e.g. 50 kg) and record the voltage.
iv) Repeat steps ii) and iii) until the blow tank is filled with the total designated mass of product.

Table 3.3 lists all the recorded results of mass and voltage. Note that the test material in this case was fly ash.

The load cell calibration factors are shown in Figure 3.8. From Figure 3.8 (a) and (b), the calibration factors for the blow tank and receiving hopper load cells are found to be 91.692 and 7.9364 (kg mv^{-1}), respectively.

Table 3.3 Mass and voltage measured by load cells.

	Voltage (mv)	
Mass of product (kg)	Blow tank load cell	Hopper load cell
0.0	0.0	0.0
50	0.5	6.0
100	1.057	11.87
150	1.624	18.6
200	2.176	24.9
250	2.696	31.27
300	3.251	37.5
350	3.798	43.8
381	4.133	47.77

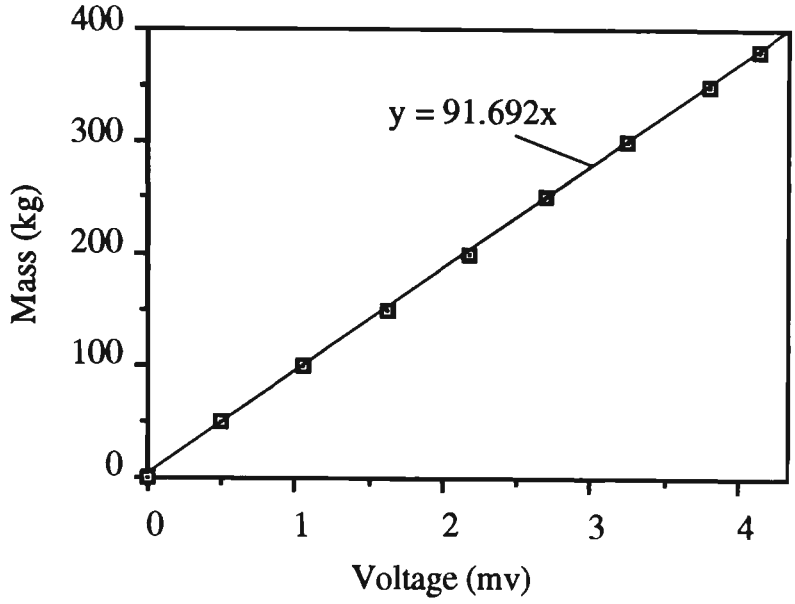

(a) Blow tank load cell.

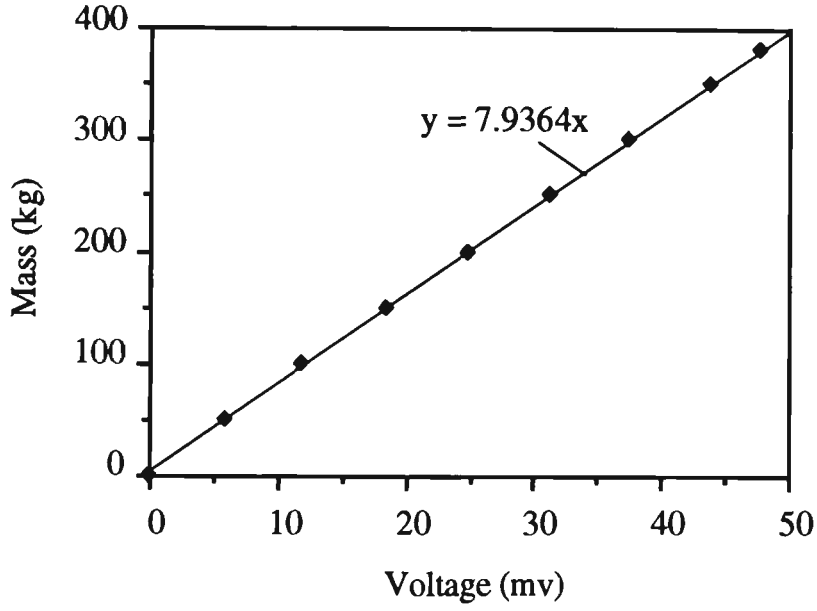

(b) Receiving hopper load cell.

Figure 3.8 Load cell calibration factors.

3.4.2 Pressure Transducer Calibration

All the pressure transducers used in the test program are calibrated by maintaining a constant pressure in the pipeline and recording simultaneously the voltages of the pressure transducers. The calibration procedure is established as follows.

i) Connect all the pressure transducers by cable to the Transducer Signal Conditioning Unit, as shown in Figure 3.6.

ii) With all the material in the receiving hopper (hopper valve and fill valve closed), close the ball valve at the end of the pipeline, vent valve and open the discharge valve (see Figure 3.1).

iii) Open the flow control valve located upstream of the pick-up point p (see Figure 3.2) and close it until a designated pressure (e.g. 200 kPag) is reached in the pipeline.

iv) Check whether there is a leak on each pressure tapping by using soapy water. If so, open the vent valve, rectify any leaky tapping points and go back to Item iii). If not, proceed to Item v).

v) Open the vent valve until there is atmospheric pressure in the pipeline, then close it.

vi) Adjust the pressure regulator to a designated pressure (e.g. 50 kPag), then open the valves to the blow tank top- and ring-air.

vii) Measure the static pressure in the pipeline by using a pressure meter and record the voltages of all the pressure transducers simultaneously after the pressure in the pipeline is very stable.

viii) Close the valves to the blow tank top- and ring-air. Repeat steps v), vi), vii) until sufficient groups of data are obtained (i.e. for different static pressures).

Typical experimental results and the calibration factor for a pressure transducer are listed in Table 3.4 and Figure 3.9.

Table 3.4 Pressure and voltage measured by a pressure transducer.

Pressure (kPag)	0.0	5.8	9.7	26.5	42.3	89.0	138.4	182.6
Voltage (mv)	0.0	0.481	0.802	1.714	3.496	7.528	11.767	15.61

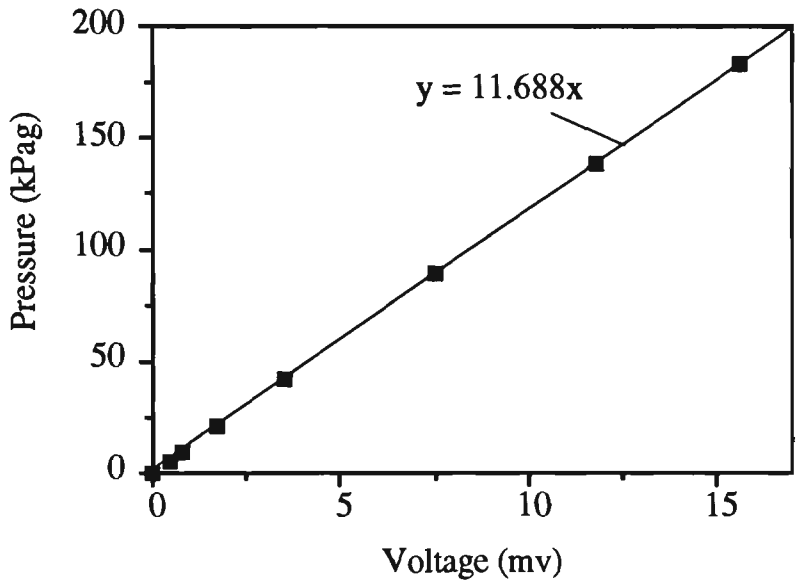

Figure 3.9 Calibration factor for a pressure transducer.

Figure 3.9 shows that the calibration factor for the pressure transducer is 11.688 (kPag mv^{-1}).

In Figure 3.4, a Porex™ Disk is used to filter the air. After several runs of conveying product, it is possible that the Porex™ Disk becomes blocked with dust. If so, the response of the pressure transducer is delayed, as shown in Figure 3.10 (i.e. see Ch. Nos. 3 and 6). However, this does not affect the steady-state calibration (value) of the transducer(s), as long as the pressure in the pipeline is very stable.

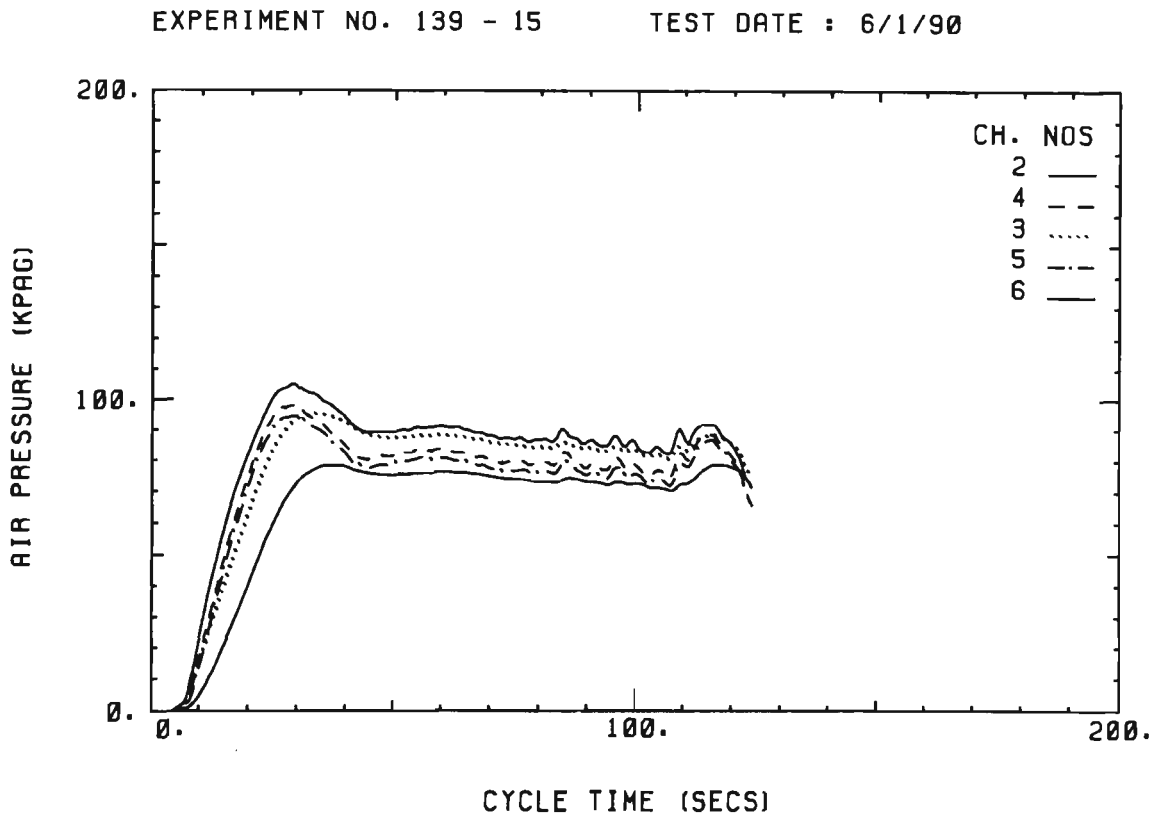

Figure 3.10 Delayed response of pressure transducer (Ch. Nos. 3 and 6).

From Figure 3.10, it is clear that the responses of Channels 3 and 6 are delayed. Therefore, the corresponding Porex™ Disks are changed to obtain the more responsive results shown in Figure 3.11. However, note that the steady-state value of pressure is not affected largely by the blocked Porex™ Disk. As transients are not being investigated in this thesis, a certain amount of delayed response can be tolerated.

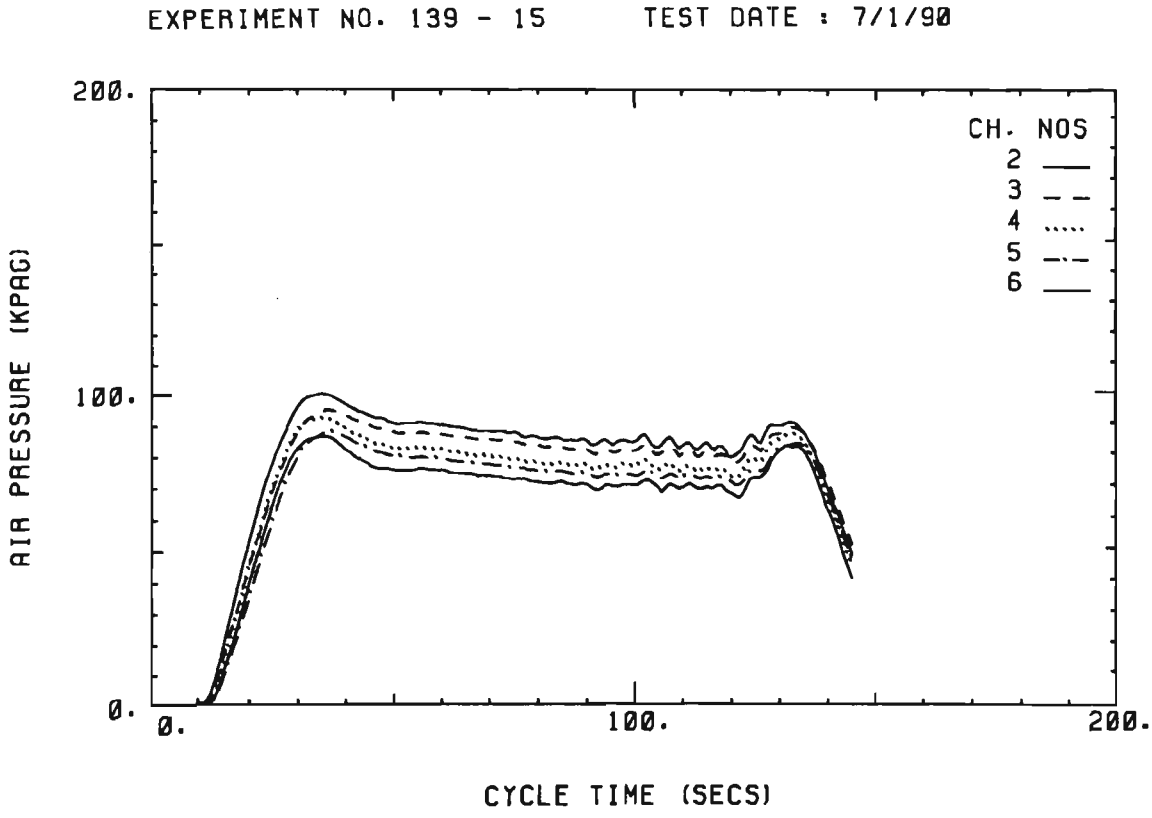

Figure 3.11 Good response of pressure transducer.

In order to obtain accurate experimental values of pressure in the blow tank and along the pipeline, it is necessary to check all the calibrated pressure transducers against a varying pressure in the pipeline. This is undertaken before and after a particular group of experiments, as shown in Figure 3.12. Note that the increasing pressures are obtained simply by 'opening up' the blow tank regulator and the decreasing pressures by venting the blow tank and also readjusting the regulator setting.

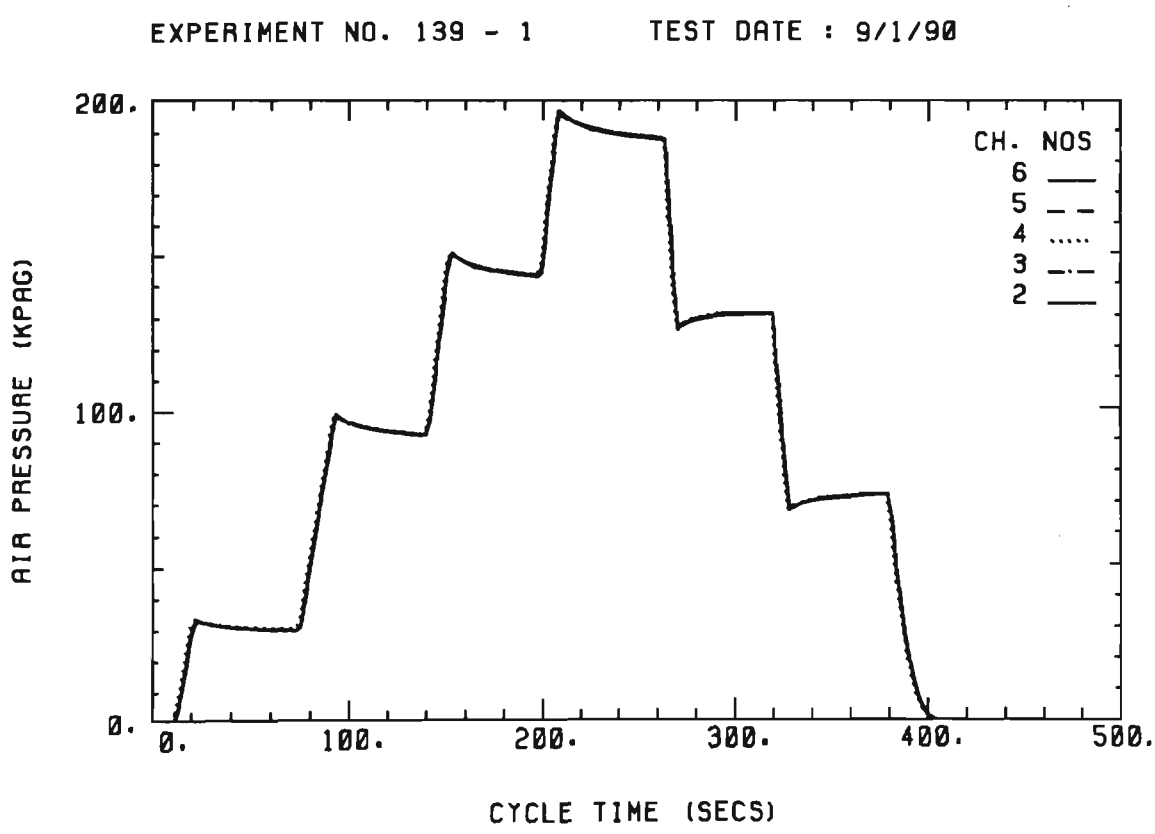

(a) Before experiments.

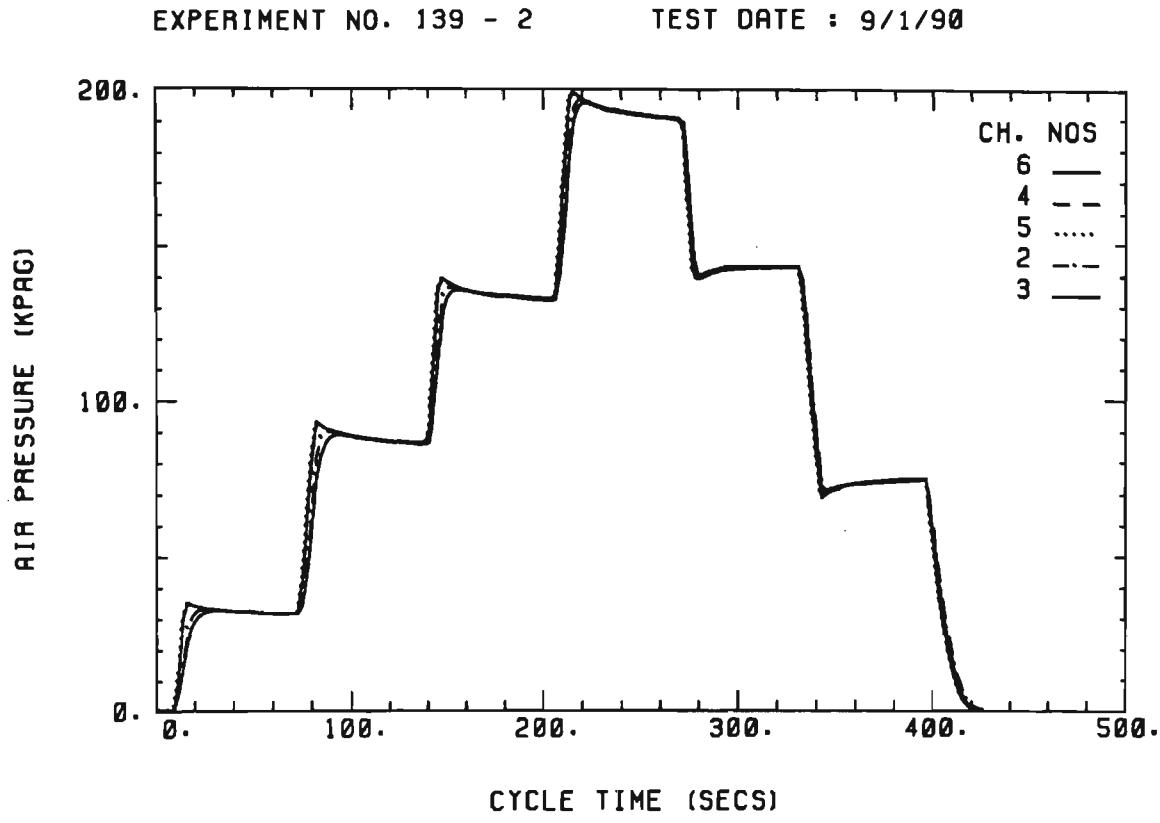

(b) After experiments.

Figure 3.12 Varying pressure in the pipeline measured by all the pressure transducers before and after a group of experiments.

Figure 3.12 clearly shows that the response of all the pressure transducers is good and the calibration factors of all the pressure transducers are accurate (i.e. the measured values of pressure are reliable and accurate).

3.5 Test Material

The product used for the majority of experiments was fly ash. The particle density and loose-poured bulk density were 2197 and 634 kg m^{-3} respectively and the size distribution is tabulated in Table 3.5 and shown in Figure 3.13. Note that from this graph, the median particle diameter was found to be 15.5 μm.

Table 3.5 Fly ash size distribution, according to Malvern 2600C laser diffraction analyser.

No.	Particle Size Range (μm)	Average Size (μm)	Mass % in Range
1	1.2 - 1.5	1.35	0.2
2	1.5 - 1.9	1.7	0.4
3	1.9 - 2.4	2.15	1.2
4	2.4 - 3.0	2.7	2.0
5	3.0 - 3.9	3.45	3.2
6	3.9 - 5.0	4.45	5.8
7	5.0 - 6.4	5.7	6.0
8	6.4 - 8.2	7.3	10.0
9	8.2 - 10.5	9.35	9.9
10	10.5 - 13.6	12.05	7.0
11	13.6 - 17.7	15.65	9.0
12	17.7 - 23.7	20.7	10.4
13	23.7 - 33.7	28.7	10.8
14	33.7 - 54.9	44.3	13.5
15	54.9 - 118.4	86.85	10.7

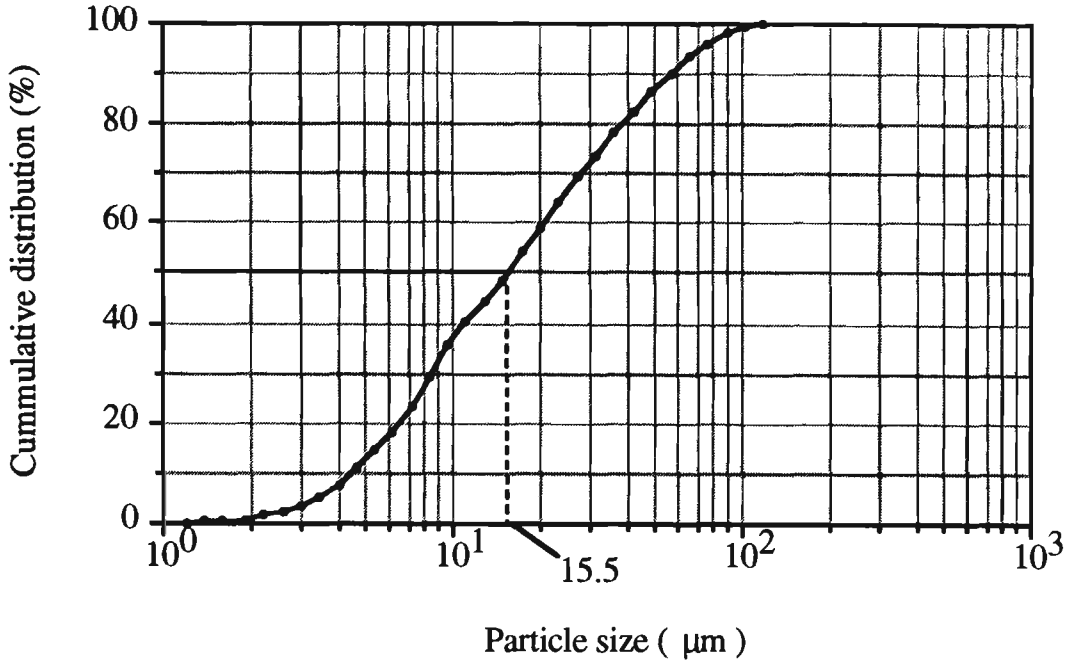

Figure 3.13 Cumulative size distribution for fly ash, according to Malvern 2600C laser diffraction analyser.

3.6 Typical Test Results

All the test bends and pipelines were tested separately with fly ash over a wide range of conveying conditions. The set-up and test conditions for each bend and pipeline are summarised in Table 3.6. A typical pressure profile along the pipeline is shown in Figure 3.14.

All the recorded data are compiled in Appendix A.

Table 3.6 Test conditions for bend and pipeline.

	Range of m*	Measured Points (see Figure 3.2)	No. of Measured Points	No. of Data
Pipeline I R=100	11 ~ 127	1 - 10	10	50
Pipeline I R=254	10 ~ 128	1 - 10	10	48
Pipeline I R=450	11 ~ 133	1 - 10	10	50
Pipeline I R=1000	13 ~ 112	1 - 10	10	47
Pipeline I Blinded-tee	11 ~ 120	1 - 10	10	46
Pipeline I	7 ~ 150	Ta - Tf, p	7	33
Pipeline II	6 ~ 150	Ta - Tf, p	7	36
Pipeline III	10 ~ 70	Ta - Tf, p	7	39
Pipeline IV	8 ~ 199	v1 - v5, p	6	36

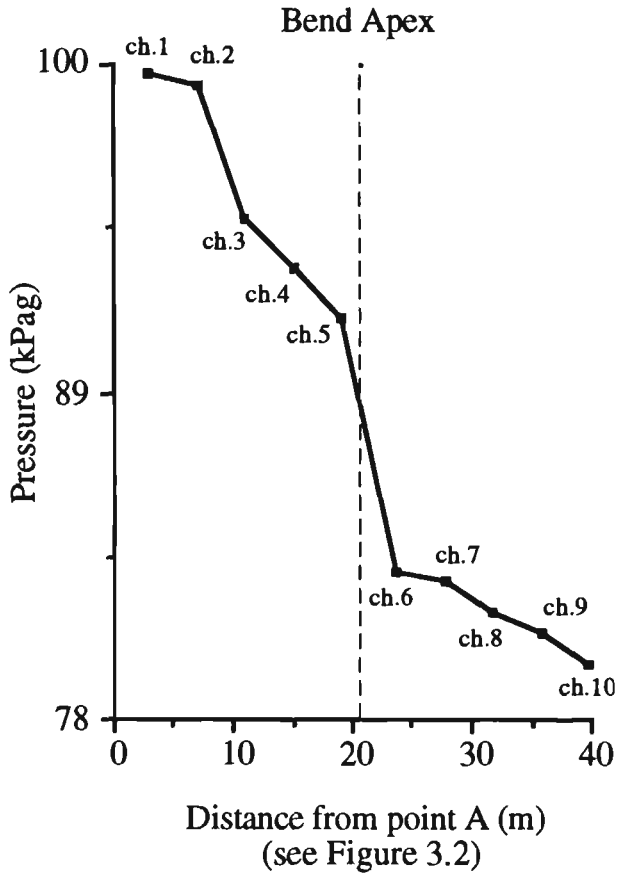

Figure 3.14 Typical profile of pressure before and after R=254 mm bend (Pre-set pressure in blow tank=160 kPag, m_S=1.443 kg s^{-1}, m_f=0.0743 kg s^{-1}).

CHAPTER 4

PRESSURE DROP DUE TO AIR-ONLY

4.1 Introduction

Conveying air is a very important component for transporting solids in a pneumatic conveying system. Without it, it is impossible to convey solids from one place to another. In many systems, the air-only component of pressure drop is significant (e.g. dilute-phase, long-distance conveying). Therefore, it is very important to predict accurately the pressure drop due to air alone. Also, it has been shown [6, 9, 42, 55, 58, 61, 66, 71] the pressure drop due to the solids-air mixture is correlated best when expressed as the sum of two functions. The first function represents the loss due to air alone and the second is related to the loss due to solids.

A potentially accurate way of estimating the total pipeline air pressure drop is to deal separately with the straight sections of pipe and bends [6, 66]. Usually, the formulae that were developed from experiments in which an incompressible fluid such as water was used and the inner surface conditions of straight pipe and bend were given [17, 23] are used widely to predict the pressure drop due to air alone in straight pipes and bends [6, 42, 61, 66]. However, in pneumatic conveying, the compressibility effect of air may be significant. Also, the inner surface of the pipe could change with time (e.g. due to wear). Hence, the applicability of these formulae is unknown.

In this chapter, the formulae based on incompressible flow are modified to allow for this compressibility effect. Then by using least squares, exponents in the modified formulae are determined by minimising the sum of the squared errors of the measured pressure along the two straight sections of pipe that are connected directly to the test bend. It is found that these exponents do not vary significantly (i.e. with respect to the 'original' incompressible formulae), as long as mean conditions (based on average air density) for each straight section of pipe and conditions at the outlet of

bend are used in the analysis. These formulae then are used to determine the air-only component of pressure drop for several existing pneumatic conveying pipelines of different length, diameter, step and bend number. The results show that these formulae are able to predict accurately not only the air-only pressure drop due to both bends and straight sections of pipe at different locations, but also the total air-only pressure drop for different configurations of pneumatic conveying pipeline.

4.2 Formulae for Incompressible Fluid

4.2.1 Straight Sections of Pipe

When fluids, such as oil, smoke, air and so on, move through a pipe, there are possibly three basic types of flow, each possessing different characteristics. The first type is called laminar flow, where the fluid flow is smooth and 'streamlined' and the trajectory of a fluid particle is predictable, not random or unstable. The second type of flow is called transitional flow. During transitional flow, the fluid particle moves from its well-behaved laminar condition into other adjacent layers in a somewhat oscillatory manner that grows in amplitude and quickly produces an unstable pattern. The third type of flow is called turbulent flow. The fluid particles move in all three directions most often in an irregular fashion. However, near the wall, the flow approaches a smooth and laminar condition.

From the Moody diagram [17]:

$R_e \leq 2300$	laminar flow
$2000 \leq R_e \leq 4500$	transitional flow
$R_e > 4500$	turbulent flow

If the fluid flow in the pipe is treated as a fully established flow in which the velocity profile does not change with respect to the streamwise direction and there is no streamwise acceleration, i.e. as in incompressible flow, it is possible to set up accurate expressions for predicting the pressure drop due to the energy loss caused by friction in both laminar and turbulent flows.

4.2.1.1 Laminar Flow

The axial velocity v at any point on the cross section of the straight section can be expressed [17] as:

$$v = \frac{\Delta p_{sf}}{4\,\mu\,\Delta L}\,(r_o^2 - r_1^2)$$

The fluid flow rate Q is evaluated as:

$$Q = \int_0^{r_o} 2\pi\, r_1\, dr_1\, v = 2\pi \int_0^{r_o} \frac{\Delta p_{sf}}{4\,\mu\,\Delta L}\,(r_o^2 - r_1^2)\, r_1\, dr_1 = \frac{\pi\,\Delta p_{sf}}{8\,\mu\,\Delta L}\, r_o^4$$

$$\therefore \quad V_f = \frac{Q}{A} = \frac{\Delta p_{sf}}{8\,\mu\,\Delta L}\, r_o^2$$

Solving this expression for Δp_{sf} yields:

$$\Delta p_{sf} = \frac{32\,\mu\,\Delta L}{D^2}\, V_f = \frac{64}{R_e}\,\rho_f\, V_f^2\, \frac{\Delta L}{2\,D}$$

Assuming $\lambda_f = \frac{64}{R_e}$ then:

$$\Delta p_{sf} = \lambda_f \rho_f V_f^2 \frac{\Delta L}{2\,D} \tag{4.1}$$

4.2.1.2 Turbulent Flow

Turbulent flow is much more complex than laminar flow. The pressure drop Δp_{sf} along the straight section of ΔL is a function of many pertinent variables, such as fluid flowing velocity V_f, fluid density ρ_f, pipe diameter D, pipe length ΔL, fluid viscosity μ and Moody pipe roughness ε. Up to now, there is still no theoretical relationship between Δp_{sf} and V_f, ρ_f, D, ΔL, μ, ε. Therefore, the dimensional analysis [43] is used to set up the relationship between these pertinent variables. Initially an expression of the form given in Equation (4.2) is considered.

$$\Delta p_{sf}=k\, V_f^a\, \rho_f^b\, D^c\, \Delta L^e\, \mu^f\, \varepsilon^h \tag{4.2}$$

Equation (4.2) normally would involve the evaluation of seven unknowns, but the number of unknowns may be reduced with the aid of dimensional analysis.

The dimensional equation corresponding to Equation (4.2) is:

$$[L^{-1}\,M\,T^{-2}]=[L\,T^{-1}]^a\,[M\,L^{-3}]^b\,[L]^c\,[L]^e\,[L^{-1}\,M\,T^{-1}]^f\,[L]^h \tag{4.3}$$

Equation (4.3) may be resolved into three component auxiliary equations:

$$L:\ -1=a-3b+c+e-f+h \tag{4.4}$$

$$M:\ 1=b+f \tag{4.5}$$

$$T:\ -2=-a-f \tag{4.6}$$

There are now six unknowns and three equations; hence three of the unknowns may be expressed in terms of the remaining three unknowns. Numerous combinations are possible. One possible combination is to express a, b, and c in terms of e, f, and h. From Equations (4.4), (4.5), and (4.6),

$$a=2-f$$

$$b=1-f$$

$$c=-e-f-h$$

Substituting these values into Equation (4.2) results in:

$$\Delta p_{sf} = k\, V_f^{2-f}\, \rho_f^{1-f}\, D^{-e-f-h}\, \Delta L^{e}\, \mu^{f}\, \varepsilon^{h}$$

This may be rewritten as:

$$\Delta p_{sf} = k \left(\frac{\mu}{\rho_f V_f D}\right)^{f} \left(\frac{\varepsilon}{D}\right)^{h} \left(\frac{\Delta L}{D}\right)^{e} \rho_f V_f^2 \qquad (4.7)$$

From experiments using incompressible fluid, e can be considered equal to 1 [29], then assuming:

$$\lambda_f = 2k \left(\frac{\mu}{\rho_f V_f D}\right)^{f} \left(\frac{\varepsilon}{D}\right)^{h} = 2k\, Re^{-f} \left(\frac{\varepsilon}{D}\right)^{h} = \Phi\left(k, Re, \frac{\varepsilon}{D}\right)$$

Therefore, an expression similar to Equation (4.1) is obtained:

$$\Delta p_{sf} = \lambda_f \rho_f V_f^2 \frac{\Delta L}{2D} \qquad (4.8)$$

Since the fluid flow is considered incompressible, up to now many semi-empirical and/or empirical formulae have been developed to calculate λ_f. Some popular formulae are listed below.

i) The Colebrook Formula gives λ_f in an implicit form:

$$\frac{1}{\sqrt{\lambda_f}} = -0.86 \ln\left[\frac{\varepsilon}{3.7\,D} + \frac{2.51}{R_e\sqrt{\lambda_f}}\right] \tag{4.9}$$

which is valid for all the three zones of turbulent flow: smooth turbulent, rough turbulent and transition between smooth and rough turbulent.

ii) Based on Equation (4.9), Swamee and Jain [60] developed an explicit equation:

$$\lambda_f = \frac{1.325}{\left[\ln\left(\frac{\varepsilon}{3.7\,D} + \frac{5.74}{R_e^{0.9}}\right)\right]^2} \tag{4.10}$$

For the ranges $10^{-6} \le \frac{\varepsilon}{D} \le 10^{-2}$ and $5\times10^3 \le R_e \le 10^8$, this equation was claimed [60] to yield λ_f within 1 percent of the Colebrook formula. Also, it may be used conveniently with an electronic calculator.

iii) In smooth turbulent flow, Blasius presented a very simple empirical formula that is valid up to about $R_e = 10^5$:

$$\lambda_f = \frac{0.316}{R_e^{0.25}} \tag{4.11}$$

Then based on Equation (4.1) or (4.8), the pressure gradient in a straight section of pipe is presented as follows:

$$\delta p_{sf} = \frac{\Delta p_{sf}}{\Delta L} = \frac{\lambda_f \rho_f V_f^2}{2 D}$$

and $$\rho_f V_f = \frac{m_f}{A}$$

$$\therefore \quad \delta p_{sf} = \frac{\lambda_f m_f}{2 D A} V_f = \Phi_1(\frac{\varepsilon}{D}, m_f, V_f) \qquad (4.12)$$

From the above formulae, it can be seen that for a given fluid mass flow rate and section of constant diameter pipe, λ_f should not vary with respect to length and δp_{sf} is a function of and proportional to the fluid velocity.

4.2.2 Bends

The fluid flow around a bend is much more complex than through a straight section of pipe. Up to now, still no theoretical formula exists to predict the pressure drop due to an incompressible fluid flowing around a bend. However, this pressure drop could be considered as a function of pipe diameter D, bend centreline radius R, fluid viscosity μ, Moody pipe roughness ε, and fluid flowing velocity V_{fo} and density ρ_{fo} at the outlet of the bend. So the dimensional analysis is used again, leading to an expression of the form given by Equation (4.13):

$$\Delta p_{bf} = k V_{fo}^{a} \rho_{fo}^{b} D^{c} R^{e} \mu^{f} \varepsilon^{h} \qquad (4.13)$$

With the aid of dimensional analysis, an expression similar to Equation (4.7) is obtained:

$$\Delta p_{bf} = k \left(\frac{\mu}{\rho_{fo} V_{fo} D}\right)^f \left(\frac{\varepsilon}{D}\right)^h \left(\frac{R}{D}\right)^e \rho_{fo} V_{fo}^2 \qquad (4.14)$$

Assuming:

$$\zeta_f = 2k \left(\frac{\mu}{\rho_{fo} V_{fo} D}\right)^f \left(\frac{\varepsilon}{D}\right)^h \left(\frac{R}{D}\right)^e = \Phi(k, R_e, \frac{\varepsilon}{D}, \frac{R}{D})$$

$$\therefore \qquad \Delta p_{bf} = \frac{1}{2} \zeta_f \rho_{fo} V_{fo}^2 \qquad (4.15)$$

Although many investigators have studied the problem of determining the bend-loss coefficient ζ_f, most have failed to obtain satisfactory correlations from their experimental results. However, from his experiments on water flow, Ito [23] has given satisfactory empirical correlations and these have been used widely. In his experiments, the pipe bends were brass castings, made up of two pieces in the plane of the curved pipe axis. Their inner surfaces were machined and polished carefully with fine sand paper to provide accurate geometrical forms. The formulae for a 90° bend [23] are rewritten, as follows:

$$\zeta_f = \frac{0.217\,\alpha}{R_e^{0.17}} \left(\frac{R}{r_o}\right)^{0.84} \qquad R_e \left(\frac{r_o}{R}\right)^2 > 91$$

$$\zeta_f = \frac{0.248\,\alpha}{R_e^{0.2}} \left(\frac{R}{r_o}\right)^{0.9} \qquad R_e \left(\frac{r_o}{R}\right)^2 < 91$$

$$\alpha = 0.95 + 17.2 \left(\frac{R}{r_o}\right)^{-1.96} \qquad \frac{R}{r_o} < 19.7$$

$$\alpha = 1.0 \quad \frac{R}{r_o} > 19.7 \tag{4.16}$$

Rewriting Equation (4.15) gives:

$$\Delta p_{bf} = \frac{\zeta_f m_f}{2 A} V_{fo} = \Phi 2(\frac{\varepsilon}{D}, m_f, V_{fo}) \tag{4.17}$$

The above equations show that, for a given bend and fluid mass flow rate, ζ_f should be constant and the pressure drop due to a bend is a function of and proportional to the fluid velocity at the outlet of the bend. Hence, bend pressure drop also depends on bend location.

4.3 Test Program

4.3.1 Experimental Facility

A schematic layout of the experimental facility is shown in Figure 3.2. Pipelines I and IV (see Table 3.1) were employed in these 'air-only' investigations. Note that the blow tank shown in Figure 3.2 was not used (i.e. the discharge valve was maintained in the closed position).

When air only is flowing through the pneumatic conveying pipeline, the pressure drop is low. Hence, a 2.0 m manometer with coloured water, as illustrated in Figure 4.1, was used to measure the various pressures along the pipeline. However, due to the relatively higher pressures occurring at the feed point (see Figure 3.2), a specially calibrated transducer was employed to measure the pressure at the pick-up point p.

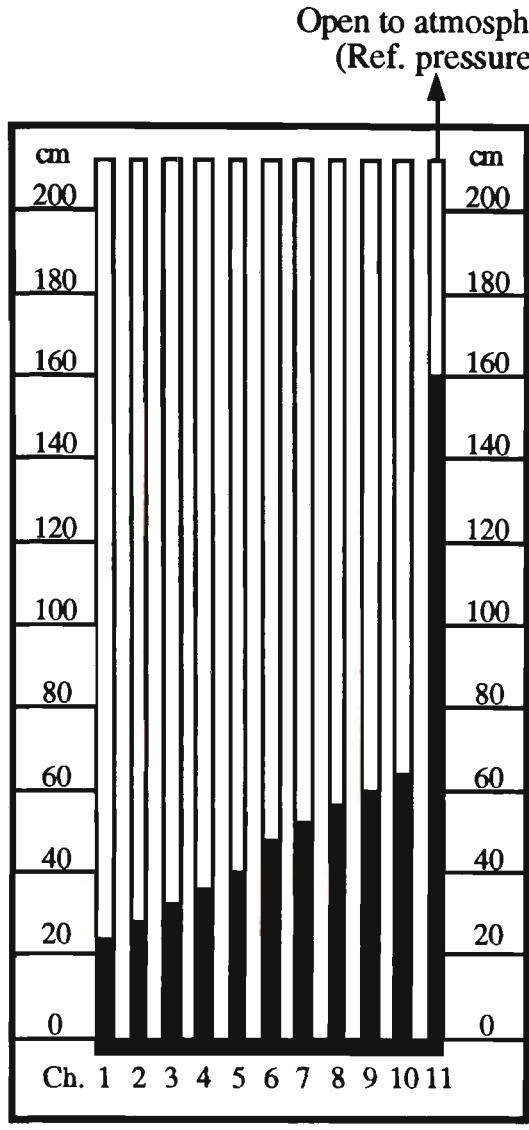

Figure 4.1 Typical reading shown on the manometer with coloured water.

4.3.2 Experimental Results

The manometer was used initially to measure static pressures at points 1-10 (see Figure 3.2). Twelve air mass flow rates (from 0.0097 to 0.065 kg s^{-1}) were selected. A typical reading from the manometer is shown in Figure 4.1 which shows clearly that the air has been accelerated fully by points 1 and 6.

Note that as stated previously a transducer was used to measure the pressure at the pick-up point p. The pressures at selected points and the pressure drops in the two long straight sections of pipe are shown in Figure 4.2 and listed in Table 4.1. Note that in this initial series of tests, the test bend shown in Figure 3.2 had a centreline radius of R=254 mm.

Secondly, the test bend (R=254 mm) was replaced with a bend having R=1000 mm. The results are listed in Table 4.2.

Finally, the bend before point 1 was replaced with a 180° bend (dashed line in Figure 3.2) and the manometer was used to measure the pressures at points v1, v5 (the distance between points v1 and v5 being 6 m). The results are listed in Table 4.3.

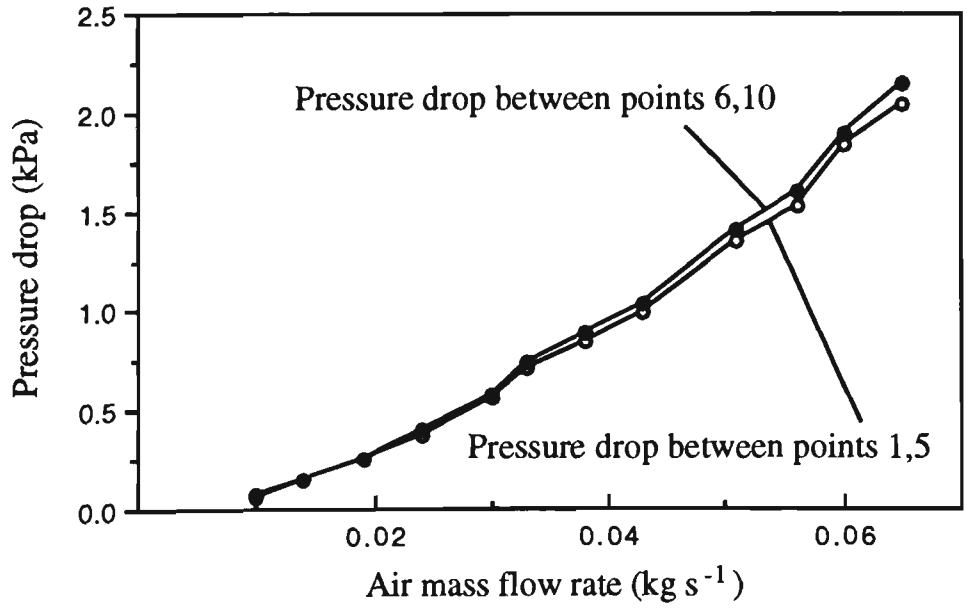

Figure 4.2 Pressure drop in straight test sections of pipe.

Table 4.1: Pressures at different points and pressure drops in two straight pipes (test bend radius=254 mm).

Exp.No.	1	2	3	4	5	6
m_f (kg s^{-1})	0.0096	0.0138	0.0188	0.0243	0.0299	0.0334
p_p (kPag)	0.493	0.915	1.537	2.433	3.563	4.53
p_1 (kPag)	0.458	0.896	1.491	2.329	3.41	4.346
p_5 (kPag)	0.399	0.75	1.237	1.958	2.855	3.637
p_6 (kPag)	0.341	0.682	1.14	1.812	2.66	3.391
p_{10} (kPag)	0.263	0.536	0.887	1.413	2.085	2.65
$\Delta p_{sf\ 1,5}$(kPa)	0.059	0.146	0.254	0.371	0.555	0.709
$\Delta p_{sf\ 6,10}$(kPa)	0.078	0.146	0.253	0.399	0.575	0.741

Continuation of Table 4.1

Exp. No.	7	8	9	10	11	12
m_f (kg s^{-1})	0.0385	0.0429	0.0505	0.0555	0.0603	0.0653
p_p (kPag)	5.52	6.63	8.78	10.48	12.17	14.06
p_1 (kPag)	5.222	6.21	8.45	9.63	11.54	13.13
p_5 (kPag)	4.384	5.21	7.103	8.106	9.704	11.09
p_6 (kPag)	4.082	4.86	6.625	7.58	9.081	10.36
p_{10} (kPag)	3.196	3.83	5.222	5.982	7.191	8.214
$\Delta p_{sf\ 1,5}$(kPa)	0.838	1.00	1.347	1.524	1.836	2.04
$\Delta p_{sf\ 6,10}$(kPa)	0.886	1.03	1.403	1.598	1.89	2.146

Table 4.2: Pressures at different points and pressure drops in two straight pipes (test bend radius=1000 mm).

Exp.No.	1	2	3	4	5	6
m_f (kg s^{-1})	0.0097	0.014	0.0185	0.0236	0.03	0.0345
p_p (kPag)	0.491	0.93	1.517	2.351	3.585	4.579
p_1 (kPag)	0.477	0.809	1.481	2.29	3.5	4.414
p_5 (kPag)	0.399	0.672	1.237	1.919	2.981	3.683
p_6 (kPag)	0.37	0.624	1.15	1.793	2.806	3.459
p_{10} (kPag)	0.292	0.477	0.926	1.413	2.231	2.709
$\Delta p_{sf\ 1,5}$(kPa)	0.078	0.137	0.244	0.371	0.519	0.731
$\Delta p_{sf\ 6,10}$(kPa)	0.078	0.147	0.224	0.38	0.575	0.75

Continuation of Table 4.2

Exp. No.	7	8	9	10	11	12
m_f (kg s^{-1})	0.0382	0.0428	0.0511	0.0544	0.0601	0.0659
p_p (kPag)	5.434	6.67	9.159	10.21	12.16	14.06
p_1 (kPag)	5.3	6.47	8.74	9.792	11.85	13.348
p_5 (kPag)	4.433	5.437	7.337	8.233	9.958	11.302
p_6 (kPag)	4.199	5.067	6.869	7.804	9.334	10.737
p_{10} (kPag)	3.245	4.014	5.427	6.09	7.385	8.506
$\Delta p_{sf\ 1,5}$(kPa)	0.867	1.033	1.403	1.559	1.892	2.046
$\Delta p_{sf\ 6,10}$(kPa)	0.954	1.053	1.442	1.714	1.949	2.231

Table 4.3: Pressures in vertical straight pipe.

Exp. No.	1	2	3	4	5	6
m_f (kg s^{-1})	0.0097	0.0138	0.0183	0.0239	0.0292	0.0341
p_{v1} (kPag)	0.516	1.004	1.637	2.65	3.702	4.93
p_{v5} (kPag)	0.487	0.945	1.549	2.524	3.508	4.667

Continuation of Table 4.3

Exp. No.	7	8	9	10	11	12
m_f (kg s^{-1})	0.0382	0.0429	0.0509	0.0552	0.0599	0.0621
p_{v1} (kPag)	5.836	7.161	9.665	11.22	13.25	13.99
p_{v5} (kPag)	5.544	6.791	9.198	10.68	12.59	13.31

4.4 Formulae for Conveying Air

Equations (4.12) and (4.17) show clearly that, for a given fluid mass flow rate and pipeline, the pressure gradient in a straight section of pipe and the pressure drop across a bend are a function of and proportional to the fluid velocity only. When an incompressible fluid is flowing steadily through a pipeline which has many bends and straight sections of pipe, its density and velocity at any point along the pipeline are constant. Hence, the pressure drop caused by any bend and the pressure gradient along any straight section of pipe are constant too. However, if the fluid density and/or the fluid flowing velocity are altered, the pressure drop caused by a bend and the pressure gradient in a straight section of pipe also will change. This also occurs in pneumatic conveying where the conveying air is compressible. For a constant air mass flow rate, the air velocity increases towards the end of the pipeline (i.e. as the pressure decreases). This fact has been confirmed by the previous experiments, as listed in Tables 4.1, 4.2 and shown in Figure 4.2. That is, $\Delta p_{sf\ 6,10} > \Delta p_{sf\ 1,5}$

demonstrating a greater velocity in the section of pipe downstream of the bend. It is clear from this information that, for a constant air mass flow rate, a straight section of pipe and a bend have different pressure drops at different locations (i.e. the pressure gradient along a straight section of pipe is variable).

Hence, the values of the exponents in Equations (4.10) or (4.11) and (4.16) are expected to be different and should be determined by experiment in which only air is flowing (because the properties of the fluid and the inner pipe surface can be different and vary with time). That is, assuming:

for bend:

$$\zeta_f = \frac{x1\ \alpha}{Re^{x2}} \left(\frac{R}{r_o}\right)^{x3} \qquad Re \left(\frac{r_o}{R}\right)^2 > 91 \tag{4.18}$$

$$\zeta_f = \frac{x4\ \alpha}{Re^{x5}} \left(\frac{R}{r_o}\right)^{x6} \qquad Re \left(\frac{r_o}{R}\right)^2 < 91 \tag{4.19}$$

$$\alpha = 0.95+17.2 \left(\frac{R}{r_o}\right)^{-1.96} \qquad \frac{R}{r_o} < 19.7 \tag{4.20}$$

$$\alpha = 1.0 \qquad \frac{R}{r_o} > 19.7 \tag{4.21}$$

for straight section:

$$\lambda_f = \frac{x7}{Re^{x8}} \tag{4.22}$$

or

$$\lambda_f = \frac{x9}{\left[\ln\left(\frac{\varepsilon}{3.7\ D} + \frac{x10}{Re^{x11}}\right)\right]^2} \tag{4.23}$$

In the experiments conducted by the author, the air temperature was 27.5°C, the atmospheric pressure was 102.1 kPa, the relative humidity was 56% and the air mass flow rate was varied between 0.0097 and 0.065 kg s^{-1}. Therefore, the Reynolds number ranged between 12782 and 85652. These numbers are much higher than 4500 and hence the flow was considered turbulent.

For the R=254 mm bend,

$$\frac{R}{r_o} = 9.676 < 19.7$$

$$R_e \left(\frac{r_o}{R}\right)^2 = 136.52 \text{ to } 914.84 > 91$$

Due to the bend geometry, only Equations (4.18), (4.20) and (4.22) or (4.23) are employed.

For the R=1000 mm bend,

$$\frac{R}{r_o} = 38.1 > 19.7$$

$$R_e \left(\frac{r_o}{R}\right)^2 = 8.805 \text{ to } 59.01 < 91$$

In this case, only Equations (4.19), (4.21) and (4.22) or (4.23) are used.

It has been shown by the previous mathematical analyses and experiments that the pressure gradient is not constant along a straight section of pipe. However, it may be sufficient to base the calculation of pressure drop due to the conveying air on the mean operating conditions (based on average air density) of the straight section of

pipe. For a bend, the flow of air is complex and hence, the conditions occurring at the outlet of the bend are used to determine pressure drop. Note that these outlet conditions are the 'effective' conditions as determined by the straight pipeline analysis (i.e. for the section of pipe downstream of the bend). It is expected that there will be differences between predicted and experimental values of pressure drop and it is impossible to obtain exact experimental data of bend pressure drop (discussed later in Chapter 6). Therefore, the exponents in these equations are determined by minimising the sum of squared errors of pressure at points 1, 5 and 6 listed in Tables 4.1, 4.2 respectively, starting from point 10 which is taken to have known flow conditions. Note that, due to several runs with an actual product (viz. fly ash), the inner surface of pipeline has become smooth with time. Hence, the pipe roughness can be considered as zero. The determined values of exponent are listed in Table 4.4, which also includes the 'previous' values (e.g. [23, 60]).

Table 4.4: Values of exponent for air-only.

Constant	Determined	Previous
x1	0.1819	0.217
x2	0.2333	0.17
x3	0.8342	0.84
x4	0.2478	0.248
x5	0.2341	0.2
x6	0.8945	0.9
x7	0.2969	0.316
x8	0.2381	0.25
x9	1.3282	1.325
x10	5.7379	5.74
x11	0.8734	0.9

The pressure at point p is predicted initially by using the above 'determined' and 'previous' values of exponent, starting from the end of pipeline. In order to determine the effect of the vertical section, the pressure at point v1 also is predicted, starting from point v5. All the agreement is very good, as shown in Figure 4.3.

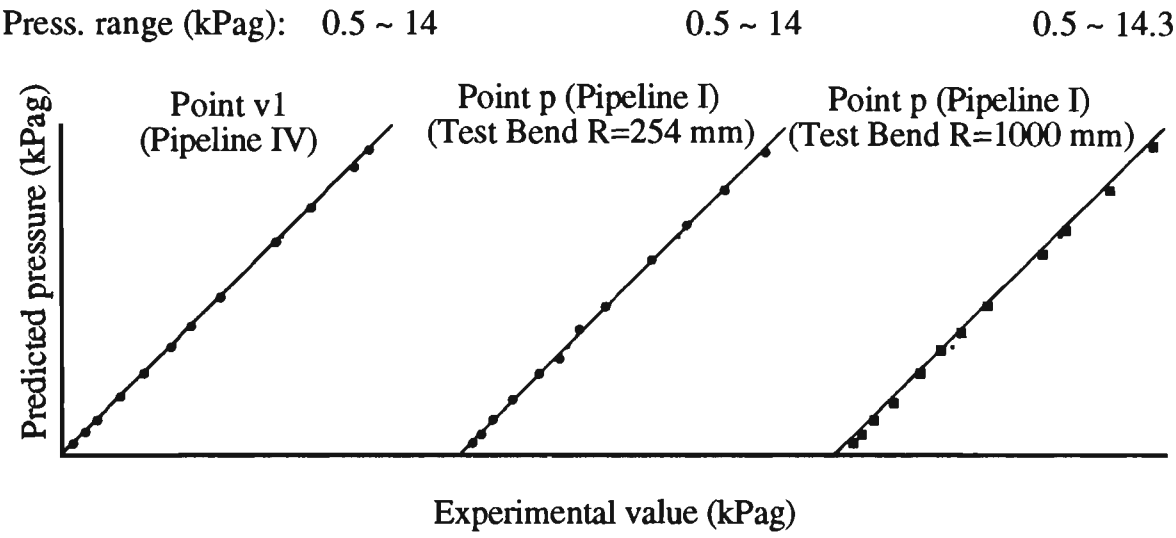

(a) By using the 'previous' values of exponent.

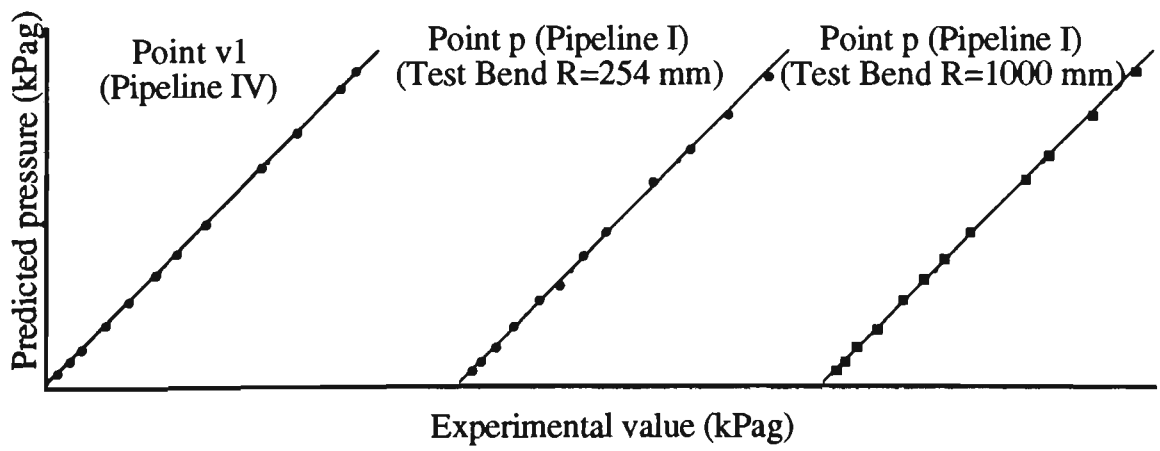

(b) By using the 'determined' values of exponent.

Figure 4.3 Predicted pressure vs experimental value at points p, v1.

From Figure 4.3 and the predictions of pressure at point v1, it is clear that the air gravity in the vertical section of pipe has little influence on the pressure drop (i.e. the vertical section can be considered as a horizontal one - in fact, this was assumed for the prediction of the total air-only pressure drop).

4.5 Prediction of Other Pipelines

Four different pipelines were tested previously [58] with air alone. The schematic layout and characteristics of these four different pipelines are depicted in Appendix B. Also, for convenience, their characteristics are summarised in Table 4.5 below.

Table 4.5: Characteristics of four different pipelines [58].

Pipeline	Diameter (m)	Length (m)	No. of Bends	No. of Straights	No. of Data	m_f range (kg s^{-1})
A1	0.069	172	5	6	13	0.07 - 0.37
A2	0.069	553	17	18	9	0.06 - 0.31
A3	0.069 0.081	564 391	17 12	13 18	8	0.06 - 0.31
A4	0.069 0.081 0.105	564 391 253	17 12 8	18 13 9	22	0.054 - 0.4

The pressure at the pick-up point for each pipeline is predicted by using the above 'determined' and 'previous' values of constant, starting from the end of pipeline. The agreement generally is very good, as shown in Figure 4.4.

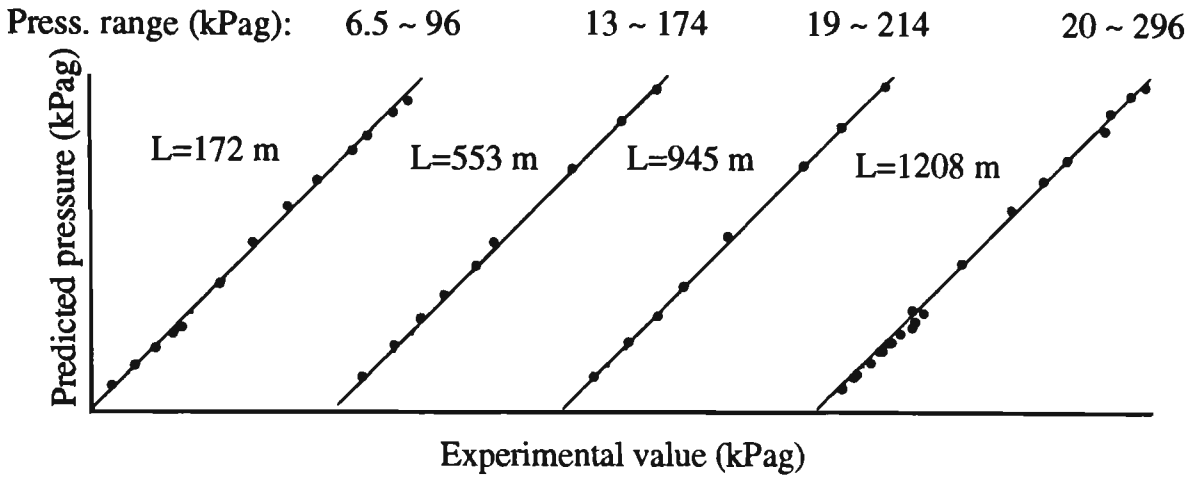

(a) By using the 'previous' values of exponent.

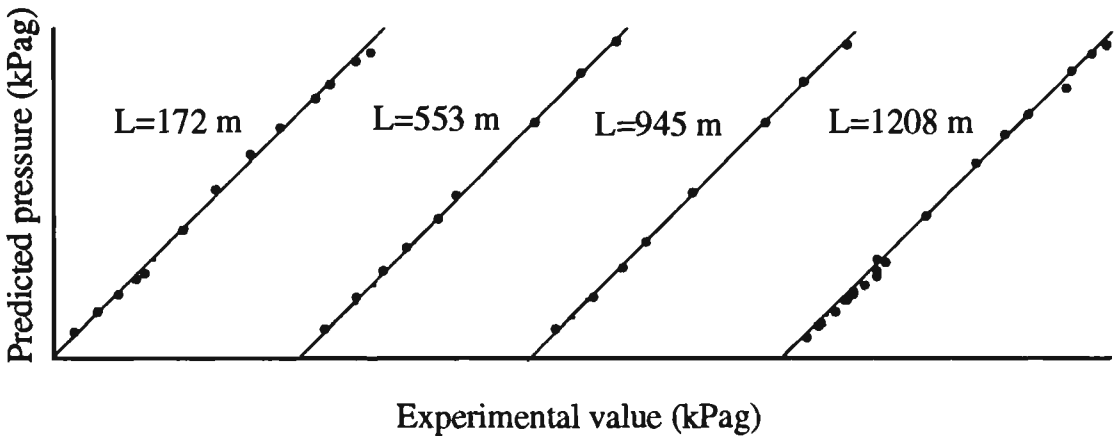

(b) By using the 'determined' values of exponent.

Figure 4.4 Predicted pressure vs experimental value at pick-up point for four different pipelines.

All the above results show that the existing formulae which were based on incompressible flow still can be employed to determine accurately the air-alone component of pressure drop in pneumatic conveying pipelines, as long as:

- the pressure drop for each component (e.g. straight pipe, bend) is determined separately starting say, from the end of the pipeline where conditions usually are known,

- the pressure drop calculation for a given straight section of pipe is based on the mean operating conditions (i.e. average air density),

- the pressure drop calculation for a given bend is based on the density and velocity which occur at the outlet of the bend.

CHAPTER 5

PRESSURE DROP DUE TO SOLIDS-AIR MIXTURE IN HORIZONTAL AND VERTICAL PIPES

5.1 Introduction

To predict accurately the total pipeline air pressure drop in pneumatic conveying, an essential step involves the determination of pressure drop due to solids-air mixture in each straight section of pipe, Δp_S. The pressure drop, Δp_S, depends on the pipe parameters (e.g. diameter, length and roughness), particle characteristics (e.g. particle size, size distribution, density, shape and moisture content), conveying conditions (e.g. air density, air velocity, air and product mass flow rates) and the relationship between the particles and pipe wall (e.g. wall friction).

In the literature, there is no lack of theoretical and empirical studies on the determination of the pressure drop, Δp_S. However, most of the theoretical correlations [61, 67, 75, 76, 78] are restricted to the dilute-phase conveying (e.g. $m^* \leq$ 20 [67], 6 [20]) of coarse particles of relatively narrow size distribution (e.g. adequately represented by a mean or median particle diameter). Also, knowledge of the particle velocity and concentration as well as their variation along the pipeline is required. The majority of pneumatic conveying systems in industry transport particles of different size, size distribution, density, shape and surface roughness [70]. The product to air mass flow rate ratios also vary considerably. Therefore, it is difficult to quantify the pressure drop, Δp_S, theoretically. As a result, empiricism has been used widely [2, 6, 8, 12, 42, 54].

A number of attempts have been made to generalise empirical correlations by determining the corresponding exponents for different products and configurations of pipeline [24, 59]. However, the materials conveyed have numerous influences on

the pressure drop, Δp_S [13, 33, 41, 62, 63, 64]. Also, it has been shown [63, 75] that there is a large scatter between the predicted and experimental values of pressure drop, Δp_S, by using the above generalised empirical correlations. The reason is that, the influences of the materials conveyed are very complicated and difficult to describe properly.

A number of researchers (e.g. Weber [63], Reed [45]) have suggested that it is more precise to determine the exponents using the data obtained from a given product. However, it is not correct to consider the assumption that the pressure gradient along the straight sections of pipe is constant [6, 7, 8, 42, 45]. Also, the accurate prediction of both dilute- and dense-phase steady-state conveying characteristics has been found quite difficult [6, 7, 8, 42, 45].

This chapter presents a new test-design procedure that uses a semi-empirical correlation, which is accurate for the test material and also applicable to dilute-/dense-phase conditions and other sizes of pipe (viz. length and/or diameter). The exponents in this new correlation are determined by minimising the sum of the squared errors of pressure along a constant straight section of pipe.

The semi-empirical correlation then is used to predict the pressure drop caused by straight pipes of different diameter and length at different locations. These results demonstrate the good accuracy and reliability of this procedure, as well as its applicability to both dilute- and dense-phase conditions. A comparison with the prediction of other existing models is included. Also, the pressure drop and the steady-state conveying characteristics of horizontal and vertical straight pipes are presented and compared.

5.2 Steady-State Conveying Characteristics of Straight Pipes

Steady-state conveying characteristics are a useful method of obtaining pertinent information to assist the designers of pneumatic conveying systems. Up to now, numerous experiments with different materials have been carried out in both horizontal and vertical straight pipes of different length and diameter. It has been found that many of the flow situations which occur in straight pipes are clearly a function of material properties [36, 77].

For fine-particle suspensions (e.g. fly ash), five identifiable flow patterns have been observed. These observations have been made either by keeping the air mass flow rate constant whilst increasing the product mass flow rate or by keeping the product mass flow rate constant whilst decreasing the air mass flow rate. In Figure 5.1, the different flow patterns are depicted as the air mass flow rate is decreased. Figure 5.1(a) shows the regime of flow in dilute-phase conveying in a horizontal straight pipe. This mode of flow is accompanied usually by high air velocities and low product to air mass flow ratios. A reduction in the air mass flow rate for a constant product mass flow rate leads to a small strand moving along the bottom of pipe (b) with a velocity lower than the top particle velocity. At still lower air flows, erratic flow appears (c). Finally a continual reduction in the air mass flow rate leads to plug flow with a stationary bed along the bottom of pipe (d) and a substantial stationary bed (e) until blockage. With the exception of (c), the regimes of flow are essentially the same in a vertical straight pipe as in a horizontal straight pipe.

The general phase diagrams or steady-state conveying characteristics for fine particles flowing in horizontal and vertical straight pipes are similar to the ones

obtained by Rizk [48], as shown in Figures 5.2 and 5.3. The pressure drop decreases and then increases, as the average air velocity (or the air mass flow rate) increases.

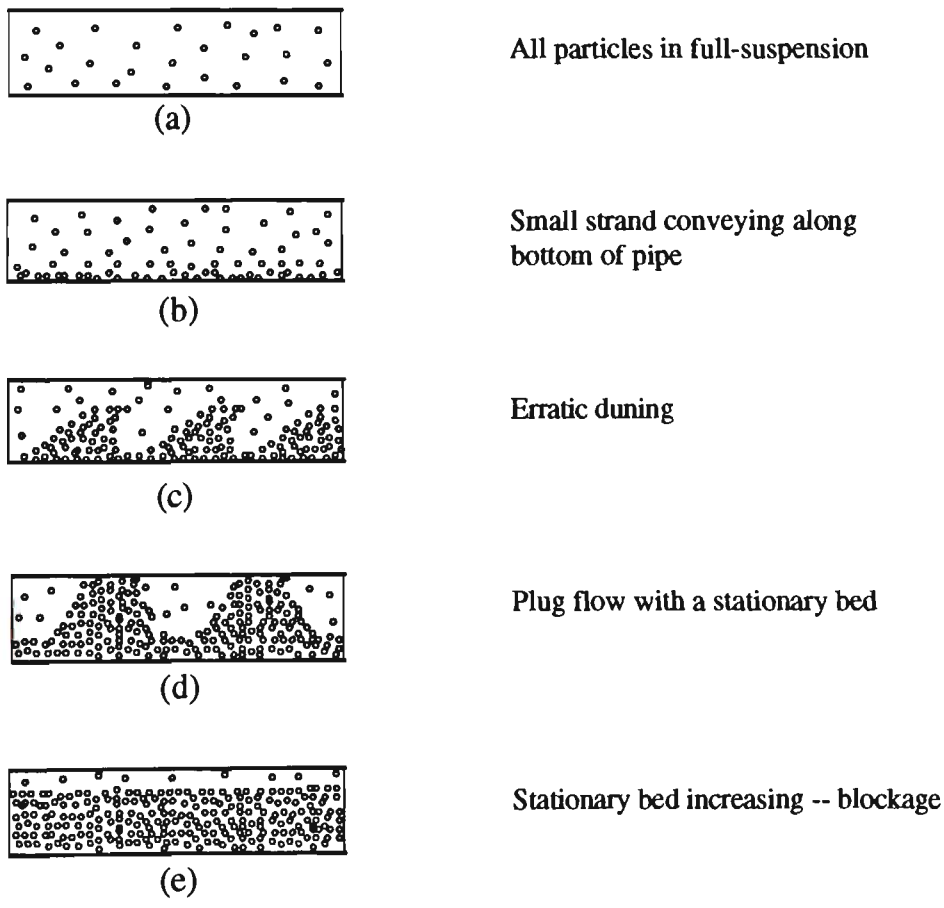

Figure 5.1 Observed modes of flow for fine particles and decreasing air flow.

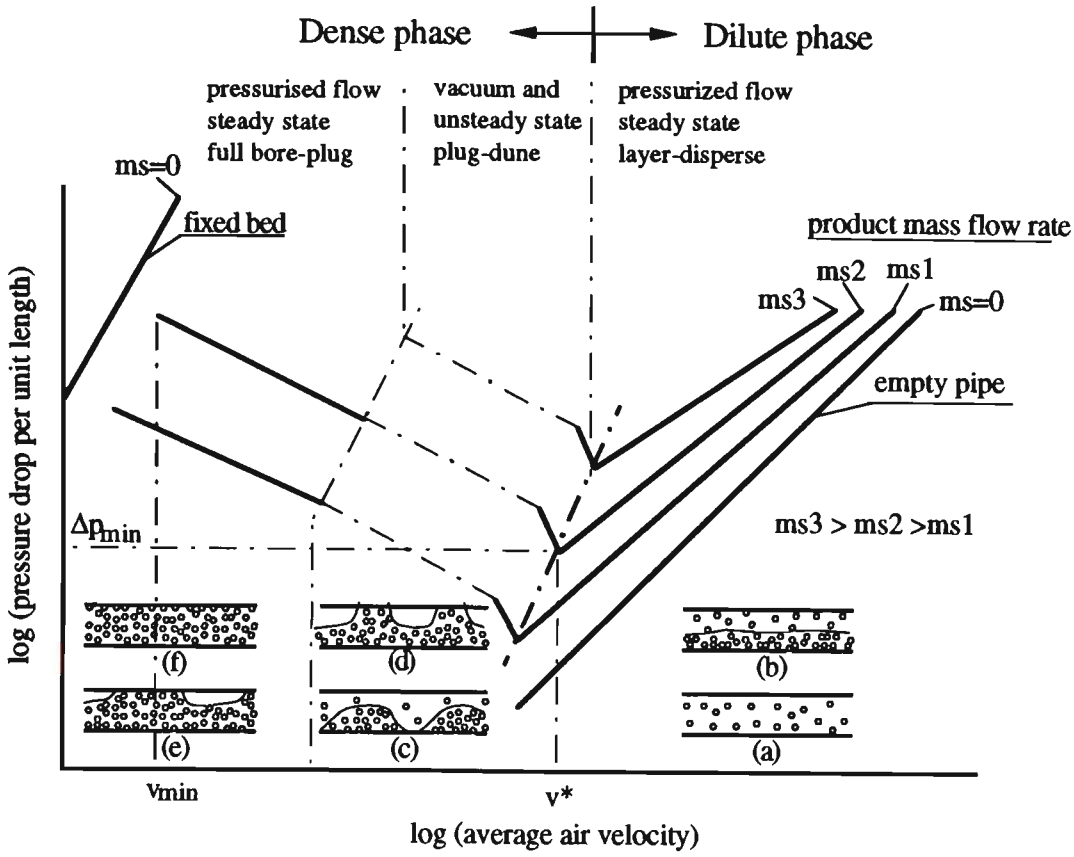

Figure 5.2 State diagram for horizontal conveying [48].

Product	Styropor - 3
Particle size	d_p = 2,385 mm
Density	ρ_S = 1050 kg m^{-3}
Pipe diameter	D = 52.6 mm
Pipe material	Stainless steel
Average pipe wall roughness	ε = 6 to 10 µm

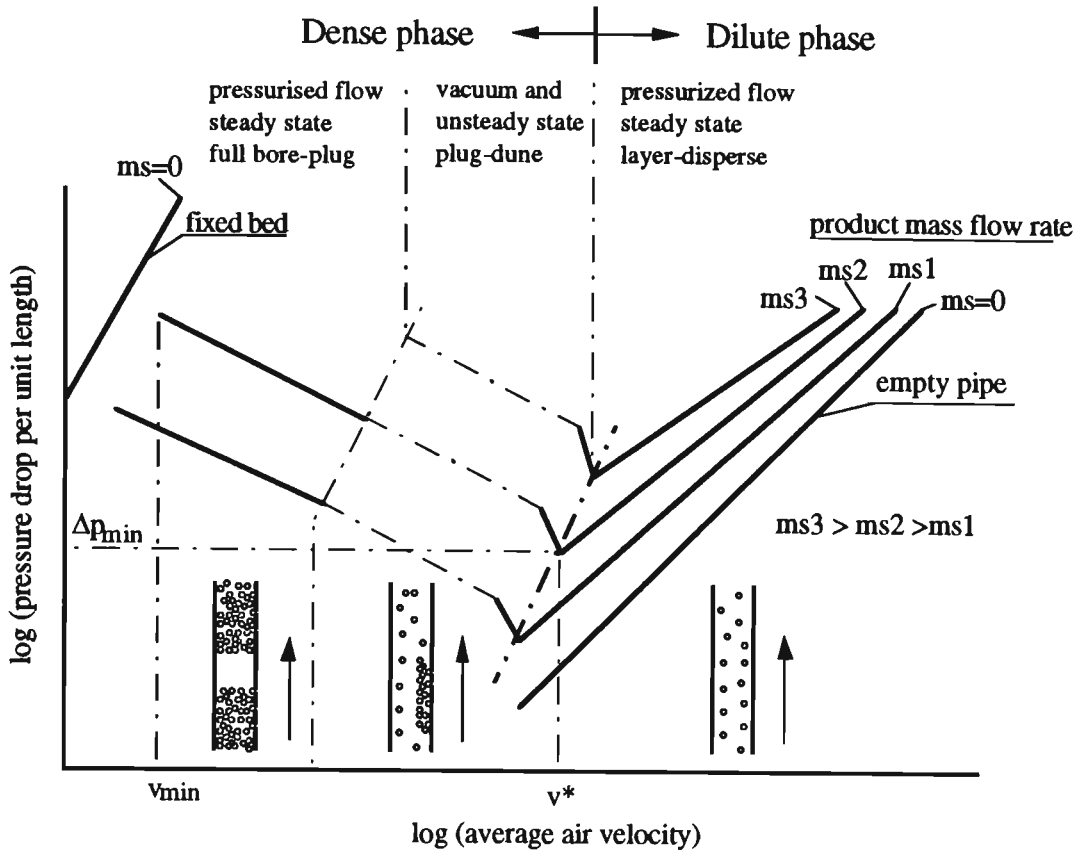

Figure 5.3 State diagram for vertical conveying [48].

Product	Styropor - 3
Particle size	d_p = 2,385 mm
Density	ρ_s = 1050 kg m^{-3}
Pipe diameter	D = 52.6 mm
Pipe material	Stainless steel
Average pipe wall roughness	ε = 6 to 10 µm

5.3 Theoretical Analysis

In deriving the necessary correlations for pressure drop prediction, the following assumption is adopted:

- Concerning the friction between a group of the particles and pipe wall, an empirical expression such as the one by Weidner [65] is applicable.

The forces acting on flowing particles, as shown in Figure 5.4, are:

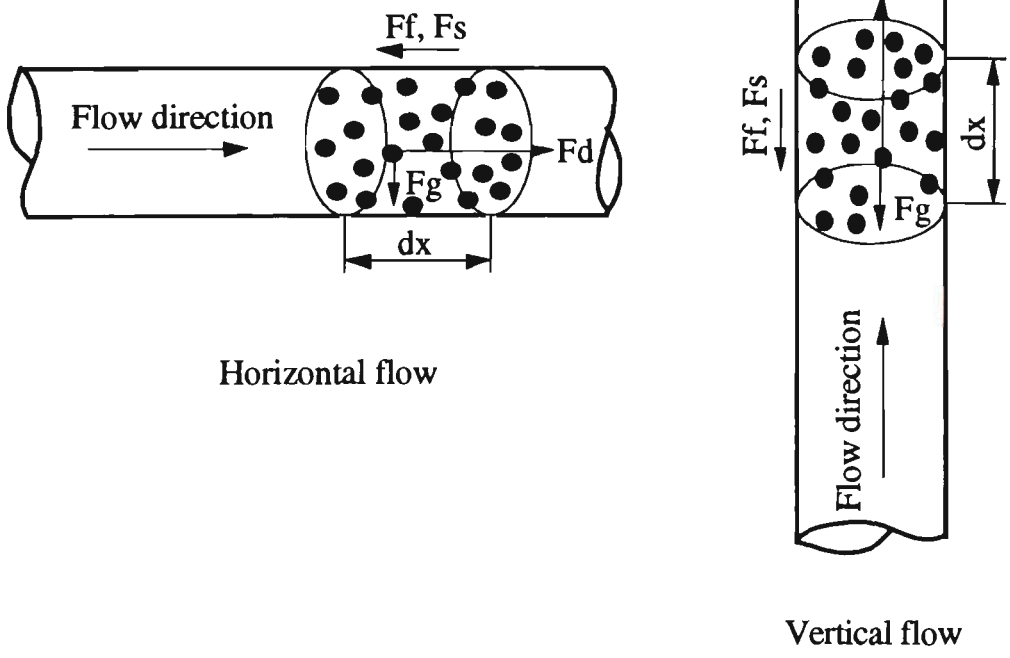

Figure 5.4 Forces acting on moving particles.

a) Drag force, F_d

This force, denoted as F_d, is due to drag and results from the conveying air. It forces the particles to flow along the straight section of pipe.

b) Frictional forces for air, F_f and for solids, F_s

For the air:

$$\tau_f = \frac{\lambda_f}{4} \rho_f \frac{v_f^2}{2}$$

$$F_f = \tau_f P_{wf} dx = \frac{\lambda_f}{4} \rho_f \frac{v_f^2}{2} P_{wf} dx$$

$$P_{wf} = \xi \pi D \qquad 0 \leq \xi \leq 1$$

$$F_f = \frac{\lambda_f}{4} \rho_f \frac{v_f^2}{2} \xi \pi D dx$$

For the solids:

$$\tau_s = \frac{\lambda_s'}{4} \rho_d \frac{v_s^2}{2} = \frac{\lambda_s'}{4} (1-\varepsilon) \rho_s \frac{v_s^2}{2}$$

$$F_s = \tau_s P_{ws} dx = \frac{\lambda_s'}{4} (1-\varepsilon) \rho_s \frac{v_s^2}{2} P_{ws} dx$$

$$P_{ws} = (1-\xi) \pi D$$

$$F_s = \frac{\lambda_s'}{4} (1-\varepsilon) \rho_s \frac{v_s^2}{2} (1-\xi) \pi D dx$$

c) Gravity force, F_g

The gravity force acting on the particles over length dx is:

$$F_g = \rho_d A\, dx\, g = (1-\varepsilon)\, \rho_s A\, dx\, g \qquad (5.1)$$

In the vertical straight section of pipe, the force due to gravity which hinders the motion of the particles is the value expressed in Equation (5.1). However, in the horizontal straight section of pipe, the force due to the gravity which produces a frictional force to hinder the motion of the particles is less than F_g and inversely proportional to the air velocity. When the air velocity is higher than the saltation velocity, all the particles are suspended. Hence, there is no friction between the particle and the pipe wall due to the gravity. When the air velocity is less than the saltation velocity, a strand slides along the bottom of the pipe and there is a friction between the strand and the pipe wall. However, it is difficult to calculate the friction separately. Therefore, the friction is always included in λ_s' [45, 63].

Compared to the gravity of solids, the gravity of the air can be neglected, which has been confirmed in Chapter 4.

Now, using the Euler Momentum Equation

For the air:

$$A\, dp_s - m_f\, dv_f - \frac{\lambda_f}{4}\, \rho_f \frac{v_f^2}{2}\, \xi\, \pi\, D\, dx - F_d = 0$$

For the solids:

$$F_d - m_s\, dv_s - \frac{\lambda_s'}{4}\,(1-\varepsilon)\,\rho_s\,\frac{v_s^2}{2}\,(1-\xi)\,\pi\,D\,dx - \beta\,(1-\varepsilon)\,\rho_s\,A\,dx\,g = 0$$

These two equations are added and then divided by A:

$$dp_s - \varepsilon\,\rho_f\,v_f\,dv_f - (1-\varepsilon)\,\rho_s\,v_s\,dv_s - \lambda_f\,\rho_f\,\frac{v_f^2}{2\,D}\,\xi\,dx$$

$$- (1-\varepsilon)\,\lambda_s'\,\rho_s\,\frac{v_s^2}{2\,D}\,(1-\xi)\,dx - \beta\,(1-\varepsilon)\,\rho_s\,dx\,g = 0$$

Denoting the velocity ratio of solid-to-air as:

$$\eta = \frac{v_s}{v_f}$$

Then: $dv_s = \eta\,dv_f$

Noting that:

$$(1-\varepsilon) = \frac{\dfrac{m^*\,\rho_f}{\rho_s\,\eta}}{1 + \dfrac{m^*\,\rho_f}{\rho_s\,\eta}} \approx \frac{m^*\,\rho_f}{\rho_s\,\eta} \qquad \left(\frac{m^*\,\rho_f}{\rho_s\,\eta} \ll 1\right)$$

$$\therefore \quad dp_s - (1+m^*\,\eta)\,\varepsilon\,\rho_f\,v_f\,dv_f - \left[\frac{\xi}{\varepsilon}\,\lambda_f + m^*\,\eta\,\lambda_s'\,(1-\xi)\right.$$

$$\left. + \beta\,\frac{2\,D\,m^*}{v_f^2\,\eta\,\varepsilon}\right]\varepsilon\,\rho_f\,v_f^2\,\frac{dx}{2\,D} = 0$$

Under isothermal conditions: $-\dfrac{dp_s}{p_s} = \dfrac{dv_f}{v_f}$

$$dp_s + (1+m^*\eta)\frac{\varepsilon v_f^2}{R_a T} dp_s - [\frac{\xi}{\varepsilon}\lambda_f + m^*\eta\lambda_s'(1-\xi) + \beta\frac{2 D m^*}{v_f^2 \eta \varepsilon}] \varepsilon \rho_f v_f^2 \frac{dx}{2D} = 0$$

$$dp_s = \frac{[\frac{\xi}{\varepsilon}\lambda_f + m^*\eta\lambda_s'(1-\xi) + \beta\frac{2 D m^*}{v_f^2 \eta \varepsilon}] \frac{\varepsilon \rho_f v_f^2}{2D}}{1 + (1+m^*\eta)\frac{\varepsilon v_f^2}{R_a T}} dx$$

If the acceleration terms are neglected

$$dp_s = [\xi\lambda_f + m^*\eta\lambda_s'(1-\xi)\varepsilon + \beta\frac{2 D m^*}{v_f^2 \eta}] \frac{\rho_f v_f^2}{2D} dx \qquad (5.2)$$

Usually, it is very difficult to calculate the actual air velocity. Therefore, the superficial air velocity is used to replace the actual air velocity.

$$v_f = \frac{m_f}{\rho_f \varepsilon A} = \frac{V_f}{\varepsilon} \qquad (5.3)$$

Substituting Equation (5.3) into Equation (5.2) results in:

$$dp_s = [\frac{\xi}{\varepsilon^2}\lambda_f + \frac{m^*\eta\lambda_s'(1-\xi)}{\varepsilon} + \beta\frac{2 D m^*}{V_f^2 \eta}] \frac{\rho_f V_f^2}{2D} dx \qquad (5.4)$$

ξ and ε are functions of and proportional to m*. Assuming that both ξ and $\varepsilon \approx 1$ (which is a good approximation for dilute-phase conditions),

then $$\frac{\xi}{\varepsilon^2} \approx 1$$

Therefore, rewriting Equation (5.4) gives:

$$dp_S = [\lambda_f + \frac{m^* \eta \lambda_S' (1-\xi)}{\varepsilon} + \beta \frac{2 D m^*}{V_f^2 \eta}] \frac{\rho_f V_f^2}{2 D} dx$$

$$\delta p_S = \frac{dp_S}{dx}$$

$$= [\lambda_f + \frac{m^* \eta \lambda_S' (1-\xi)}{\varepsilon} + \beta \frac{2 D m^*}{V_f^2 \eta}] \frac{\rho_f V_f^2}{2 D}$$

Assuming:

$$\lambda_S = \frac{\eta \lambda_S' (1-\xi)}{\varepsilon} + \beta \frac{2 D}{V_f^2 \eta}$$

$$\delta p_S = (\lambda_f + m^* \lambda_S) \frac{\rho_f V_f^2}{2 D} \qquad (5.5)$$

Hence, the pressure drop Δp_S over ΔL is:

$$\Delta p_S = (\lambda_f + m^* \lambda_S) \frac{\rho_f V_f^2}{2 D} \Delta L \qquad (5.6)$$

Note that:

$\lambda_S = \lambda_{Sh}$, $\lambda_S' = \lambda_{Sh}'$, $\beta = 0$ in horizontal straight sections of pipe.

and $\lambda_S = \lambda_{Sv}$, $\lambda_S' = \lambda_{Sv}'$, $\beta = 1$ in vertical lift sections,

$\beta = -1$ in vertical drop sections.

5.4 Dimensional Analysis

Equation (5.5) clearly shows that the pressure drop due to the solids-air mixture in the straight section of pipe is the sum of two functions. The first function represents the loss due to air alone and the second is related to the loss due to solids. The formulae for calculating λ_f have been set up already in Chapter 4. Also, λ_s is the function of many influential parameters, such as particle size, size distribution, density, shape, pipe diameter, superficial air velocity, air density, impact between particles, friction between particles and pipe wall, etc. It is very difficult to set up analytic relationships between λ_s and these influential parameters. So this section is concerned mainly with calculating λ_s by using the dimensional analysis [43].

Although the pressure drop Δp_s due to solids over ΔL can not be expressed theoretically, it is clear that Δp_s is a function of many pertinent variables, such as superficial air velocity V_f, air density ρ_f, pipe diameter D, pipe length ΔL, air viscosity μ, pipe roughness ε, product mass flow rate m_s, particle density ρ_s, mean particle diameter d_p, particle shape factor z and the friction coefficient between the pipe wall and solids υ. For a given product and pipe material, it can be assumed that d_p, z, ρ_s and υ are constant. Based on the dimensional analysis [43], an expression of the form given in Equation (5.7) is considered initially.

$$\Delta p_{ss} = k\, V_f^{a}\, \rho_f^{b}\, D^{c}\, \Delta L^{e}\, \mu^{f}\, \varepsilon^{h}\, m_s^{i} \tag{5.7}$$

With the aid of dimensional analysis, an expression similar to Equation (4.7) is obtained:

$$\Delta p_{ss} = k \left(\frac{\mu}{\rho_f V_f D}\right)^{f} \left(\frac{\varepsilon}{D}\right)^{h} \left(\frac{\Delta L}{D}\right)^{e} \left(\frac{m_s}{\rho_f V_f D^2}\right)^{i} \rho_f V_f^2 \tag{5.8}$$

Comparing Equations (5.6) and (5.8) results in:

$$\lambda_S = 2\,k\,(\frac{\pi}{4})^i\,Re^f\,(\frac{\varepsilon}{D})^h\,(\frac{\Delta L}{D})^{e-1}\,m^{*i-1}$$

$$= 2\,k\,(\frac{\pi}{4})^i\,m^{*i-1}\,V_f^{-f}\,\rho_f^{-f}\,(\frac{\mu}{D})^f\,(\frac{\varepsilon}{D})^h\,(\frac{\Delta L}{D})^{e-1}$$

For a given pipe material and conveying air temperature, μ and ε can be assumed constant. Also, k may be a function of m*, V_f, ρ_f, D and ΔL.

$$\therefore \qquad \lambda_S = \Phi(m^*, V_f, \rho_f, D, \Delta L)$$

ΔL has been included in Equation (5.6) and

$$Fr = \frac{V_f}{\sqrt{g\ D}}$$

Therefore, λ_S is assumed as:

$$\lambda_S = x1\ m^{*x2}\ Fr^{x3}\ \rho_f^{x4} \qquad (5.9)$$

5.5 Pressure Gradient in Straight Pipes

Rewriting Equation (5.5) gives:

$$\delta p_S = (\lambda_f + m^*\,\lambda_S)\,\frac{m_f}{2\ D\ A}\,V_f \qquad (5.10)$$

It can be seen from Equation (5.9) that λ_s is a function of V_f. So from Equation (5.10), it is clear that, for a given product, pipe material, product and air mass flow rate, δp_s is a function of V_f. Due to the compressibility of air, for a constant air mass flow rate the superficial air velocity increases towards the end of the pipeline (i.e. as the pressure decreases). Therefore, the pressure gradient at any point along a straight section of pipe is not constant.

Based on the experimental data of pressure along straight pipes, a number of researchers [6, 7, 8, 42, 45, 46] have assumed that the pressure gradient is constant. The determination of the pressure gradient in a straight section of pipe is shown in Figure 5.5. Note that all the selected points are beyond any bend effects.

In Chapter 3, numerous experiments were carried out with fly ash over a wide range of conveying conditions for different pipelines. By using the method shown in Figure 5.5, the pressure gradients in the two horizontal straight sections of pipe, which were directly upstream and downstream of the R=254 mm test bend (see Figure 3.2), were obtained. Some of the pressure gradients are listed in Table 5.1. Note that the values of δp_{su} and δp_{sd} were obtained using the traditional method given in Figure 5.5.

From Table 5.1, it is clear that, for constant product and air mass flow rates, two straight sections of pipe have different pressure gradients (i.e. a straight section of pipe causes different pressure drops at different locations). Therefore, the pressure gradient at any point along a straight section of pipe is not constant.

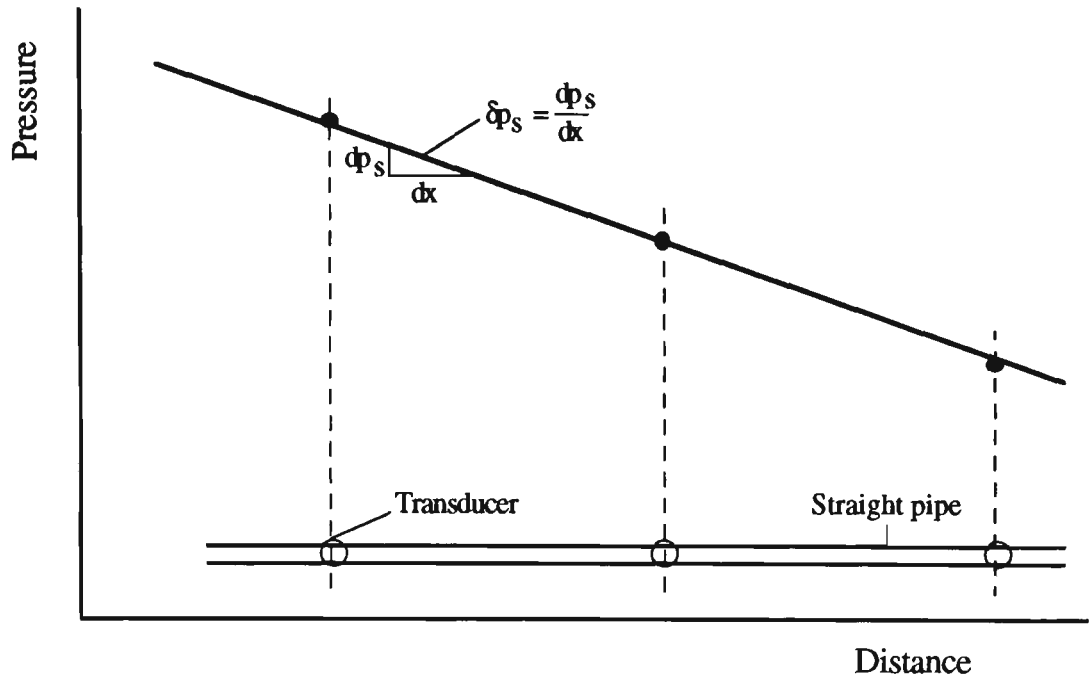

Figure 5.5 Traditional determination of pressure gradient in a straight pipe.

Table 5.1 Some pressure gradients in two straight pipes connected to R=254 bend.

Pre-set pressure in blow tank: 160 kPa g						
m_f (kg s^{-1})	0.0743	0.0699	0.0591	0.0474	0.0362	0.0236
m_s (kg s^{-1})	1.443	1.548	1.776	2.037	2.275	2.455
δp_{su} (kPa m^{-1})	0.425	0.481	0.364	0.522	0.634	0.803
δp_{sd} (kPa m^{-1})	0.222	0.231	0.389	0.478	0.614	0.663

In order to predict accurately the pressure drop caused by a straight section of pipe, especially by a long straight section of pipe which usually causes a high pressure drop, the mean conditions (based on average air density) on the straight section of pipe are used. Hence, Equations (5.6) and (5.9) are rewritten as:

$$\Delta p_S = (\lambda_f + m^* \lambda_S) \frac{\rho_{fm} V_{fm}^2}{2 D} \Delta L \qquad (5.11)$$

$$\lambda_S = x1 \; m^{*x2} \; F_{rm}^{x3} \; \rho_{fm}^{x4} \qquad (5.12)$$

5.6 Determination of Exponents in Equation (5.12)

It has been demonstrated [13, 33, 41, 62, 63, 64] that the materials conveyed have numerous influences on pressure drop. These influences are very complicated and have not been described properly. They only can be determined by undertaking pneumatic conveying experiments. Hence, the exponents in Equation (5.12) should be determined empirically and are valid only for a given product [45, 63].

Test rig Pipelines I, II, III, IV (see Figure 3.2) and Pipelines A1, A2, A3, which have been used to convey the same fly ash [58] (see Figures B.1, B.2 and B.3), comprise numerous straight sections of pipe of different length and diameter. Most of these straight pipes are horizontal. Also, numerous pressure transducers are installed at the selected points along each pipeline. Hence, the experimental values of pressure drop for horizontal straight pipes of different length and diameter and one vertical straight pipe (ΔL=8 m, D=52.5 mm in Pipeline IV) are available. The characteristics of some selected horizontal straight sections of pipe and one vertical straight section of pipe are listed in Table 5.2.

For a given product (e.g. fly ash), it is expected that the determination of the exponents in Equation (5.12) is based on the experimental values of pressure along a constant diameter straight section of pipe and that the subsequent equation is able to

predict accurately the pressure along straight pipes of different length, diameter and at different locations.

Table 5.2 Characteristics of selected horizontal and vertical pipes.

Straight pipe*	D (m)	ΔL (m)	m* range	No. of data	Location
SP1	0.0525	4.0	7 ~ 150	36	Horizontal
SP2	0.0525	15.3	6 ~ 150	36	Horizontal
SP3	0.0805	17.0	10 ~ 70	36	Horizontal
SP4	0.0690	48.5	3 ~ 76	38	Horizontal
SP5	0.0525	4.5	8 ~ 199	36	Vertical

* SP1: Td - Tc in Pipeline I
SP2: Td - Tc in Pipeline II
SP3: Td - Tc in Pipeline III
SP4: Te1 - Te2 in Pipeline A1
SP5: v5 - v3 in Pipeline IV

5.6.1 Horizontal Straight Pipe

Based on the experimental data of pressure along a constant diameter straight section of pipe, such as SP1, exponents x1, ..., x4 are determined by minimising the sum of the squared errors of pressure drop. The determined values of exponent are listed in Table 5.3.

Then the pressures along straight pipes SP2, SP3 and SP4 are predicted by using the above determined values of exponent. All the agreement is quite good, as shown in Figure 5.6.

Table 5.3 Values of exponent for straight pipe.

Exponent	Value (Horizontal)	Value (Vertical)
x1	5.3062	5.5306
x2	-0.4366	-0.128
x3	-1.9341	-1.7769
x4	-0.1175	-0.5069

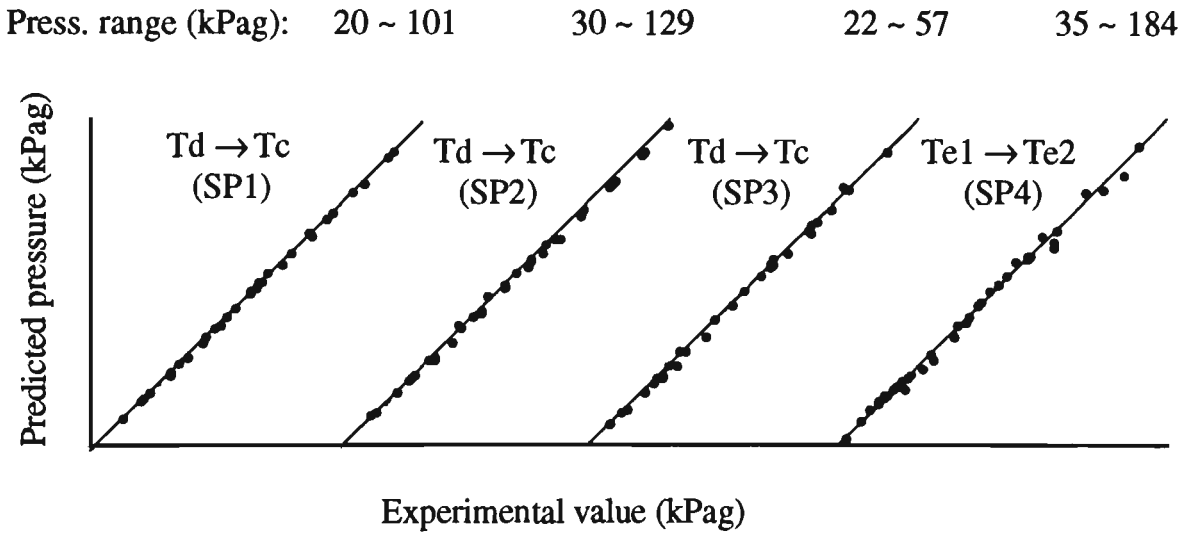

Figure 5.6 Predicted pressure vs experimental value in straight pipes of different length and diameter at different locations.

(Note: Td → Tc means the predicted pressure at Tc, starting from Td)

Also the steady-state conveying characteristics of the horizontal straight section of pipe at different locations are predicted, as depicted in Figure 5.7.

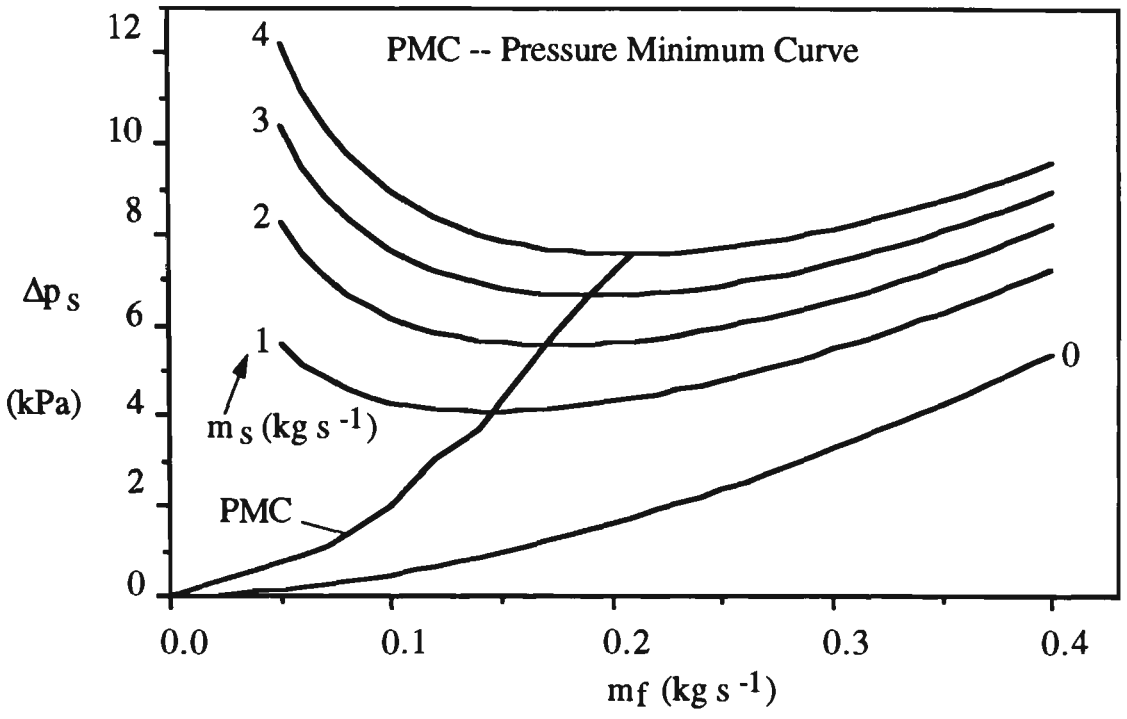

(a) $\rho_{fe} = 1.8$ kg m^{-3}.

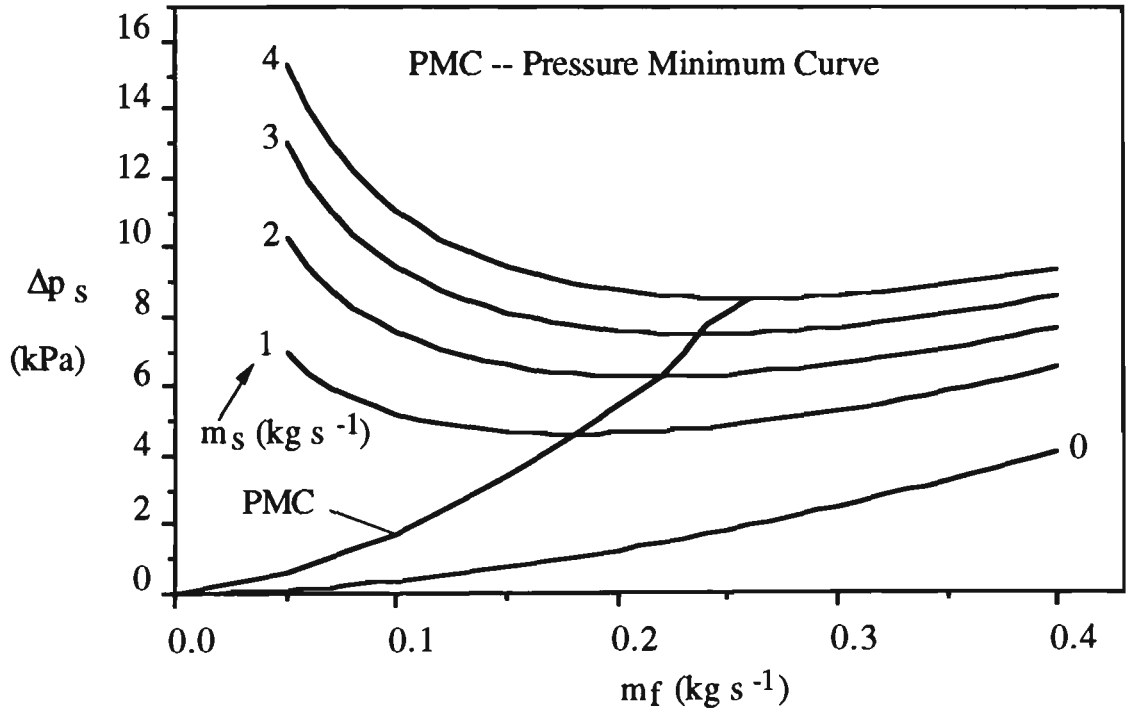

(b) $\rho_{fe} = 2.39$ kg m^{-3}.

Figure 5.7 Steady-state conveying characteristics of a horizontal straight pipe (ΔL=20 m, D=80.5 mm) at different locations.

5.6.2 Vertical Straight Pipe

Due to the difference in flow patterns between vertical and horizontal straight pipes, the above determined values of exponent for the horizontal cannot be used directly for the vertical. Similar to the horizontal straight section of pipe, exponents x1, ..., x4 are determined by minimising the sum of the squared error of pressure drop in SP5. The determined values of exponent also are listed in Table 5.3.

Because there is only one vertical straight section of pipe along which the pressure was measured, the above determined values of exponent cannot be applied to other vertical straight pipes of different length and diameter. However, good results have been obtained in the horizontal straight sections of pipe. Hence, similar good results are expected in vertical straight pipes of different length and diameter. The steady-state conveying characteristics of the vertical straight section of pipe at different locations are predicted, as shown in Figure 5.8.

All the results shown in Figures 5.6, 5.7 and 5.8 demonstrate the good accuracy and reliability of the above procedure, as well as the applicability to the both dilute- and dense-phase conditions.

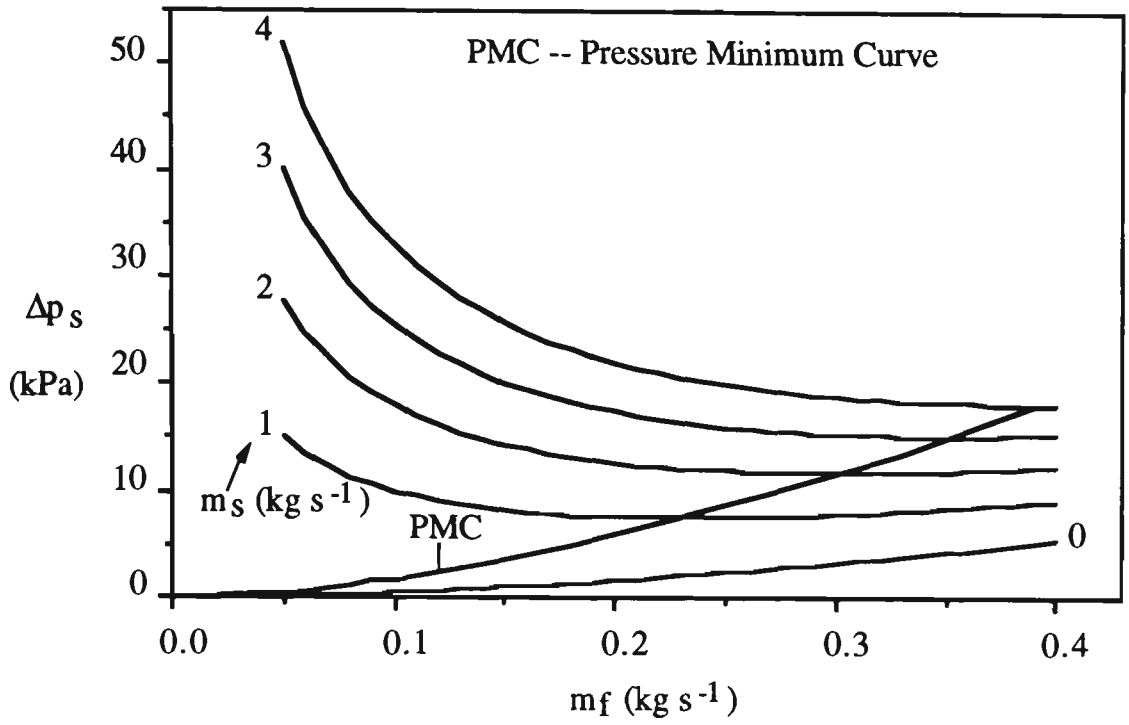

(a) ρ_{fe} = 1.8 kg m^{-3}.

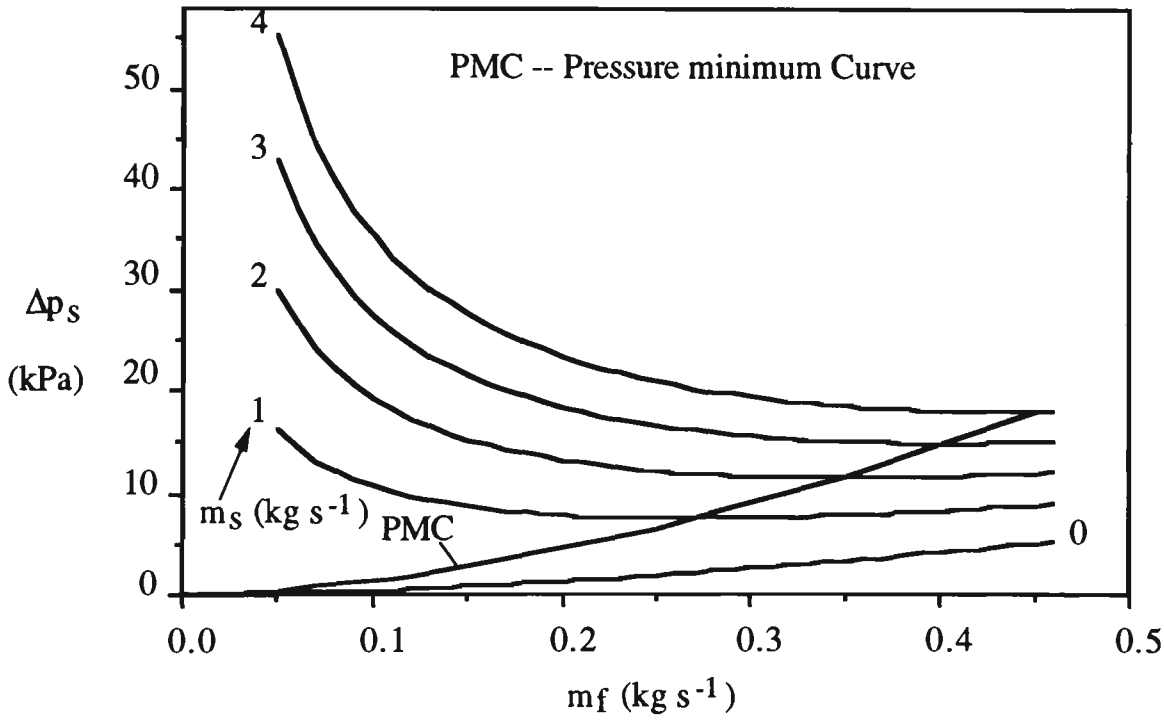

(b) ρ_{fe} = 2.39 kg m^{-3}.

Figure 5.8 Steady-state conveying characteristics of a vertical straight pipe (ΔL=20 m, D=80.5 mm) at different locations.

5.6.3 Comparison between Horizontal and Vertical Straight Pipes

The flow of the solids-air mixture along a horizontal straight pipe is very different to vertical lift [48, 62]. In the case of horizontal conveying, the driving force of the conveying air acts horizontally. The gravitational force, however, acts vertically. The flow of the conveying air must, therefore, produce driving forces and transverse 'carrying' forces. In order to transport the solids in suspension, additional forces must be occurring besides buoyancy. In the case of vertical lift conveying, forces act as carrying and driving forces and are directed exactly opposite to the weight of the solids (see Figure 5.4). So it is expected that, for the same product and air mass flow rate and air density at the pipe exit, the pressure drops caused by horizontal and vertical straight pipes which have the same geometry should be different.

On comparing Figures 5.7 and 5.8, it is clear that the pressure drop caused by the vertical straight pipe is always higher than by the horizontal straight pipe. Also, for a given product (e.g. fly ash), the ratio of the vertical to horizontal straight pipe pressure drop is a function of pipe location, diameter, air and product mass flow rates, as indicated in Figure 5.9. However, by comparing Figure 5.9 (a) with Figure 5.9 (b) and Figure 5.9 (c) with Figure 5.9 (d), the influence of pipe length on the ratio can be neglected. Hence, the ratios cannot be considered as a factor of 2.0, which has been used commonly [8].

It is interesting to note that at very low values of loading (i.e. m*), the ratio of the vertical to horizontal straight pipe pressure drop is less than 1. See Figure 5.9 (c) and (d). This can be explained that in very dilute-phase conveying, the friction between the solids-air mixture and the pipe wall is significant and the number of

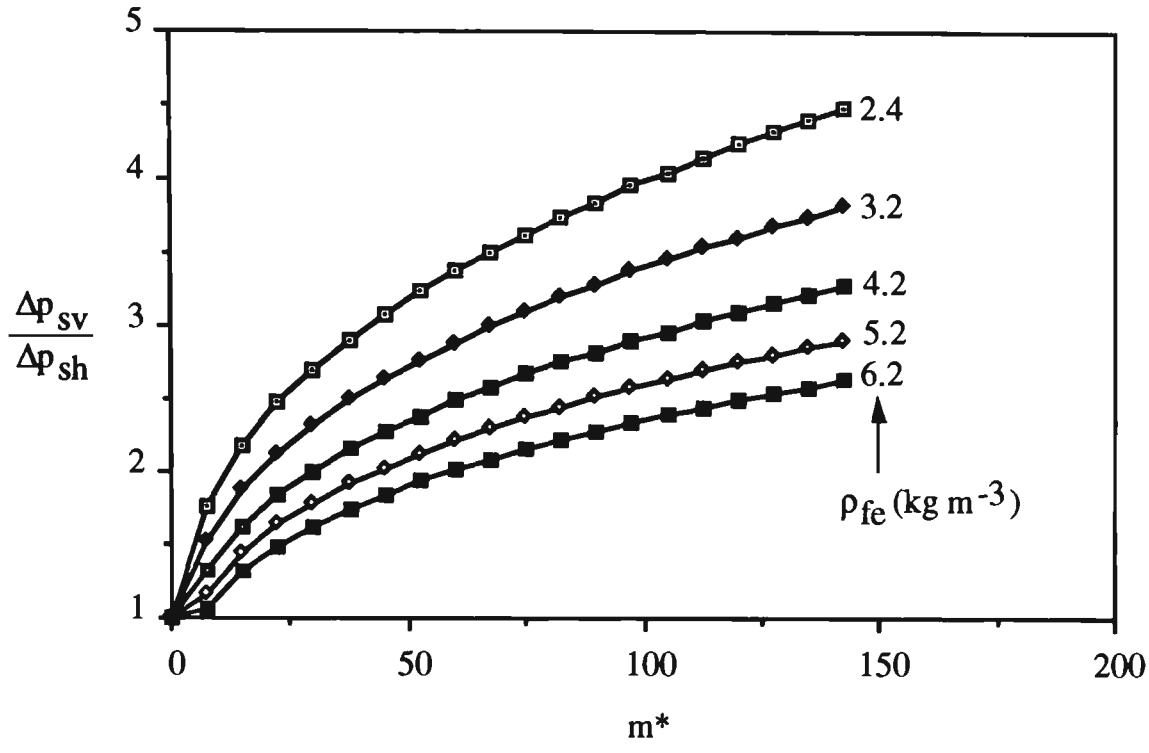

(a) D=52.5 mm, ΔL=20.0 m, m_f=0.02 kg s^{-1}, m_s=0.0 ~ 3.0 kg s^{-1}

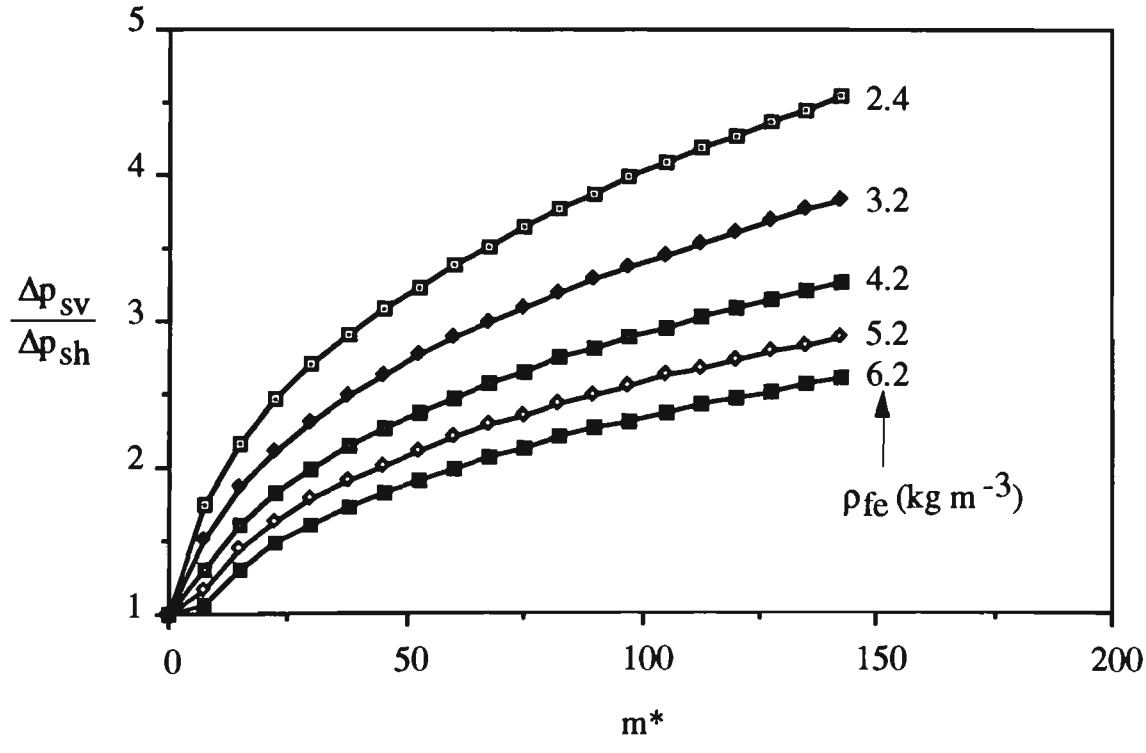

(b) D=52.5 mm, ΔL=50.0 m, m_f=0.02 kg s^{-1}, m_s=0.0 ~ 3.0 kg s^{-1}

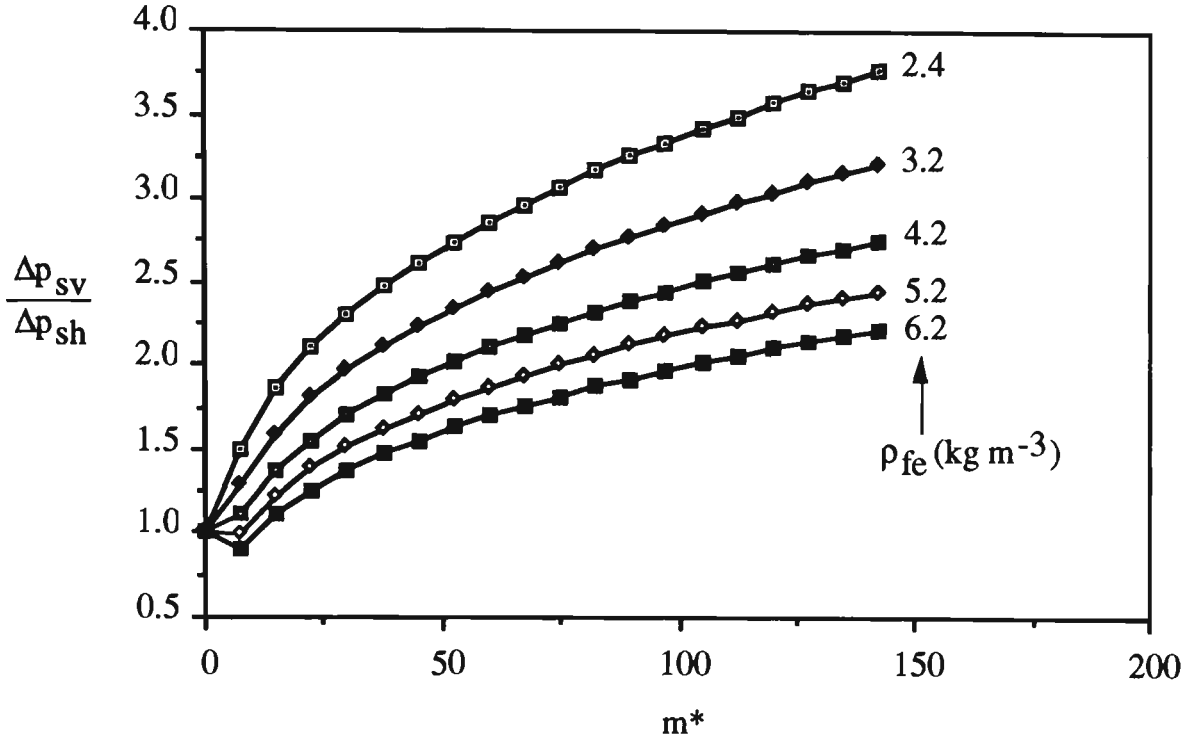

(c) D=80.5 mm, ΔL=20.0 m, m_f=0.02 kg s^{-1}, m_S=0.0 ~ 3.0 kg s^{-1}

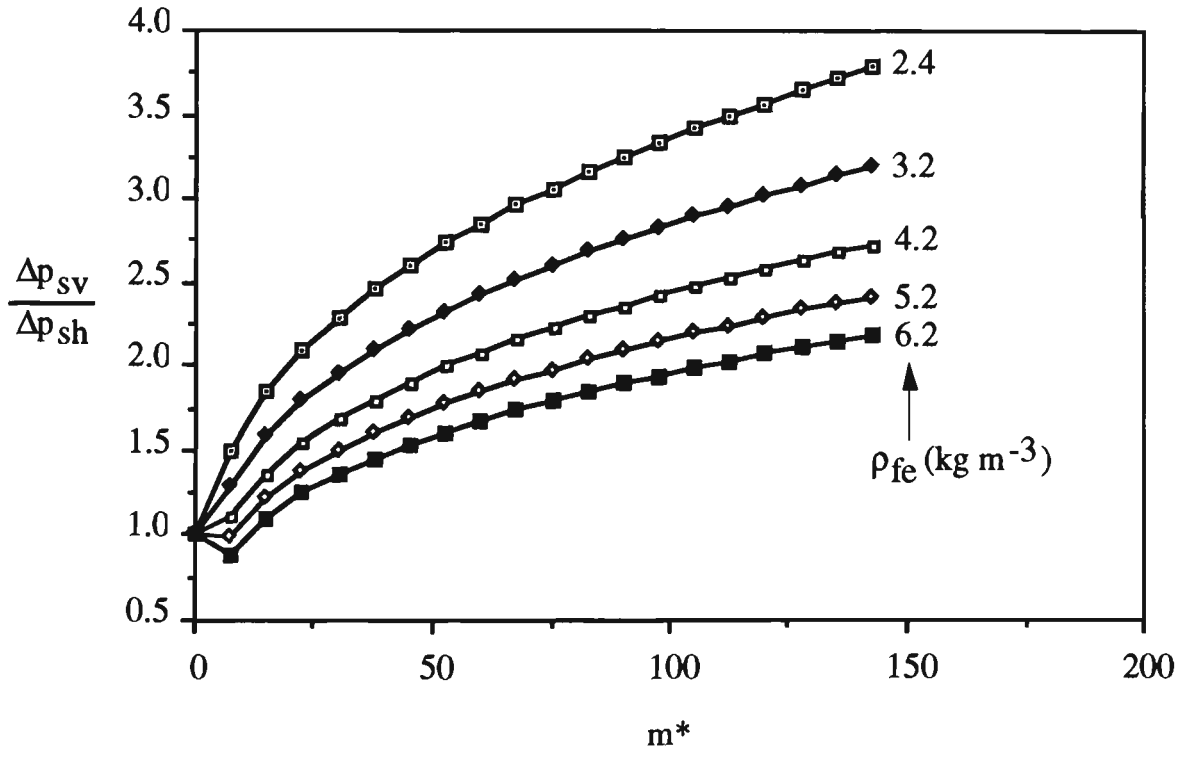

(d) D=80.5 mm, ΔL=50.0 m, m_f=0.02 kg s^{-1}, m_S=0.0 ~ 3.0 kg s^{-1}

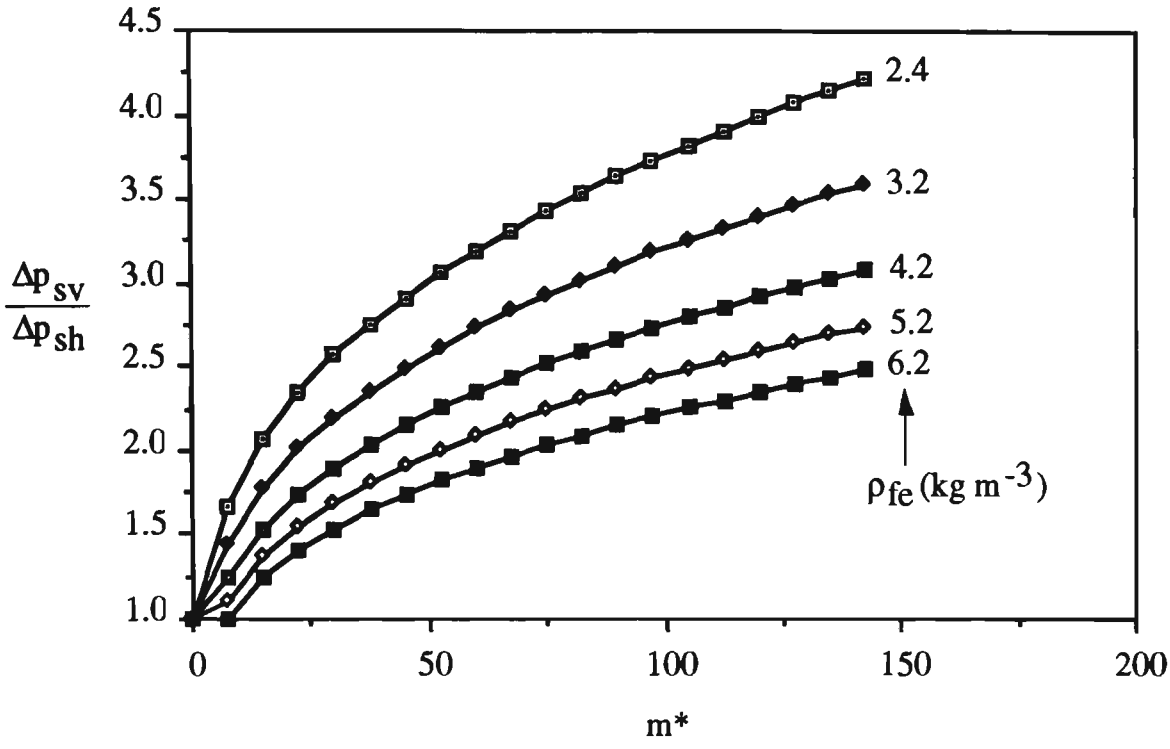

(e) D=80.5 mm, ΔL=50.0 m, m_f=0.04 kg s^{-1}, m_s=0.0 ~ 6.0 kg s^{-1}

Figure 5.9 Ratio of vertical to horizontal straight pipe pressure drop at different locations and pipe diameter, length.

contact between the particles and the pipe wall in a horizontal pipe is higher than in a vertical pipe, especially in the straight section of pipe with a big diameter.

Also, the horizontal and vertical straight pipes have different steady-state conveying characteristics (see Figures 5.7 and 5.8). In fact, from Figures 5.7 and 5.8, it can be seen that, to achieve a minimum pressure drop (for a given product mass flow rate) in a vertical pipe, a higher value of air mass flow rate is required (i.e. compared with a horizontal pipe). The reasons are:

- in the vertical pneumatic transport of fly ash, the weight of the solids is the most influential parameter; only at the very high air and particle velocities does the friction between the solids-air mixture and the pipe wall becomes significant;

- in horizontal pneumatic transport, however, the friction which is proportional to the air and particle velocities is always dominant; only at very low air/particle velocity does the friction due to the weight of the solids become an influential parameter.

Similar results also have been obtained by Rizk [48]. In his experiments, the test products are:

Styropor (spherical): d_p = 0.135, 2.38 and 5.65 mm

ρ_s = 1050 kg m^{-3}

Polysytrol-475K (Oval cylindrical):

d_p = 1.776, 2.56 and 3.15 mm

ρ_s = 1050 kg m^{-3}

Polysytrol-168N (Oval cylindrical):

d_p = 1.776, 2.56 and 3.15 mm

ρ_s = 1695 kg m^{-3}

5.7 Evaluation of Existing Correlations

Up to now, numerous experiments on different products have been carried out by researchers [2, 12, 21, 44, 54] in both horizontal and vertical straight pipes of different

length and diameter. Many empirical correlations have been set up for the prediction of pressure drop caused by vertical or horizontal straight pipe but based on certain products, pipe materials and conveying conditions. Therefore, still the general applicability of each correlation is limited. However, numerous designers still are interested in using the existing correlations for pneumatic conveying design, even though different products and/or conveying conditions may be involved.

In order to assist the designers to select the 'most accurate and reliable' correlation, some researchers [1, 38] have collected and analysed numerous experimental data of pressure drop in vertical and/or horizontal straight pipes and then have selected the 'best' correlation by evaluating several existing correlations or proposed a new generalised expression. For example, refer to Stegmaier [59] and Schade [51]. However, contradictory findings quite often are found in the literature (i.e. different investigators have obtained different 'best' correlations). Also, there is a large scatter between the predicted and experimental values of pressure drop (i.e. using the selected or generalised empirical correlations) [63, 75]. The main reason is that the influences of the conveyed materials and the limitations of the correlations have not been taken into account. This is confirmed by the following sections.

5.7.1 Existing Correlations

Equation (5.11) can be rewritten as:

$$\Delta p_S = \lambda_t \frac{\rho_{fm} V_{fm}^2}{2 D} \Delta L$$

where λ_t is the total friction factor in a straight pipe.

On calculating the total friction factor, λ_t, two basic models are used. Model A assumes that the air and solid contributions are additive and Model B assumes that the total friction factor, λ_t, is a multiple of the air friction factor, λ_f. Thus, for Model A the functional form of the correlation is:

$$\lambda_t = \lambda_f + \gamma \lambda_s \tag{5.13}$$

where γ is a constant.

For Model B, the functional form of the correlation is:

$$\lambda_t = \lambda_f (\theta + \omega)^n \tag{5.14}$$

where θ is a constant (usually equal to unity), n is an exponent which may be a function of the solid properties or the flow variable and ω is a function of solid properties and the flow variable.

The existing correlations evaluated in this study are based on both Models A and B and listed in Table 5.4.

It must be pointed out here that one may find in the literature other correlations, such as the ones by Koncheski et al. [27], Richardson et al. [47], Rose et al. [80] and so on. However, these correlations are excluded from the present study for one or more of the following reasons:

Table 5.4 Existing correlations for predicting pressure drop in straight pipes.

Investigator	Pipe Location*	Correlation
Dogin et al. [12]	H	$\lambda_t = \lambda_f + 6.6\times10^{-6}\ m^* \left(\frac{d_p}{D}\right)^{0.1} Re^{0.4}\ Fr_m^{-0.5}\ \frac{\rho_s}{\rho_{fm}}$
Hetsroni et al. [79]	H	$\lambda_t = \lambda_f + 8\times10^{-7}\ m^* \left(\frac{d_p}{D}\right)^{0.1} Re^{0.4}\ Fr_m^{-0.5}\ \frac{\rho_s}{\rho_{fm}}$
Hitchcock et al. [21]	H	$\lambda_t = \lambda_f + 0.003\ m^{*0.9}\ Fr_m^{-0.5} \left(\frac{d_p}{D}\right)^{-0.9}$
Pfeffer et al. 1 [44]	H	$\lambda_t = \lambda_f\ (1+m^*)^{0.3}$
Pfeffer et al. 2 [44]	H	$\lambda_t = \lambda_f\ (1+4.0\ Re^{-0.32}\ m^*)$
Pfeffer et al. 3 [44]	H	$\lambda_t = 7.6\ \lambda_f\ m^{*0.45}\ Re^{-0.21}$
Michaelides [37]	V & H	$\lambda_t = \lambda_f + 0.076\ \frac{m^*}{\sqrt{Fr_m}}$
Belden et. al. [2]	V	$\lambda_t = (1+m^*)\ [0.049+0.22\ \frac{m^*}{(1+m^*)^2}]\ Re^{-0.2}$
Richards et al. [46]	V	$\Delta p_s = (1+m^*)\ \rho_{fm}\ V_{fm}^2 + (1+m^*)\ g\ \Delta L\ (1+17.5\ \sqrt{\frac{D}{\Delta L}})\ \rho_{fm}$
Shimizu et al. [54]	V	$\lambda_t = \lambda_f\ (1+0.379\ m^*)$

* H - Horizontal, V - Vertical.

- they require knowledge of flow parameters, such as particle velocity;
- they only pertain to a very specific flow regime (e.g. slug-flow, dense-phase, etc.);
- the information provided is of a graphical nature.

5.7.2 Method and Result of Evaluation

The method used for evaluation is to find out how well a given correlation predicts pressure drop under the same conditions of particular experiments. Initially, all correlations are arranged to yield the pressure drop in straight pipes. A relative deviation of the experimental data and those predicted by the correlations is defined:

$$\hat{e}_i = \frac{\Delta p_{se} - \Delta p_{sc}}{\Delta p_{se}} \tag{5.15}$$

where Δp_{se} is the value observed in the experiment and Δp_{sc} is the value calculated by the correlation under the same conditions of the experiment.

From the relative deviation an average relative deviation e, an average absolute deviation |e| and a standard deviation σ of the error are obtained as follows:

$$e = \frac{1}{N} \sum_{i=1}^{N} \hat{e}_i$$

$$|e| = \frac{1}{N} \sum_{i=1}^{N} |\hat{e}_i|$$

$$\sigma = \sqrt{\frac{1}{N-1} \sum_{i=1}^{N} (\hat{e}_i - e)^2}$$

where N is the number of experimental data.

Using the experimental values of pressure drop due to conveying fly ash in straight pipes, SP1, SP2, SP3, SP4 and SP5 (see Table 5.2), Table 5.5 lists e, |e| and σ for all the correlations (see Table 5.4). Note that the correlations developed from horizontal straight pipes (e.g. the expressions proposed by Dogin et al. [12], Hetsroni et al. [79], Hitchcock et al. [21], Pfeffer et al. [44] and Michaelides [37]) are used for straight pipes, SP1, SP2, SP3 and SP4 and the correlations from vertical straight pipes (e.g. by Belden et al. [2], Richards et al. [46], Shimizu et al. [54] and Michaelides [37]) are used for straight pipe, SP5. Then the data from all four horizontal straight pipes are combined in one set of data and the correlations from horizontal straight pipes are compared with this large data bank. The results also are given in Table 5.5. Figures 5.10 and 5.11 show these results in graphical form for some of the 'better' correlations.

The standard deviation yields essentially the same information as the average absolute relative deviation. However, the standard deviation is biased mostly by the very high relative deviations (because of the squaring operation), while the average absolute relative deviation treats equally high or low relative deviations. For this reason the author places more importance on a low value of |e| rather than σ.

At this point, it must be emphasised that a good correlation is characterised by a value of e which is close to zero (no bias towards overpredicting or underpredicting) and low |e| which signifies that the absolute errors are not large. A low value of σ will ensure that the spread of the deviations from their mean value is not high and this may account for the consistency of a correlation.

Table 5.5 Values of e, |e| and σ for the existing correlations.

No.	Correlation		SP1	SP2	SP3	SP4	SP5	All H Data (SP1-SP4)*
1	Dogin	e	-8.1521	-5.5976	-6.6537	-9.2960	-	-7.4583
		|e|	8.1521	5.5976	6.6537	9.2960	-	7.4583
		σ	3.7455	2.2291	1.8816	1.5486	-	2.8373
2	Hetsroni	e	-0.1828	-0.0587	-0.1565	-1.3596	-	-0.4663
		|e|	0.4261	0.3289	0.2864	1.3596	-	0.6240
		σ	0.5535	0.3947	0.3161	0.3519	-	0.6861
3	Hitchcock	e	-90.4925	-61.0553	-79.7896	-91.8994	-	-80.7891
		|e|	90.4925	61.0553	79.7896	91.8994	-	80.7891
		σ	33.1219	17.8355	16.6466	16.0528	-	24.9947
4	Pfeffer 1	e	0.8816	0.7787	0.8221	0.2870	-	0.6787
		|e|	0.8816	0.7787	0.8221	0.3402	-	0.6932
		σ	0.1914	0.1600	0.1037	0.2901	-	0.3153
5	Pfeffer 2	e	0.6635	0.6211	0.7502	0.3109	-	0.5761
		|e|	0.6635	0.6211	0.7502	0.314	-	0.5770
		σ	0.1532	0.1155	0.0711	0.1694	-	0.2154

Continuation of Table 5.5

No.	Correlation		SP1	SP2	SP3	SP4	SP5	All H Data (SP1-SP4)*
6	Pfeffer 3	e	0.8271	0.7364	0.8033	0.4111	-	0.6844
		|e|	0.8271	0.7364	0.8033	0.4111	-	0.6844
		σ	0.1676	0.1424	0.0844	0.1634	-	0.2232
7	Michaelides	e	-1.9015	-1.4943	-1.0781	-2.9908	0.1353	-1.9043
		|e|	1.9307	1.5279	1.0781	2.9908	0.3468	1.9199
		σ	1.0523	0.7271	0.4231	0.7742	0.4112	1.0578
8	Belden	e	-	-	-	-	0.7328	-
		|e|	-	-	-	-	0.7328	-
		σ	-	-	-	-	0.1836	-
9	Richards	e	-	-	-	-	-1.6620	-
		|e|	-	-	-	-	1.6220	-
		σ	-	-	-	-	0.3816	-
10	Shimizu	e	-	-	-	-	0.6593	-
		|e|	-	-	-	-	0.6603	-
		σ	-	-	-	-	0.2081	-

* All data of four horizontal straight pipes.

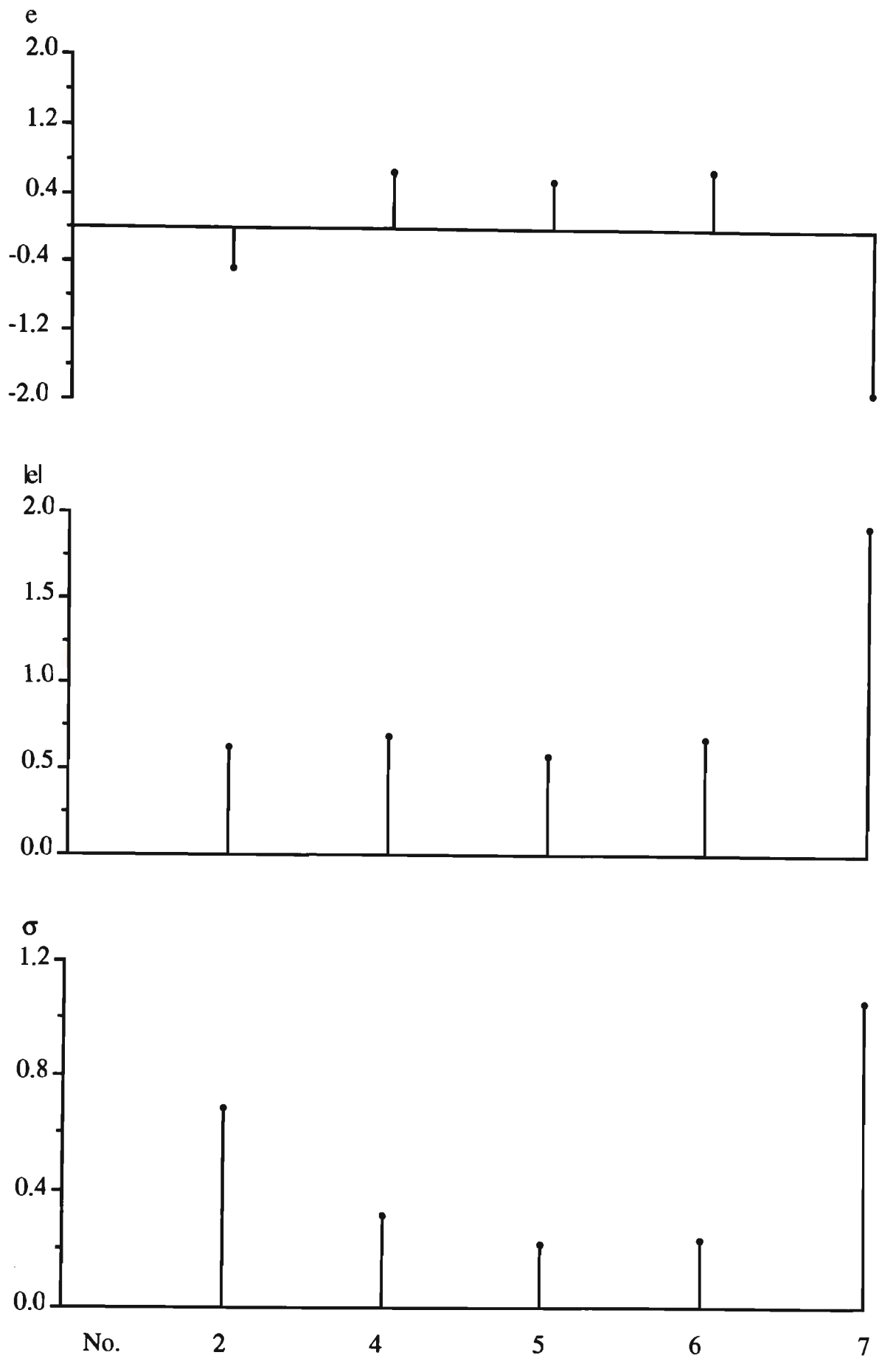

Figure 5. 10 Graphical representation of results for all horizontal straight pipe data.

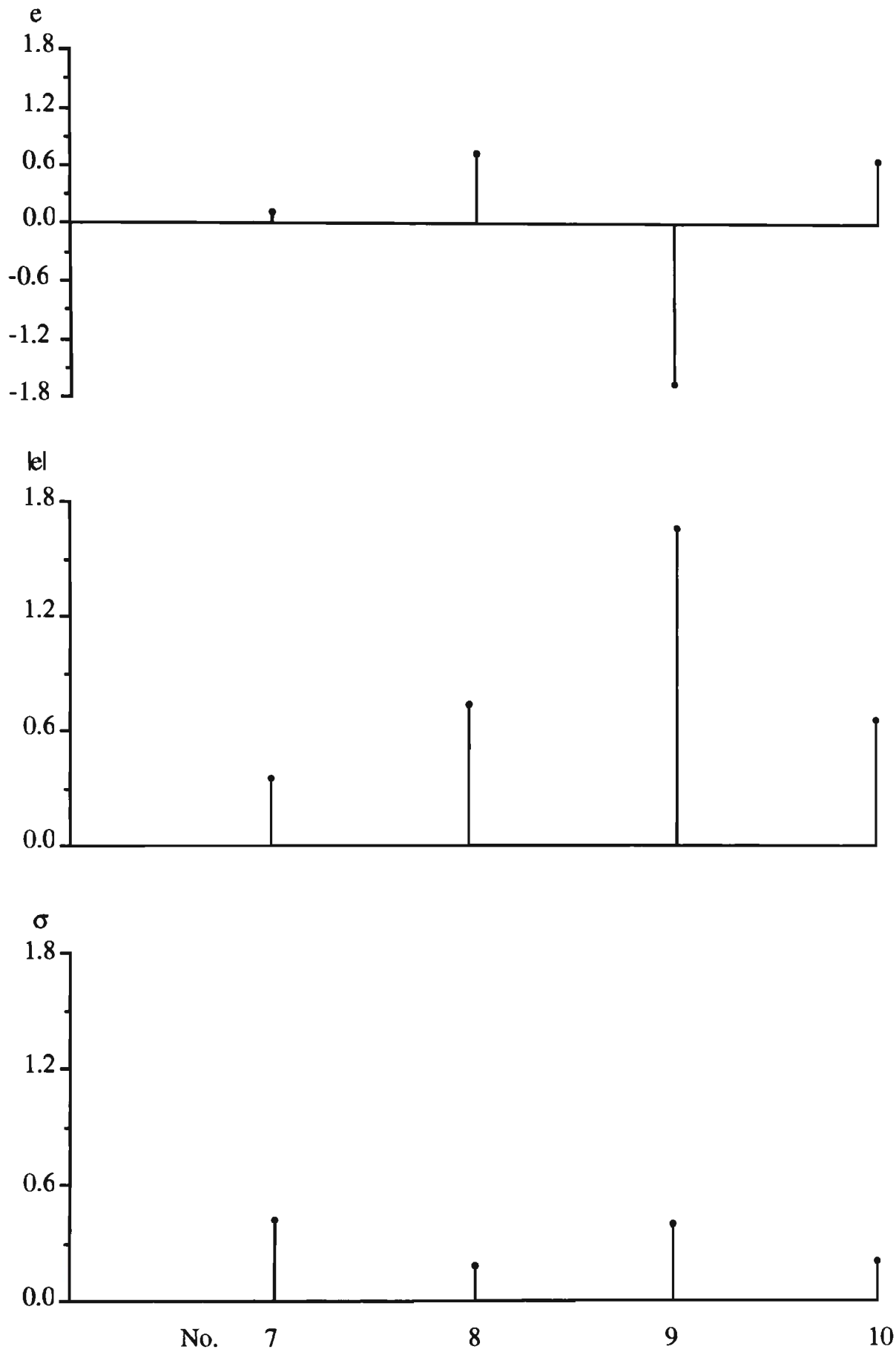

Figure 5.11 Graphical representation of results for vertical straight pipe data.

It is apparent from the results given in Table 5.5, Figures 5.10 and 5.11 that, for fly ash, the expression proposed by Michaelides [37] is the 'best' for the vertical straight pipes and the expression proposed by Hetsroni et al. [79] for the horizontal straight pipes. Figure 5.12 shows the predictions by Hetsroni's and Michaelides's expressions. When compared with the results in Figure 5.6, high scatter is evident. Usually, a pneumatic conveying pipeline comprises many straight sections of pipe connected by bends. During the prediction of total pipeline air pressure drop, the accumulation of errors by these expressions may be very high (discussed later in Chapter 7). Also, for all the above selected correlations, it is clear that, when $m_f \rightarrow 0$, $\Delta p_s \rightarrow 0$, as shown in Figures 5.13 and 5.14.

Comparing Figure 5.13 with Figure 5.7 (b) and Figure 5.14 with Figure 5.8 (b), significant differences can be seen clearly.

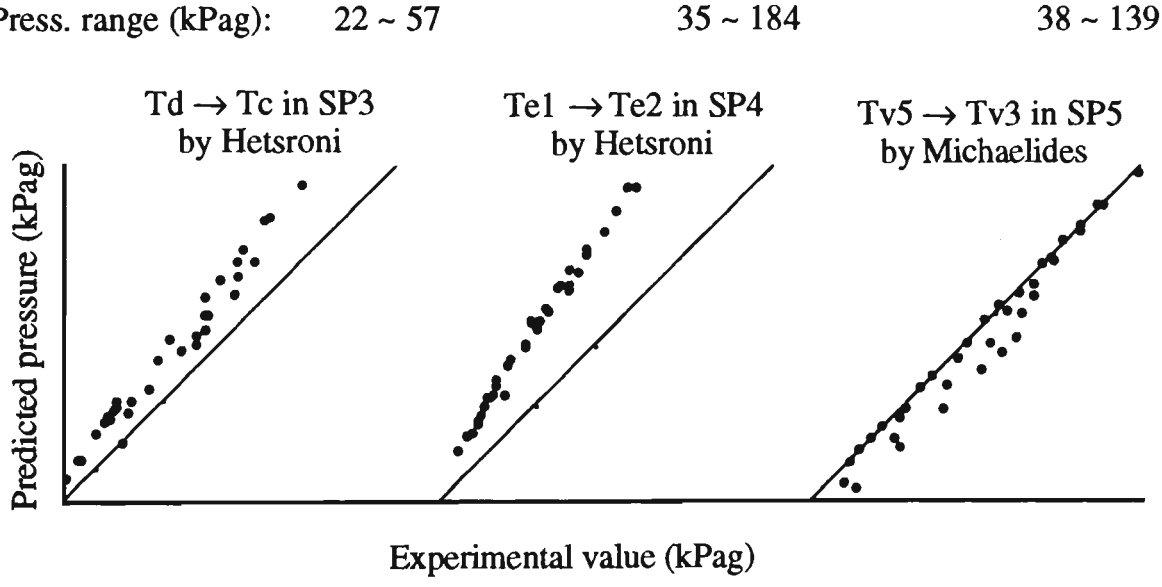

Figure 5.12 Predicted pressure vs experimental value along horizontal and vertical straight pipes

(Note: Tc → Td means the predicted pressure at Td, starting from Tc).

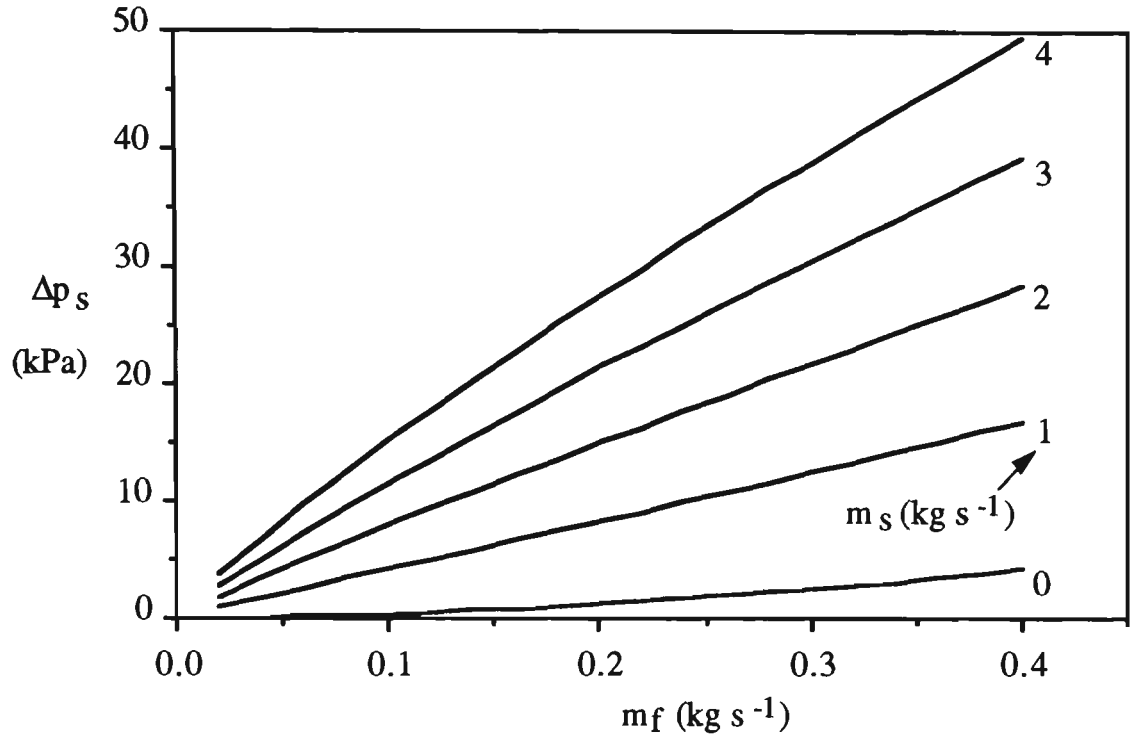

Figure 5.13 Steady-state conveying characteristics of a horizontal straight pipe (ΔL=20 m, D=80.5 mm, ρ_{fe}=2.39 kg m^{-3}) by Hetsroni et al. [79].

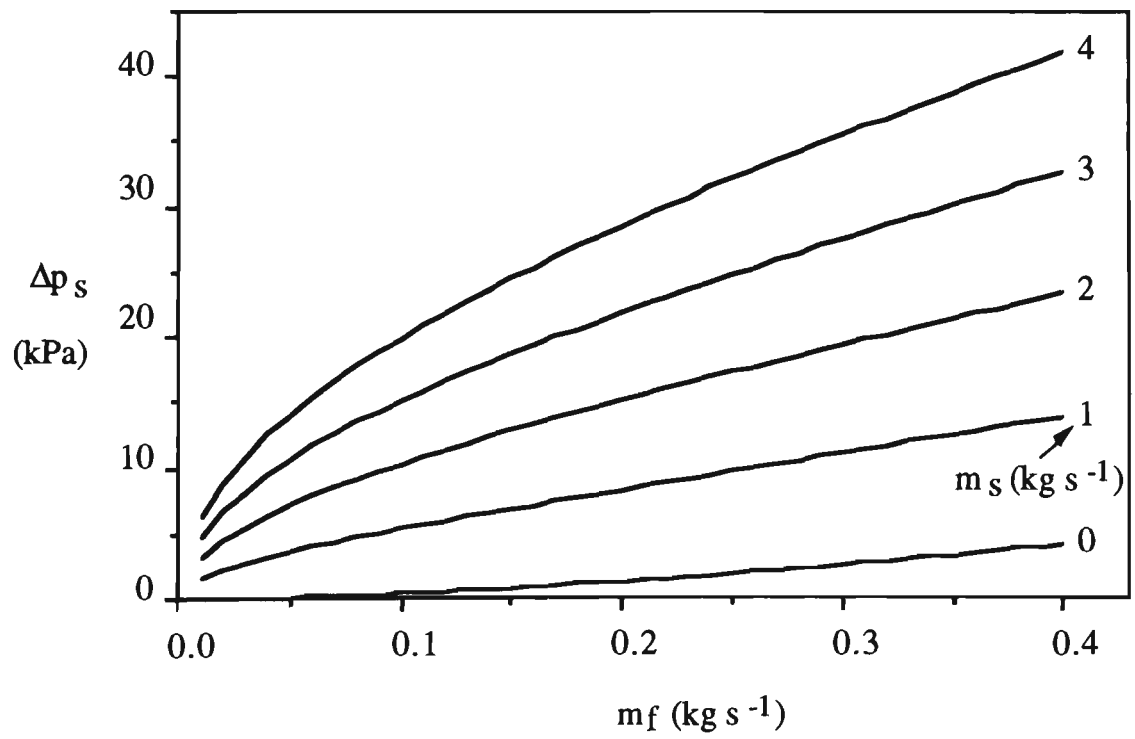

Figure 5.14 Steady-state conveying characteristics of a vertical straight pipe (ΔL=20 m, D=80.5 mm, ρ_{fe}=2.39 kg m^{-3}) by Michaelides [37].

CHAPTER 6

PRESSURE DROP DUE TO SOLIDS-AIR MIXTURE THROUGH BENDS

6.1 Introduction

Due to their ease of use and installation, bends are a common feature in pneumatic conveying pipelines. However, bends also may have a significant influence on the total pressure drop of a particular pipeline system. To predict accurately the total pipeline air pressure drop, it is important to determine the pressure drop caused by bends at different locations.

The flow of the solids-air mixture through a bend is significantly more complicated than through a straight section of pipe. Chapter 4 has shown the complex nature of flow around a bend, even for air-only conditions. However, the pressure drop caused by a bend still can be considered as a function of several variables, such as bend geometry (e.g. pipe diameter, bend radius), particle characteristics (e.g. particle size, size distribution, density, shape and moisture content), bend location (e.g. air density, velocity at the outlet of the bend), conveying conditions (e.g. product and air mass flow rates) and a relationship between particles and the pipe wall (e.g. wall friction).

Although the exact calculation of the pressure drop in the bend is highly complex, considerable research has been undertaken theoretically and empirically, especially for bends of different radius [3, 6, 7, 8, 10, 16, 18, 22, 26, 28, 31, 32, 35, 42, 45, 52, 53, 55, 61, 66]. However, the theoretical analysis is based on assumptions that the particles are coarse, rigid, of uniform size and are conveyed in very dilute-phase (e.g. $m^* \leq 5.3$ [16]). Also, the theoretical method requires knowledge of the fraction of particles sliding along and impacting against the bend wall, as well as, the particle velocities at the entrance and exit of the bend. Properties such as the coefficient of

restitution and particle drag coefficient also must be known. All these factors limit the applicability of the theoretical approach, especially when having to analyse small, irregular-shaped and/or mixed-size particles.

As far as the empirical approaches are concerned, contradictory results quite often are found in the literature. For example, some advocate that short radius bends exhibit low pressure loss [7, 32], whilst others claim the opposite [42, 52, 66], whereas some also conclude that there exists an optimal ratio of bend radius to pipe diameter [40, 53]. Some possible explanations for these discrepancies are that researchers have

- tested pipelines comprising different radius bends and derived conclusions based on only the total pipeline air pressure drop [40, 53] (i.e. the pressure drop caused by a bend is dependent on its location; also, bends of different radii produce different pressure profiles along a pipeline; hence, they are subjected to different operating conditions and cannot be compared on the same basis), or

- used two long straight pipes connected to the test bend and based their conclusions on the direct measurements of bend pressure drop [7, 32, 42, 52, 66]. This is explained further below.

The pressure drop caused by a bend is defined as the sum of two components [4, 6, 28]. One component is located in the bend itself and the other occurs in the straight section of pipe immediately downstream from the bend for the re-acceleration of the particles. Therefore, the pressure drop caused by a bend cannot be measured directly. Its determination should be based on the pressures acting along the two

long straight sections of pipe. Compared with the pressure along the connecting straight sections of pipe, bend pressure drop is low. Hence, a small fluctuation in pressure along the two long straight sections of pipe is expected to have a great influence on the values of bend pressure drop. Therefore, it is difficult to obtain exact values of bend pressure drop. Also, it is inaccurate to determine the exponents in the empirical correlations by using such experimental data. Therefore, it is believed that these existing empirical correlations and techniques cannot predict accurately the pressure drop caused by bends at different locations.

In this chapter, four different radius bends (viz. R=100, 254, 450 & 1000 mm) and one blinded-tee bend connected by two long straight sections of pipe (D=52.5 mm ID) are tested with fly ash over a wide range of conveying conditions (see Chapter 3). The detailed mathematical and dimensional analyses are carried out and a semi-empirical correlation is set up. The exponents in the semi-empirical correlation are determined by minimising the sum of the squared errors of pressure along the upstream straight section of pipe, starting at a point of known pressure in the downstream pipe. This correlation then is used to predict the pressure drop caused by bends at different locations. The results show that this correlation is reliable and accurate. Also, one of the conclusions in this work is that longer radius bends produce a lower pressure drop.

6.2 Mathematical Analysis

When the solids-air mixture enters a bend, the bend causes flow separation (see Figure 6.1) due to the high inertia of the solid particles. This results in the particles impinging on the outer side of the bend and sliding along the outside wall of the

bend. Friction between the particles and the wall slows down the particles considerably, which then have to be accelerated back to their original velocity once the bend has been passed. Thus, the pressure drop occurs not only in the bend itself, but also behind it, mainly due to re-acceleration [4, 28].

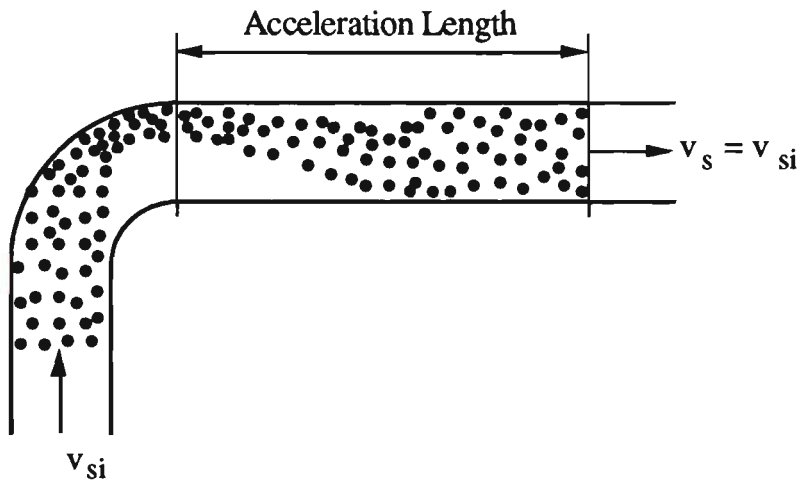

Figure 6.1 Deceleration and re-acceleration of solids due to a bend.

6.2.1 Flow through Bend

To derive the necessary correlations, the following assumptions [28] are adopted:

- The elemental section R dϕ is considered as a short straight pipe.

- All particles slide along the outside wall of the bend.

The forces acting on the particles are shown in Figure 6.2.

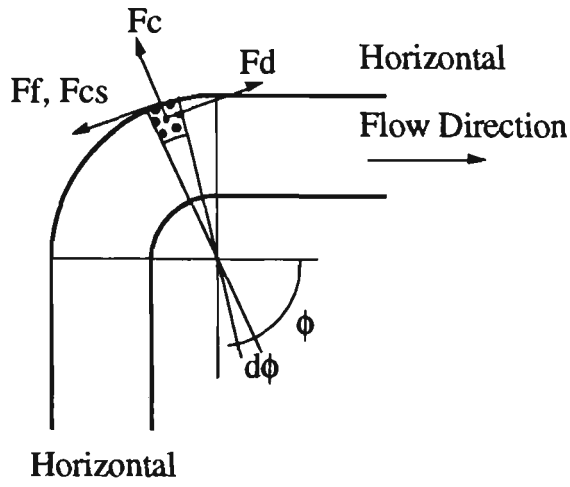

Figure 6.2 Forces acting on sliding particles in a horizontal-horizontal bend.

a) Drag force, F_d

This force, designated as F_d, is due to drag and produced by the conveying air. It maintains the motion of the particles.

b) Centrifugal force, F_c

$$F_c = \rho_d A R d\phi \frac{v_s^2}{R} = (1-\varepsilon) \rho_s A v_s^2 d\phi$$

c) Frictional forces, F_f and F_{cs}

For the air:

$$\tau_f = \frac{\lambda_f}{4} \rho_f \frac{v_f^2}{2}$$

$$F_f = \tau_f P_{wf} R d\phi = \frac{\lambda_f}{4} \rho_f \frac{v_f^2}{2} P_{wf} R d\phi$$

$$P_{wf} = \xi \pi D \qquad 0 \le \xi \le 1$$

$$F_f = \frac{\lambda_f}{4} \rho_f \frac{v_f^2}{2} \xi \pi D R \, d\phi$$

For the solids:

$$F_{cs} = F_c \upsilon = (1-\varepsilon) \rho_s A v_s^2 \upsilon \, d\phi$$

Using the Euler Momentum Equation

For the air:

$$A \, dp_b - m_f \, dv_f - \frac{\lambda_f}{4} \rho_f \frac{v_f^2}{2} \xi \pi D R \, d\phi - F_d = 0$$

For the solids:

$$F_d - m_s \, dv_s - (1-\varepsilon) \rho_s A v_s^2 \upsilon \, d\phi = 0$$

These two equations are added and then divided by A:

$$dp_b - \varepsilon \rho_f v_f \, dv_f - (1-\varepsilon) \rho_s v_s \, dv_s - \lambda_f \rho_f \frac{v_f^2}{2 D} \xi R \, d\phi$$

$$- (1-\varepsilon) \rho_s v_s^2 \upsilon \, d\phi = 0$$

Denoting the velocity ratio of solid-to-air as:

$$\eta = \frac{v_s}{v_f}$$

Then: $dv_s = \eta\, dv_f$

$$dp_b - (1+m^*\eta)\,\varepsilon\,\rho_f\,v_f\,dv_f - \xi\,\lambda_f\,\rho_f\,v_f^2\frac{R\,d\phi}{2\,D} - (1-\varepsilon)\,\rho_s\,v_s^2\,\upsilon\,d\phi = 0$$

Under isothermal conditions: $-\frac{dp_b}{p_b} = \frac{dv_f}{v_f}$

$$dp_b + (1+m^*\eta)\frac{\varepsilon\,v_f^2}{R_a\,T}\,dp_b - \xi\,\lambda_f\,\rho_f\,v_f^2\frac{R\,d\phi}{2\,D} - (1-\varepsilon)\,\rho_s\,v_s^2\,\upsilon\,d\phi = 0$$

Note: $(1-\varepsilon) \approx \frac{m^*\,\rho_f}{\rho_s\,\eta}$

$$dp_b = \frac{\xi\,\lambda_f\frac{\rho_f\,v_f^2}{2\,D} + \eta\;m^*\,\rho_f\,v_f^2\,\frac{\upsilon}{R}}{1 + (1+m^*\eta)\,\frac{\varepsilon\,v_f^2}{R_a\,T}}\,R\,d\phi$$

$$\therefore \quad \Delta p_{b1} = \int_{p_{bo}}^{p_{be}} dp_b$$

$$= \int_0^{\frac{\pi}{2}} \frac{\xi\,\lambda_f + 2\,D\,\eta\;m^*\,\frac{\upsilon}{R}}{1 + (1+m^*\eta)\,\frac{\varepsilon\,v_f^2}{R_a\,T}}\,\frac{\rho_f\,v_f^2}{2\,D}\,R\,d\phi \qquad (6.1)$$

Also, the superficial air velocity is used to replace the actual air velocity.

$$v_f = \frac{m_f}{\rho_f\,\varepsilon\,A} = \frac{V_f}{\varepsilon} \qquad (6.2)$$

Substituting Equation (6.2) into Equation (6.1) results in:

$$\Delta p_{b1} = \int_0^{\frac{\pi}{2}} \frac{\frac{\xi}{\varepsilon^2}\lambda_f + 2\,D\,\eta\,m^*\,\frac{\upsilon}{\varepsilon^2 R}}{1 + (1+m^*\,\eta)\,\frac{V_f^2}{\varepsilon\,R_a\,T}} \rho_f \frac{V_f^2}{2\,D} R\,d\phi \qquad (6.3)$$

6.2.2 Flow after Bend - Reacceleration

The particles, after leaving the bend, are re-accelerated by the conveying air to the same velocity with which they entered the bend. Using the impulse theorem results in [28]:

$$\Delta p_{b2} = \frac{m_s}{A}(v_\infty - v_{so})$$

$$\therefore \qquad \Delta p_b = \Delta p_{b1} + \Delta p_{b2}$$

However, as ε, ξ and η are functions of m* and the particle properties, they are difficult to determine, especially for small, irregular-shaped and mixed-size particles. Hence, it is not easy to integrate Equation (6.3). Also, it is very difficult to obtain the particle velocity at the outlet of bend, v_{so}. Therefore, it is assumed that the pressure drop occurring in the bend and for the solid re-acceleration is all in the bend [4, 28].

It has been shown [6, 42, 55, 58, 61, 66, 69] that, the pressure drop due to the solids-air mixture is correlated best when expressed as the sum of two functions. The first

function represents the loss due to air alone and the second is related to the loss due to solids. Therefore, it is assumed that:

$$\Delta p_b = (\zeta_f + m^* \zeta_s) \frac{\rho_{fo} V_{fo}^2}{2} \tag{6.4}$$

6.3 Dimensional Analysis

The formulae for calculating ζ_f have been obtained already in Chapter 4. This section mainly sets up formulae for calculating ζ_s.

The pressure drop due to solids through a bend Δp_{bs} can be considered as a function of many pertinent variables, such as superficial air velocity V_{fo} and density ρ_{fo} at the outlet of the bend, pipe diameter D, bend radius R, air viscosity μ, pipe roughness ε, product mass flow rate m_s, particle density ρ_s, mean particle diameter d_p, particle shape factor z and friction coefficient between pipe wall and particle υ. For a given product and pipe material, d_p, z, ρ_s and υ are constant. By using the dimensional analysis [43], an expression of the form given in Equation (6.5) is considered initially.

$$\Delta p_{bs} = k\, V_{fo}^a\, \rho_{fo}^b\, D^c\, R^e\, \mu^f\, \varepsilon^h\, m_s^i \tag{6.5}$$

With the aid of dimensional analysis, an expression similar to Equation (4.7) or (5.8) is obtained:

$$\Delta p_{bs} = k \left(\frac{\mu}{\rho_{fo} V_{fo} D}\right)^f \left(\frac{\varepsilon}{D}\right)^h \left(\frac{R}{D}\right)^e \left(\frac{m_s}{\rho_{fo} V_{fo} D^2}\right)^i \rho_{fo} V_{fo}^2$$

(6.6)

Comparing Equations (6.4) and (6.6) results:

$$\zeta_S = 2\,k\,(\frac{\pi}{4})^i\,Re^f\,(\frac{\varepsilon}{D})^h\,(\frac{R}{D})^e\,m^{*i-1}$$

$$= 2\,k\,(\frac{\pi}{4})^i\,m^{*i-1}\,V_{fo}^{-f}\,\rho_{fo}^{-f}\,(\frac{\mu}{D})^f\,(\frac{\varepsilon}{D})^h\,(\frac{R}{D})^e$$

For a given pipe material and conveying air temperature, μ and ε can be assumed constant. Also, k may be a function of m^*, V_{fo}, ρ_{fo}, D and R.

$$\therefore \qquad \zeta_S = \Phi(m^*,\ V_{fo},\ \rho_{fo},\ D,\ R)$$

then ζ_S is assumed:

$$\zeta_S = y1\ m^{*y2}\ Fr_o^{y3}\ (\frac{R}{D})^{y4} \qquad (6.7)$$

6.4 Determination of Exponents in Equation (6.7)

As mentioned in Chapter 5, the conveyed materials have numerous influences on pressure drop. So the exponents in the empirical correlations such as Equation (6.7) should be determined empirically and are valid only for a given product [45, 63].

Usually, for a given product the determination of the exponents in Equation (6.7) is based on the experimental data of pressure drop caused by the bend [6, 7, 8, 42, 45, 52, 66]. However, the pressure drop caused by a bend is defined as the sum of two components. One component is located in the bend itself. The remainder occurs in

the straight section of pipe immediately downstream from the bend for the re-acceleration of particles. Hence, bend pressure drop cannot be measured directly. Therefore, the method shown in Figure 6.3, the so-called traditional method, is used commonly to determine bend pressure drop [6, 7, 8, 42, 45, 52, 66]. The step change in pressure is considered equivalent to the loss caused by the bend. Note that Figure 6.3 is the same as Figure 2.1 and repeated here for convenience.

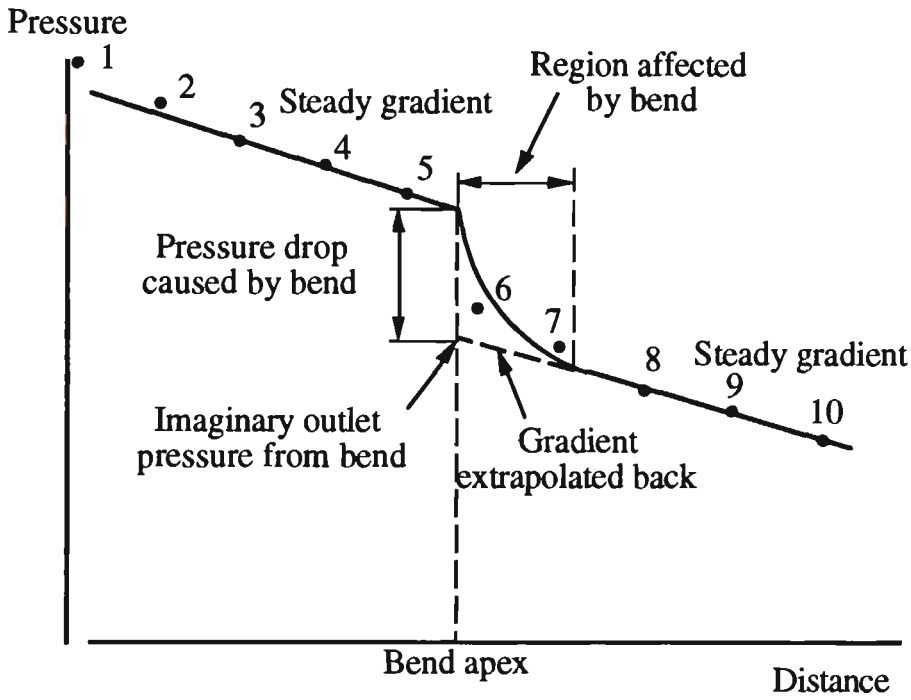

Figure 6.3 Traditional method used to determine pressure drop caused by bend.

However, it has been shown clearly in Chapters 4 and 5 that the pressure gradient at any point along a straight section of pipe is not constant. Also, compared to the static pressure along the straight sections of pipe such as at points 1-10, bend pressure

drop is low. Hence, a small fluctuation in pressure at points 3, 4, 5, 8, 9 or 10 is expected to have a great influence on the values of bend pressure drop. An example is given in Table 6.1, which shows that a ±1.81% change in static pressure can result in a ±62.8% change in bend pressure drop (i.e. based on the traditional method).

In experiments, the instruments used to measure the pressure along the pipeline always have measuring and/or reading errors which easily could accumulate to a value of ±1.81%. Therefore, it is difficult to obtain exact values of bend pressure drop. Hence, it is inaccurate to base the determination of exponents in the empirical correlations on the 'incorrect' experimental data of bend pressure drop.

To minimise the effect of this small influence of pressure fluctuation along the two long straight sections of pipe, the exponents in Equation (6.7) are determined by minimising the sum of the squared errors of pressure along the upstream straight section of pipe (e.g. at points 3, 4 and 5), starting at a point (e.g. point 8, 9 or 10) of known pressure in the downstream pipe (see Figure 3.2 and Table 3.6). The pressure drop caused by the straight section of pipe is calculated individually (e.g. by using the equations developed in Chapter 5) and the conditions occurring at the outlet of the bend are used to determine the bend pressure drop. Note that these outlet conditions are the 'effective' conditions as determined by the straight pipeline analysis (i.e. for the section of pipe downstream of the bend).

Based on the experimental data of pressure along the two straight sections of pipe upstream and downstream of the different radius test bends (e.g. R=100, 254, 450 and 1000 mm) for conveying fly ash (see Table 3.6), the determined values of exponent in Equation (6.7) are listed in Table 6.2.

Table 6.1: Different bend pressure drops obtained by using the traditional method.

Conveyed material: fly ash, m_s =1.573 kg s^{-1}, m_f =0.0335 kg s^{-1}, R=254 mm						
Transducer Ch.	3	4	5	8	9	10
Pressure p (kPag)	59.602	57.863	**55.156**	46.868	44.720	42.635
Distance s (m) from Point A or B (see Figure 3.2)	11.016	15.016	19.016	10.946	14.946	18.946
Relationship between p and s	p = 65.885 - 0.55575 s			p = 52.649- 0.52912 s		
Length (m)	20.792			20.622		
Δp_b (kPa)	Δp_b = 65.885 - 0.55575 × 20.792 - 52.649 = 1.681					
Pressure p (kPag)	59.602	57.863	**56.156**	46.868	44.720	42.635
Relationship between p and s	p = 64.342 - 0.43075 s			p = 52.649- 0.52912 s		
Δp_b (kPa)	Δp_b = 64.342 - 0.43075 × 20.792 - 52.649 = 2.737					
Relative deviation	For ch. 5 = $\frac{56.156-55.156}{55.156}$ 100% = 1.81% For bend pressure drop = $\frac{2.737-1.681}{1.681}$ 100% = 62.82%					
Pressure p (kPag)	59.602	57.863	**54.156**	46.868	44.720	42.635
Relationship between p and s	p = 67.429 - 0.68075 s			p = 52.649- 0.52912 s		
Δp_b (kPa)	Δp_b = 67.429-0.68075 × 20.792 - 52.649 = 0.626					
Relative deviation	For ch. 5 = $\frac{54.156-55.156}{55.156}$ 100% = -1.81% For bend pressure drop = $\frac{0.626-1.681}{1.681}$ 100% = -62.76%					

Table 6.2: Values of exponent for bend.

Exponent	Radius bend	Blinded-tee bend
y1	0.0052	0.0148
y2	0.4900	0.4683
y3	1.1182	1.1457
y4	-0.1286	-

However, no correlation has been found useful in predicting the air-only pressure drop through the blinded-tee bend. Therefore, the following equations are used directly to predict the pressure drop due to the solids-air mixture through the blinded-tee bend.

$$\Delta p_b = m^* \zeta_s \frac{\rho_{fo} V_{fo}^2}{2}$$

$$\zeta_s = y1\ m^{*y2}\ F_{ro}^{y3} \tag{6.8}$$

The determined values of exponent in Equation (6.8) also are listed in Table 6.2.

6.5 Steady-State Conveying Characteristics of Bend

By using the above 'determined' values of exponent, the steady-state conveying characteristics of bend for conveying fly ash are predicted. For example, refer to Figure 6.4, which clearly shows that the bend has significantly different pressure drops at different locations. Also, as $m_f \rightarrow 0$, $\Delta p_b \rightarrow 0$, which is agrees with the results obtained by other researchers [6, 42, 52, 66].

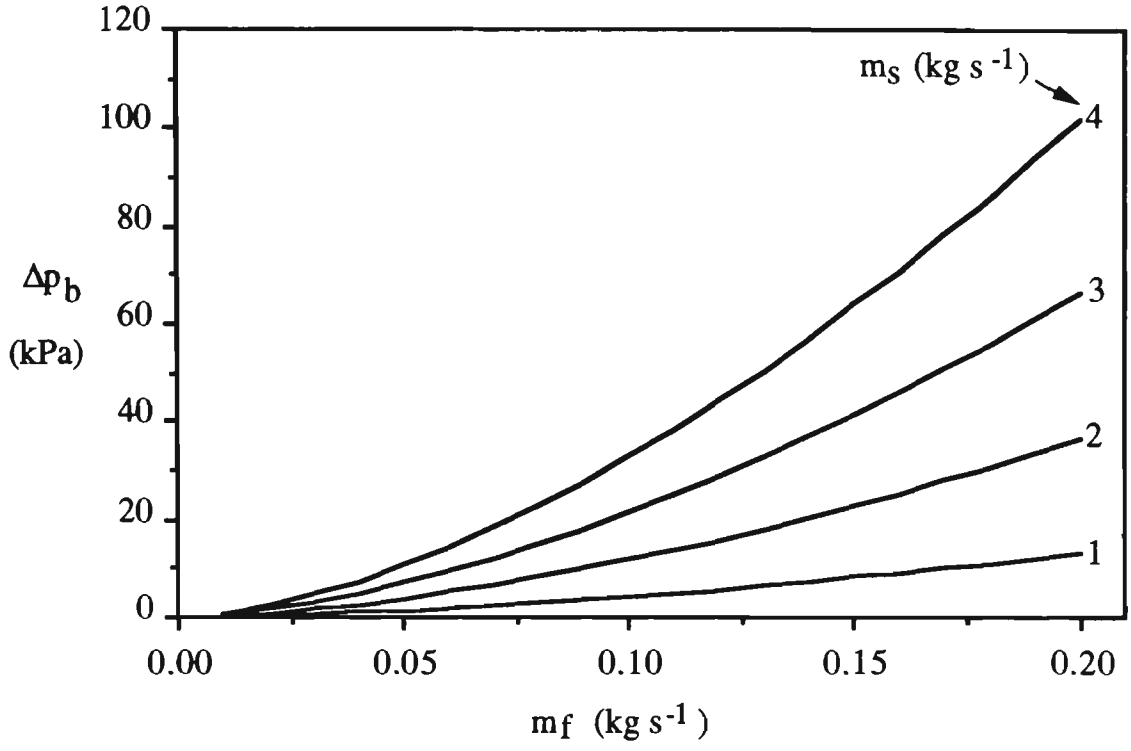

(a) ρ_{fo} = 1.8 (kg m^{-3}).

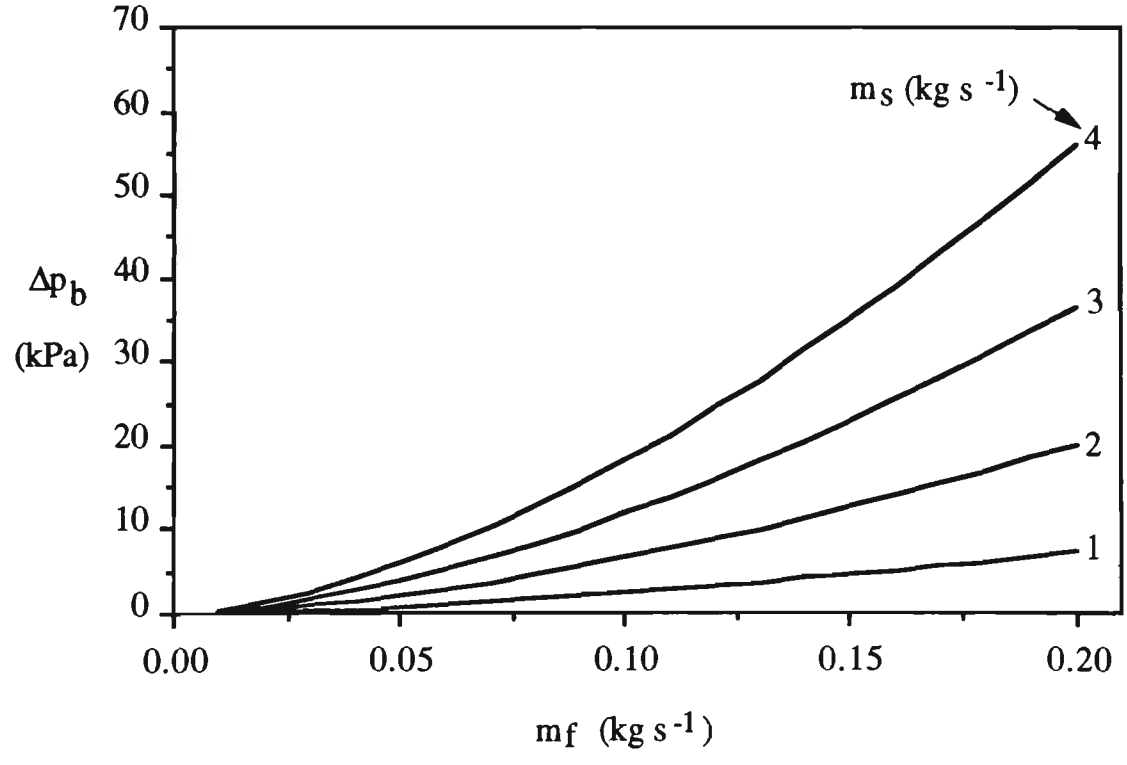

(b) ρ_{fo} = 2.39 (kg m^{-3}).

Figure 6.4 Steady-state conveying characteristics of R=254 mm bend (D=52.5 mm) at different locations.

6.6 Pressure Drop Caused by Different Geometry Bends

Also, by using the above 'determined' values of exponent, the pressure drop caused by the bends of different radius and the blinded-tee bend for conveying fly ash at different locations are predicted, as shown in Figure 6.5.

From Figure 6.5, it is evident that longer radius bends produce a lower pressure drop and the blinded-tee bend causes much higher pressure drops than radius bends. However, at high product to air mass flow ratios, m*, the bends of different radius nearly cause the same pressure drop. The reason is that:

when the particles pass a horizontal-horizontal radius 90° bend, the relationship between the velocities of the particle at the inlet and outlet of the bend is [18]:

$$v_{so} = v_{si}\, e^{(-\upsilon \frac{\pi}{2})}$$

The above equation shows that the radius of the bend has no effect on velocity losses for bends in the horizontal plane.

However, the centrifugal force acting on the particles is a function of the bend radius, as given by:

$$F_c = m \frac{v_s^2}{R}$$

The corresponding frictional force is:

$$F_{cs} = F_c\, \upsilon = m \frac{v_s^2}{R} \upsilon$$

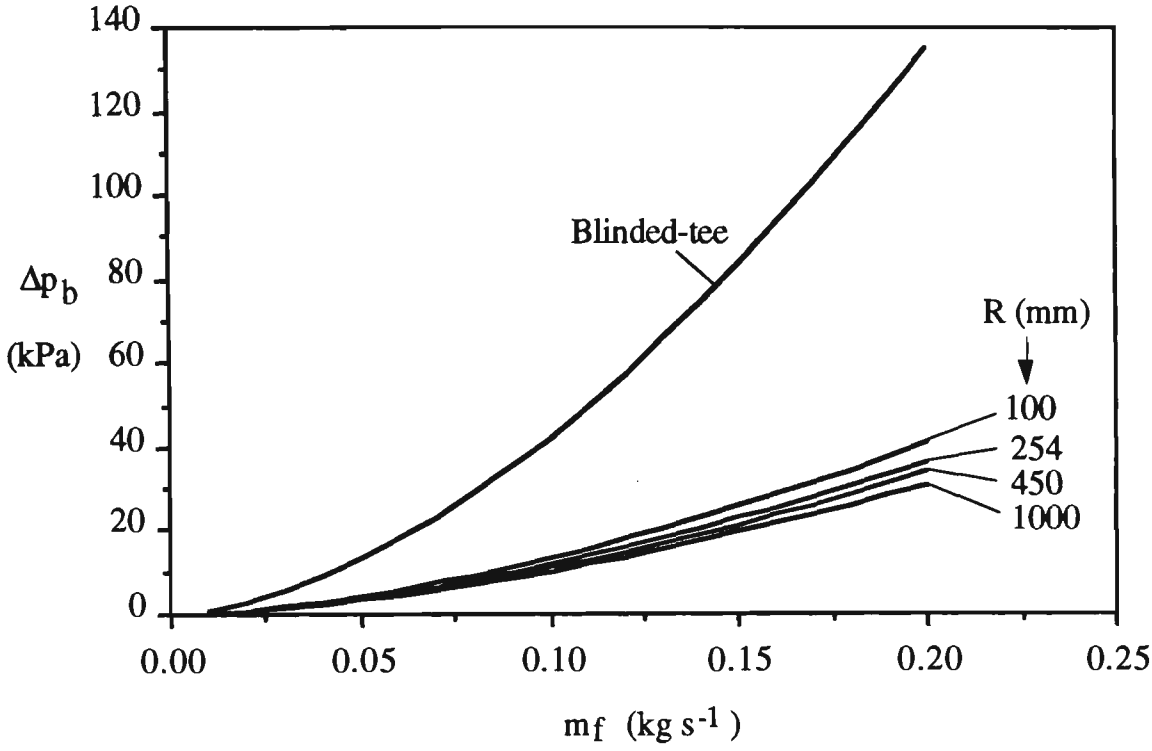

(a) $\rho_{fo} = 1.8$ (kg m^{-3}).

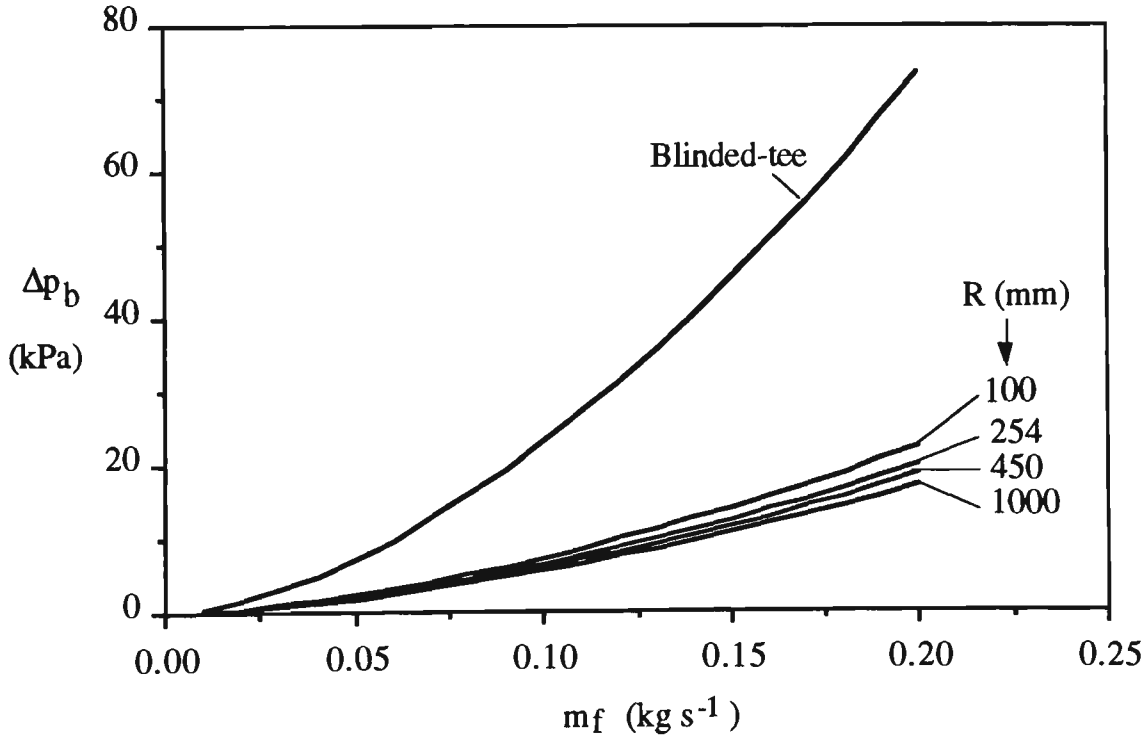

(b) $\rho_{fo} = 2.39$ (kg m^{-3}).

Figure 6.5 Pressure drop caused by different radius bends and blinded-tee bend at different locations (D=52.5 mm, m_S=2.0 kg s^{-1}).

As mentioned previously, the pressure drop caused by a bend is the sum of two components. One component is located in the bend itself. The remainder occurs in the straight section of pipe immediately downstream of the bend for the re-acceleration of the particles. For the same v_{so}, bends of different radii will cause the same pressure drop for the re-acceleration of the particles. However, the frictional force hindering the motion of the particles is inversely proportional to the bend radius. Therefore, there is a higher frictional force acting on the particles in the shorter radius bends, which results in the higher pressure drop.

At high product to air mass flow ratios, particle velocity is low. Therefore, the influence of the bend radius on the frictional force is not great. Hence, the bends of different radius cause nearly the same pressure drop.

Also, from Figure 6.5, it is possible that a short radius bend could cause a lower pressure drop than a long radius bend, if the two bends are at different locations along the same pipeline. Hence, as the bends of different geometry would produce different pressure profiles along a pipeline, they should be compared on the basis of total pipeline air pressure drop. Figure 6.6 illustrates a pipeline comprising a number of bends (e.g. seven bends) which have the same size and at any one time the same geometry. Five different bend geometries (blinded-tee, R=100, 254, 450 and 1000 mm) are considered and compared for this purpose. Note that the correlations for straight pipes in Chapter 5 are suitable for long straight pipes where particles can be fully accelerated. Hence, the distance between any two bends is long (e.g. equal to 20m in Figure 6.6). By using the above determined correlations for bends and straight pipes, the total pipeline air pressure drop is predicted for conveying fly ash, as shown in Figure 6.7.

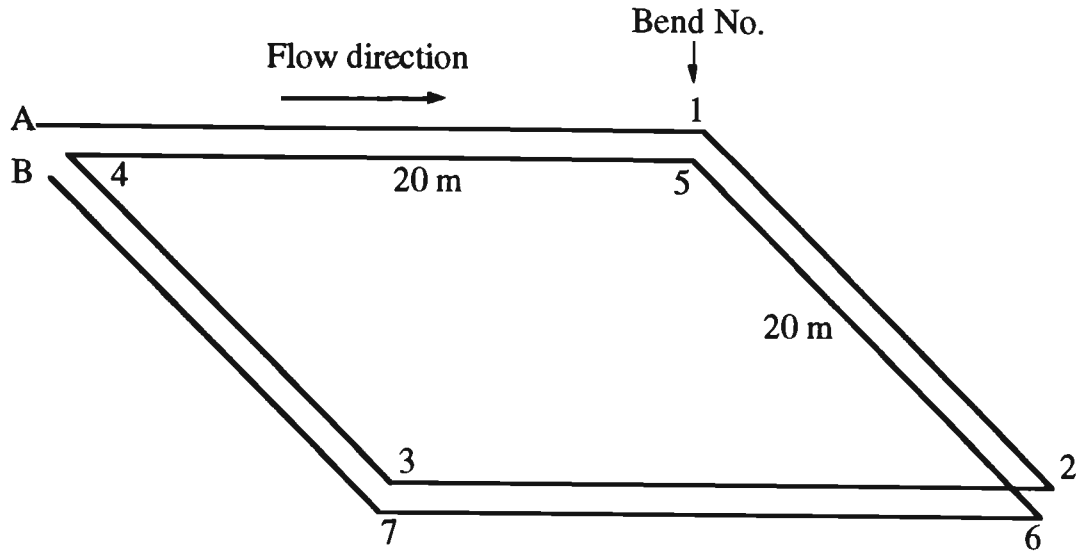

Figure 6.6 Pipeline comprising bends and long straight pipes.

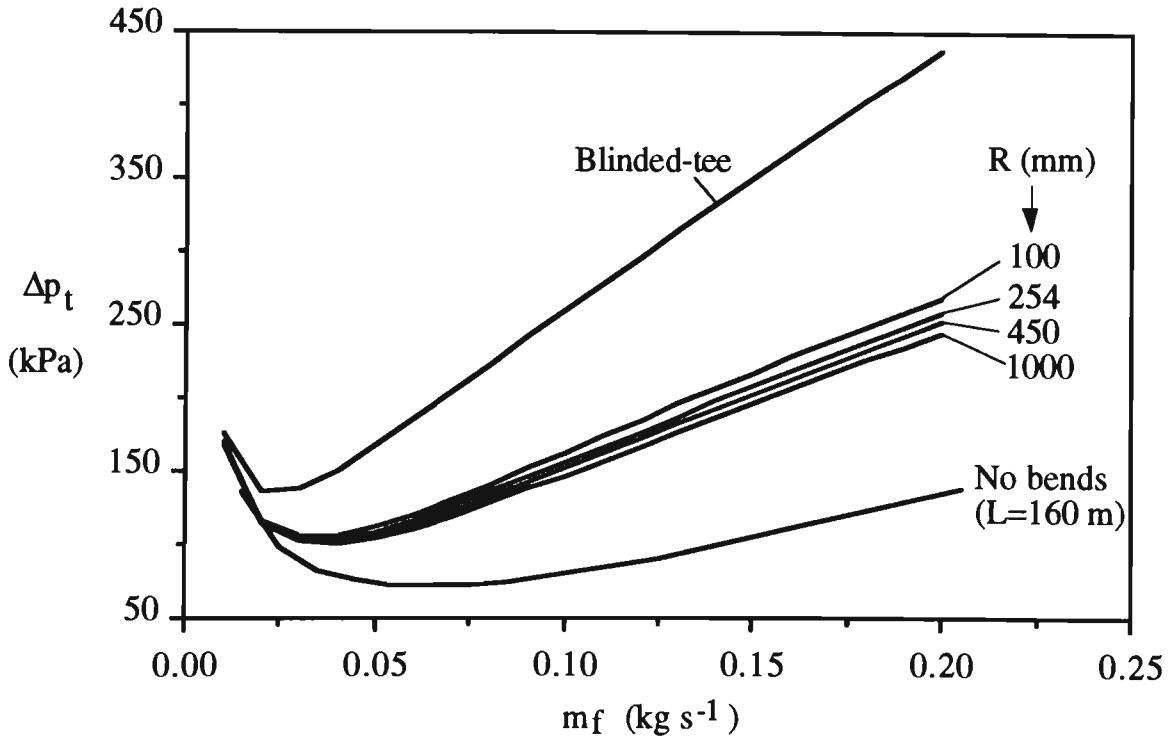

Figure 6.7 Total pipeline air pressure drop in pipeline comprising bends of different geometries (D=52.5 mm, m_S=2.0 kg s^{-1}).

From Figure 6.7, it is also evident that longer radius bends produce lower pressure drops and all the radius bends cause nearly the same pressure drop in dense-phase conveying.

6.7 Influence of Bend Location and Number on Total Pipeline Air Pressure Drop

6.7.1 Influence of Bend Location

Figure 6.4 clearly shows that the location of a bend has a significant influence on pressure drop. A similar result is presented in Figure 5.7 for straight pipes. Also, from these two figures, it can be found that the pressure drop caused by a straight section of pipe is depedent on air density at the pipe exit, and the pressure drop caused by a bend is inversely proportional to the air density at the bend outlet. In a pipeline, there are many bends and straight sections of pipe which are at different locations. Therefore, they affect each other considerably.

Figure 6.8 illustrates a pipeline where bend 3 is allowed to have different locations. Therefore, the bends and straight pipes before bend 3 also are expected to have different relative locations (due to the varying air density at their exit or outlet). Figure 6.9 shows the influence of the bend location on the total pipeline air pressure drop. It is clear from these findings that bend location has a great influence on total pipeline air pressure drop.

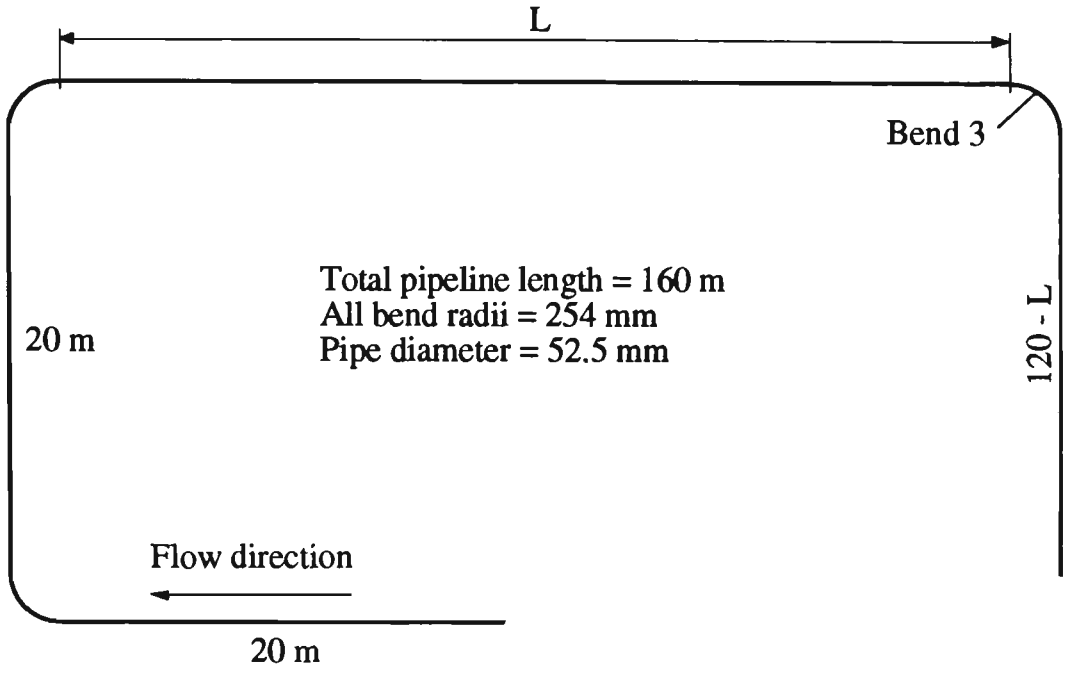

Figure 6.8 Pipeline comprising bend of varying location.

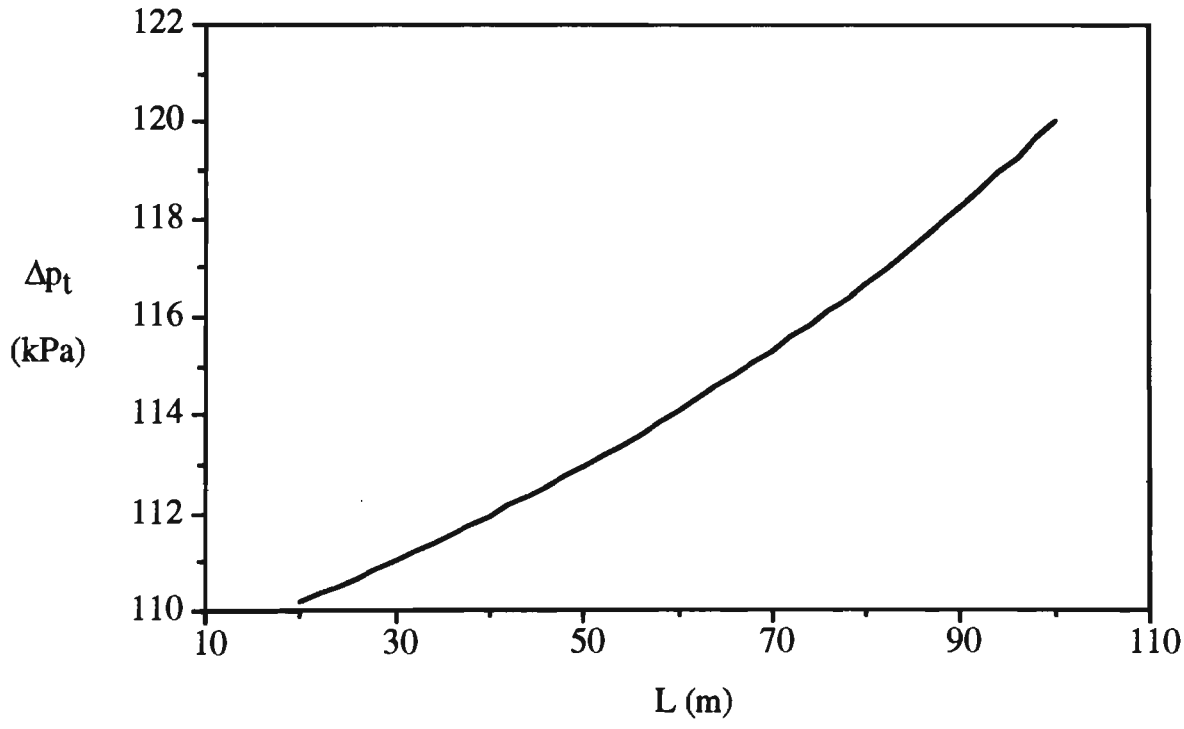

Figure 6.9 Influence of bend location on total pipeline air pressure drop (m_S=2.0 kg s^{-1}, m_f=0.1 kg s^{-1}).

6.7.2 Influence of Bend Number

As particles are required to be conveyed from one place to another, numerous configurations of pipeline are used for this purpose. There is no doubt that these configurations of pipeline have different total pipeline air pressure drops, even though they may have the same total effective length. The main reason is that these configurations of pipeline comprise different numbers and/or locations of bend.

Table 6.3 lists six configurations of pipeline, each comprising a different number of bends. Each pipeline has a total effective length of 120 m. The pressure drops for conveying fly ash in each pipeline is shown in Figure 6.10. Thus graph clearly shows that the total pipeline air pressure drop is proportional to the number of bends.

Table 6.3 Pipeline comprising different number of bends and straights.

No. of Bends	No. of Straights	Effective Length of Each Straight
0	1	120 m
1	2	60 m
2	3	40 m
3	4	30 m
4	5	24 m
5	6	20 m

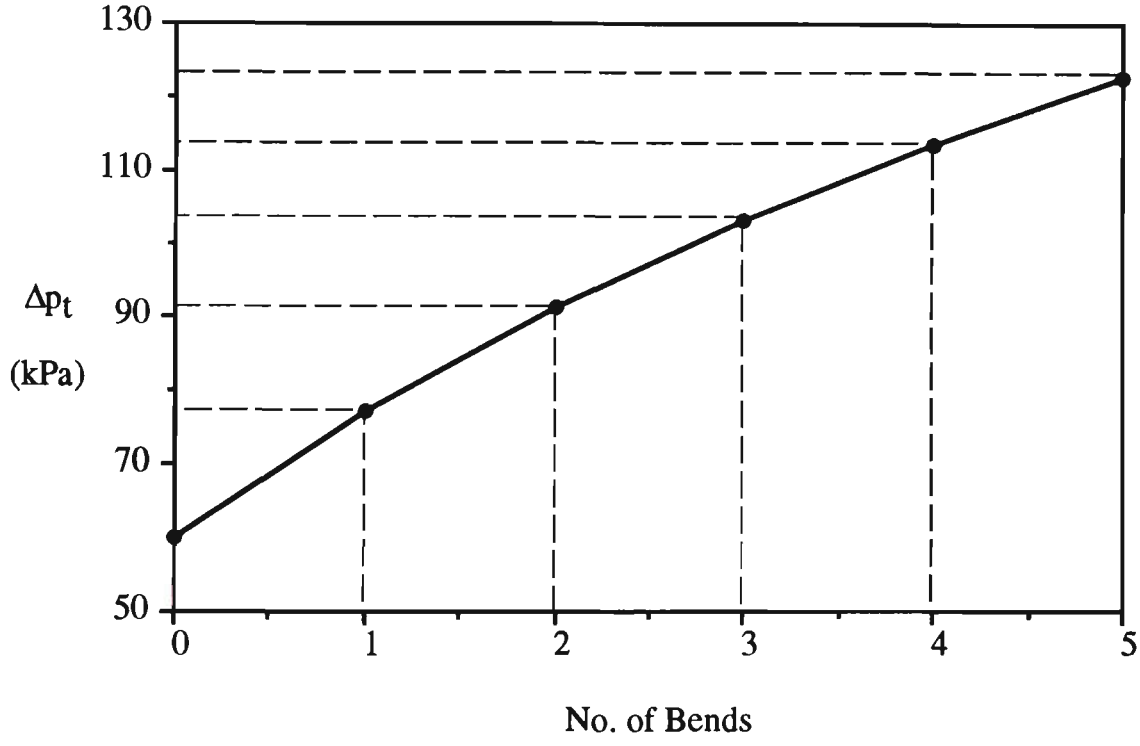

Figure 6.10 Influence of bend number on total pipeline air pressure drop (R=254 mm, D=52.5 mm, m_S=2.0 kg s^{-1}, m_f=0.1 kg s^{-1}).

6.8 Comparison with Other Correlations

To date, many correlations for calculating the pressure drop caused by radius bends have been developed [10, 14, 26, 35, 42, 45, 52, 53, 55, 56]. Some of these correlations [14, 52, 66] have been used widely. However, it is not accurate to use the correlation in EEUA [14]:

$$\Delta p_{tb} = N_b F_3 (1 + m^*) \frac{\rho_{fo} V_{fo}^2}{2} \tag{6.9}$$

directly to predict the pressure drop caused by a bend at different locations. The reason is that Equation (6.9) may be inaccurate unless the mean conditions for the pipeline (i.e. average air velocity), which comprises many bends and straight sections of pipe, are substituted. Therefore, this equation is evaluated more fully in Chapter 7 for predicting **total** pipeline air pressure drop.

Hence, in this section, the correlations (Equations (6.4) and (6.7)) are compared with the expressions by Schuchart [52] and Westman [66]. The correlations proposed by Schuchart and Westman are as follows.

Schuchart:

$$\frac{\Delta p_{bs}}{\Delta p_{ss}} = 210 \left(\frac{2R}{D}\right)^{-1.15} \tag{6.10}$$

Westman:

$$\Delta p_b = (\zeta_f + \zeta_s) \frac{\rho_{fo} V_{fo}^2}{2}$$

$$\zeta_s = \frac{5.4\ m * 1.293}{F_{ro}^{0.84} \left(\frac{2R}{D}\right)^{0.39}} \qquad (6.11)$$

ζ_f is the same as in Chapter 4.

As mentioned previously, exact experimental values of bend pressure drop cannot be obtained. Also, compared with the pressure along the pipeline, bend pressure drop is low. Therefore, all the correlations are compared by predicting the pressures at points Ta-Tf along Pipelines I, II and III (see Figure 3.2). Note that the pressure drop caused by the horizontal straight pipe is calculated by using the correlations in Chapter 5. The results predicted by each correlation are shown in Figures 6.11, 6.12 and 6.13.

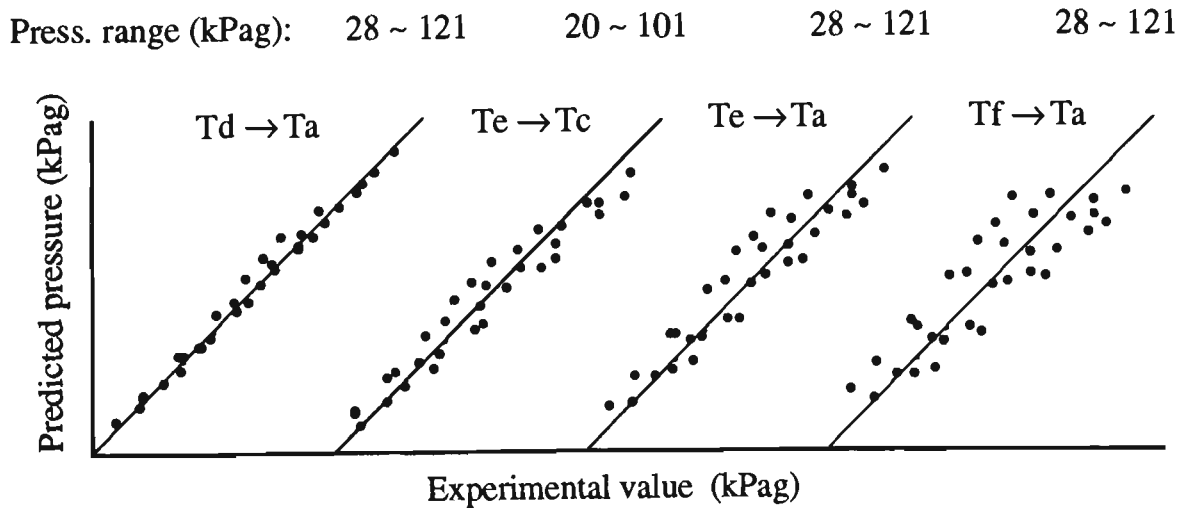

(a) Pipeline I.

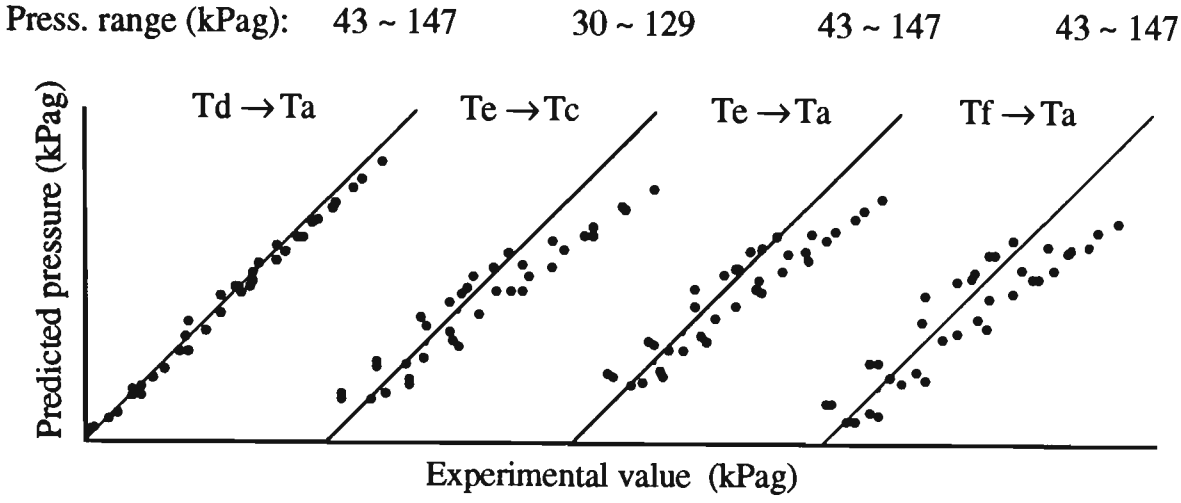

(b) Pipeline II.

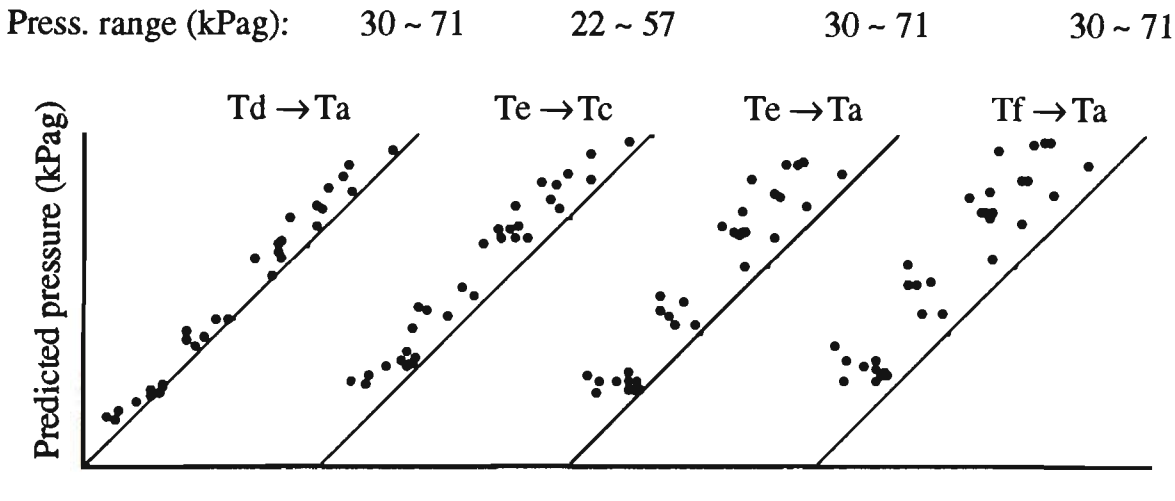

(c) Pipeline III.

Figure 6.11 Predicted pressure vs experimental value by Schuchart [52] correlation.

(Note: Td → Ta means the predicted pressure at Ta, starting from Td)

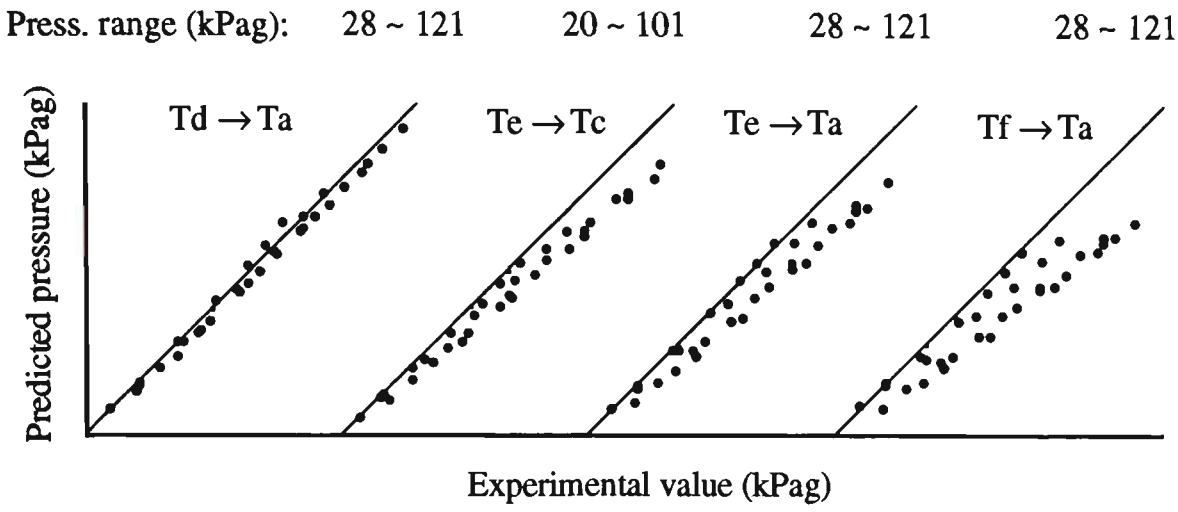

(a) Pipeline I

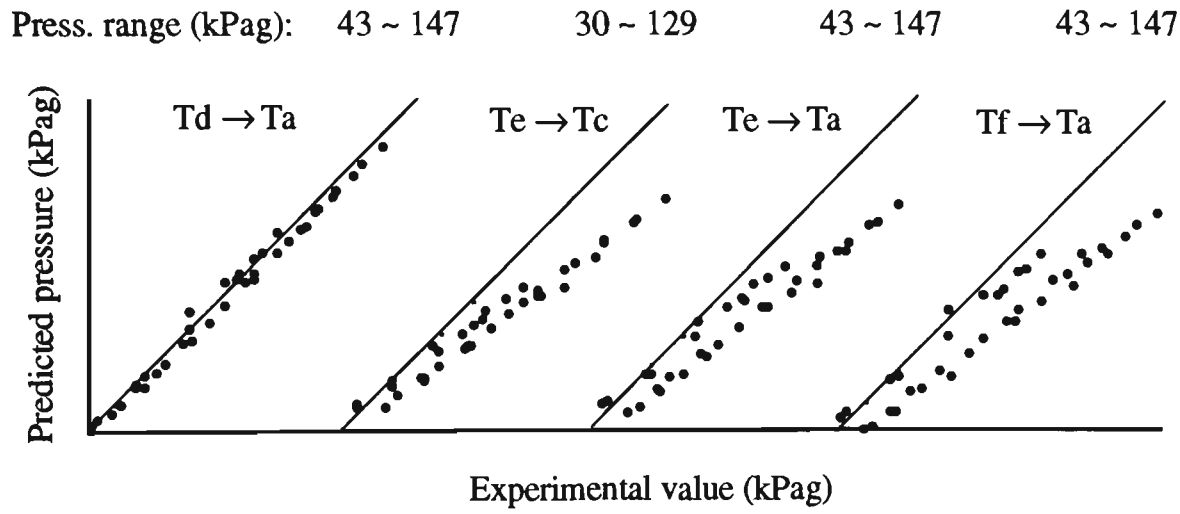

(b) Pipeline II

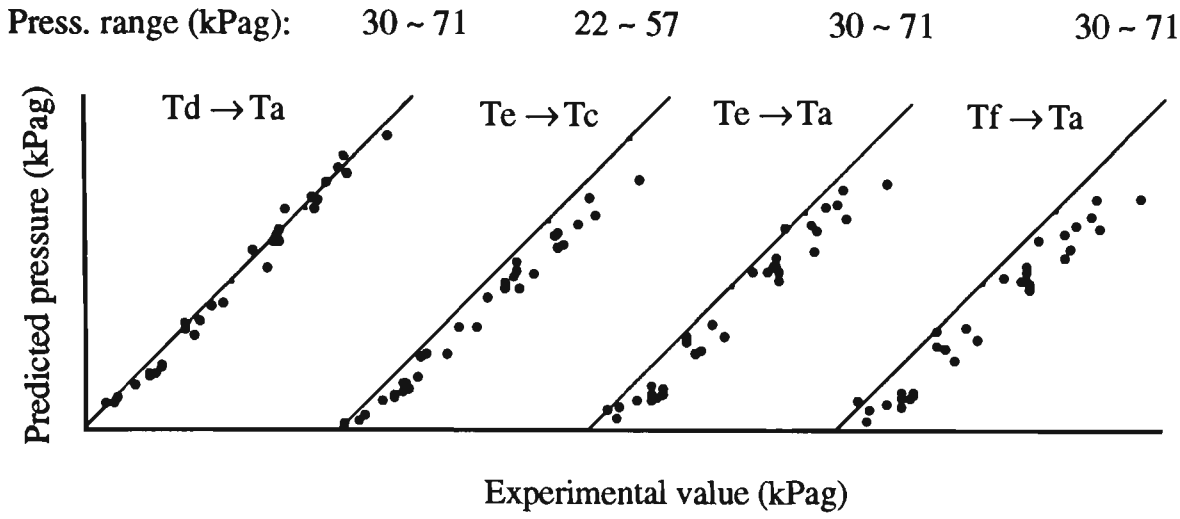

(c) Pipeline III

Figure 6.12 Predicted pressure vs experimental value by Westman [66] correlation.

(Note: Td → Ta means the predicted pressure at Ta, starting from Td)

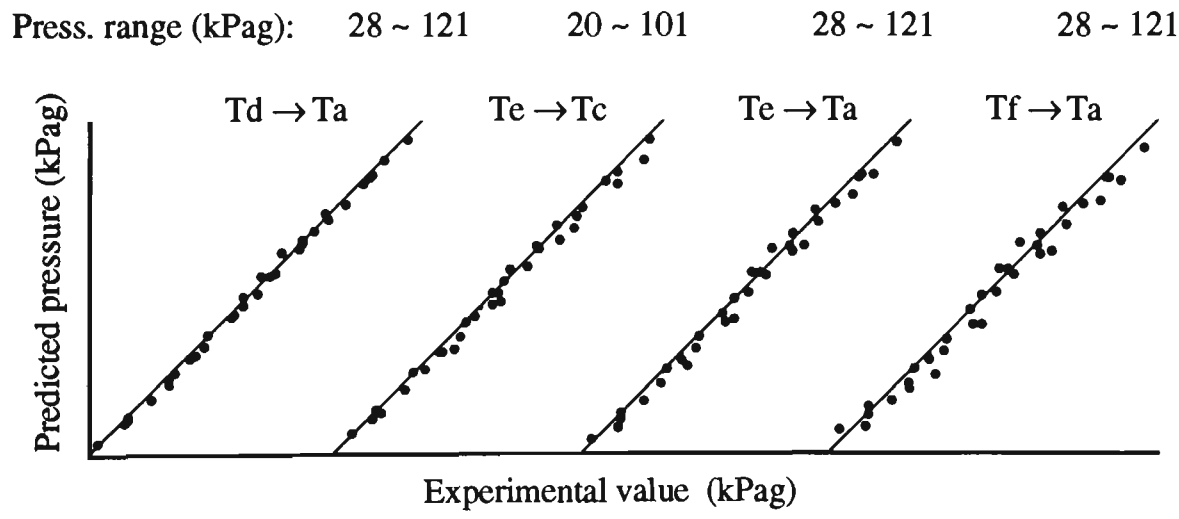

(a) Pipeline I

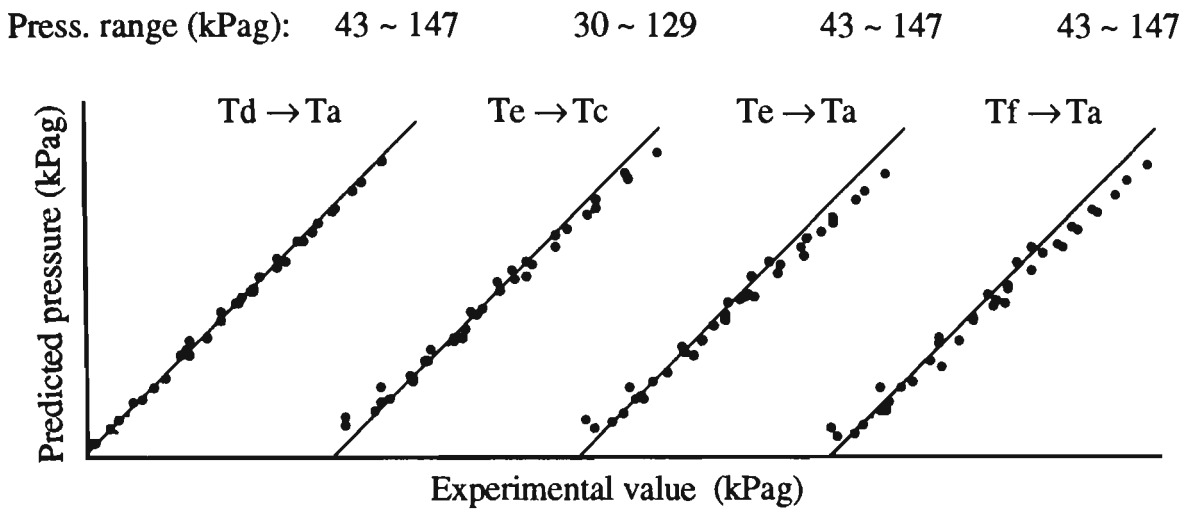

(b) Pipeline II

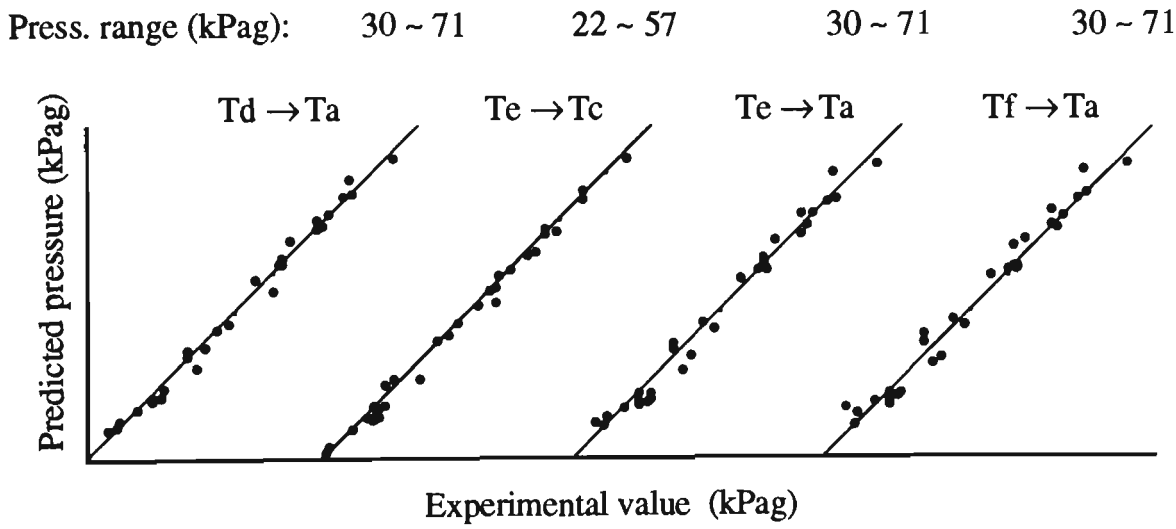

(c) Pipeline III

Figure 6.13 Predicted pressure vs experimental value by author's correlation.

(Note: Td → Ta means the predicted pressure at Ta, starting from Td)

From Figures 6.11, 6.12 and 6.13, it is clear that there is great scatter between the predicted and experimental pressure along the pipeline by using the correlations of Schuchart [52] and Westman [66]. The reasons are:

- the determination of the exponents in these two empirical correlations was based on the experimental data of bend pressure drop obtained by using the traditional method shown in Figure 6.3,

- the products tested by Schuchart [52] and Westman [66] had different size, size distribution, density, shape, and surface roughness, as listed in Table 6.4.

Table 6.4: Particle properties used by different investigators.

Investigator	Material	ρ_S (kg m^{-3})	Equiv. Diameter (μm)
Schuchart [52]	Quartz beads	2610	1490 ~ 2960
	Polymide plastic	1140	2180
Westman [66]	Alathon	877	3410
	Alathon	924	3380
	Polyster	1298	3400
	Polyster	1320	3510
Author	Fly ash	2197	15.5

Similar results have been obtained by other researchers [5, 10, 25, 42, 55, 66]. That is, the correlations based on given products cannot predict accurately the pressure drop for conveying other products.

CHAPTER 7

SCALE-UP PROCEDURES FOR PNEUMATIC CONVEYING SYSTEM DESIGN

7.1 Introduction

An accurate estimation of the total pipeline air pressure drop is considered widely to be one of the most important aspects of pneumatic conveying system design. Since there are numerous influential parameters, such as velocity, particle properties and material, the determination of the total pipeline air pressure drop in pipelines of different length, diameter, step and bend number is based largely on the scale-up of test rig data.

Over the past two decades, many scale-up procedures have been developed and used quite extensively [6, 9, 14, 34, 39, 45, 58, 68, 71, 72]. However, most of these scale-up procedures have not taken into account:

- the geometry, number and/or location of bends,
- the number and/or location of straight pipes,
- the influence of the conveyed material(s),
- relatively short pipe lengths (e.g. between bends), and/or
- a variable pressure gradient along straight sections of pipe.

These disadvantages may preclude the reliable and accurate scale-up of test rig data to full-scale installations.

In Chapters 5 and 6, the correlations for calculating the pressure drop caused by straight sections of pipe and bends at different locations have been set up and they are accurate and reliable for the test material (viz. fly ash). However, these correlations are suitable only for pipelines containing long straight sections of pipe where particles can be re-accelerated fully. When these correlations are applied to

pipelines comprising many short pipe lengths, the total pipeline air pressure drop still may not be predicted accurately.

In this chapter, a new scale-up procedure is proposed, in which the test bends and straight sections of pipe are considered at the same time (i.e. dealt with as one unit). Note that the correlations for the straight pipes remain unchanged, whereas the correlations for the bends are modified and the exponents in the modified correlations are determined by minimising the sum of the squared errors of pressure along a simple configuration of constant diameter pipeline. The test section of the pipeline comprises one short and two long straight pipes and two bends. These correlations predict accurately the pipeline pressure for other different configurations of single- and stepped-diameter pipeline (containing short lengths of pipe) and for a wide range of operating conditions.

7.2 Steady-State Pipeline Conveying Characteristics

If a pneumatic conveying system is to be designed or upgraded to ensure satisfactory and efficient operation, it is suggested that as much information as possible be obtained on the bulk solid to be handled (e.g. physical properties, conveying performance). It is very important for efficient and reliable design, that any conveying performance data be summarised in a convenient and workable form. One technique is shown in Figure 7.1, which is referred to as the steady-state pipeline conveying characteristics. It clearly displays the variation of steady-state m_s (the product mass flow rate, kg s^{-1}) with respect to m_f (the supplied air mass flow rate, kg s^{-1}) and Δp_t (the total pipeline air pressure drop, kPa). Based on the information

shown in Figure 7.1, it is easy to select the operating conditions for the system to be designed or upgraded.

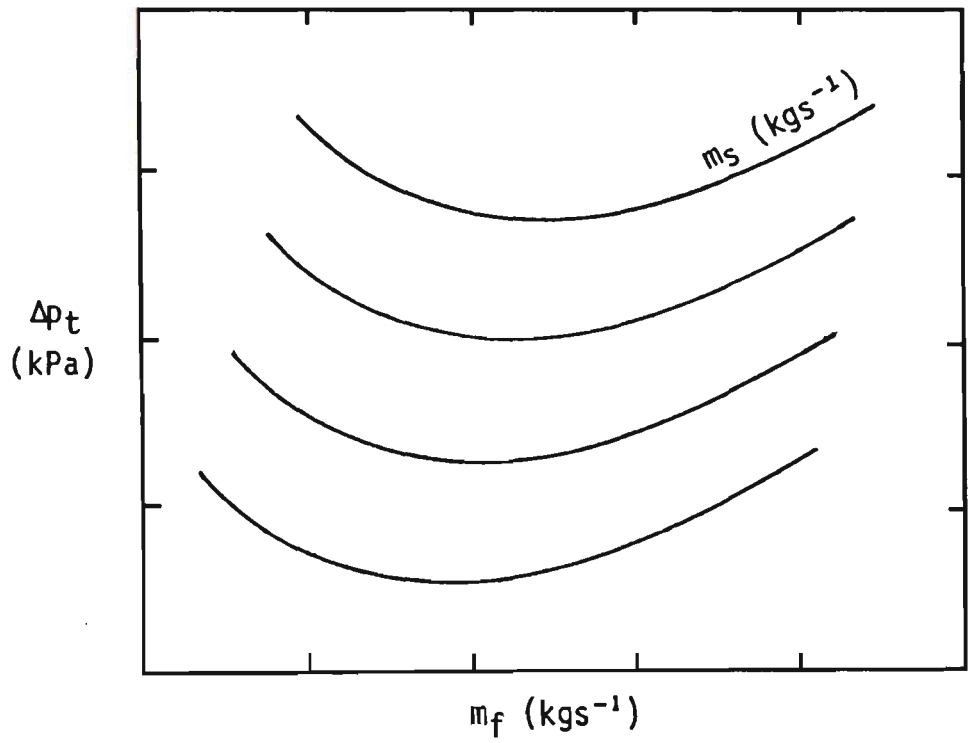

Figure 7.1 General form of steady-state conveying characteristics for a given material and pipeline configuration.

Figures 5.7, 5.8 and 6.4 clearly display that, a straight section of pipe or bend has significantly different steady-state conveying characteristics at different locations (i.e. different air density at the exit of straight pipe or bend). Hence, it is expected that also there are significantly different steady-state conveying characteristics for different configurations of pipeline (i.e. comprising different number and/or location of bends and straight sections of pipe). Figures 7.2 to 7.6 illustrate the steady-state conveying characteristics of Pipelines I, II, III, A1 and A2. Note that the m_S curves are obtained by using interpolation techniques.

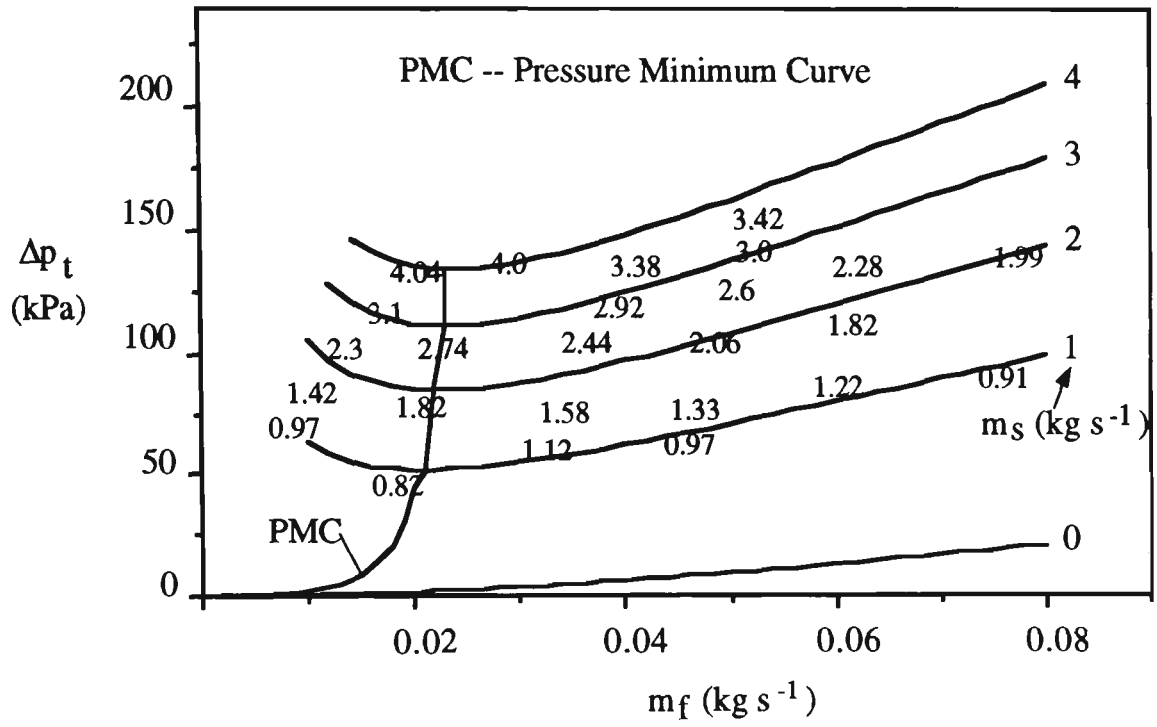

Figure 7.2 Steady-state conveying characteristics of Pipeline I and fly ash (L=102 m, D=52.5 mm, R=254 mm).

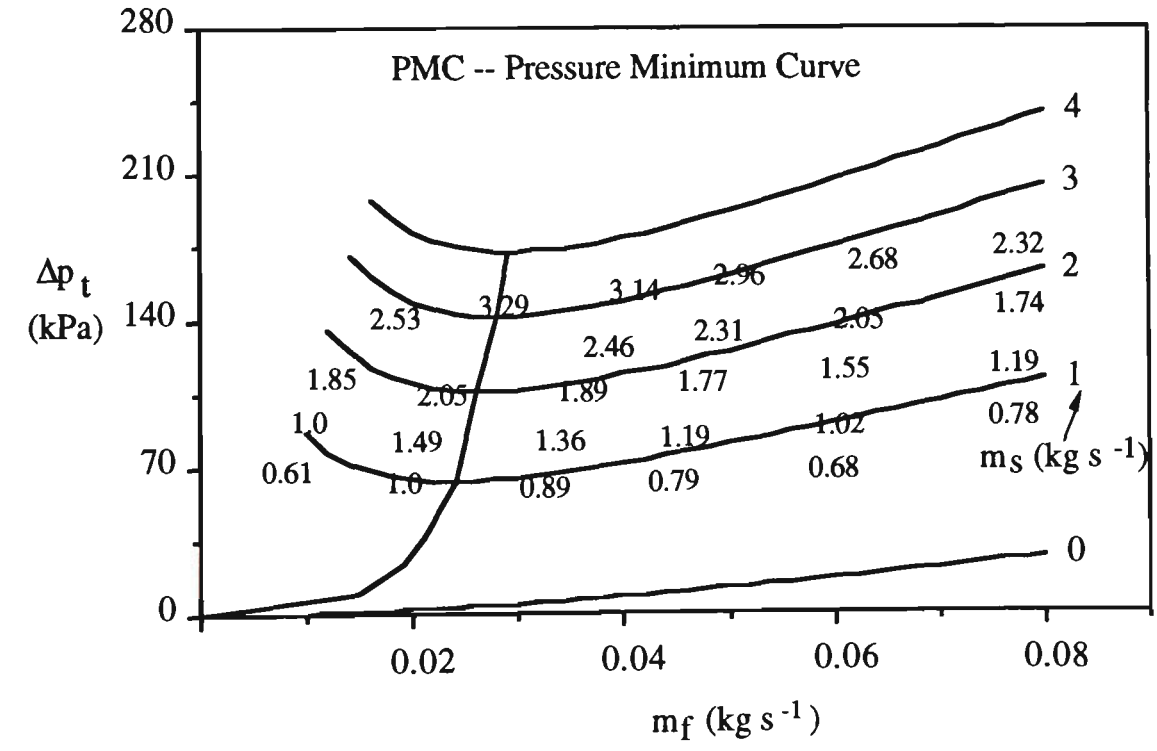

Figure 7.3 Steady-state conveying characteristics of Pipeline II and fly ash (L=135 m, D=52.5 mm, R=254 mm).

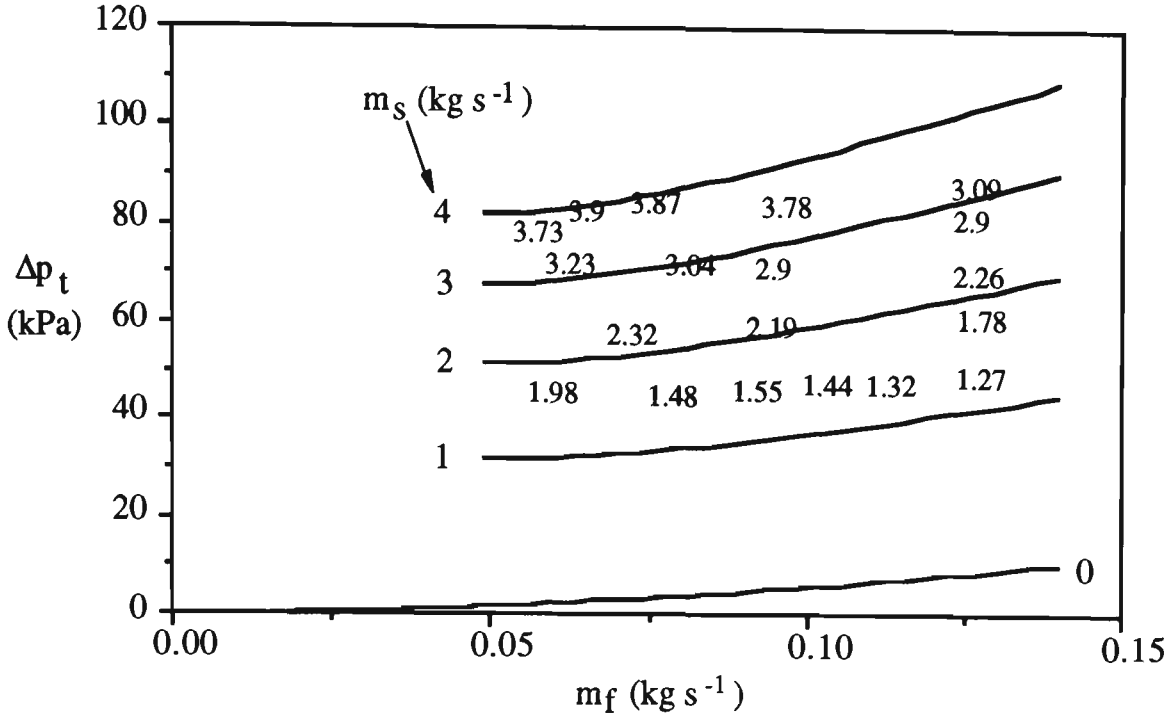

Figure 7.4 Steady-state conveying characteristics of Pipeline III and fly ash (L=137 m, D=80.5 mm, R=254 mm).

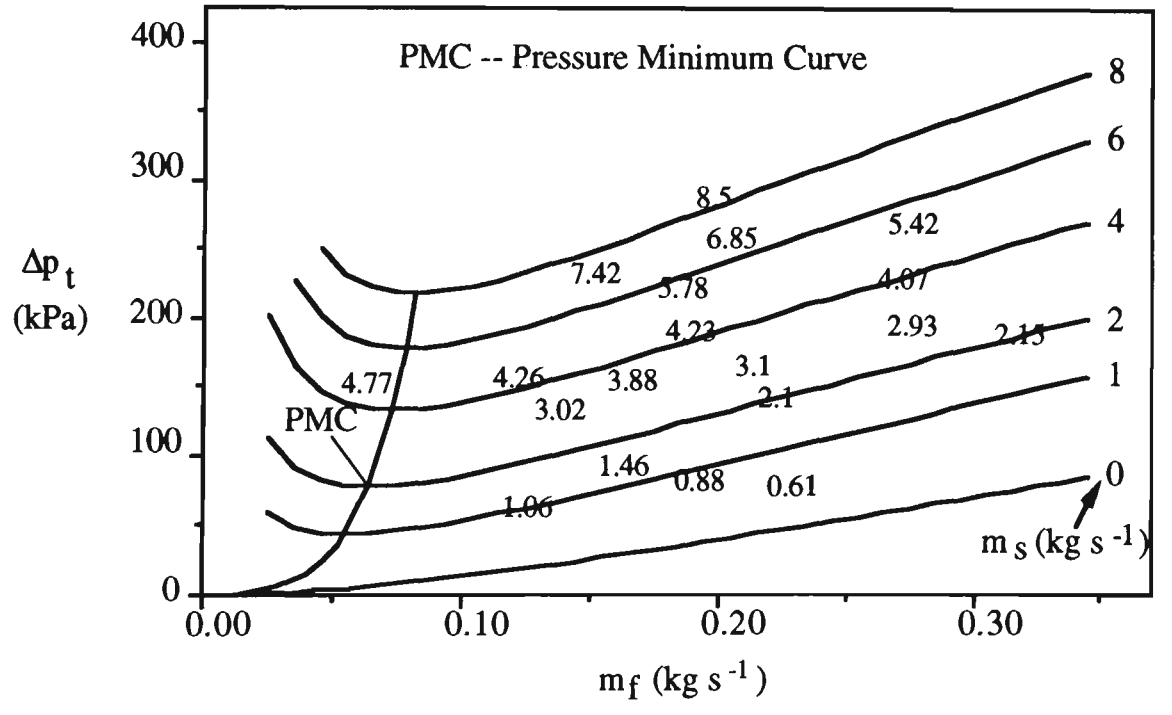

Figure 7.5 Steady-state conveying characteristics of Pipeline A1 and fly ash (L=172 m, D=69 mm, R=1000 mm).

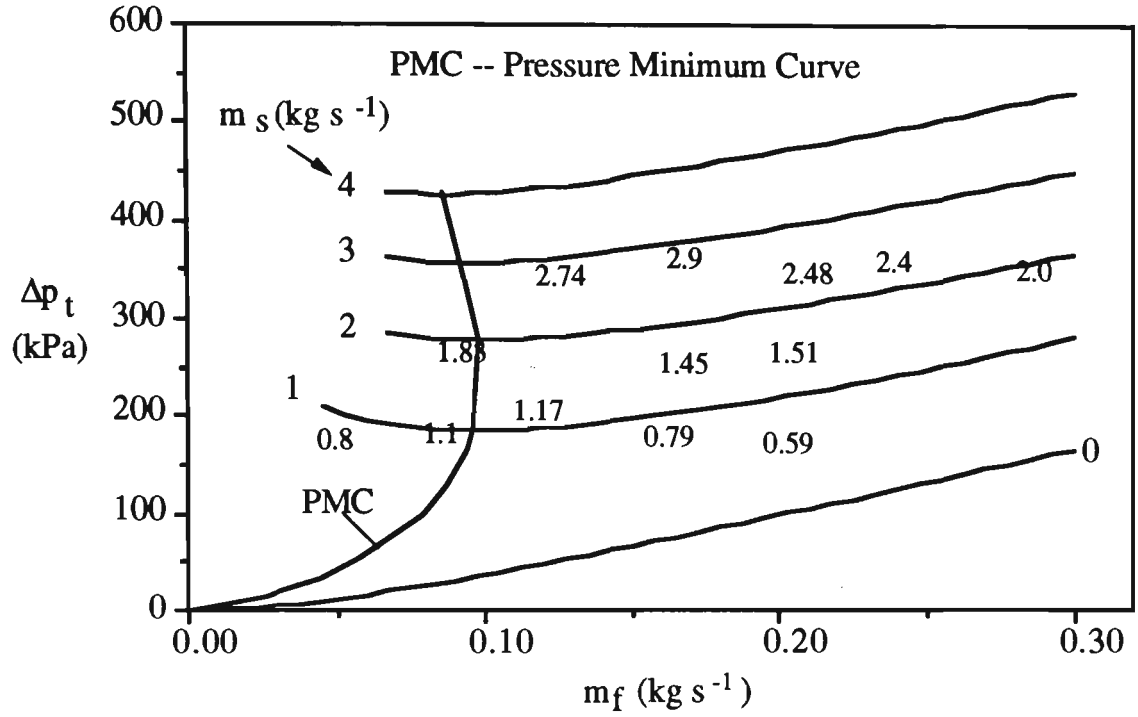

Figure 7.6 Steady-state conveying characteristics of Pipeline A2 and fly ash (L=554 m, D=69 mm, R=1000 mm).

7.3 Prediction of Total Pipeline Air Pressure Drop by Using Existing Scale-up Procedures

To date, many scale-up procedures have been developed [6, 9, 14, 34, 39, 45, 58, 68, 71, 72] and some of these have been used quite extensively. In this section, various 'popular' scale-up procedures are evaluated, by predicting the total pipeline air pressure drop for Pipelines I, II, III, A1 and A2 and conveying fly ash.

7.3.1 Existing Scale-up Procedures

7.3.1.1 Based on Test Rig Data

The scale-up procedure (i.e. scale-up of m_S with respect to pipeline length and diameter) proposed by Mills et al. [39] and Mason et al. [34] is very simple. That is:

$$m_{S2} = m_{S1} \frac{L_1}{L_2} \left(\frac{D_2}{D_1}\right)^2 \quad \text{for constant solids pressure drop and } m_f D^{-2} \tag{7.1}$$

where subscript 1 refers to the test rig and 2 to the actual plant.

Based on Equation (7.1) and the steady-state conveying characteristics obtained from three products (fly ash/cement mix, PVC powder and screened coke) and four different test rigs, Wypych and Arnold [68] developed a similar but empirical based scale-up equation:

$$m_{S2} = m_{S1} \frac{L_1'}{L_2'} \left(\frac{D_2}{D_1}\right)^{2.8} \tag{7.2}$$

where L_1' and L_2' represent values of L_1 and L_2 adjusted to allow for any differences between the number (and type) of bends used on the test rig and actual plant. For example:

$$L_1' = L_1 + 4\,N_b$$

$$L_2' = L_2 + 4\,N_b$$

7.3.1.2 Direct Prediction

EEUA [14] presents equations to predict directly the total pipeline air pressure drop:

$$\Delta p_t = \Delta p_{ta} + \Delta p_{ts} + \Delta p_{tb} \tag{7.3}$$

where Δp_t is the total pipeline air pressure drop, Δp_{ta} is the pressure drop due to the acceleration of the particles from rest, Δp_{ts} is the pressure drop due to the friction between the particles and the pipe wall along the pipeline, and Δp_{tb} is the sum of the pressure drop caused by all bends in the pipeline.

$$\Delta p_{ta} = F_1 (1 + m^*) \frac{\rho_{fav} V_{fav}^2}{2}$$

$$\Delta p_{ts} = F_2 (1 + m^*) \frac{\rho_{fav} V_{fav}^2}{2 D} L$$

$$\Delta p_{tb} = F_3 N_b (1 + m^*) \frac{\rho_{fav} V_{fav}^2}{2} \tag{7.3a}$$

where: V_{fav} is the average superficial velocity in the pipeline

$$\rho_{fav} = \frac{m_f}{V_{fav} A}$$

The values of F_1 vary with the design of the powder feeding arrangements and are suggested between 2 and 3. For approximate design, a value of 2.5 is conventionally used. The co-efficient F_2 includes a number of indeterminate variables, and varies widely for different materials, product to air mass flow rate ratios, pipe wall

conditions and air velocity. For a conservative design, the recommended value of F_2 [14] is taken from the top line of the hatched area, as shown in Figure 7.7. In order to calculate F_2 easily, the equations in Figure 7.8 are set up and used. Also, F_3 is calculated by using the equations in Figure 7.9.

All the above existing scale-up procedures treat the pipeline as a single entity. However, the total pipeline air pressure drop also can be predicted by dealing separately with bends and straight sections of pipe. The pressure drops caused by straight pipes are calculated by correlations of Hetsroni [79] (for horizontal straight pipe) or Michaelides [37] (for vertical straight pipe) (see Chapter 5). The bend pressure drop is calculated by correlations of Schuchart [52] or Westman [66] (see Chapter 6).

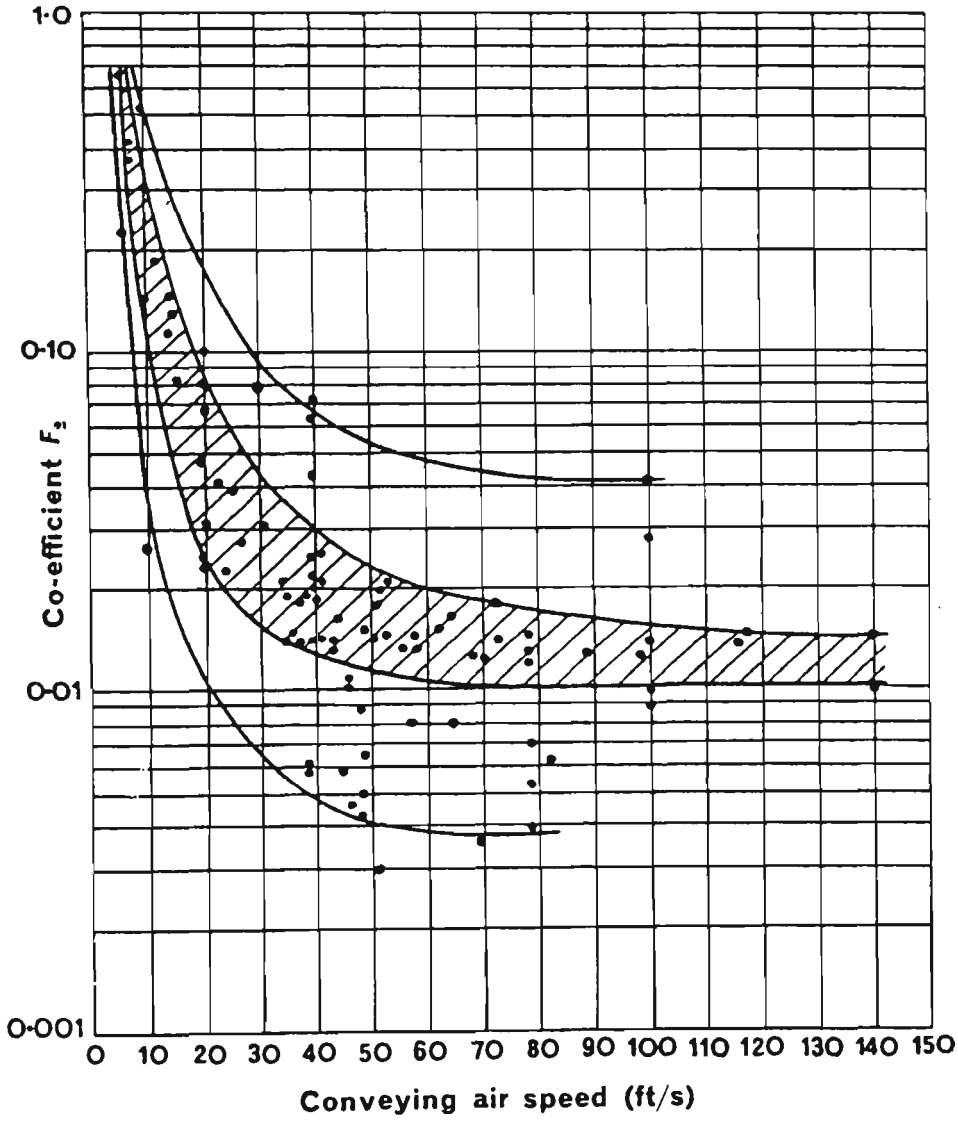

Figure 7.7 Values of the co-efficient F_2, plotted against the mean superficial air velocity V_{fav} for a large number of controlled tests .

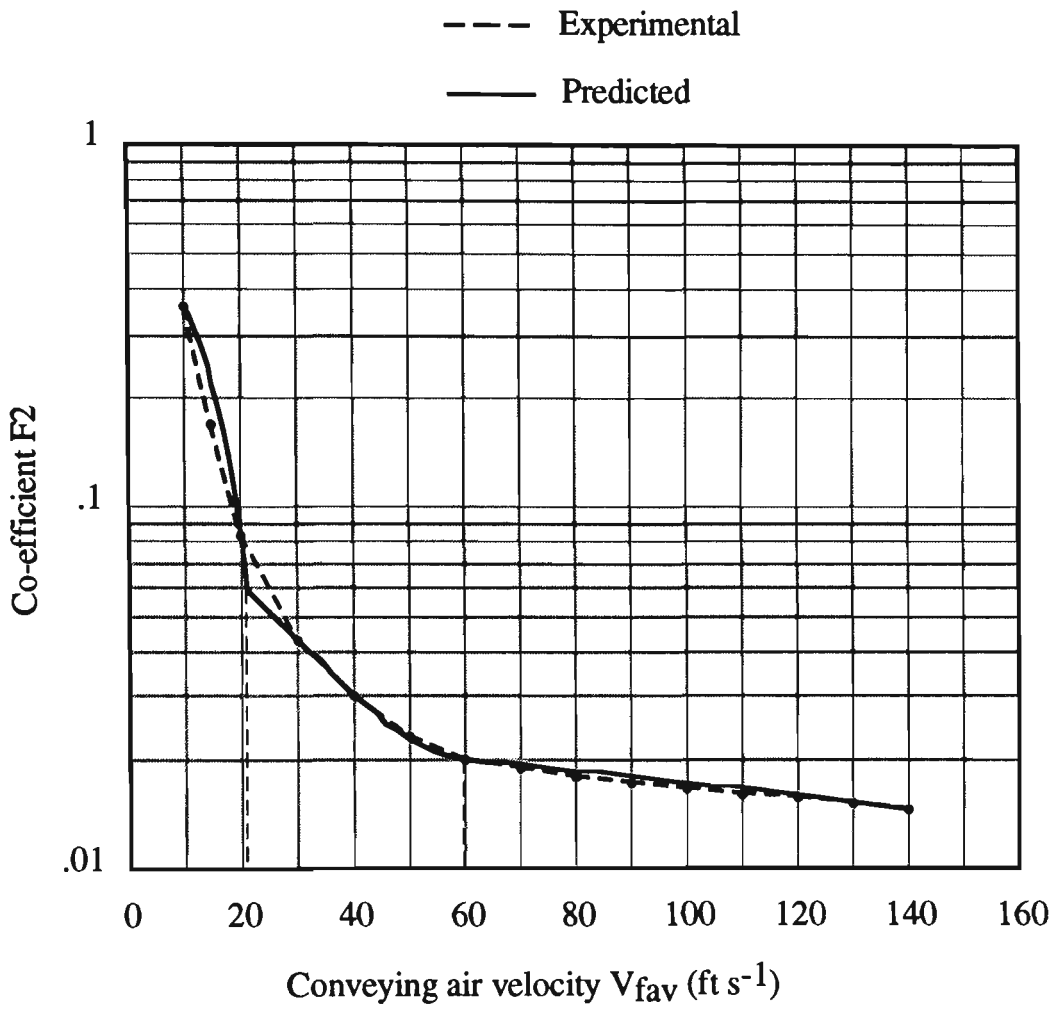

Figure 7.8 Relationship between F_2 and V_{fav}.

Equations in Figure 7.8:

$V_{fav} \leq 20.875$: $F_2 = 0.637 - 2.77 \times 10^{-5} V_{fav}$

$20.875 \leq V_{fav} \leq 60$: $F_2 = 0.111 - 3.01 \times 10^{-3} V_{fav} + 2.5 \times 10^{-5} V_{fav}^2$

$60 \leq V_{fav} \leq 140$: $F_2 = 2.413 \times 10^{-2} - 6.875 \times 10^{-5} V_{fav}$

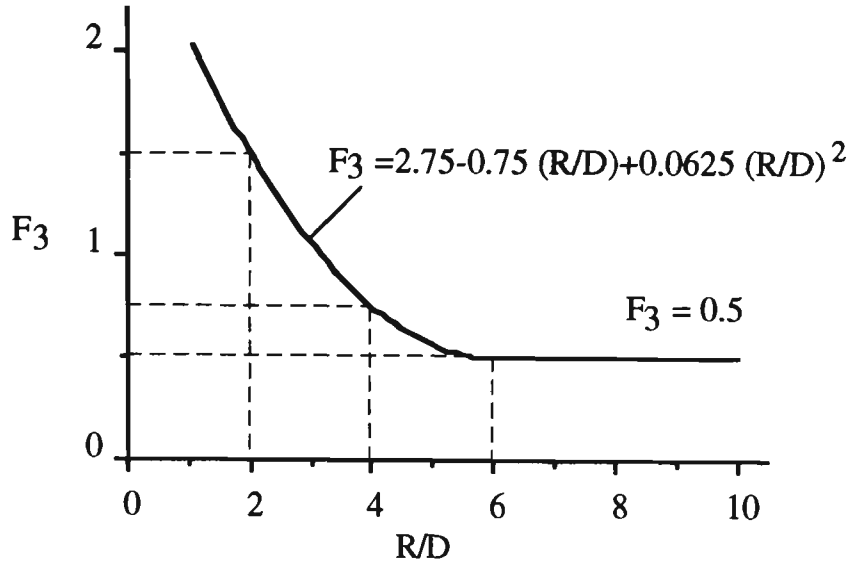

Figure 7.9 Relationship between F3 and R/D

7.3.2 Results of Prediction

Length: the scale-up equations, Equations (7.1) and (7.2), are used to scale up the data of Pipeline A1 (L=172 m, D=69 mm, 5 bends, R=1000 mm) presented in Figure 7.5 to Pipeline A2 (L=554 m, D=69 mm, 17 bends, R=1000 mm). The following calculation can be made:

$$m_{s1} = \frac{L_2}{L_1} m_{s2} = \frac{554}{172} m_{s2} = 3.221\, m_{s2} \qquad \text{By Equation (7.1)}$$

$$m_{s1} = \frac{L_2'}{L_1'} m_{s2} = \frac{554+4\times17}{172+5\times4} m_{s2} = 3.24\, m_{s2} \qquad \text{By Equation (7.2)}$$

The scale-up results are depicted in Figures 7.10 and 7.11.

Diameter: applying the scale-up equations, Equations (7.1) and (7.2), to the data of Pipeline II (L=135 m, D=52.5 mm, R=254 mm) presented in Figure 7.3 results in the 'predicted' conveying characteristics of Pipeline III (L=137 m, D=80.5 mm, R=254 mm), as shown in Figures 7.12 and 7.13, where:

$$m_{s1} = \left(\frac{D_1}{D_2}\right)^2 m_{s2} = \left(\frac{52.5}{80.5}\right)^2 m_{s2} = 0.425\, m_{s2} \qquad \text{By Equation (7.1)}$$

$$m_{s1} = \left(\frac{D_1}{D_2}\right)^{2.8} m_{s2} = \left(\frac{52.5}{80.5}\right)^{2.8} m_{s2} = 0.302\, m_{s2} \qquad \text{By Equation (7.2)}$$

Length and Diameter: the data of Pipeline I (L=102 m, D=52.5 mm, R=254 mm) presented in Figure 7.2 are scaled up to Pipeline III (L=137 m, D=80.5 mm, R=254 mm) by using Equations (7.1) and (7.2). The results are shown in Figures 7.14 and 7.15, where:

$$m_{s1} = \frac{L_2}{L_1}\left(\frac{D_1}{D_2}\right)^2 m_{s2} = \frac{137}{102}\left(\frac{52.5}{80.5}\right)^2 m_{s2}$$

$$= 0.571\, m_{s2} \qquad \text{By Equation (7.1)}$$

$$m_{s1} = \frac{L_2'}{L_1'}\left(\frac{D_1}{D_2}\right)^{2.8} m_{s2} = \frac{137+4\times9}{102+4\times9}\left(\frac{52.5}{80.5}\right)^{2.8} m_{s2}$$

$$= 0.379\, m_{s2} \qquad \text{By Equation (7.2)}$$

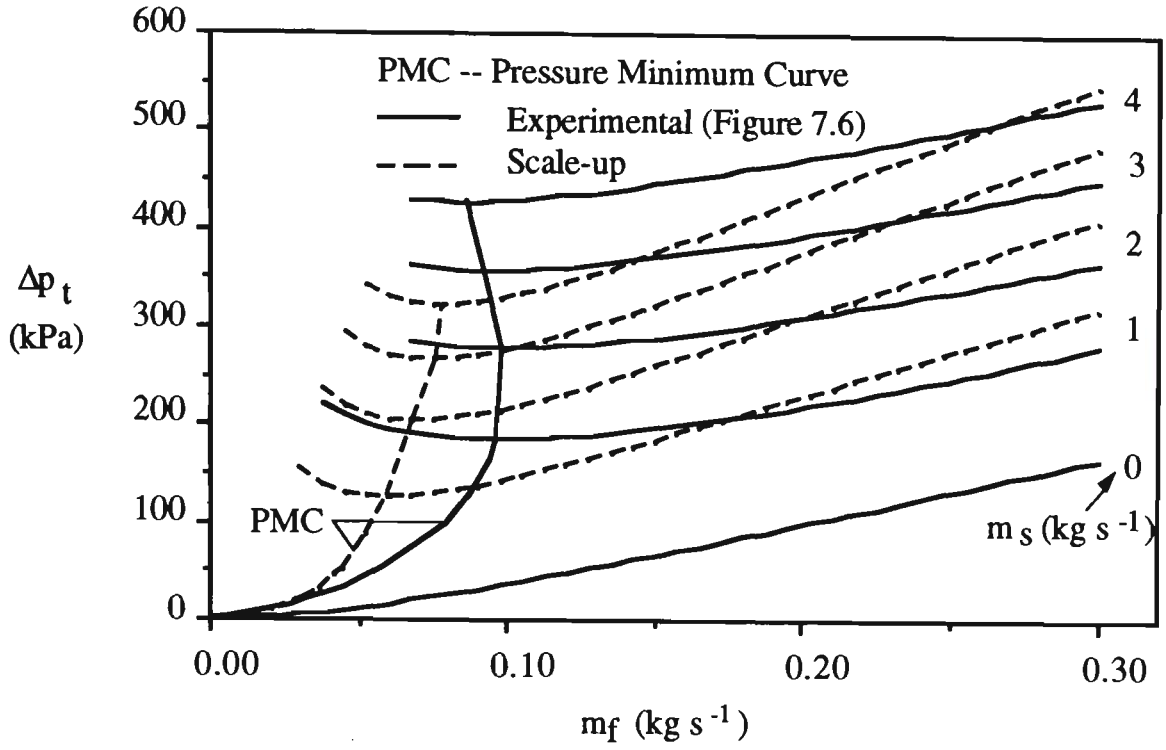

Figure 7.10 Scale-up conveying characteristics of Pipeline A2 (L=553 m, D=69 mm) from Pipeline A1 (L=172 m, D=69 mm) based on Equation (7.1).

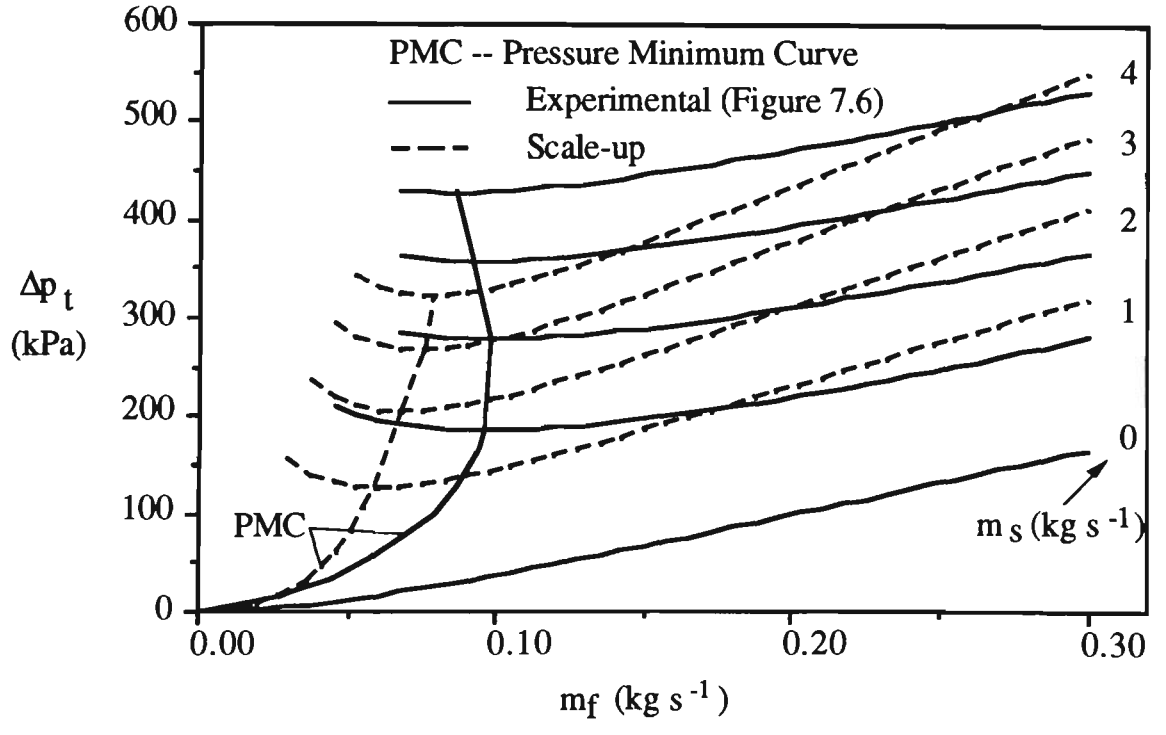

Figure 7.11 Scale-up conveying characteristics of Pipeline A2 (L=553 m, D=69 mm) from Pipeline A1 (L=172 m, D=69 mm) based on Equation (7.2).

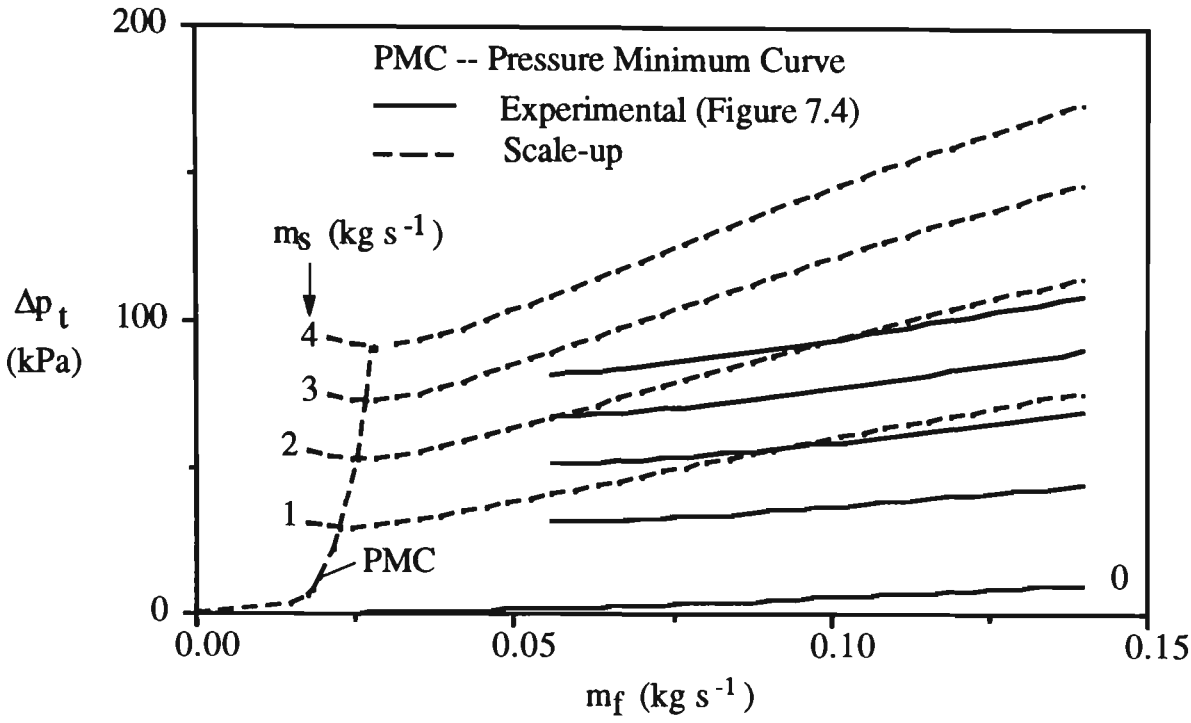

Figure 7.12 Scale-up conveying characteristics of Pipeline III (L=137 m, D=80.5 mm) from Pipeline II (L=135 m, D=52.5 mm) based on Equation (7.1).

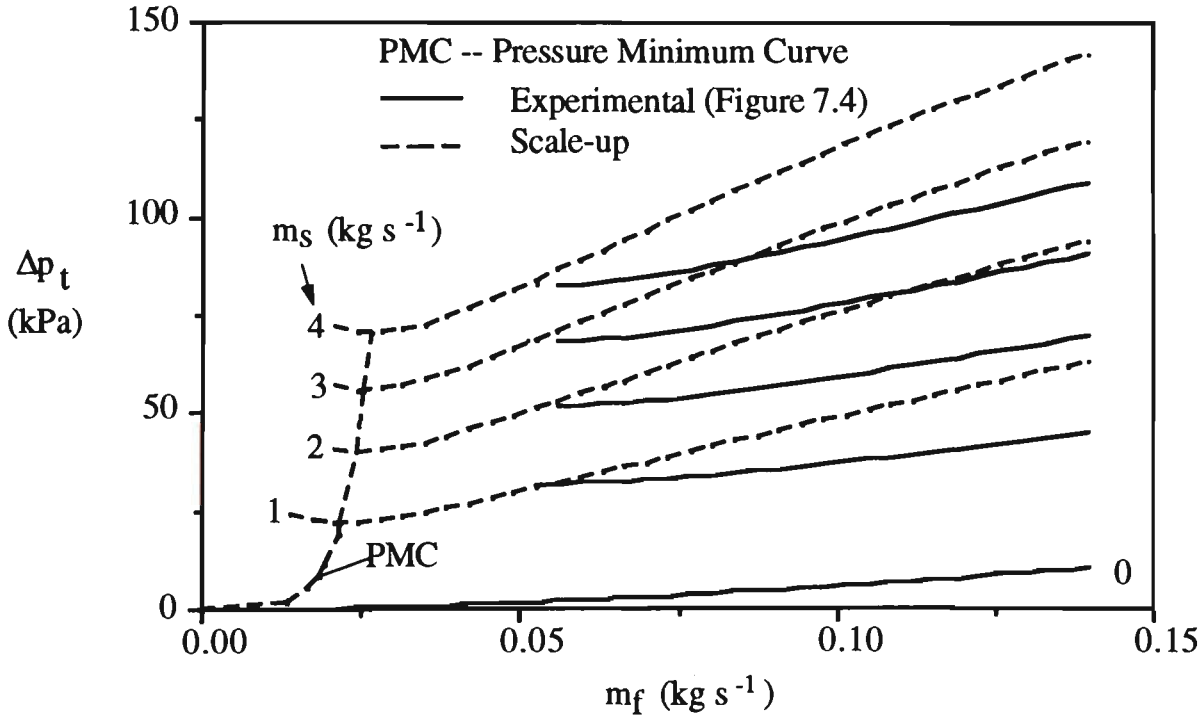

Figure 7.13 Scale-up conveying characteristics of Pipeline III (L=137 m, D=80.5 mm) from Pipeline II (L=135 m, D=52.5 mm) based on Equation (7.2).

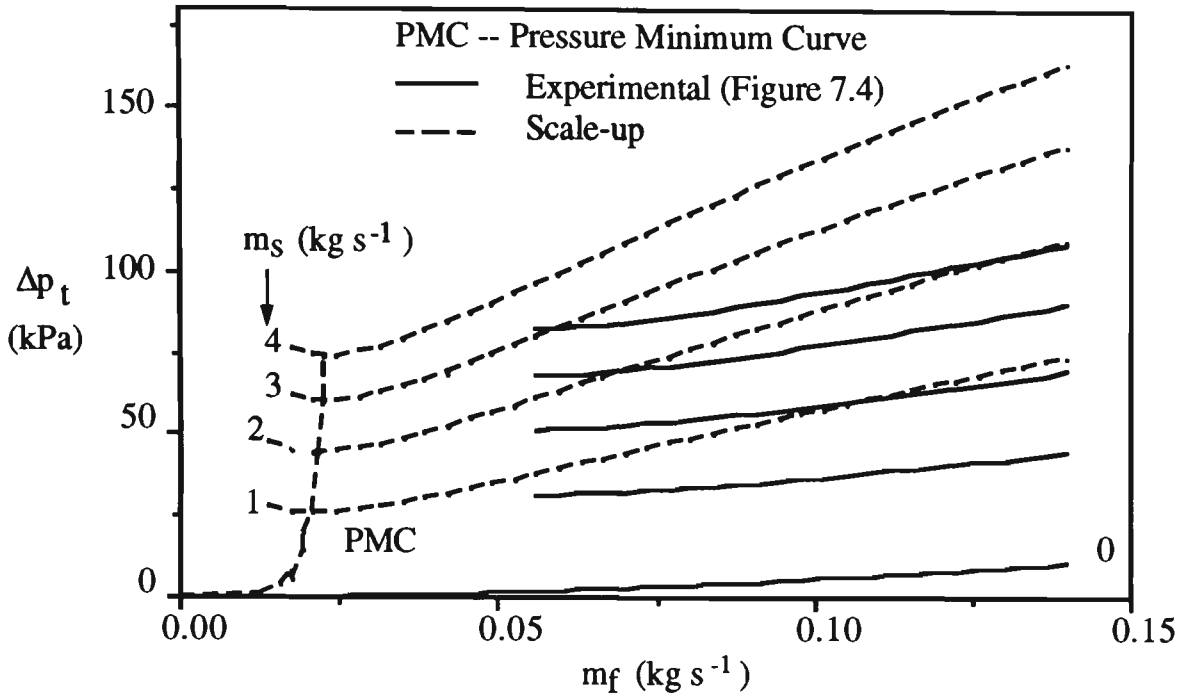

Figure 7.14 Scale-up conveying characteristics of Pipeline III (L=137 m, D=80.5 mm) from Pipeline I (L=102 m, D=52.5 mm) based on Equation (7.1).

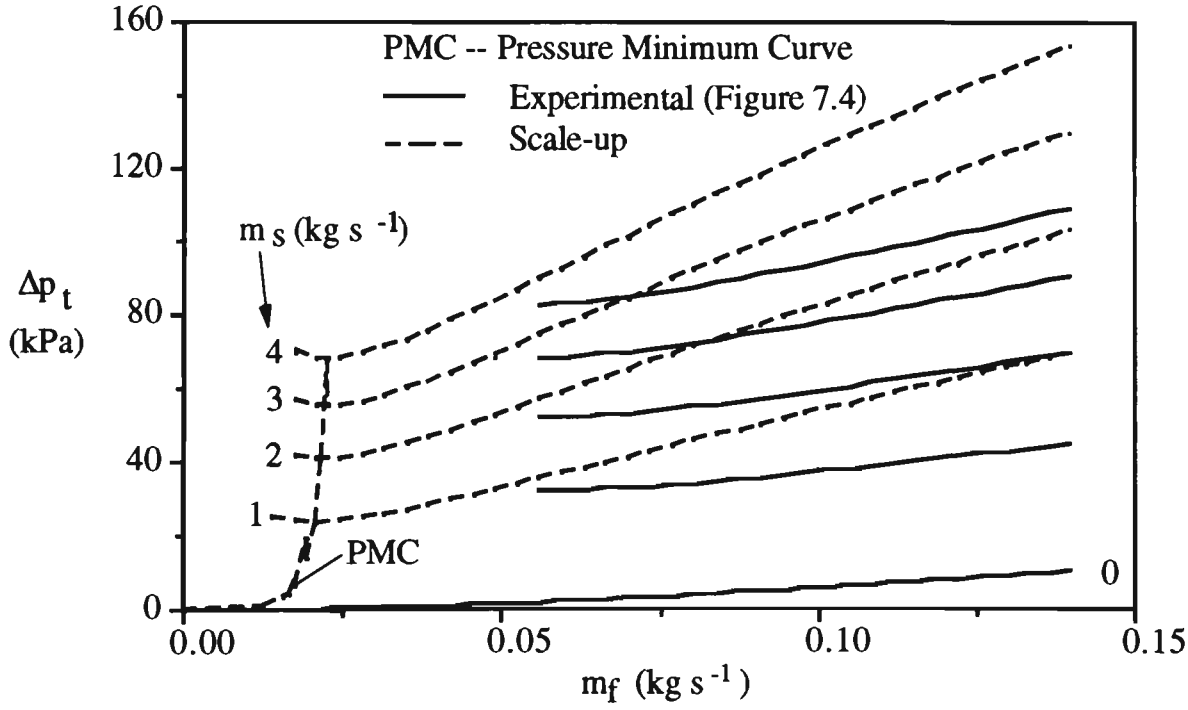

Figure 7.15 Scale-up conveying characteristics of Pipeline III (L=137 m, D=80.5 mm) from Pipeline I (L=102 m, D=52.5 mm) based on Equation (7.2).

Based on the values of several parameters (e.g. pipe diameter, bend radius, pipeline effective length, product and air mass flow rates), Equation (7.3) is used to predict the total pipeline air pressure drop. However, the total pipeline air pressure drops in Pipelines I, II, III, A1 and A2 are found to be overpredicted significantly. One of the main reasons is that the co-efficient F_2 is too conservative. An example is given below.

Example:

Known conditions: (in Pipeline I)

Δp_t=61.15 kPa, m_s=1.12 kg s^{-1}, m_f=0.0325 kg s^{-1},

D=52.5 mm, R=254 mm, L=102 m,

N_b=9

Based on the known conditions:

F_1=2.5 F_3=0.58

V_{fav}=10.16 m s^{-1} =33.34 ft s^{-1}

(T=293.15 K, R_a=287.1 N m kg^{-1} K^{-1})

ρ_{fav}=1.48 kg m

From Figure 7.7 or equations in Figure 7.8:

F_2= 0.038

The calculated pressure drops are:

$$\Delta p_{ta}=6.77 \text{ kPa} \qquad \Delta p_{ts}=200 \text{ kPa} \qquad \Delta p_{tb}=14.14 \text{ kPa}$$

$$\Delta p_t=\Delta p_{ta}+\Delta p_{ts}+\Delta p_{tb}=6.77+200+14.14=220.91 \text{ kPa}$$

The calculated total pipeline air pressure drop (220.91 kPa) is much higher than the experimental value (61.15 kPa).

Also, the total pipeline air pressure drops in Pipelines I, II, III, A1, A2 and A3 are predicted by dealing separately with bends and straight pipes [37, 52, 79], as shown in Figures 7.16 and 7.17. The predicted steady-state conveying characteristics of Pipeline I is shown in Figure 7.18.

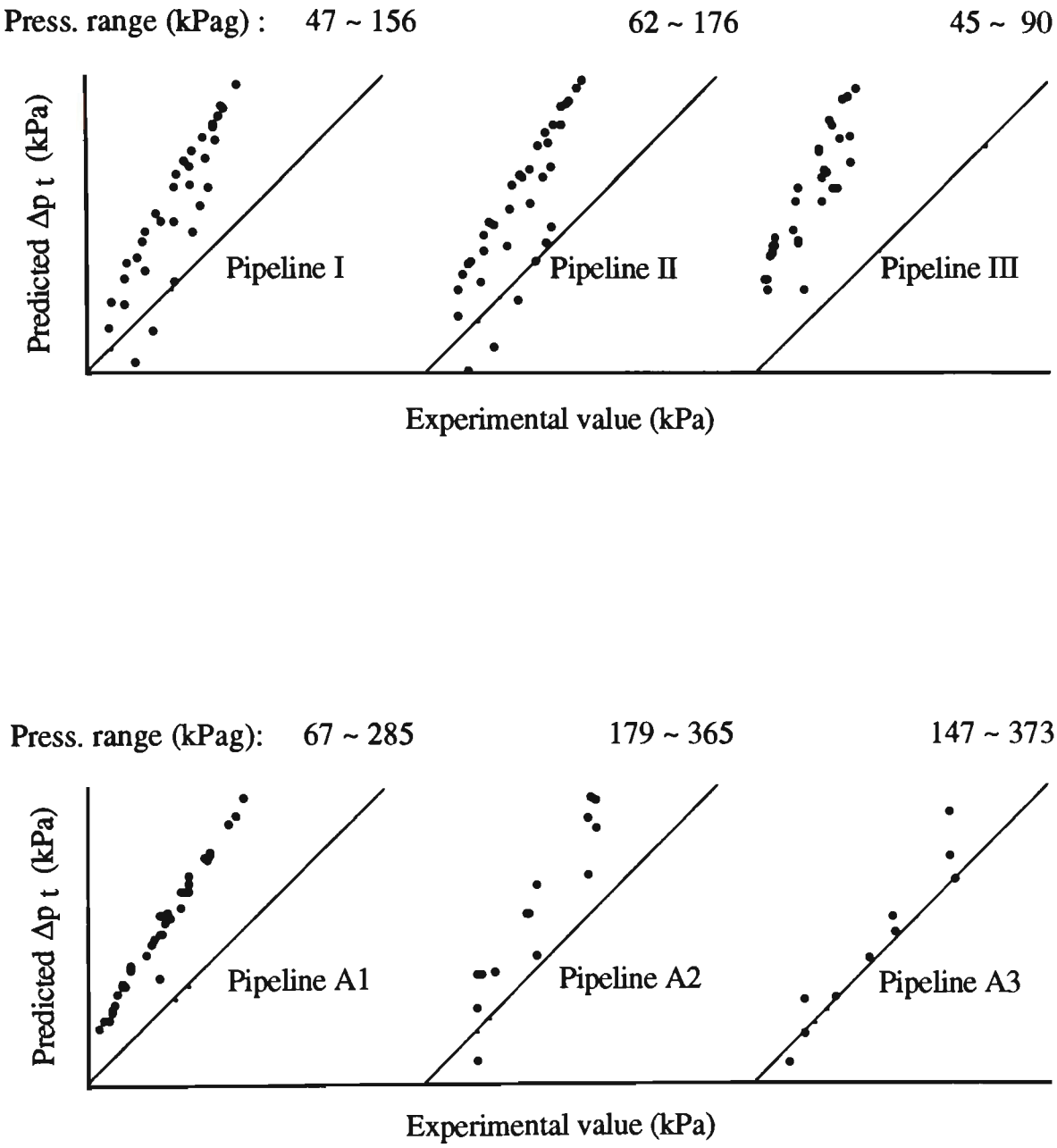

Figure 7.16 Predicted total pipeline air pressure drop vs experimental value in different pipelines by correlations of Hetsroni [79], Michaelides [37] and Schuchart [52].

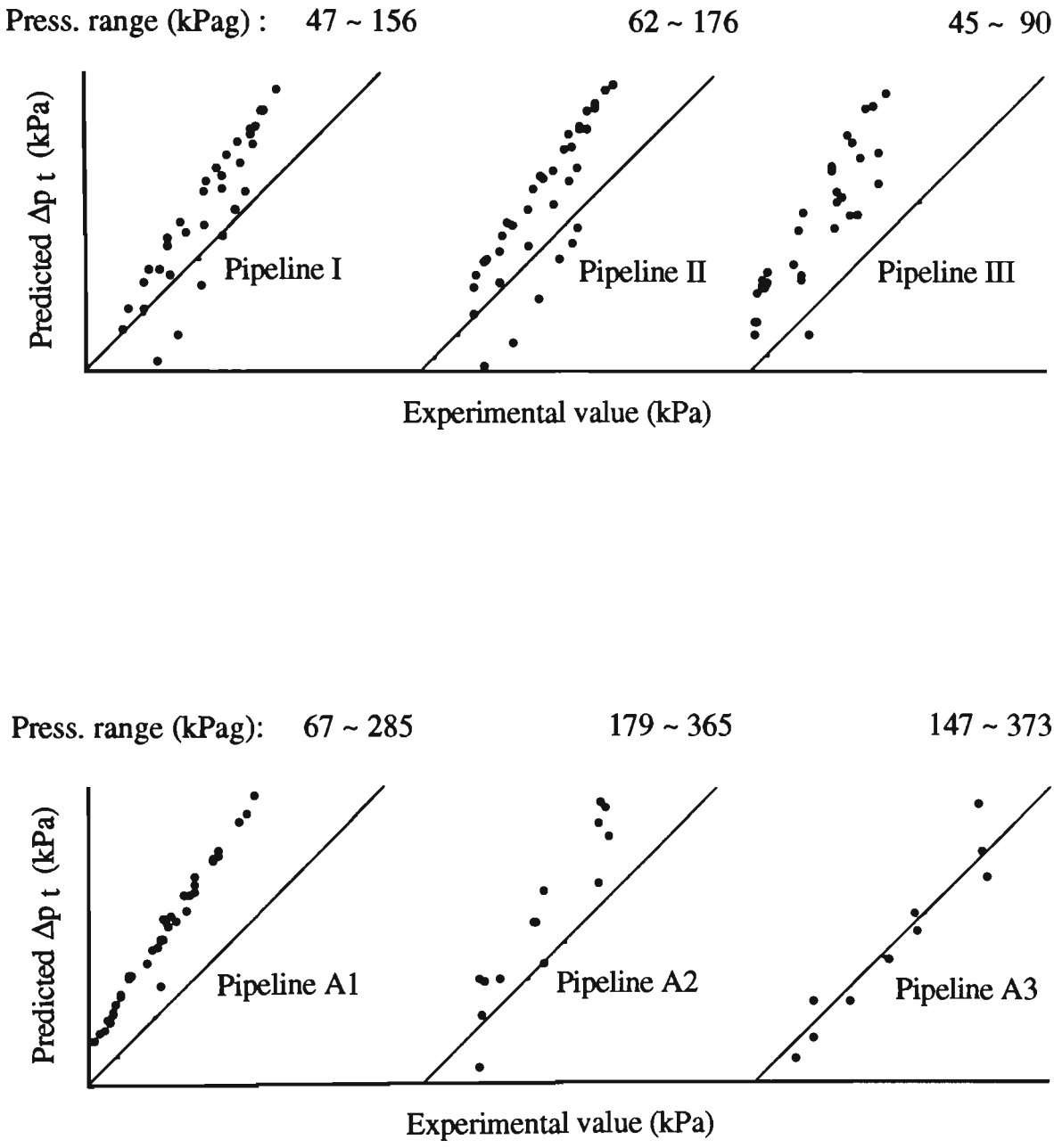

Figure 7.17 Predicted total pipeline air pressure drop vs experimental value in different pipelines by correlations of Hetsroni [79], Michaelides [37] and Westman [66].

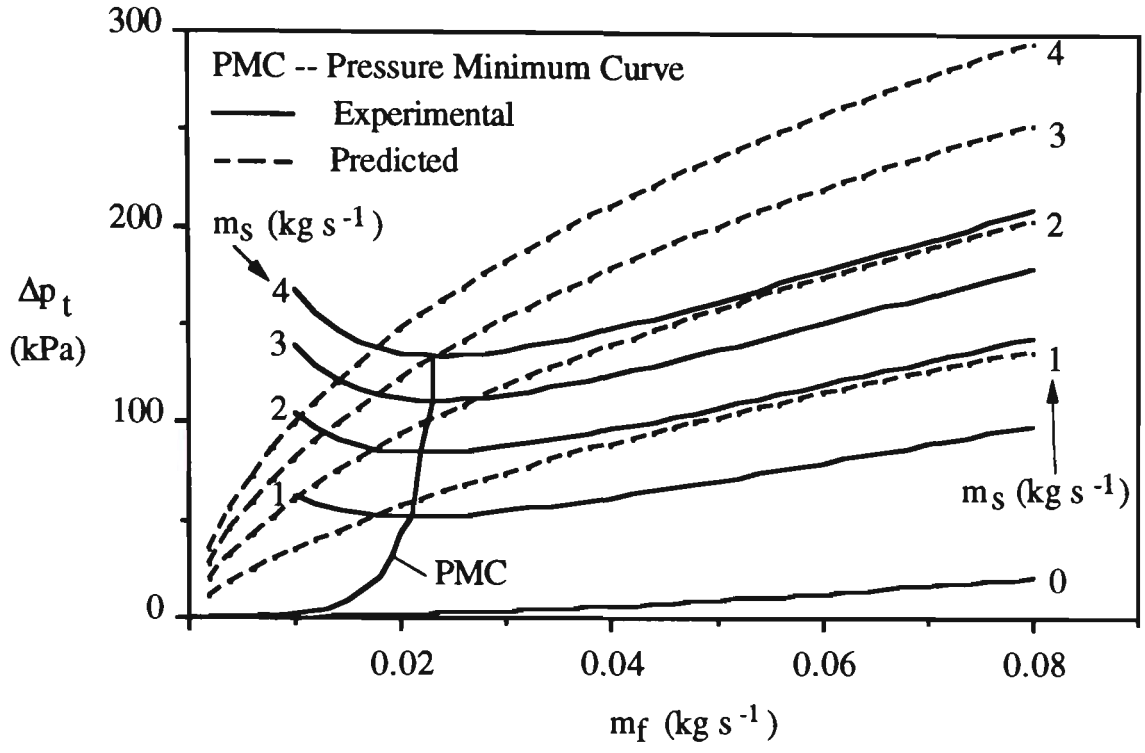

Figure 7.18 Steady-state conveying characteristics of Pipeline I predicted by correlations of Hetsroni [79], Michaelides [37] and Westman [66].

As mentioned in Chapter 5, the correlations of Hetsroni [79] and Michaelides [37] are the 'best' ones for predicting the pressure drop of conveying fly ash along horizontal and vertical straight sections of pipe, respectively. However, these correlations obviously are not accurate. Therefore, the pressure drops in the horizontal and vertical straight pipes are predicted by the correlations developed in Chapter 5. However, the bend pressure drop still is calculated by the correlations of Schuchart [52] or Westman [66]. The results of the total pipeline air pressure drop in Pipelines I, II, III, A1, A2 and A3 are shown in Figures 7.19 and 7.20.

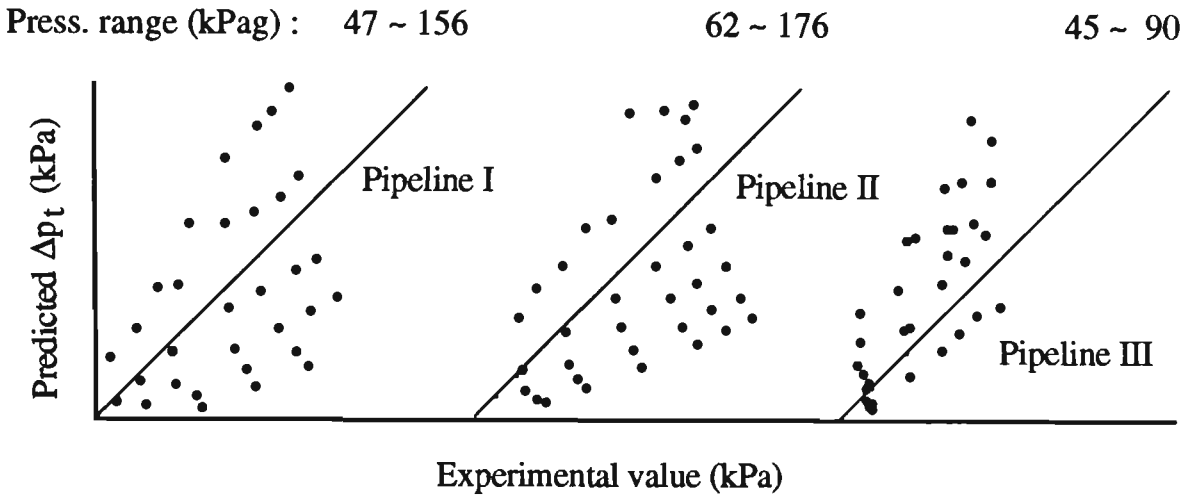

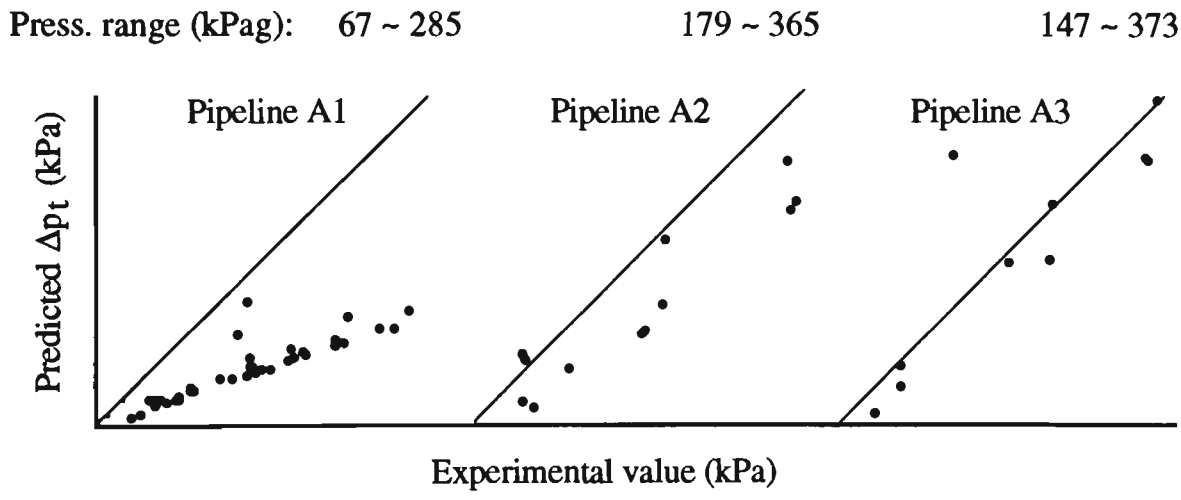

Figure 7.19 Predicted total pipeline air pressure drop vs experimental value in different pipelines by correlations in Chapter 5 and of Schuchart [52].

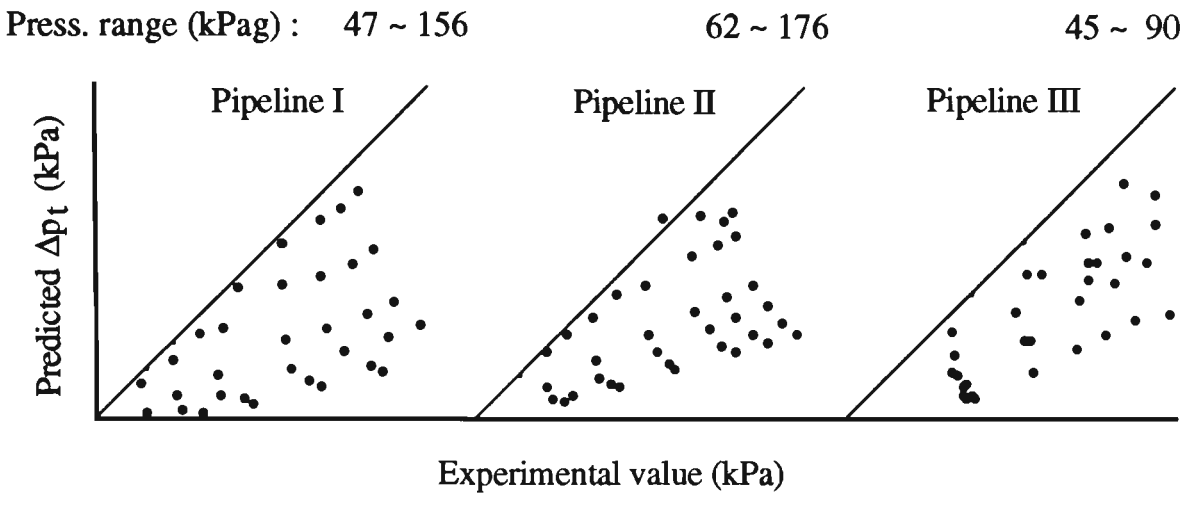

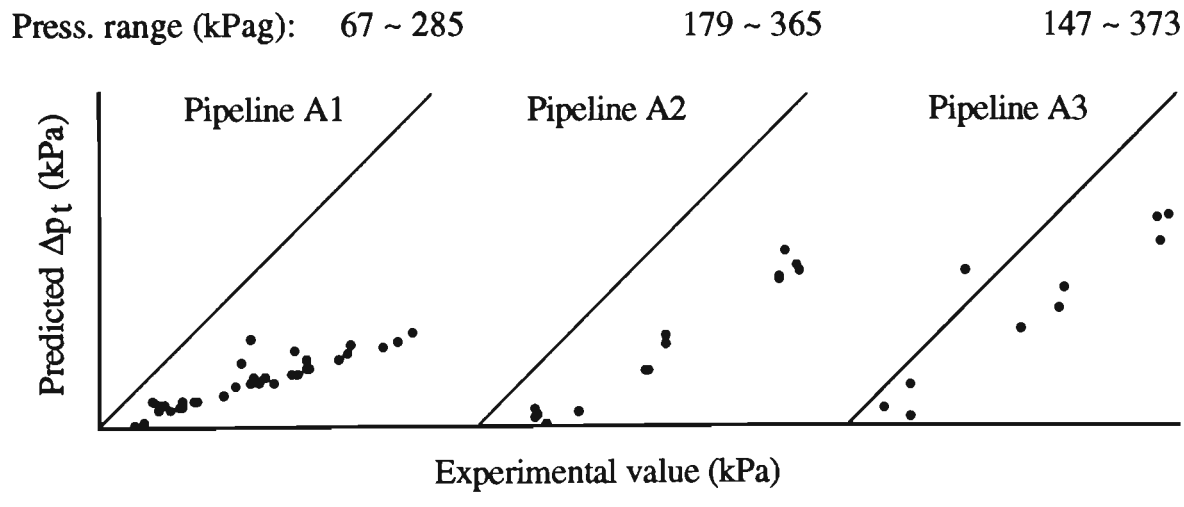

Figure 7.20 Predicted total pipeline air pressure drop vs experimental value in different pipelines by correlations in Chapter 5 and of Westman [66].

From Figures 7.10 to 7.20, it is evident that the existing scale-up equations in general cannot predict accurately the steady-state conveying characteristics. For example:

- the general shape of the m_s curves, when predicted from the test rig, tends to be retained during scale-up, as shown in Figures 7.10 to 7.15, whereas the 'experimental' curves show the opposite (i.e. different shape),

- the values of m_s, as predicted by Equations (7.1) and (7.2) and when compared with available experimental data, are found to be inaccurate for a given value of m_{f2} and Δp_{t2} (see Figure 7.12 to 7.15),

- as $m_f \rightarrow 0$, $\Delta p_t \rightarrow 0$ (see Figure 7.18),

- by using Equation (7.3), the total pipeline air pressure drops in all pipelines (e.g. Pipelines I, II, III, A1, A2 and A3) are overpredicted significantly.

The reasons for these discrepancies are that these existing equations have not taken into account:

- the geometry, number and/or location of bends,

- the number and/or location of straight pipes,

- relatively short pipe lengths (e.g. between bends),

- the influences of the conveyed materials.

It has been claimed that the correlations developed in Chapters 5 and 6 can predict accurately the pressure drop caused by both bends and straight pipes at different locations and for a wide range of operating conditions. Therefore, the total pipeline pressure drops in Pipelines I, II, III, A1, A2 and A3 are predicted by using these correlations, as shown in Figure 7.21. Note that: the vertical drop section Si (see Figure 3.2) in Pipelines I, II and III is considered as a short horizontal one; the equation for predicting the pressure drop in the vertical straight pipe in Chapter 5 is used for the vertical lift section Sb; all bends (e.g. horizontal-vertical or vertical-horizontal) are assumed as horizontal-horizontal bends. This information is assumed also in the following calculations.

Comparing results in Figure 7.21 with results in Figures 7.10 to 7.17, 7.19 and 7.20 and by Equation (7.3), shows that:

- it is much more accurate to deal separately with bends and straight pipes than to treat the total pipeline as a single entity,

- the conveyed materials have numerous influences on the pressure drop so that the existing correlations cannot be used directly for different materials.

However, most of the total pipeline air pressure drop in Pipelines I, II, III, A1, A2 and A3 still are underpredicted (see Figure 7.21). The reason is that Pipelines I, II, III, A1, A2 and A3 contain several short straight pipes. Also, the correlations in

Chapters 5 and 6 are suitable only for the long straight sections of pipe where the particles can be re-accelerated fully and the bends connected by such long straight pipes. For the bends connected by short straight pipes (downstream), particles are decelerated again before they have been accelerated fully in the straight pipe upstream of the second bend. Therefore, more pressure drop is required for the re-acceleration of the particles after the second bend has been passed.

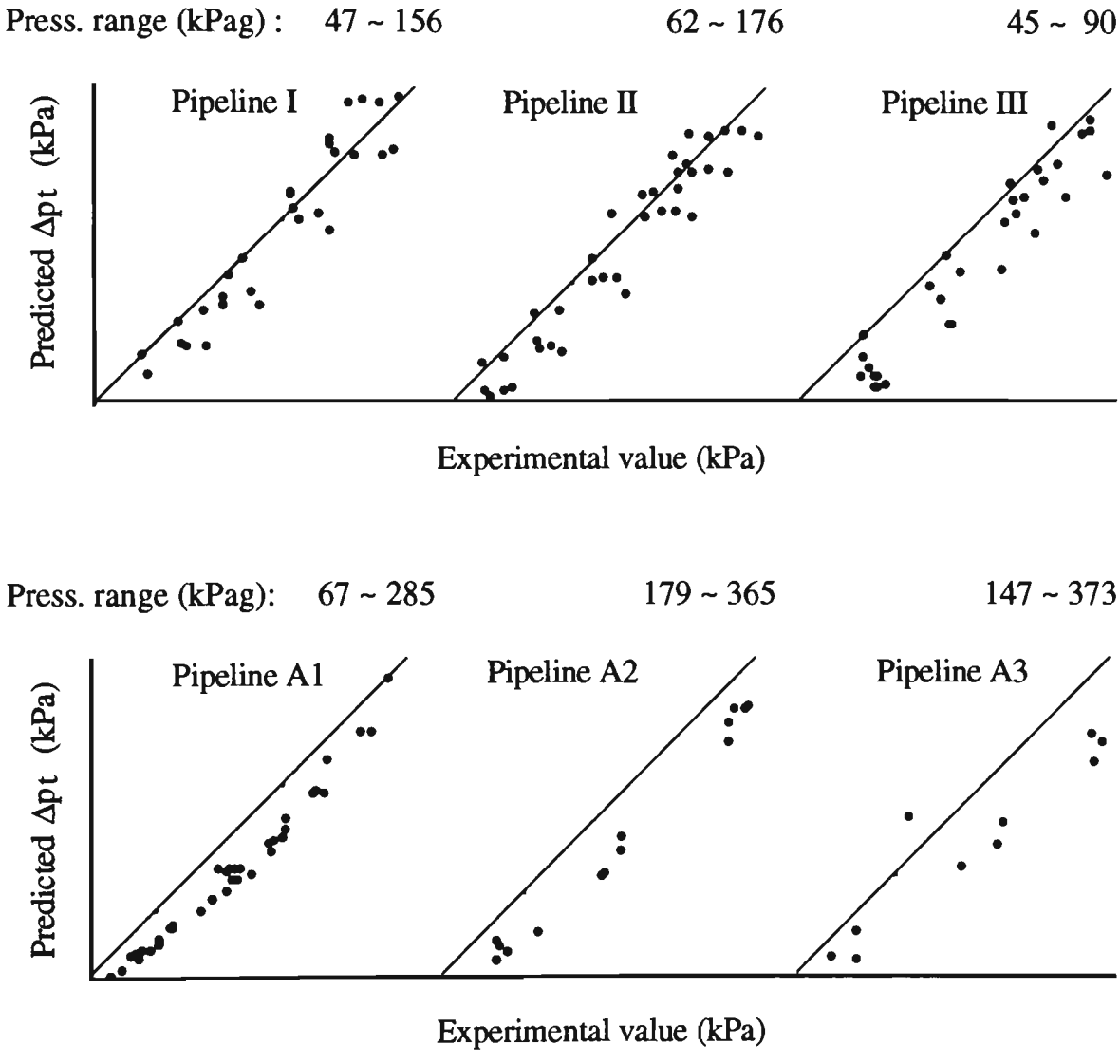

Figure 7.21 Predicted total pipeline air pressure drop vs experimental value in different pipelines by Equations (5.11), (5.12), (6.4) and (6.7).

7.4 Concept of New Scale-up Procedure

It is evident from Section 7.3 that the following aspects should be considered for the accurate and reliable scale-up of test rig data to full-scale installations that comprise relatively short straight sections of pipe.

- The geometry, location and number of bends and straight sections of pipe should be taken into account (different configurations of pipeline produce different total pipeline air pressure drops and steady-state conveying characteristics, even though these configurations of pipeline have the same total effective length).

- Allowance should be made during scale-up for the relatively short straight sections of pipe that are used commonly in industry.

- The influences of the conveyed materials also should be taken into account.

However, the latter influences are very complicated and have not been described properly. These influences can be determined only by pneumatic conveying experiments. In this thesis project, the conveyed material is given (e.g. fly ash).

In order to develop scale-up procedures which not only are reliable and accurate but also can be employed widely, the following two aspects also should be considered.

- Confidence is required in scaling-up test rig data obtained from any constant diameter of pipeline to other pipelines of different length, diameter, bend number and step.

- The configuration of the test rig pipeline should be as simple as possible and reproduced easily by other researchers.

According to the above criteria, a simple configuration of pipeline as shown in Figure 7.22 is designed for determining the exponents in the empirical correlations (e.g. Equations (5.12) and (6.7)).

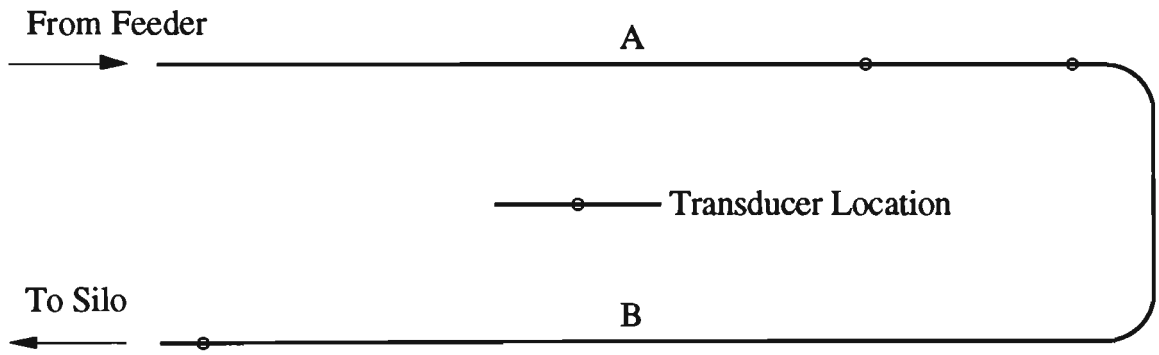

Figure 7.22 Basic configuration of pipeline used to develop new scale-up procedure.

In this pipeline, there are bends, as well as long and short straight sections of pipe. Therefore, it is still very important to predict accurately the pressure along the long straight sections of pipe. Hence, the correlations set up in Chapter 5 still remain unchanged. Only the exponents in Equation (6.7) are re-determined by minimising the sum of the squared errors of pressure measured by the transducers in straight section A, starting from the point in straight section B where the other transducer is

installed (see Figure 7.22). All the transducers in straight sections A and B are installed beyond any bend effects.

7.5 Scale-up Investigation

Equation (6.7) shows that ζ_S is a function of R. Therefore, the experimental data obtained from Pipelines I and A1 are used together to determine the exponents in Equation (6.7). The exponents in Equation (6.7) are determined by minimising the sum of the squared errors of pressure at points Tc, Td, Tc3 and Tc4, starting from points Te and Te1 respectively. The determined values of exponent are listed in Table 7.1.

Table 7.1: Values of exponent in new scale-up procedure.

	Equation (6.7)	Equation (7.4)		
Exponent	Based on data from Pipeline I & A1*	Based on data from Pipeline I*	Based on data from Pipeline III	Based on data from Pipeline A1*
x1	5.3062	5.3062	5.3144	5.3062
x2	-0.4366	-0.4366	-0.4170	-0.4366
x3	-1.9341	-1.9341	-1.9504	-1.9341
x4	-0.1175	-0.1175	-0.1263	-0.1175
y1	0.0062	0.0085	0.0076	0.0520
y2	0.5020	0.1654	0.0753	0.6580
y3	0.7901	1.3335	1.4591	0.6730
y4	0.2449	0.0129	-0.0262	-1.4950

* Note that values of x1, x2, x3 and x4 are the same as in Table 5.3.

Then by using the above 'determined' values of exponent, the total pipeline air pressure drops in Pipelines I, II, III, A1, A2 and A3 are predicted. The agreement is not good, as shown in Figure 7.23 which is similar to Figure 7.21.

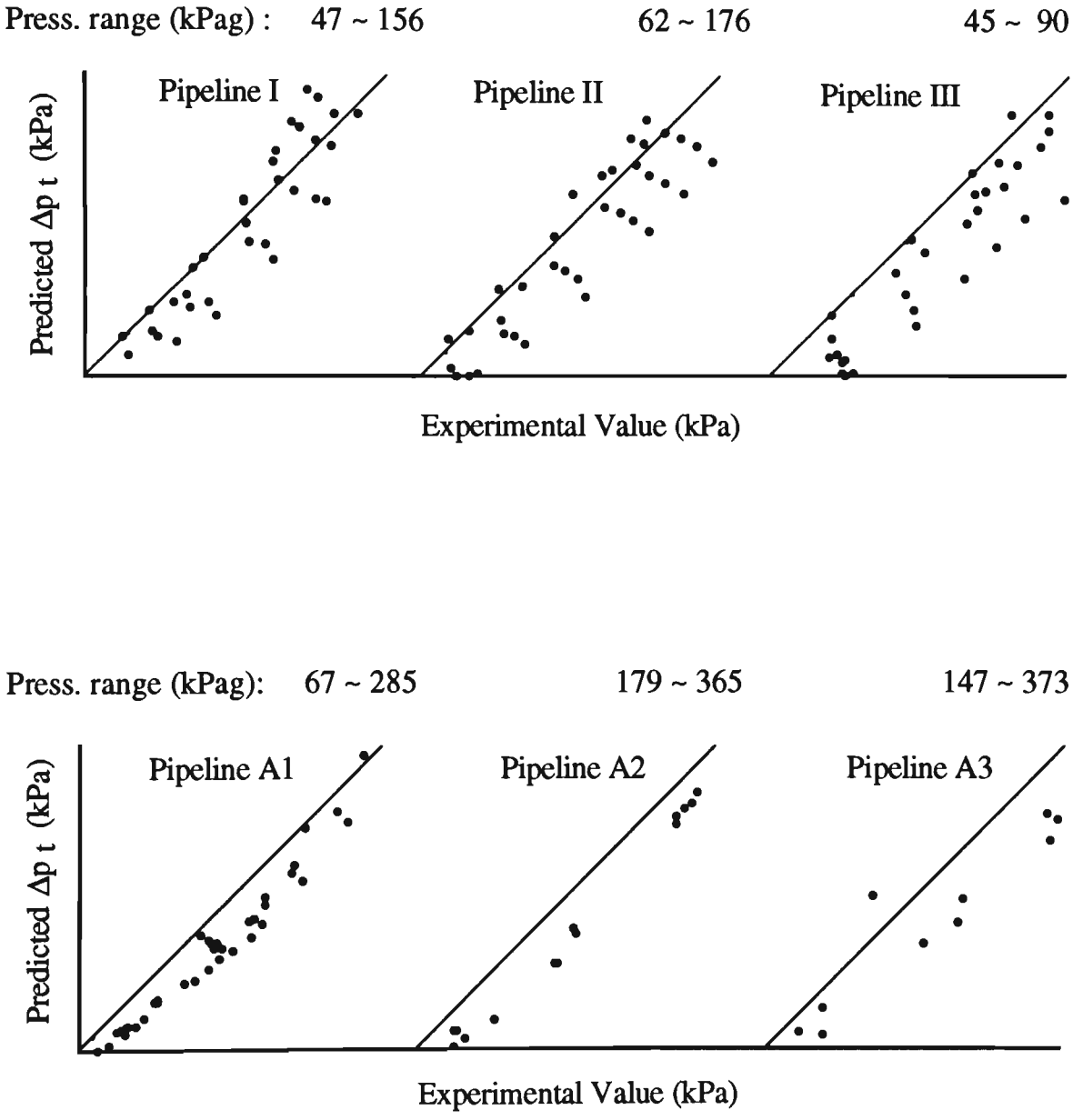

Figure 7.23 Predicted total pipeline air pressure drop vs experimental value in different pipelines based on data from Pipelines I and A1.

The reason is that the situation in Figure 7.22 is very different from the configuration where there are two long straight pipes with a bend between them. The pressure drop for the re-acceleration of the particles in the former configuration of pipeline is higher than in the latter one. Also, the pressure drop for the re-acceleration of the particles is added into the bend pressure drop. Therefore, Equation (6.7) which is suitable for the configuration of pipeline with one bend and two long straight pipes should be modified. The modified equation is as follows.

$$\zeta_s = y1\ m^{*y2}\ F_{ro}^{y3}\ \rho_{fo}^{y4} \qquad (7.4)$$

Also, the exponents y1, ..., y4 are determined empirically and only valid for the given product and bend geometry.

Firstly, the experimental data obtained from Pipeline I are used to determine the exponents in Equation (7.4) by minimising the sum of the squared errors of pressure at points Tc, Td in section Sd, starting from point Te in Section Sf (see Figure 3.2). The determined values of exponent are listed also in Table 7.1.

Then by using the above correlations, the total pipeline air pressure drop and selected pressures in Pipelines I, II and III are predicted, starting from the end of pipeline or points along the pipeline. All the agreement is quite good, some of the predictions being shown in Figure 7.24. Also, the steady-state characteristics of Pipelines I, II and III are predicted accurately, as shown in Figure 7.25.

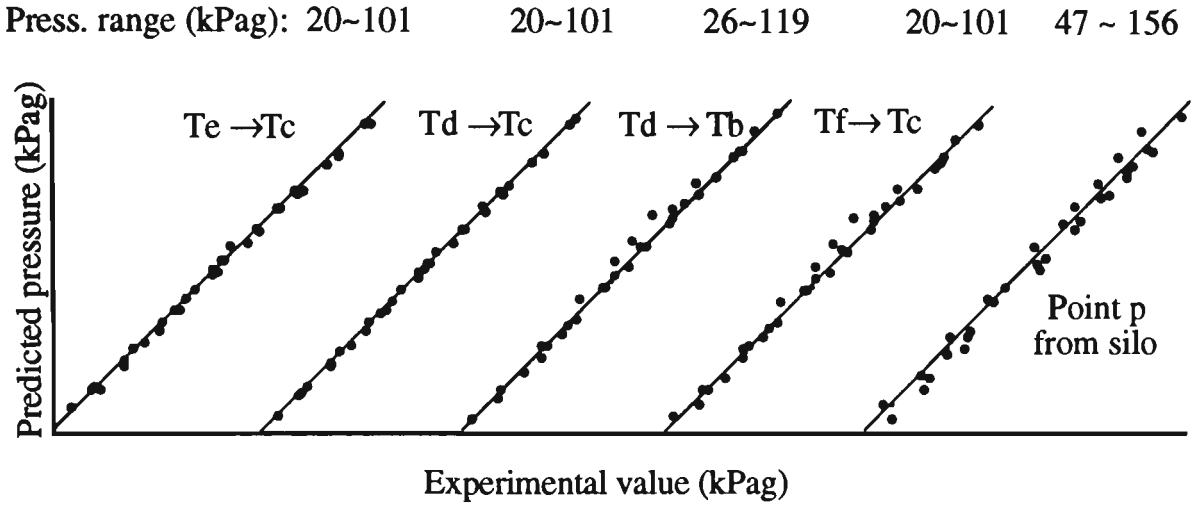

(a) Pipeline I (L=102 m, D=52.5 mm).

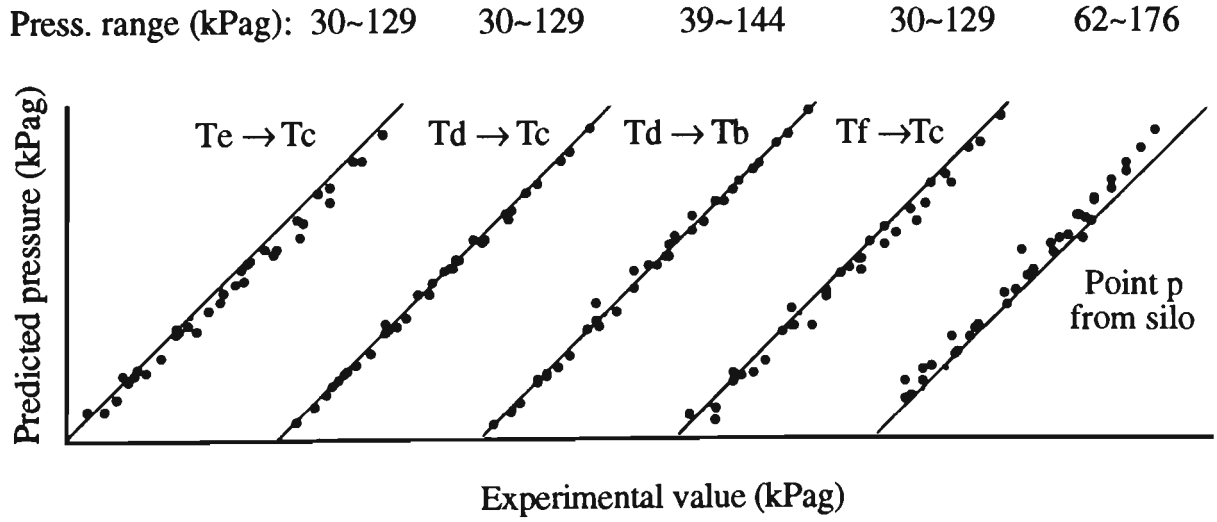

(b) Pipeline II (L=135 m, D=52.5 mm).

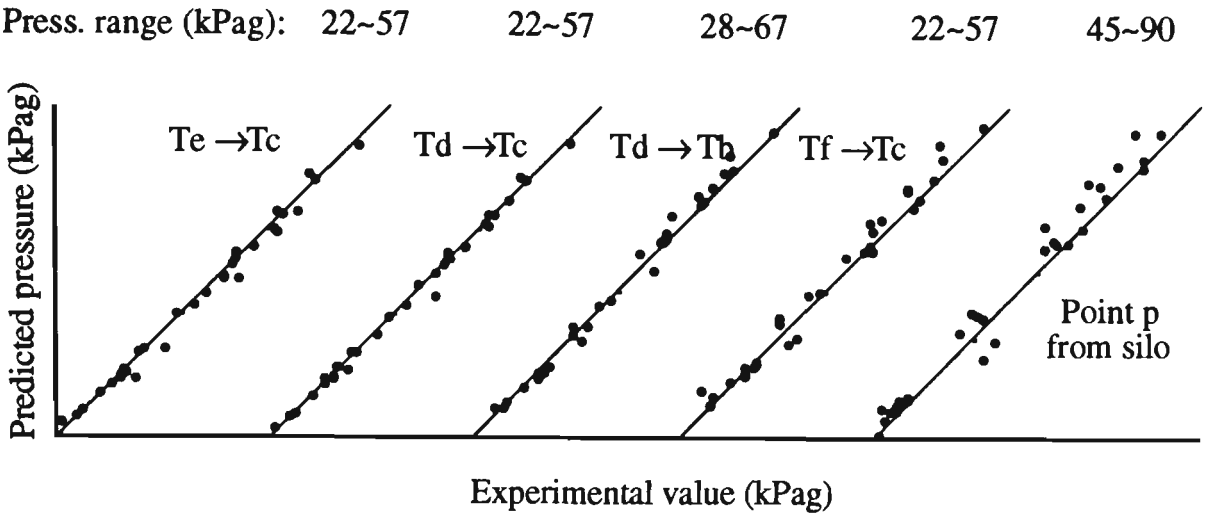

(c) Pipeline III (L=137 m, D=80.5 mm).

Figure 7.24 Predicted pressure vs experimental value based on data from Pipeline I.

(Note: Te → Tc means the predicted pressure at Tc, starting from Te)

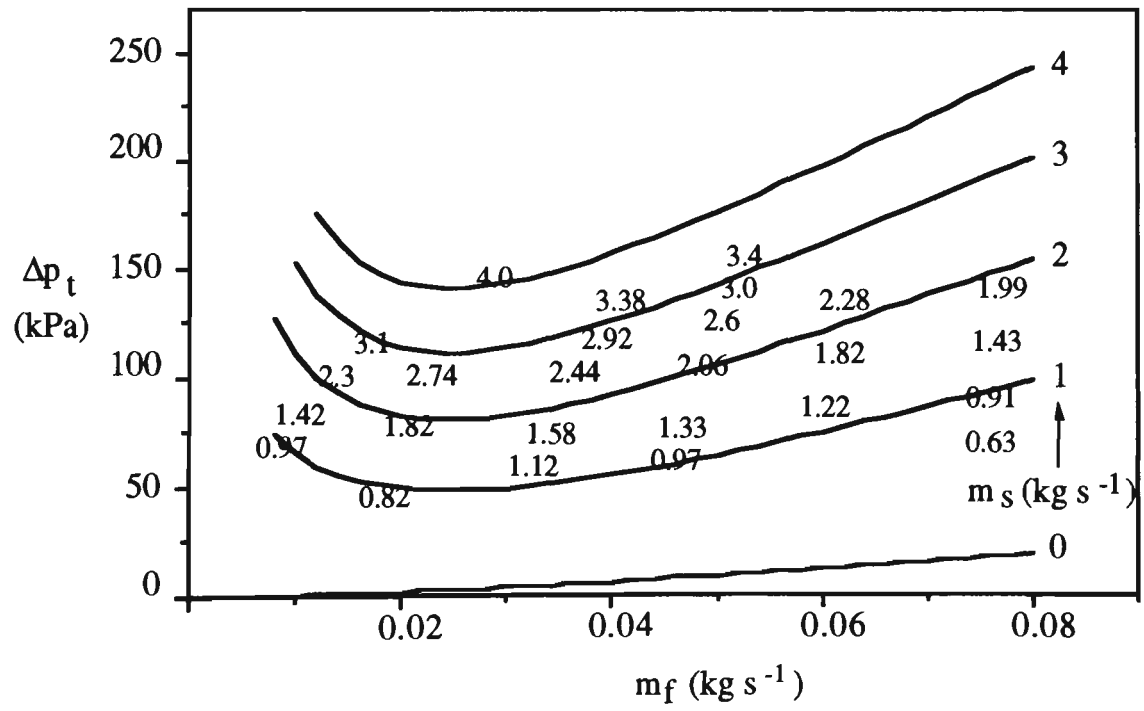

(a) Pipeline I (L=102 m, D=52.5 mm).

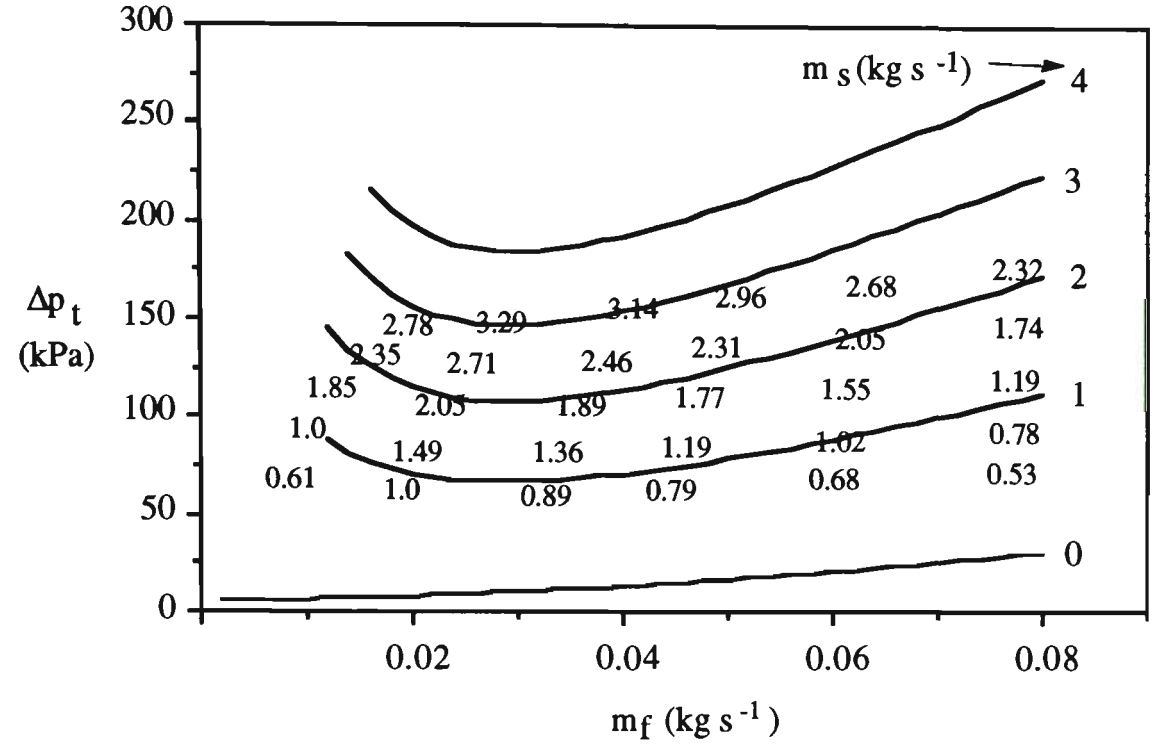

(b) Pipeline II (L=135 m, D=52.5 mm).

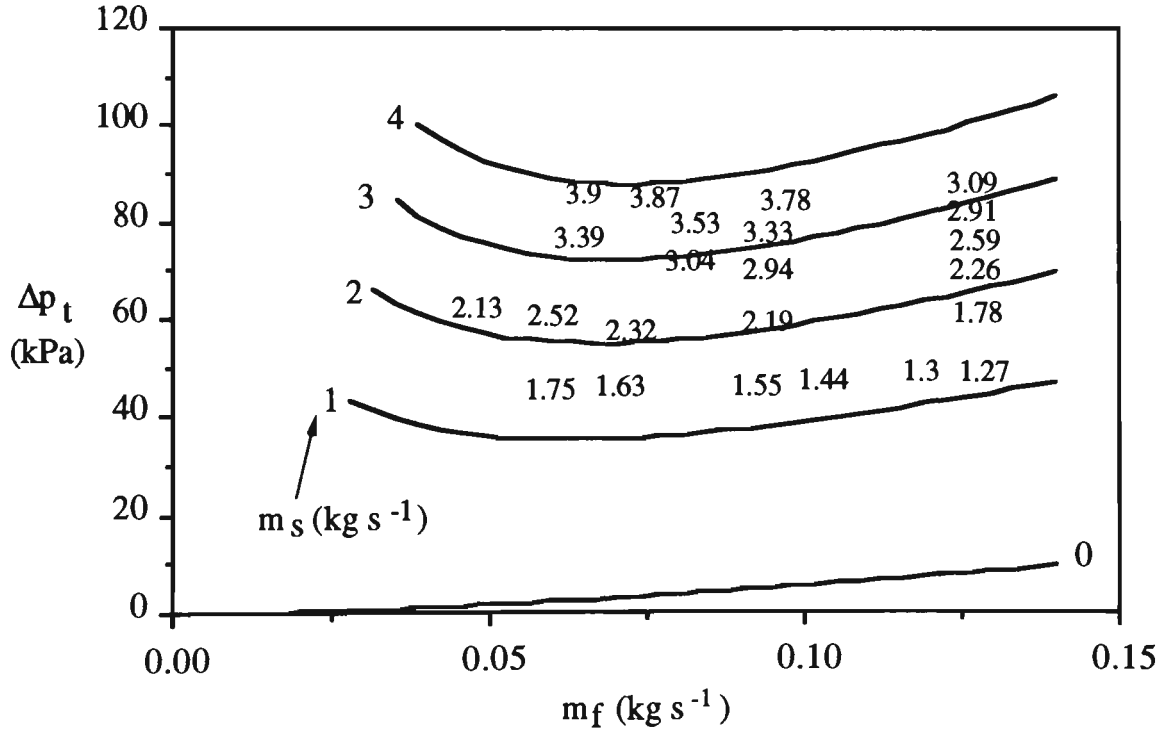

(c) Pipeline III (L=137 m, D=80.5 mm).

Figure 7.25 Predicted steady-state conveying characteristics of Pipelines I, II and III based on data from Pipeline I.

It is required ultimately to scale-up test rig data obtained from any constant diameter pipeline to other pipelines of different length, diameter, bend number and step. Hence, secondly, the data obtained from Pipeline III are used to determine the exponents in Equations (5.12) and (7.4). Similarly, the exponents are determined by minimising the sum of the squared errors of pressure at points Tc, Td in section Sd, starting from point Te in section Sf. The determined values of exponent are listed in Table 7.1. Note that exponents x1, ..., x4 have been determined firstly.

Then also by using these formulae, the total pipeline air pressure drop and selected pressures in Pipeline I, II and III are predicted, starting from the end of pipeline or points along the pipeline. All the agreement still is very good, some of the predictions being shown in Figure 7.26.

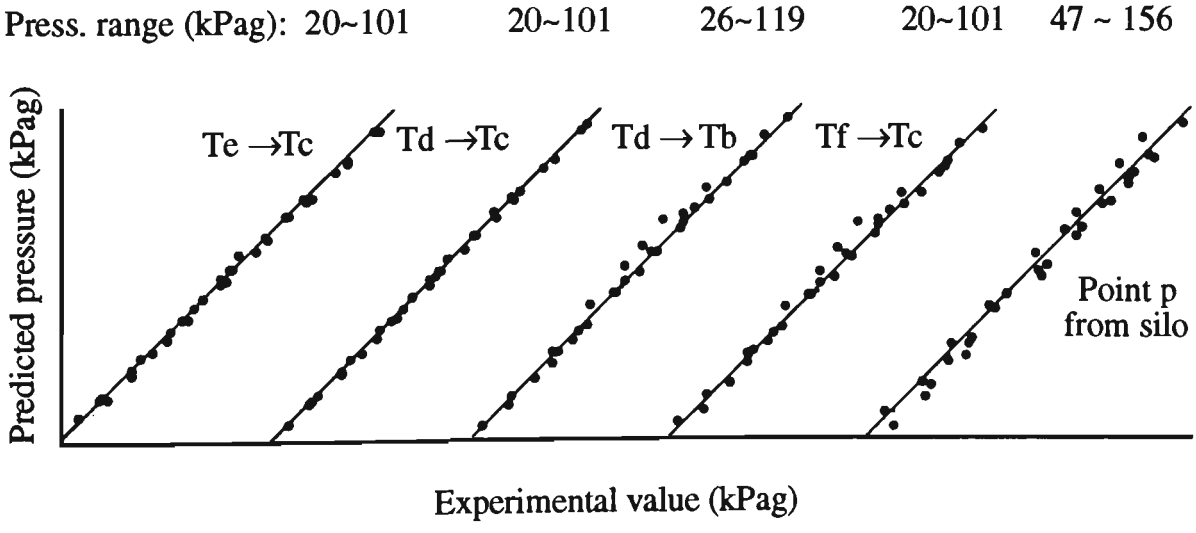

(a) Pipeline I (L=102 m, D=52.5 mm).

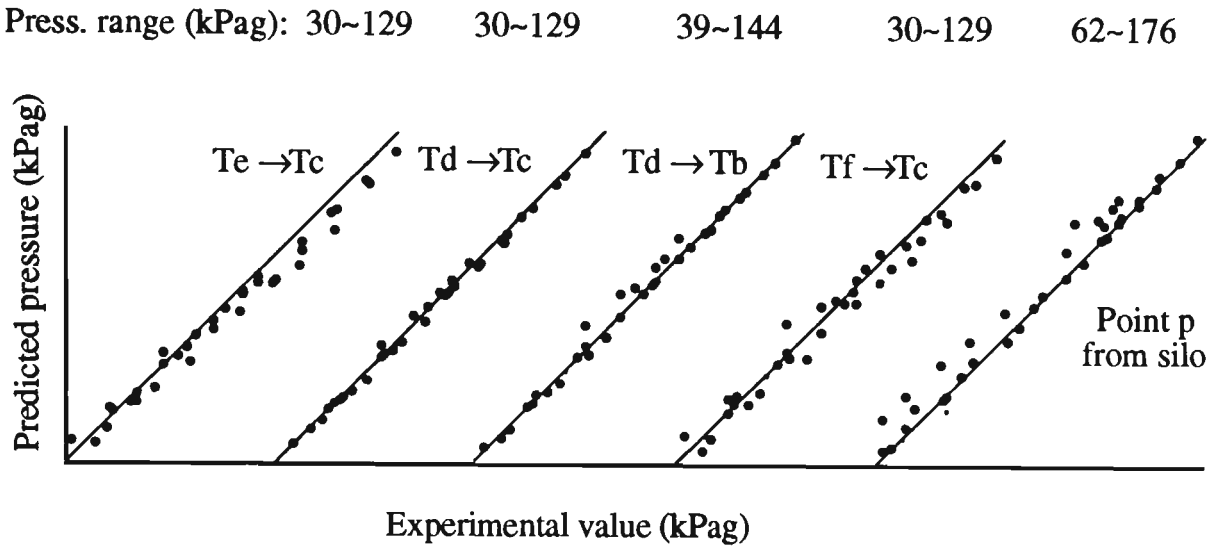

(b) Pipeline II (L=135 m, D=52.5 mm).

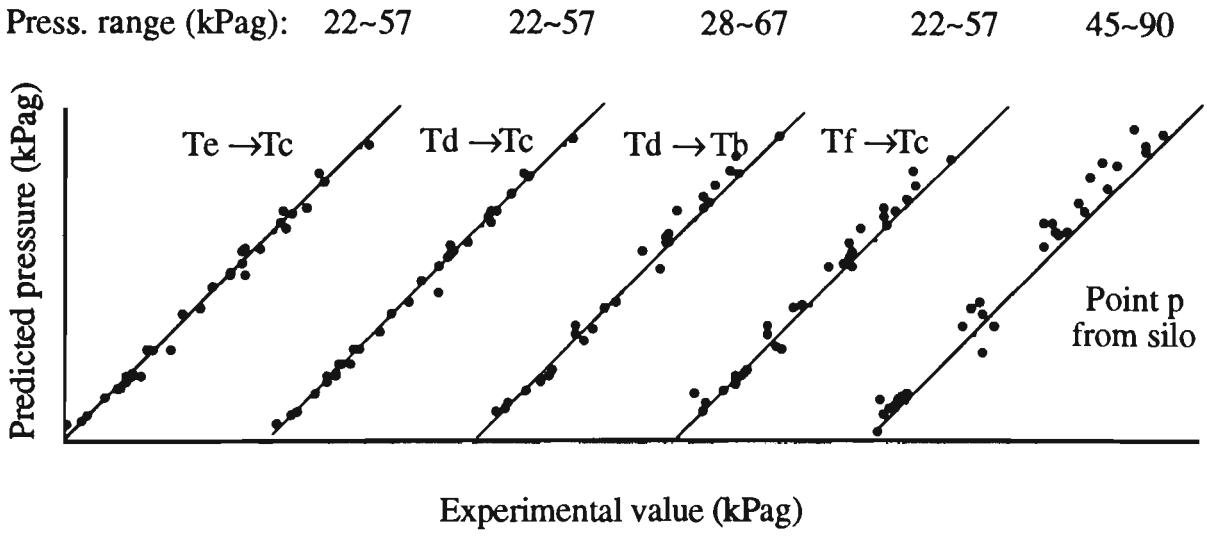

(c) Pipeline III (L=137 m, D=80.5 mm).

Figure 7.26 Predicted pressure vs experimental value based on data from Pipeline III.

(Note: Te → Tc means the predicted pressure at Tc, starting from Te)

As mentioned previously, exponents y1, ..., y4 are determined empirically and are only valid for the given product and bend geometry. Pipelines I, II and III have bends with R=254 mm. However, Pipelines A1, A2 and A3 have bends with R=1000 mm. Therefore, exponents y1, ..., y4 should be determined again, based on the data from the pipeline comprising the R=1000 mm bends. Similarly, the exponents are determined by minimising the sum of the squared errors of pressure at points Tc3 and Tc4, starting from point Te1 (see Figure B.1). The determined values of exponent are listed also in Table 7.1.

Then the total pipeline air pressure drop and selected pressures in Pipelines A1, A2 and A3 are predicted by using the above formulae, starting from the end of pipeline or points along the pipeline. The agreement generally is quite good, as illustrated in Figure 7.27.

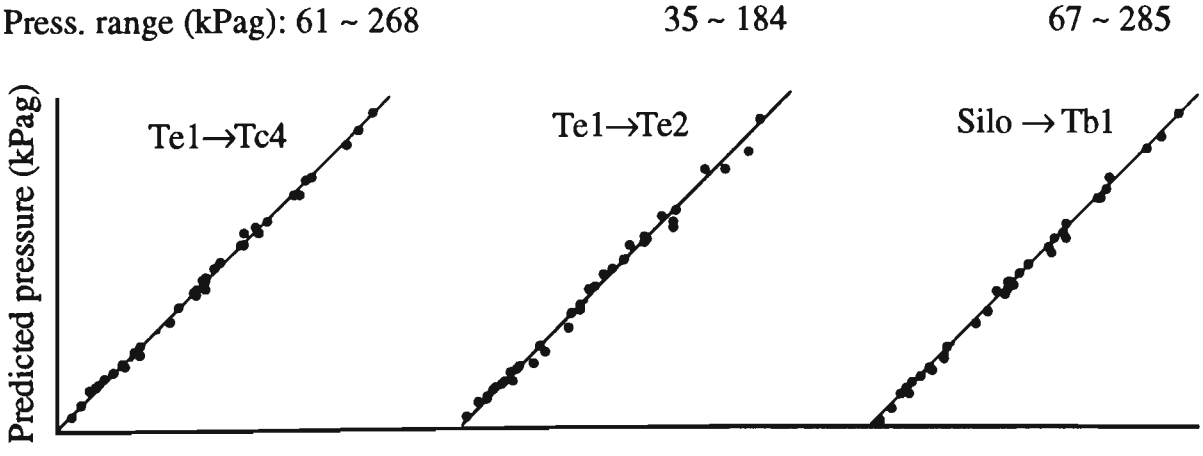

(a) Pipeline A1 (L=172 m, D=69 mm).

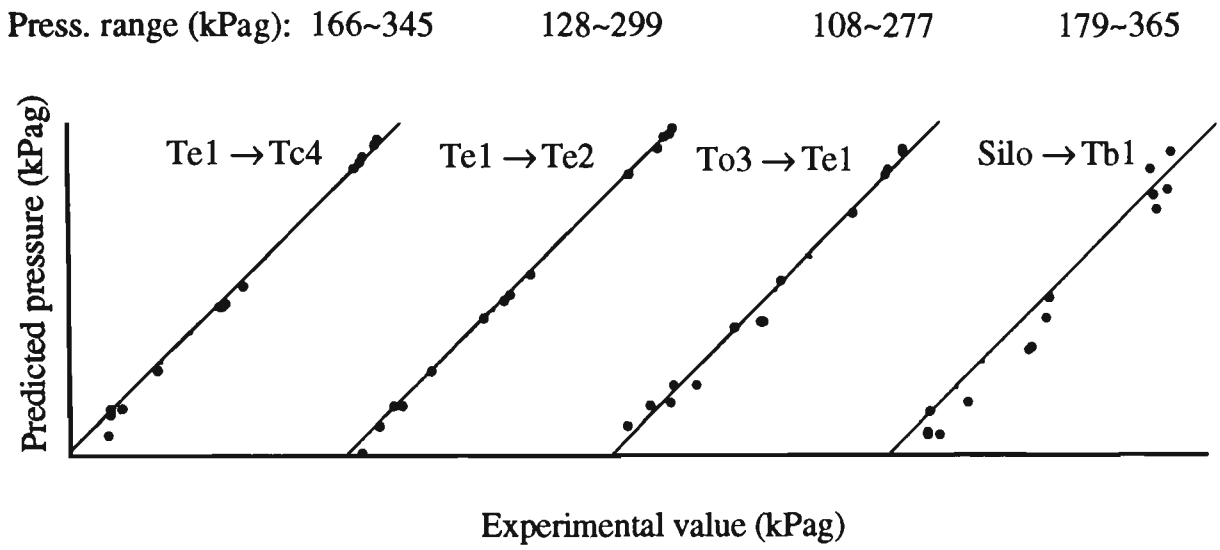

(b) Pipeline A2 (L=554 m, D=69 mm).

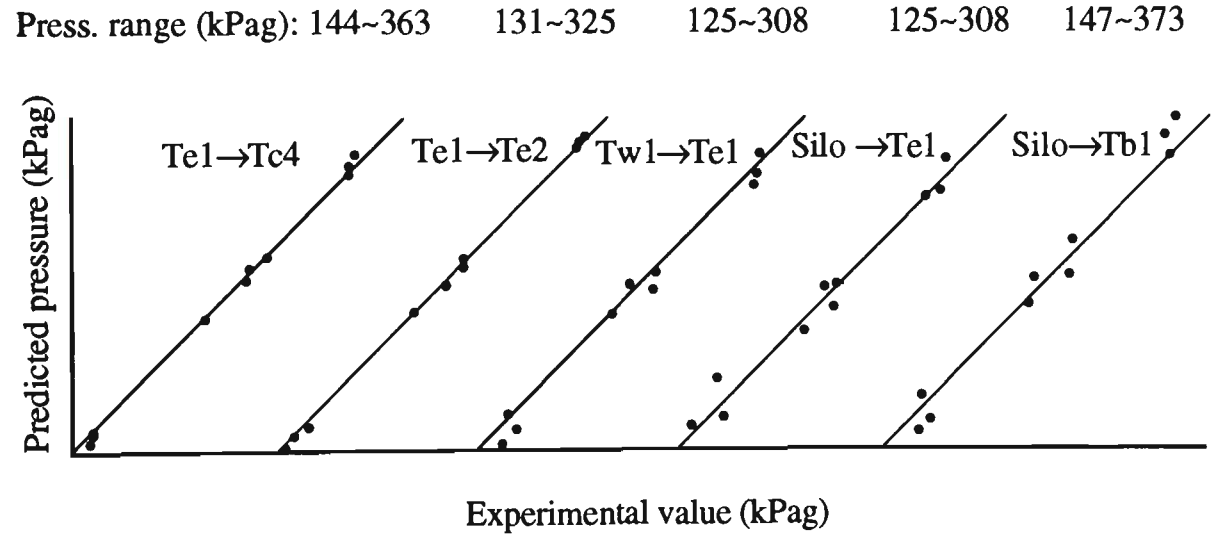

(c) Pipeline A3 (L=945 m, D=69/81 mm).

Figure 7. 27 Predicted pressure vs experimental value based on data from Pipeline A1.

(Note: Te1 → Tc4 means the predicted pressure at Tc4, starting from Te1)

7.6 Pressure Drop due to Bends of Different Radii

As described in Chapter 6, longer radius bends produce a lower pressure drop. This conclusion was derived from the bends connected by long straight sections of pipe. In industry, however, relatively short straight sections of pipe are used commonly. Figures 7.21 and 7.23 have shown clearly that the correlations from Chapters 5 and 6 cannot predict accurately the total pipeline air pressure drop in pipelines comprising short straight pipes. Therefore, the correlation for bend pressure drop should be modified (see Equation 7.4). The exponents in the modified correlation are determined by using the data obtained from the pipeline as shown in Figure 7.22. Based on the 'determined' values of exponent in the modified equation for conveying fly ash (as used in Section 7.5), the pressure drops caused by the bends of different radius are shown in Figure 7.28.

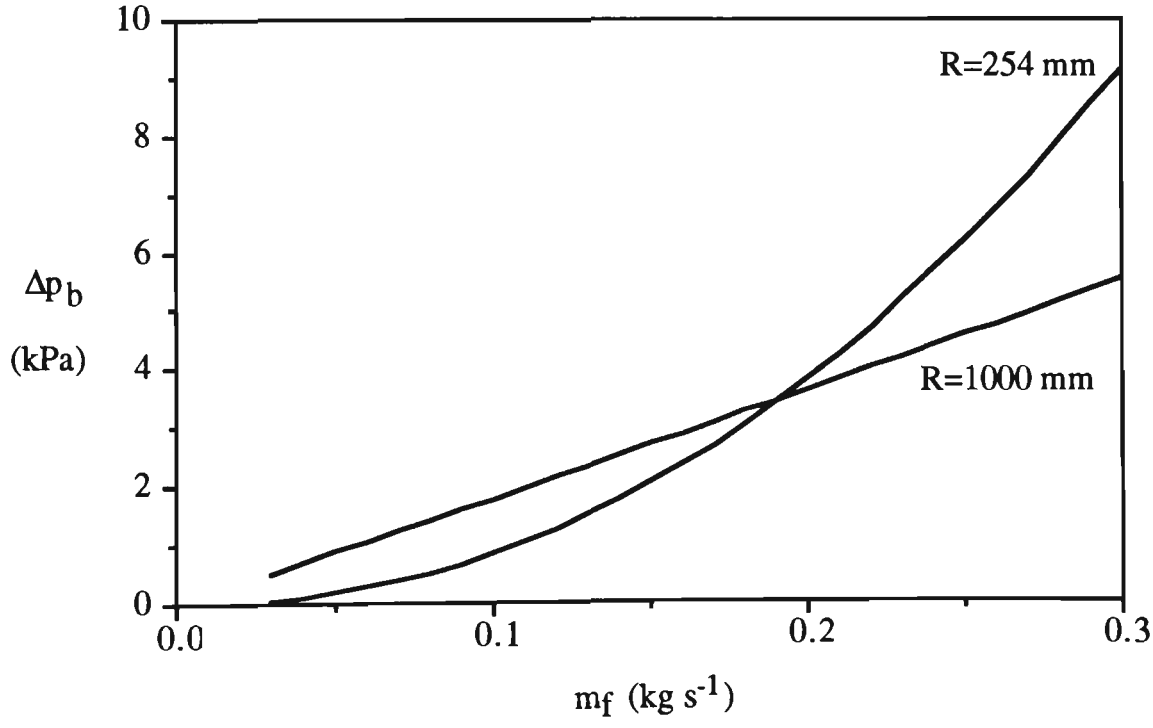

(a) $\rho_{fo} = 1.8$ kg m^{-3}.

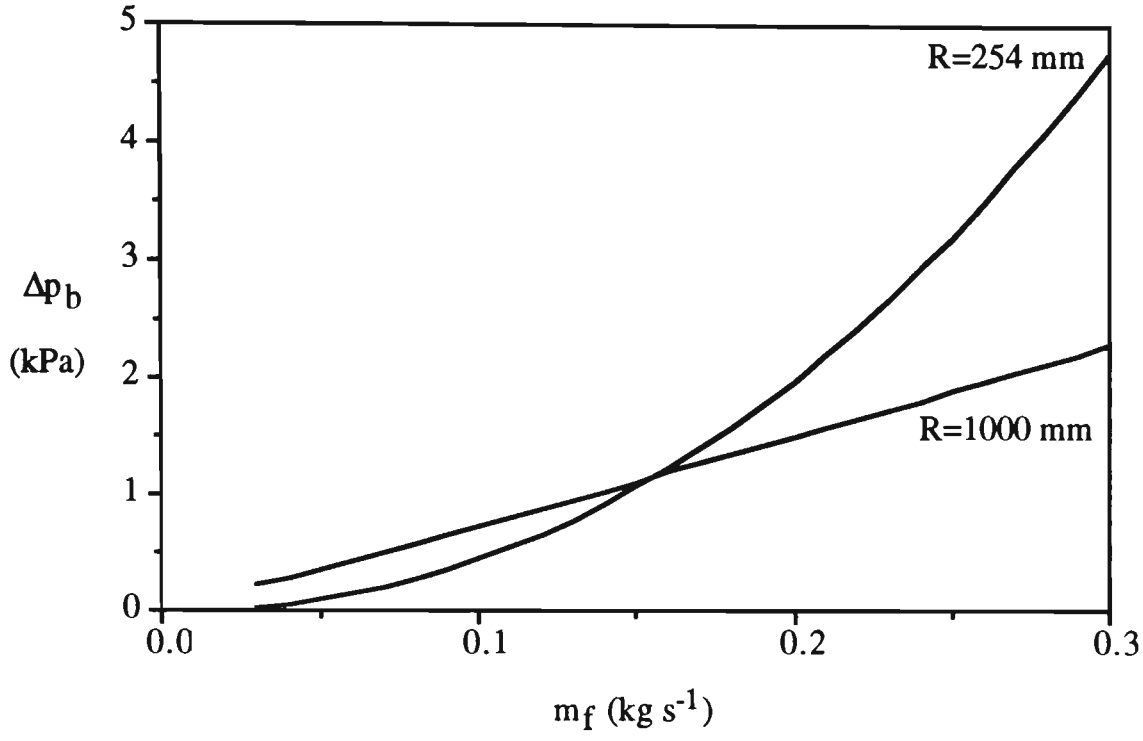

(b) $\rho_{fo} = 2.39$ kg m^{-3}.

Figure 7.28 Pressure drop caused by bends of different radius at different locations for conveying fly ash (D=80.5 mm, m_S=2.0 kg s^{-1}).

Also, based on the total pipeline air pressure drop in a pipeline comprising short straight sections of pipe (e.g. from silo to point Ta in Pipeline III, see Figure 3.2), the pressure drops caused by the bends of different radius are compared. The results are illustrated in Figure 7.29.

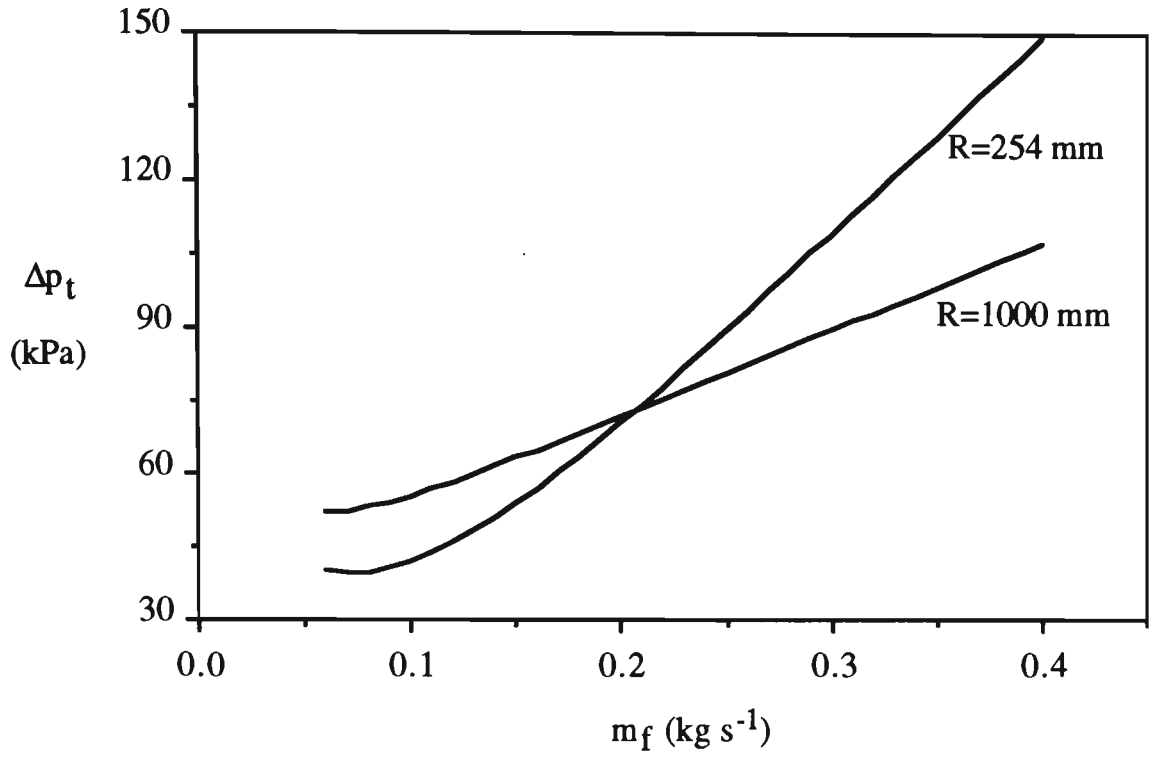

Figure 7.29 Total pipeline air pressure drop from silo to point Ta in Pipeline III ($D=80.5$ mm, $m_S=2.0$ kg s^{-1}).

Figures 7.28 and 7.29 show that, for a constant product mass flow rate (e.g. $m_S=2.0$ kg s^{-1}), longer radius bends produce a higher pressure drop at low air mass flow rates and a lower pressure drop at high air mass flow rate. The reason is as follows.

According to Haag [18]:

$$v_{so} = v_{si}\, e^{(-\mu \frac{\pi}{2})} \tag{7.5}$$

The change in solids velocity along the pipeline shown in Figure 7.22 is depicted in Figure 7.30.

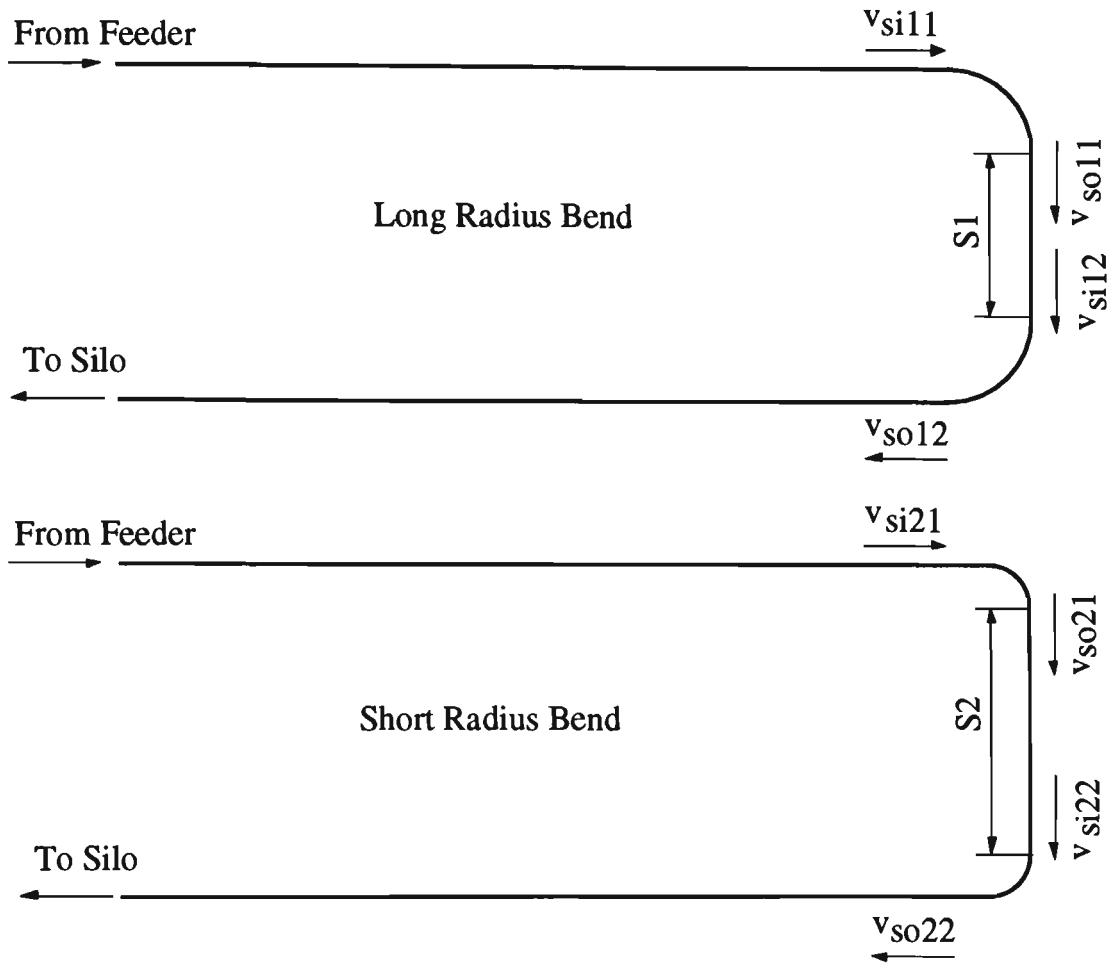

Figure 7.30 Velocity profile along a pipeline comprising bends of different radius and short straight pipe.

If $v_{si11} = v_{si21}$, then from Equation (7.5), $v_{so11} = v_{so21}$. However, since S1 < S2, so $v_{si12} < v_{si22}$, which results in $v_{so12} < v_{so22}$. In Chapter 6, the bend pressure drop was defined as the sum of two components. One component is located in the bend itself, whilst the other occurs in the straight section of pipe immediately downstream from the bend for the re-acceleration of the particles. Usually, the latter is much higher than the former. Therefore, it is expected that longer radius bends will produce a higher pressure drop. However, in very dilute phase conveying, the particle velocity is very high. Therefore, the bend radius has a great influence on the frictional force hindering the motion of the particles. Hence, the pressure drop

located in the bend itself becomes dominant which results in the shorter radius bend producing a higher pressure drop.

CHAPTER 8

APPLICATIONS

8.1 Introduction

The total pipeline air pressure drop can be considered as a function of the following three factors:

- particle properties (e.g. particle size, size distribution, density and shape),

- configuration of pipeline (e.g. pipe diameter, length, bend number and location),

- conveying conditions (e.g. air density, velocity, product and air mass flow rates).

In Chapter 7, a new scale-up procedure was developed for the prediction of the total pipeline air pressure drop and it was demonstrated to have good accuracy and reliability. However, the test material was only fly ash and the scale-up procedure did not include any particle properties. Therefore, it is not known that this scale-up procedure still can be used for other materials which have significantly different particle properties.

In this chapter, two other materials (pulverised brown coal and plastic pellets) are investigated and conveyed in different configurations of pipeline (e.g. Pipelines I, III, A1, A2 and A4). The experimental data from each configuration of pipeline are employed to examine the above scale-up procedure.

These results also demonstrate the good accuracy and reliability of this new scale-up procedure.

8.2 Test Materials

The particle density (air pycnometer) and loose-poured bulk density (according to IS06770) of each test material (pulverised brown coal and plastic pellets) are listed in Table 8.1.

Table 8.1: Particle and bulk densities of test materials.

Material	Particle density (kg m^{-3})	Bulk density (kg m^{-3})	d_p (μm)
Pulverised brown coal	1488	437	25.8
Plastic pellets	834	458	3750**
Fly ash*	2197	634	15.5

* Quoted here again for ease of comparison.

**Equivalent volume diameter.

The plastic pellets are cylindrical in shape and of uniform size (e.g. 4 mm diameter, 2.2 mm long). However, the pulverised brown coal has a wide size distribution, as shown in Table 8.2 and Figure 8.1.

From Figure 8.1 and Table 8.2, it is clear that the pulverised brown coal also is a very fine powder. These two test materials have significantly different particle properties (i.e. compared with the fly ash, see Table 8.1 or Section 3.5).

Table 8.2: Pulverised brown coal size distribution, according to Malvern 2600C laser diffraction analyser.

No.	Particle size range (μm)	Average size (μm)	Mass % in range
1	5.8 - 7.2	6.5	7.0
2	7.2 - 9.0	8.1	5.4
3	9.0 - 11.4	10.2	5.5
4	11.4 - 14.5	12.95	4.9
5	14.5 - 18.5	16.5	5.2
6	18.5 - 23.7	21.1	7.9
7	23.7 - 30.3	27.0	8.1
8	30.3 - 39.0	34.65	8.8
9	39.0 - 50.2	44.6	8.9
10	50.2 - 64.6	57.4	7.6
11	64.6 - 84.3	74.45	7.1
12	84.3 - 112.8	98.55	6.2
13	112.8 - 160.4	136.6	3.9
14	160.4 - 261.7	211.05	2.0
15	261.7 - 312.0	286.85	0.1

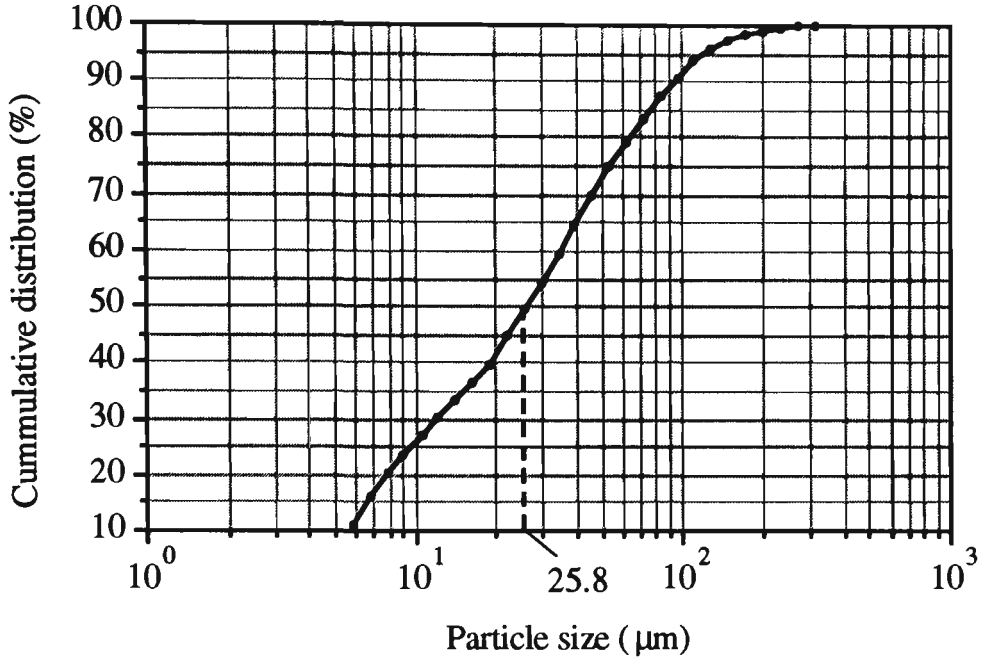

Figure 8.1 Cumulative size distribution for pulverised brown coal according to Malvern 2600C laser diffraction analyser.

8.3 Conveying Pipelines

Different configurations of pipeline were employed to convey the above two test materials, as summarised in Table 8.3.

Table 8.3: Conveying pipelines.

Material	Pipeline
Pulverised brown coal	A1, A2, A4
Plastic pellets	I, III

8.4 Test Results

The two test materials were subjected to a wide range of conveying conditions. All the pressure transducers were believed to be installed beyond any bend effects. The range of test conditions for each product is listed in Table 8.4.

Table 8.4: Test conditions.

	Material				
	Pulverised brown coal			Plastic pellets	
	Pipeline				
	A1	A2	A4	I	III
Range of m*	3.6 - 63.4	0.5 - 19.4	0.7 - 20.9	4.1 - 18.4	5.4 - 12.9
No. of measured points	5	9	8	6	6
No. of data	26	22	19	23	30

Figures 8.2 to 8.6 show the steady-state conveying characteristics of Pipelines I, III, A1, A2 and A4. Note that the m_S curves were obtained by using interpolation techniques.

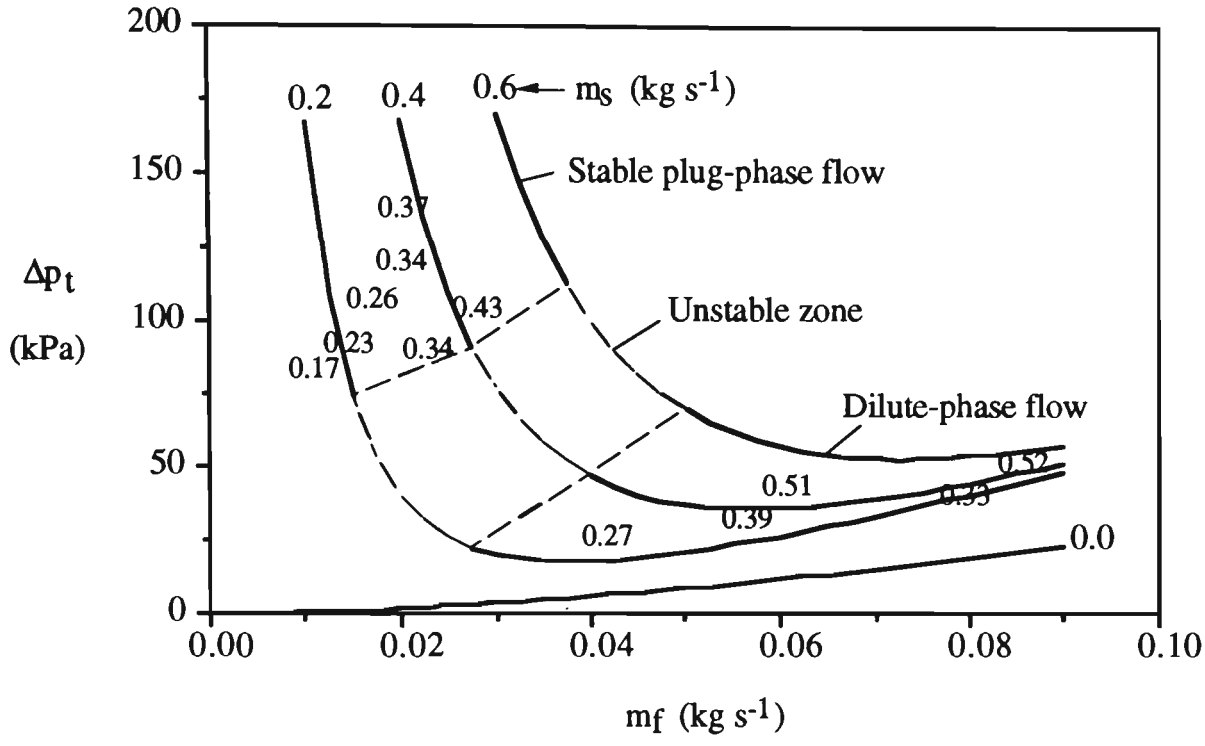

Figure 8.2 Steady-state conveying characteristics of Pipeline I and plastic pellets (L=102 m, D=52.5 mm, R=254 mm).

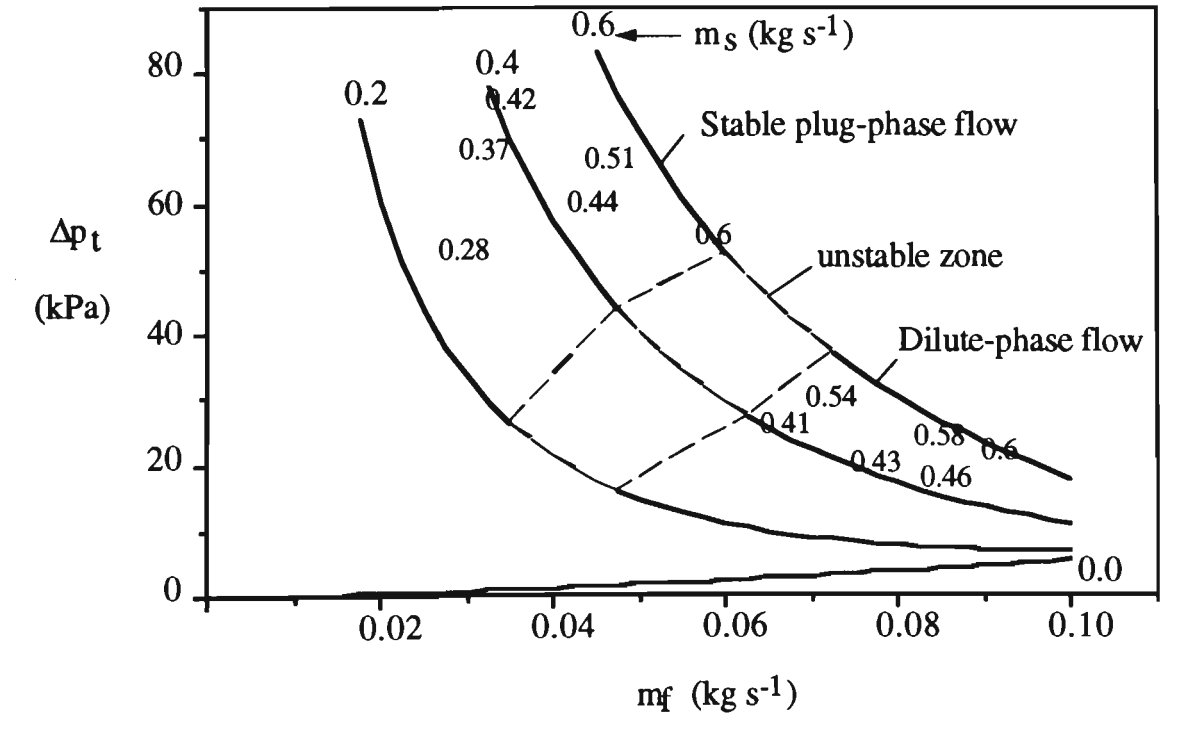

Figure 8.3 Steady-state conveying characteristics of Pipeline III and plastic pellets (L=137 m, D=80.5 mm, R=254 mm).

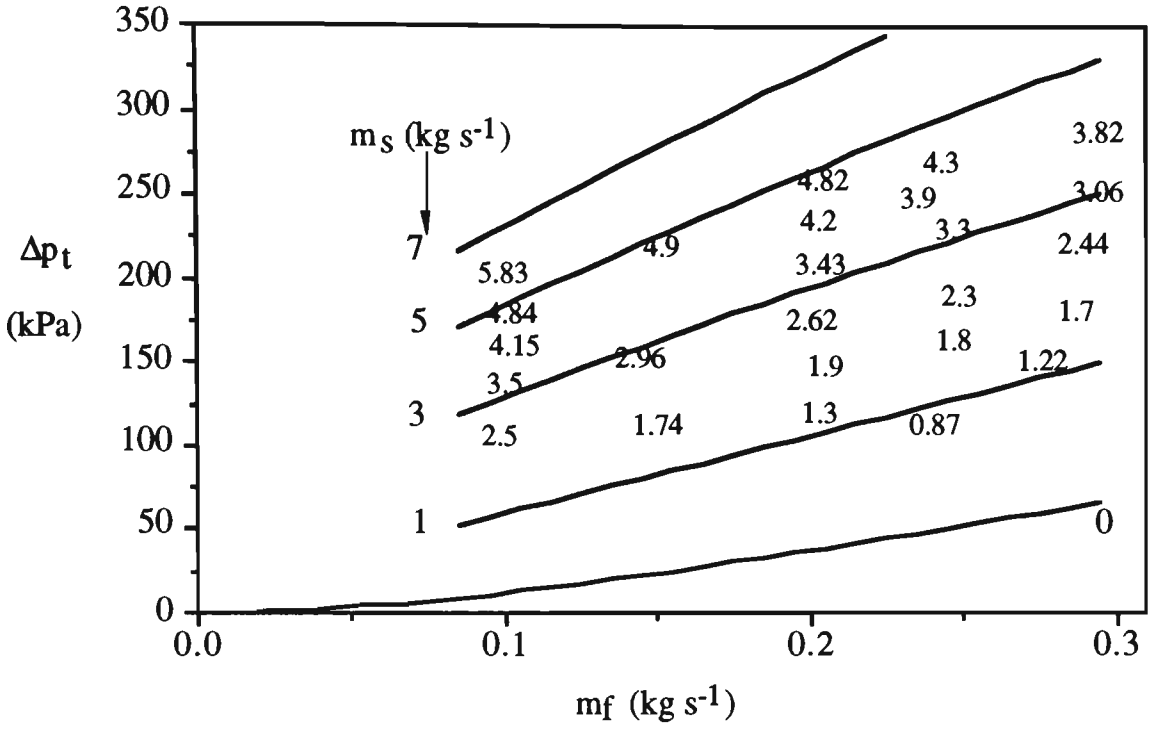

Figure 8.4 Steady-state conveying characteristics of Pipeline A1 and pulverised brown coal (L=172 m, D=69 mm, R=1000 mm).

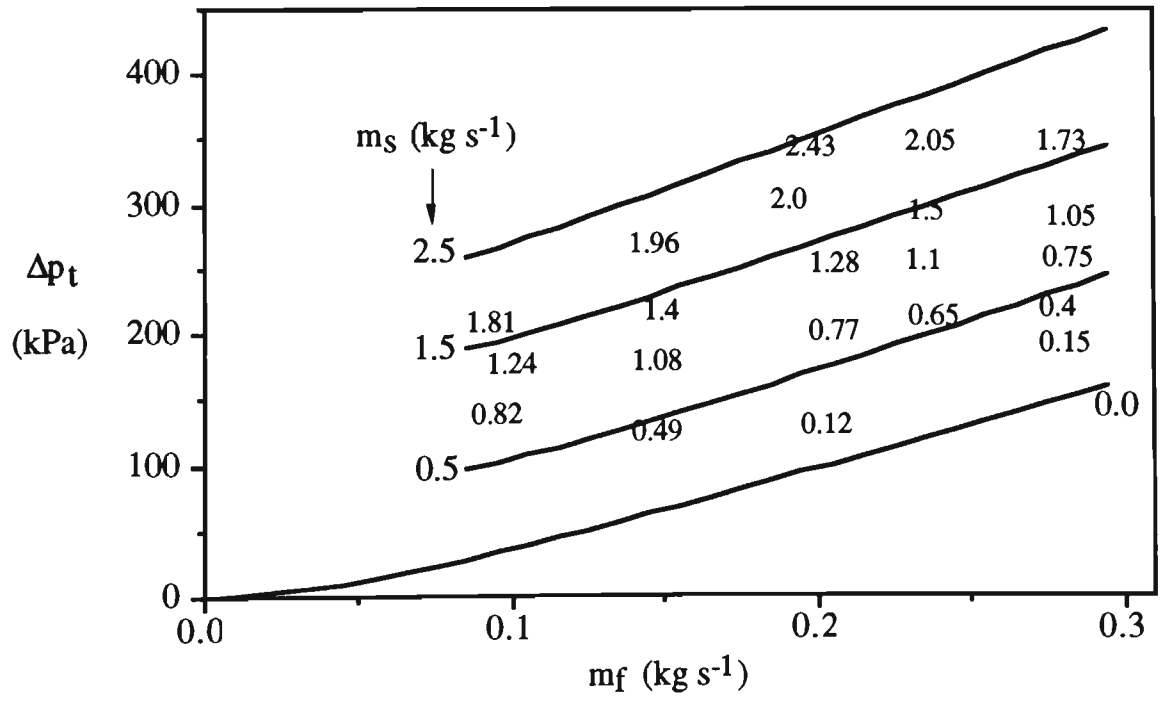

Figure 8.5 Steady-state conveying characteristics of Pipeline A2 and pulverised brown coal (L=553 m, D=69 mm, R=1000 mm).

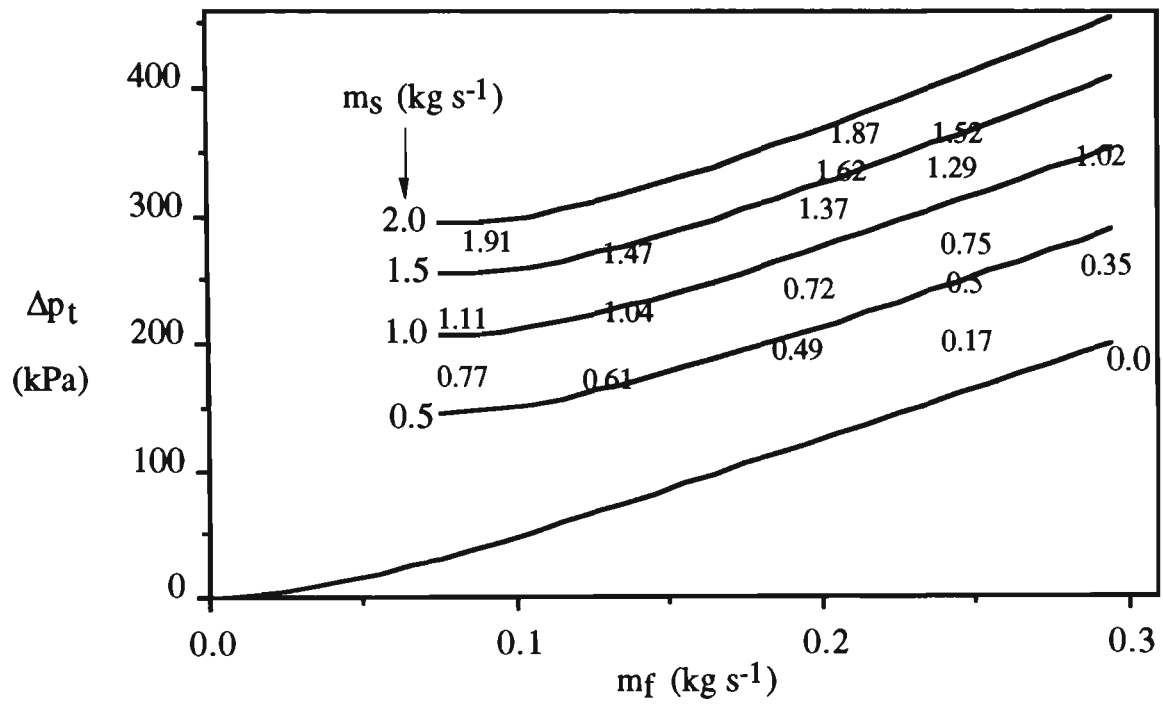

Figure 8.6 Steady-state conveying characteristics of Pipeline A4 and pulverised brown coal (L=1208 m, D=69/81/105 mm, R=1000 mm).

8.5 Application of New Scale-Up Procedure

As described in Chapters 5 and 6, the exponents in the empirical correlations should be determined empirically and are valid only for a given product and bend geometry. Therefore, it is expected that the exponents in the empirical correlations have different values for pulverised brown coal and plastic pellets.

8.5.1 Pulverised Brown Coal

8.5.1.1 Straight Pipes

There are several straight sections of pipe in Pipelines A1, A2 and A4. The pressure drops in some straight pipes were measured by using two pressure transducers (e.g. points Te1 and Te2 in Pipeline A1). Therefore, the exponents in Equations (5.12) can be determined by minimising the sum of the squared errors of pressure at one point (e.g. Point Te2), starting from another point (e.g. point Te1) in Pipeline A1. The determined values of the exponent are listed in Table 8.5.

Table 8.5: Values of exponent in Equation (5.12).

Exponent	Pulverised brown coal Based on data from Pipeline A1	Plastic pellets Based on data from Pipeline I
x1	1.0	0.9042
x2	-0.2665	0.7981
x3	-1.4467	-2.0861
x4	-0.6626	-0.1021

8.5.1.2 Bends

In order to predict accurately the total pipeline air pressure drop in pipelines comprising short straight pipes, the modified empirical correlation (e.g. Equation

(7.4)) is used to predict the bend pressure drop. Hence, the exponents in Equation (7.4) are determined by minimising the sum of the squared errors of pressure at points Tc3 and Tc4, starting from point Te1 in Pipeline A1. The determined values of the exponent are listed in Table 8.6.

Table 8.6: Values of exponent in Equation (7.4).

Exponent	Pulverised brown coal Based on data from Pipeline A1	Plastic pellets Based on data from Pipeline I
y1	1.0	2.3071
y2	-0.0071	-0.6195
y3	0.0984	-0.6513
y4	0.1968	5.0488

8.5.1.3 Pressure in Different Pipeline Configurations

With the exponents in Equations (5.12) and (7.4) being determined already for pulverised brown coal, the pressures along the different configurations of pipeline (e.g. Pipelines A2 and A4) can be predicted. Figure 8.7 shows the relationship between the predicted and experimental pressures at selected points in Pipelines A2 and A4.

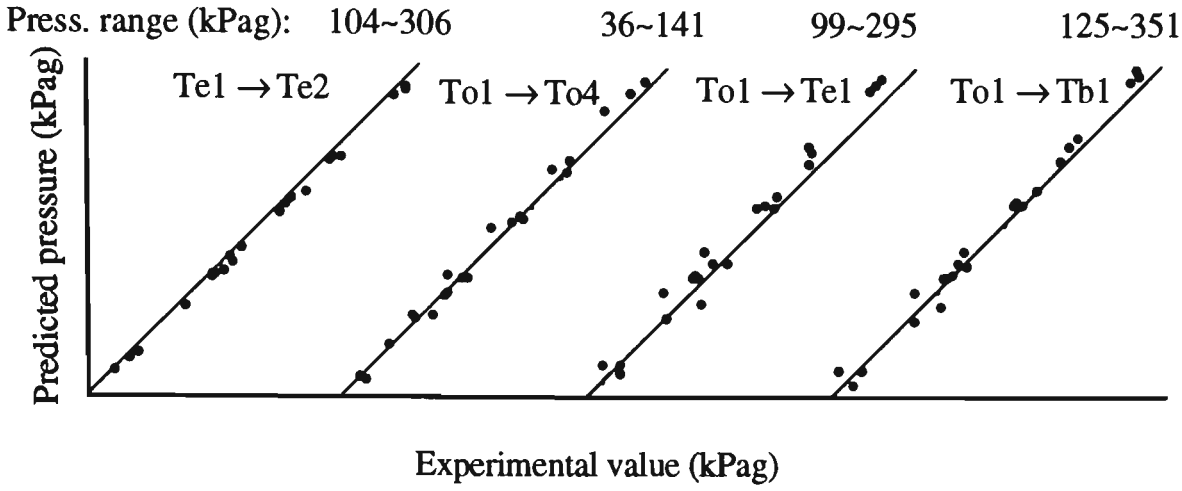

(a) Pipeline A2 (L=553 m, D=69 mm, R=1000 mm).

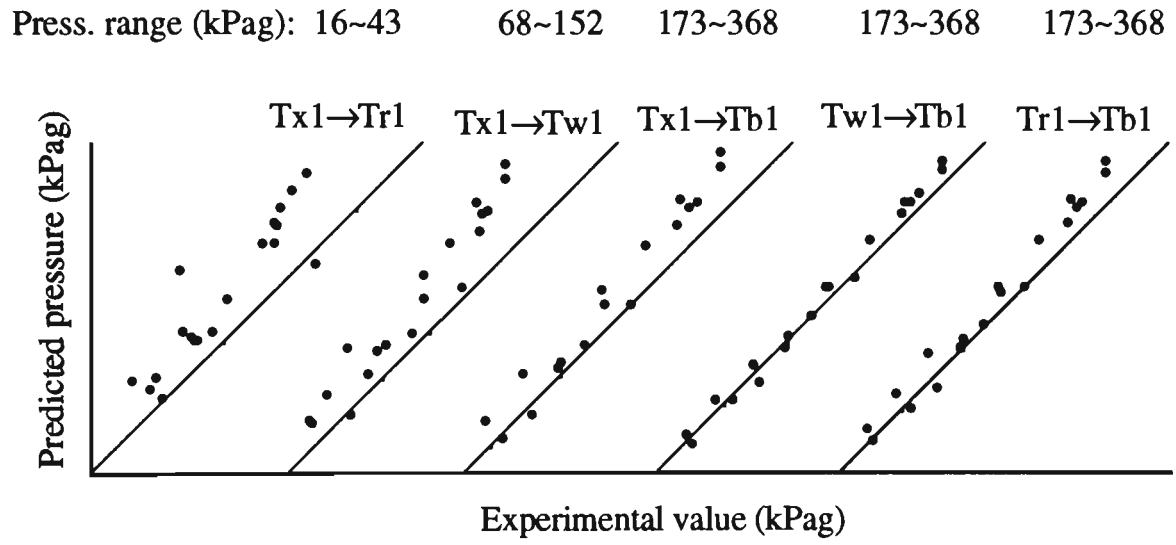

(b) Pipeline A4 (L=1200 m, D=69/81/105 mm, R=1000 mm).

Figure 8.7 Predicted pressure vs experimental value at selected points in different configurations of pipeline for conveying pulverised brown coal, based on data from Pipeline A1.

(Note: Te1 → Te2 means the predicted pressure at Te2, starting from Te1)

8.5.2 Plastic Pellets

8.5.2.1 Straight Pipes

The exponents in Equation (5.12) are determined by minimising the sum of the squared errors of pressure at point Tc, starting from point Td in Pipeline I. The determined values of the exponent are listed also in Table 8.5.

The pressure drops in other straight sections of pipe in Pipelines I and III are predicted by using the above determined values of the exponent. All the agreement is very good, as shown in Figure 8.8.

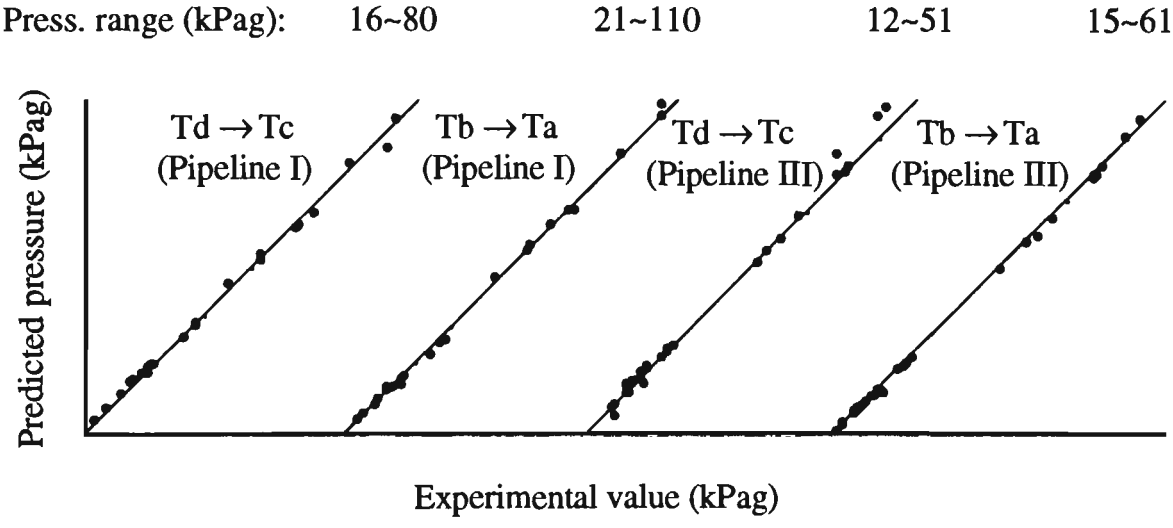

Figure 8.8 Predicted pressure vs experimental value in straight pipes of different length and diameter at different locations for conveying plastic pellets, based on data from Pipeline I.

(Note: Td → Tc means the predicted pressure at Tc, starting from Td)

8.5.2.2 Bends

The exponents in Equation (7.4) are determined by minimising the sum of the squared errors of pressure at the points Tc and Td, starting from the point Te. The determined values of the exponent are also listed in Table 8.6.

8.5.2.3 Pressure in Different Pipeline Configurations

By using the above correlations for the bends and straight pipes, the pressures at selected points in Pipelines I and III are predicted, some of which are shown in Figure 8.9.

All the above results demonstrate the good accuracy, reliability and applicability of the new scale-up procedure developed in Chapter 7 (i.e. for different materials and configurations of pipeline).

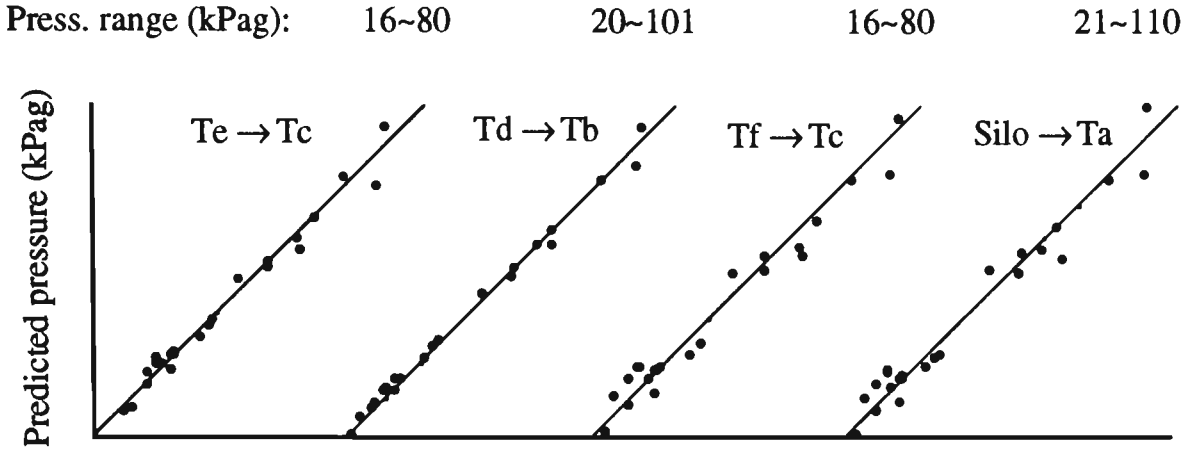

(a) Pipeline I (L=102 m, D=52.5 mm).

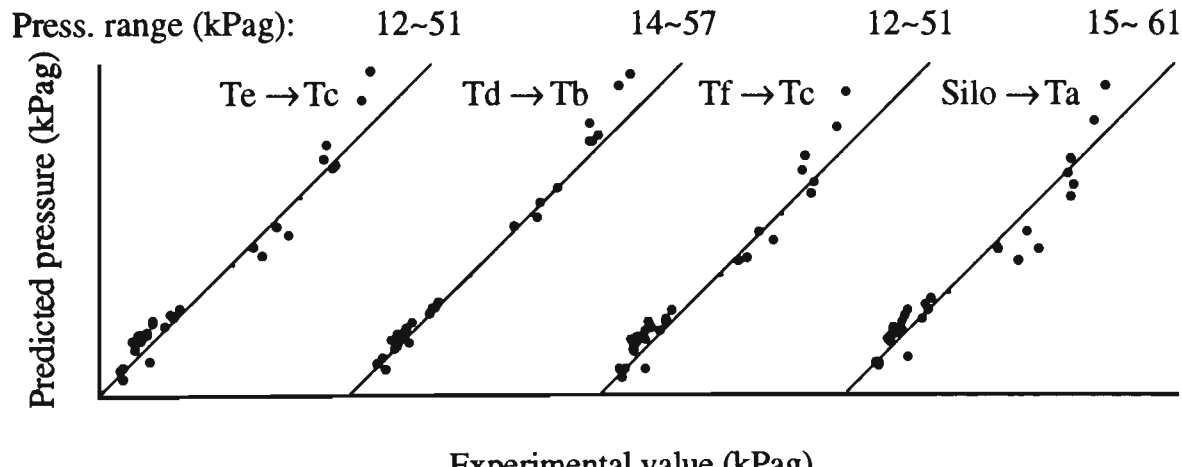

(b) Pipeline III (L=137 m, D=80.5 mm).

Figure 8.9 Predicted pressure vs experimental value at selected points in different configurations of pipeline for conveying plastic pellets, based on data from Pipeline I.

(Note: Te → Tc means the predicted pressure at Tc, starting from Te)

8.6 Influence of Particle Property on Pressure Drop

Comparing the values of the exponent in Equations (5.12) and (7.4) for fly ash, pulverised brown coal and plastic pellets shows that there are significantly different values of exponent. Refer to Table 8.7.

Table 8.7: Values of exponent in Equations (5.12) and (7.4) for different materials.

Exponent	Value (Fly ash)		Value (Brown coal)	Value (Plastic pellets)
x1	5.3062		1.0	0.9042
x2	-0.4366		-0.2665	0.7981
x3	-1.9341		-1.4467	-2.0861
x4	-0.1175		-0.6626	-0.1021
y1	0.0085 *1	0.052 *2	1.0 *3	2.3071 *4
y2	0.1654	0.658	-0.0071	-0.6195
y3	1.3335	0.673	0.0984	-0.6513
y4	0.0129	-1.495	0.1968	5.0488

Note: *1 R=254 mm *2 R=1000 mm *3 R=1000 mm *4 R=254 mm

Using these values of exponent, the pressure drops for conveying different materials through bends, straight pipes and pipelines are predicted respectively, as depicted in Figures 8.10, 8.11 and 8.12.

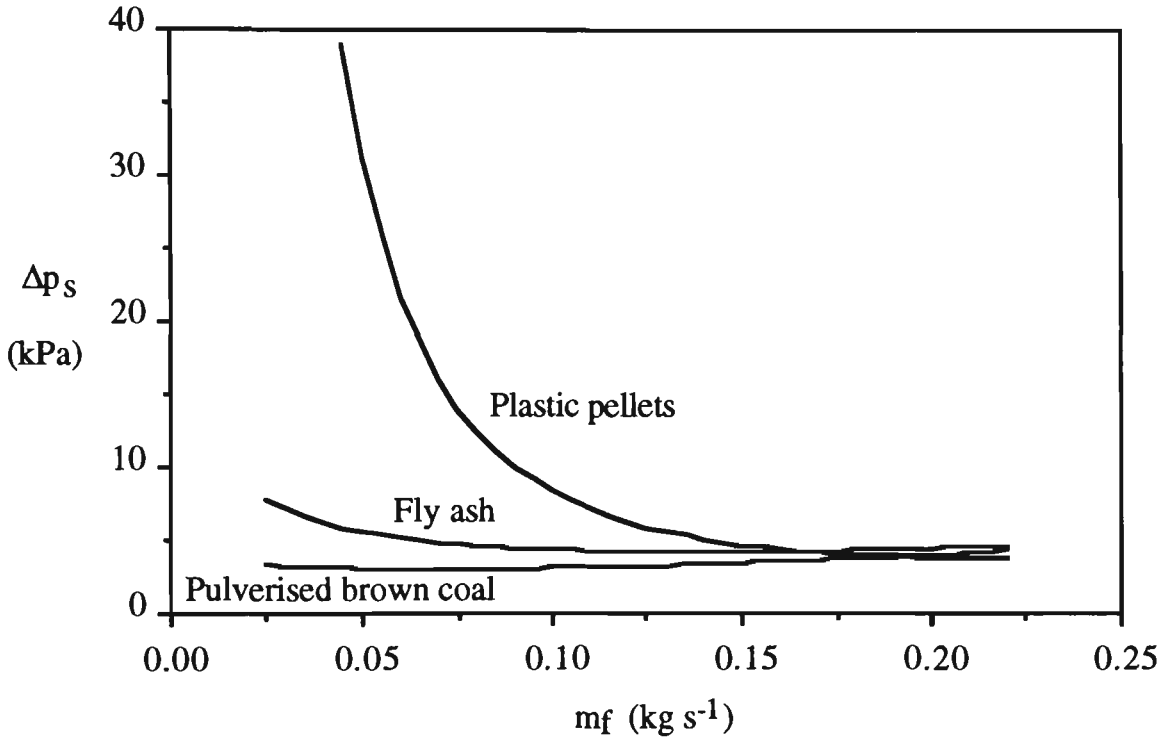

Figure 8.10 Pressure drop caused by a horizontal straight pipe for conveying different materials (D=80.5 mm, ΔL=20 m, ρ_{fe}=1.8 kg m^{-3}, m_s=1.0 kg s^{-1}).

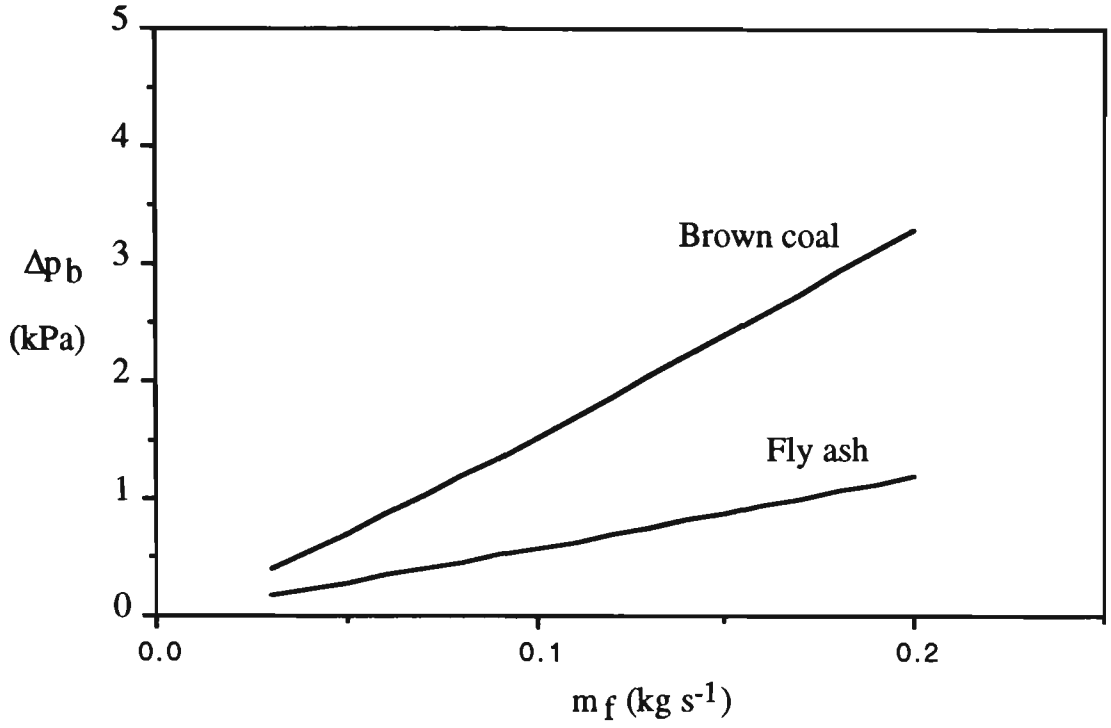

(a) R=1000 mm

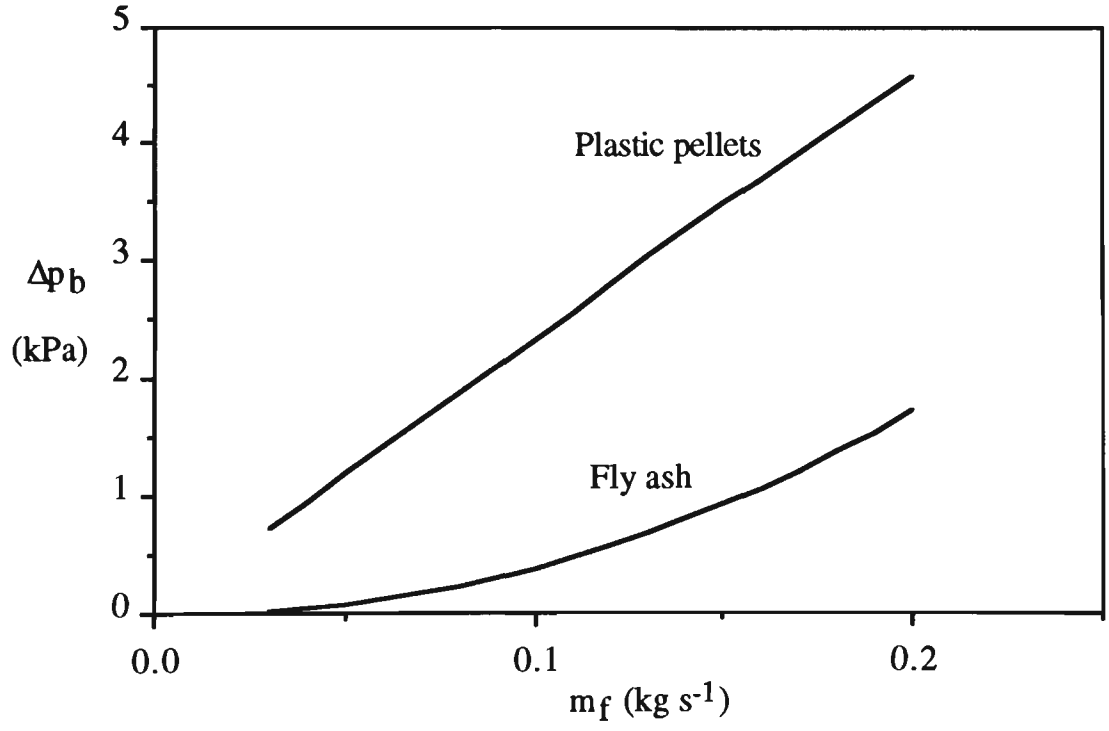

(b) R=254 mm

Figure 8.11 Pressure drop caused by horizontal-horizontal bend for conveying different materials (D=80.5 mm, ρ_{fo}=1.8 kg m^{-3}, m_s=1.0 kg s^{-1}).

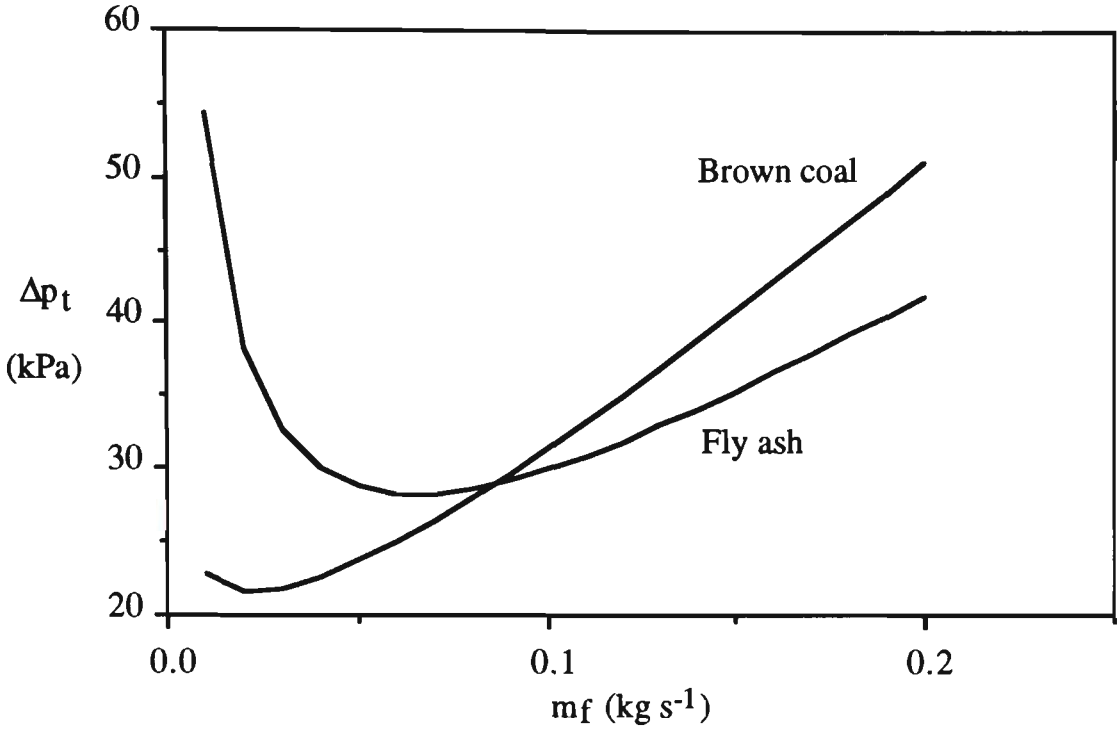

(a) R=1000 mm

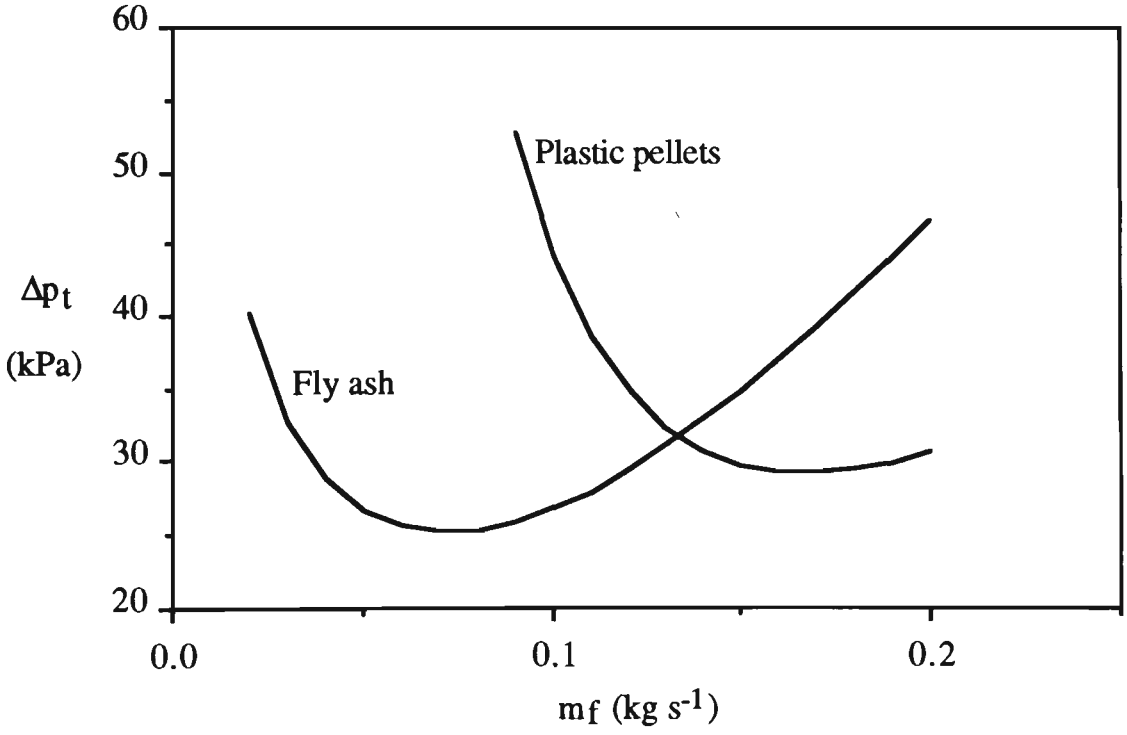

(b) R=254 mm

Figure 8.12 Pressure drop between silo and point Ta in Pipeline III for conveying different materials (m_S=1.0 kg s^{-1}).

From Figures 8.10 and 8.12, it can be seen that to achieve minimum pressure drop of conveying plastic pellets (for a given product mass flow rate), a higher value of air mass flow rate is required (i.e. compared with the conveying of fly ash and pulverised brown coal). The main reason is that the plastic pellets form plugs easily in the pipeline, even when the air mass flow rate is high. During plug flow, the pressure drop increases quickly as the air mass flow rate decreases. For a given pipeline, the length and number of plugs are a function of the product and air mass flow rates.

For fine particles, the plug flow is achieved only when the air mass flow rate is low. Any further decrease in air mass flow rate results in pipeline blockage.

Figures 8.10 to 8.12 clearly show that the conveyed materials have numerous influences on pressure drop.

CHAPTER 9

CONCLUSIONS AND SUGGESTIONS FOR FURTHER WORK

9.1 Conclusions

To consider the effect of short straight sections of pipe on total pipeline air pressure drop in pneumatic conveying, a new scale-up procedure (described in Chapter 7) was developed. To verify the new scale-up procedure developed in this thesis, numerous experiments on several products (e.g. fly ash, pulverised brown coal, plastic pellets) with significantly different properties and in configurations of pipeline of different length, diameter, bend number and step were carried out. From the above work, several conclusions can be made.

a) The scale-up procedure described in this thesis essentially is a test-design procedure. To determine the values of exponents in empirical correlations (e.g. Equation (5.12) and (7.4)), pressure along the pipeline (e.g. as shown in Figure 7.22) should be measured accurately. A technique for accurately calibrating the pressure transducers that are used to measure pressure along the pipeline was developed, whereby a stable pressure in the pipeline is employed to obtain the pressure transducer calibration factors and then all the calibrated pressure transducers are used to measure a varying pressure.

b) An accurate way of estimating total pipeline air pressure drop is to deal separately with bends and straight pipes, starting from the end of the pipeline where conditions usually are known.

c) It has been shown [6, 9, 42, 55, 58, 61, 66, 71] that the pressure drop due to the solids-air mixture (through straight pipes and bends) is correlated best when expressed as the sum of two functions. The first function represents the loss due to air alone and the second is related to the loss due to solids. In many

systems, the air-only component of pressure drop is significant (e.g. dilute-phase, long-distance conveying). Therefore, it is very important to predict accurately the pressure drop due to air alone. Based on numerous experiments on air-only in configurations of pipeline of different length, diameter, bend number and step, it was found (see Chapter 4) that the existing formulae which are suitable for incompressible flow still can be employed to determine accurately the air-only component of pressure drop as long as mean conditions for each straight section of pipe (based on average air density) and conditions at the outlet of each bend are used (e.g. density, velocity).

d) It was demonstrated experimentally and mathematically that the pressure gradient at any point along a straight section of pipe is not constant (see Chapter 5). Therefore, on calculating pressure drop in a straight section of pipe, especially in a long straight section of pipe which usually causes high pressure drop, the mean conditions (based on average air density) for the straight section of pipe should be used.

e) For a straight section of pipe and the same exit pressure, the pressure drop in a vertical location always is higher than that in a horizontal location. The ratio of the vertical to horizontal straight pipe pressure drop is a function of the air density at the pipe exit, the pipe diameter, the product and air mass flow rates. Hence, the ratios cannot be considered as a factor of 2, which has been used commonly [8]. Also, the steady-state conveying characteristics in a vertical location are different from those in a horizontal location. To achieve a minimum pressure drop (for a given product mass flow rate) in a vertical pipe, a higher value of air mass flow rate is required (i.e. compared with a horizontal pipe).

f) Pressure drop caused by a bend is the sum of two components. The first component is located in the bend itself and the second occurs in the straight section of pipe immediately downstream from the bend for the re-acceleration of particles. Therefore, the bend pressure drop cannot be measured directly. Compared with the pressure along straight sections of pipe downstream and upstream of the bend, the bend pressure drop is low. Hence, if the determination of bend pressure drop is based on the traditional method shown in Figure 6.3, a small fluctuation in pressure along the straight sections of pipe has a great influence on the values of bend pressure drop (see Table 6.1). Therefore, the conditions occurring at the outlet of the bend are used to determine the bend pressure drop. It should be noted that these outlet conditions are the 'effective' conditions as determined by the straight pipeline analysis (i.e. for the section of pipe downstream of the bend).

g) As a bend is connected by two long straight sections of pipe, longer radius bends produce a lower pressure drop. However, when short straight pipes are used between the bends, longer radius bends cause a higher pressure drop at low air mass flow rate and a lower pressure drop at high air mass flow rate (i.e. compared with short radius bends). In dense-phase conveying, the difference in pressure drop caused by long radius and short radius bends is not significant. However, blinded-tee bends always produce much a higher pressure drop than radius bends.

h) It has been demonstrated that bend location and number have significant influences on the total pipeline air pressure drop (see Figures 6.9 and 6.10), especially in dilute-phase conveying. Therefore, in designing pneumatic

conveying systems, the bend location and number should be taken into account.

i) For the pipeline without short straight sections of pipe, the values of exponents determined by the procedure presented in Chapters 5 and 6 can be used directly to predict total pipeline air pressure drop. For a pipeline with short straight pipes, the values of exponents for straight sections remain unchanged. However, the correlation for bends is modified and the exponents in the modified correlation are determined by experimental data from a simple configuration of pipeline shown in Figure 7.22, where there are two bends and three straight sections of pipe, two long and one short.

j) The new scale-up procedure does not include any particle properties. For a new product, it is necessary to conduct experiments in a pipeline with the sample of new product. The exponents are determined empirically and are valid only for the test material.

9.2 Suggestions for Further Work

More tests should be carried out on the numerous materials which have significantly different properties, to investigate and obtain a relationship between the exponents in Equations (5.12) and (6.4) or (7.4) and particle properties (e.g. density, particle size and size distribution).

For a given product, total pipeline air pressure drop in configurations of pipelines of different diameter, length, bend number and step can be predicted accurately by

using the procedures in this thesis. For general applications of pneumatic conveying in industry, more research needs to be carried out to minimise gas consumption (hence, energy costs) and/or product damage in both existing and new industrial plants. This requires investigations into its effect on minimum transport behaviour and scale-up procedures.

The work completed in this thesis has been concerned with horizontal and vertical straight sections of pipe. The work needs to be extended to inclines which are used commonly in industry.

All bends considered in this thesis were located horizontal to horizontal. Therefore, more research and tests need to be carried out for other bend orientations (e.g. downwards/upwards horizontal to vertical, upwards/downwards vertical to horizontal).

Compared to horizontal straight sections of pipe, vertical straight sections of pipe have different steady-state conveying characteristics. In this thesis, only one vertical pipe with length of 8 m and diameter of 52 mm was employed for the pressure measurements. So more work needs to be extended to verticals of different length and diameter.

Pipelines with big diameter (e.g. D=150, 200 mm) are used commonly in industry. The biggest pipe diameter used in this thesis was 105 mm. Therefore, more research should be carried out to investigate whether the scale-up procedure developed in this thesis is able to predict pressure accurately along the pipeline with big diameter.

CHAPTER 10

REFERENCES

1. Arastoopour, H., Modi, M. V., Punwani, D. V. and Talwalkar, A. T., A Review of Design Equations for Dilute-Phase Gas-Solids Horizontal Conveying Systems for Coal and Related Materials, 14th Annual Powder & Bulk Solids Conference/Exhibition, Rosemont, Illinois, 15-18 May, 1990. Proc. of the Technical Program, pp. 339-356.

2. Belden, D. H. and Kassel, L. S., Pressure Drops Encountered in Conveying Particles of Large Diameter in Vertical Transfer Lines, Int. and Eng. Chem. 41, 1949, pp. 1174-1178.

3. Bodner, S. S., Effects of Bend Configuration on Dilute-Phase Pneumatic Transport, Pneumatech I, Int. Conf. on Pneumatic Conveying Technology, Stratford-Upon-Avon, England, 3-5 May 1982. Organised by the Powder Advisory Centre, London, England. Proc. of the Technical Program.

4. Bohnet, M., Advances in the Design of Pneumatic Conveyings, International Chemical Engineering, Vol. 25, No. 3, July, 1985, pp. 387-405.

5. Bonnin, J. C. and Bouard, R., Bends in Air-Cement Flow, Pneumatech 4, Int. Conf. on Pneumatic Conveying Technology, Glasgow, Scotland, 26-28 June, 1990. Organised by the Powder Advisory Centre, London, England. Proc. of the Technical Program, pp. 61-90.

6. Bradley, M. S. A., Approaches to Dealing with the Problem of Energy Loss due to Bends, 13th Annual Powder & Bulk Solids Conference/Exhibition, Rosemont, Illinois, 9-12 May, 1988. Proc. of the Technical Program, pp. 705-715.

7. Bradley, M. S. A., Pressure Losses Caused by Bends in Pneumatic Conveying Pipelines: Effects of Bend Geometry and Fittings, 14th Annual Powder & Bulk Solids Conference/Exhibition, Rosemont, Illinois, 15-18 May, 1989. Proc. of the Technical Program, pp. 681-694.

8. Bradley, M. S. A., An Improved Method of Predicting Pressure Drop along Pneumatic Conveying Pipelines, 3rd International Conference on Bulk Materials, Storage, Handling and Transportation, Newcastle, N.S.W., 27-29 June, 1989. Organised by the Institution of Engineers, Australia, pp. 282-288.

9. Chambers, A. J. and Marcus, R. D., Pneumatic Conveying Calculations, 2nd Int. Conf. on Bulk Materials Storage, Handling and Transportation, Wollongong, 7-9 July, 1986. Organised by the Institution of Engineers, Australia. Preprints of Papers, pp. 49-52.

10. Cornish, G. K. and Charity, L. F., Pressure Drop in Elbows of a Pneumatic Conveying System, Transactions of the ASAE, Vol. 9, No. 1, 1966, pp. 29-31.

11. Cuerten, H.-J., Industrial Applications of Long-Distance Pneumatic Conveying, Pneumatech 2, Int. Conf. on Pneumatic Conveying Technology, Canterbury, England, 4-6 September, 1984. Organised by the Powder Advisory Centre, London, England. Proc. of the Technical Program, pp. 149-157.

12. Dogin, M.E. and Lebedev, V.P., Dependence of the Resistance in Pneumatic Conveying Pipelines on the Fundamental Parameter of the Two-Phase Flow, Journal of International Chemical Engineering, Vol. 2, No. 1, January, 1962, pp. 64-67.

13. Duckworth, R. A. and Kakka, R. S., The Influence of Particle Size on the Frictional Pressure Drop Caused by the Flow of a Solid-Gas Suspension in a Pipe, Pneumotransport 1, 1st Int. Conf. on the Pneumatic Transport of Solids in Pipes, Cambridge, 6-8 September, 1971. Organised by BHRA Fluid Engineering, Cranfield, Bedford, England, pp. C3(29-44).

14. The Engineering Equipment Users Association, Pneumatic Handling of Powdered Materials, E.E.U.A. Handbook, No. 15, 1963. Constable and Company Ltd..

15. Flain, R. J., Pneumatic Conveying: how the System is Matched to the Material Process Engineering, November, 1972, pp. 88-90.

16. Ghosh, D. P. and Kalyanaraman, K., Pressure Drops due to Solids around Horizontal Elbow Bends during Pneumatic Conveyance, J. Agric. Engng Res., Vol. 15, No. 2, 1970, pp. 117-128.

17. Granger, R. A., Fluid Mechanics, Holt, Rinehart and Winston, Sydney, 1985, pp. 481-586.

18. Haag, A., Velocity Losses in Pneumatic Conveyor Pipe Bends, British Chemical Engineering, Vol. 12, No. 1, January, 1967, pp. 65-66.

19. Hariu, H. and Molstad, M. C., Pressure Drop in Vertical Tubes in Transport of Solids by Gases, Ind. Eng. Chem., 41, 1148 (1949).

20. Hinkle, B. L., Acceleration of Particles and Pressure drops Encountered in Horizontal Pneumatic Conveying, Thesis (PhD), Georgia Institute of Technology, 1953.

21. Hitchcook, J. A. and Jones, C., The Pneumatic Conveying of Spheres through Straight Pipes, Br. J. Appl. Phys., 9, 1958, pp. 218-222.

22. Ikemori , K. and Munakata, H., A New Method of Expressing Pressure Drop in Horizontal Pipe Bend in Pneumatic Transport of Solids, Pneumotransport 2, 2nd Int. Conf. on the Pneumatic Transport of Solids in Pipes, Guildford, England, 5-7 September, 1973. Organised by BHRA Fluid Engineering, Cranfield, Bedford, England, pp A3(33-47).

23. Ito, H., Pressure Losses in Smooth Pipe Bends, Trans. ASME, 1959, Paper 59-Hyd-4.

24. Jones, J. H., Braun, W. G., Daubert, T. E. and Allendorf, H. D., Estimation of Pressure drop for Vertical Pneumatic Transport of Solids, AIChE J., Vol. 13, No. 3, p. 608, 1967.

25. Klinzing, G. E., A Comparison of Pressure Losses in Bends between Recent Data and Models for Gas-Solid Flow, The Canadian Journal of Chemical Engineering, Vol. 58, 1980, pp. 670-672.

26. Klueter, H. H., Puckett, H. B., Beaty, H. H. and Olver, E. F., Medium-Pressure Pneumatic Feed Conveying, Agricultural Engineering, Vol. 43, No. 10, 1962, pp. 572-575.

27. Koncheski, J.L., George, T.J. and Craig, J.G., Air and Power Requirements for the Pneumatic Transport of Crushed Coal in Horizontal Pipelines, Trans. ASME J. Eng. Int., 97, 1975, pp. 94-101.

28. Kovacs, T. L., Calculation of Pressure-Drop in Horizontal and Vertical Bends Inserted in Pneumatic Conveying Pipes, Pneumotransport 1, 1st Int. Conf. on the Pneumatic Transport of Solids in Pipes, Cambridge, 6-8 September, 1971. Organised by BHRA Fluid Engineering, Cranfield, Bedford, England, C4(45 - 55).

29. Li, S. G., Fluid Mechanics in Engineering, Mechanical Industry Publishing House, China, 1986.

30. Marcus, R. D. and Bettman, R., Refinements to the Design of Long Distance Pneumatic Conveying Systems, Pneumatech 3, Int. Conf. on Pneumatic Conveying Technology, Jersey, Channel Islands, England, 24-26 March, 1987. Organised by the Powder Advisory Centre, London, England. Proc. of the Technical Program, pp. 335-352.

31. Marcus, R. D., Hilbert, J. D. and Klinzing, G. E., The Flow through Bends in Pneumatic Conveying Systems, Notes for Short Course on Pneumatic Conveying of Bulk Solids, TUNRA Bulk Solids Handling Research

Association, The University of Newcastle, N.S.W., Australia, September, 1983.

32. Marcus, R. D., Hilbert, J. D. and Klinzing, G. E., Flow through Bends and Acceleration Zones in Pneumatic Conveying Systems, Bulk Solids Handling, Vol. 5, No. 4, August, 1985, pp. 769-774.

33. Mason, J. S. and Boothroyd, R. D., Comparison of Friction Factors in Pneumatically-Conveyed Suspensions Using Different-Sized Particles in Pipes of Varying Size, Pneumotransport 1, 1st Int. Conf. on the Pneumatic Transport of Solids in Pipes, Cambridge, 6-8 September, 1971. Organised by BHRA Fluid Engineering, Cranfield, Bedford, England, pp. C1(1-16).

34. Mason, J. S., Mills, D., Reed, A. R. and Woodcock, C. R., Conveying Performance Characteristics for Dilute and Dense Phase, Pneumatic Conveying of Bulk Materials, Session B2/B3, Intensive Short Course Notes. Thames Polytechnic, London, England, December, 1983.

35. Mason, J. S. and Smith, B. U., Pressure Drop and Flow Behaviour for the Pneumatic Transport of Fine Particles around 90 Degree Bends, Pneumotransport 2, 2nd Int. Conf. on the Pneumatic Transport of Solids in Pipes, Guildford, England, 5-7 September, 1973. Organised by BHRA Fluid Engineering, Cranfield, Bedford, England, pp. A2(17-32).

36. Meyers, S. and Marcus, R. D., The State Diagram for Fine-Particle Gas/Solids Suspensions, Bulk Solids Handling, Vol. 5, No. 4, August, 1985, pp. 131-134.

37. Michaelides, E. E., Motion of Particles in Gases: Average Velocity and Pressure Loss, Journal of Fluids Engineering, 1987.

38. Michaelides, E. E. and Roy, I., An Evaluation of Several Correlations Used for the Prediction of Pressure Drop in Particulate Flows, Int. Conf. on Pneumatic Conveying Technology, Jersey, Channel Islands, England, 24-26

March, 1987. Organised by the Powder Advisory Centre, London, England. Proc. of the Technical Program, pp. 127-141.

39. Mills, D., Mason, J. S. and Stacey, R. B., A Design Study for the Pneumatic Conveying of a Fine Particulate Material, Solidex 82, The Solids Handling Conference, Harrogate, England, 30 March-1 April, 1982. Trinty Publishing (Conferences) Ltd., Oxbridge, Middlesex, England, 1982, pp. c1-c75.

40. Mills, D. and Mason, J. S., The Influence of Bend Geometry on Pressure Drop in Pneumatic Conveying System Pipelines, 10th Powder and Bulk Solids Conference/Exhibition, Rosemont, Illinois, 1985. Proc. of the Technical Program, pp. 203-214.

41. Morikawa, Y. and Sakamoto, S., Flow Characteristics of Mixed Size Particles in Horizontal Pneumatic Conveying, Bulk Solids Handling, Vol. 5, No. 3, June, 1985, pp. 61-65.

42. Morikawa, Y., Tsuji, Y., Matsui, K. and Jittani, Y., Pressure Drops due to Pipe Bends in Air-Solids Two Phase Flows: Circular and Elliptical Bends, Int. J. Multiphase Flow, Vol. 4, 1978, pp 575-583.

43. Murphy, G., Similitude in Engineering, The Ronald Press Company, New York, 1950.

44. Pfeffer, R., Rosetti, S. and Licklein, S., Analysis and Correlation of Heat Transfer Coefficient and Heat Transfer Data for Dilute Gas-Solid Suspension, NASA, TN-D 3603, 1966.

45. Reed, A. R. and Bradley, M. S. A., Advances in the Design of Pneumatic Conveying Systems, Bulk Solids Handling, Vol. 11, No.1, March, 1991, pp. 93-97.

46. Richards, P. C. and Wiersma, M. A. S., Pressure Drop in Vertical Pneumatic Conveying, Pneumotransport 2, 2nd Int. Conf. on the Pneumatic Transport of

Solids in Pipes, Guildford, England, 5-7 September, 1973. Organised by BHRA Fluid Engineering, Cranfield, Bedford, England, pp. A1(1-15).

47. Richardson, J. F. and McLeman, M., Pneumatic Conveying, Part II: Solids Velocities and Pressure Gradients in a One-Inch Horizontal pipe, Trans. Inst. Chem Eng., 38, 1960, pp. 257-266.

48. Rizk, F., A Comparison between Horizontal and Vertical Pneumatic Conveying Systems Considering the Optimal Operating Conditions, Journal of Powder & Bulk Solids Technology, Vol. 7, No. 3, 1983, pp 5-11.

49. Roski, H.-J., The Influence of Stepped Pipelines in Pneumatic Long-Distance Transport of Building Materials, Pneumatech 3, Int. Conf. on Pneumatic Conveying Technology, Channel Islands, England, 24-26 March, 1987. Organised by the Powder Advisory Centre, London, England. Proc. of the Technical Program, pp. 311-333.

50. Rosseti, S. J., Concepts and Criteria for Gas-Solids Flow, Handbook of Fluids in Motion, Ed. Nicholas P. Cheremisinoff and Ramesh Gupta, Ann Arbor: Ann Arbor Science Publishers, 1983, pp. 635-652.

51. Schade, B., Zum Übergang Sprung-Strähnenförderung bei der Horizontalen Pneumatischen Feststofförderung, Dissertation, University of Karlsruhe, 1987.

52. Schuchart, P., Widerstandsgesetze beim pneumatischen Transport in Rohrkrümmern, Chemie-Ing.-Techn. 40. Jahrg. 1968, pp. 1060-1067.

53. Segler, G., Pneumatic Grain Conveying, Braunschweig, 1951.

54. Shimizu, A. Echigo, R., Hasegawa, S. and Hishida, M., Experimental Study on the Pressure Drop and the Entry Length of the Gas-Solid Suspension Flow in a Circular Tube, Int. J. Multi. Flow, Vol. 4, 1978, pp. 53-64.

55. Singh, B. and Wolfe, R. R., Pressure Losses due to Bends in Pneumatic Forage Handling, Transactions of the ASAE, 1972, pp. 246-248.

56. Sproson, J. C., Gray, W. A. and Haynes, J., Pneumatic Conveying of Coal, Pneumotransport 2, 2nd Int. Conf. on the Pneumatic Transport of Solids in Pipes, Guildford, England, 5-7 September, 1973. Organised by BHRA Fluid Engineering, Cranfield, Bedford, England, pp. B2(15-31).

57. Sproson, J. C., Gray, W. A. and Haynes, J., Pneumatic Transport of Coal, 3rd Int. Conf. on the Pneumatic Transport of Solids in Pipes, Bath, England, 7-9 April, 1976. Organised by BHRA Fluid Engineering, Cranfield, Bedford, England, pp. A6(57-73).

58. Stebbins, K. W., Pneumatic Conveying of Fly Ash, Internal Research Report, University of Wollongong, N.S.W., Australia, December, 1989.

59. Stegmaier, W., Zur Berechnung der horizontalen pneumatischen Förderung feinkörniger Stoffe, Fördern und Heben, Vol. 28, No. 5/6, 1978, pp. 363-366.

60. Swamee, P. K. and Jain, A. K., Explicit Equations for Pipe-Flow Problems, J. Hydr. Div., Proc. ASCE, May, 1976, pp. 657-664.

61. Tsuji, Y., Prediction of Pressure Drop and Optimal Design of Dilute Phase Pneumatic Conveying Systems, Pneumatech I, Int. Conf. on Pneumatic Conveying Technology, Stratford-Upon-Avon, England, 3-5 May 1982. Organised by the Powder Advisory Centre, London, England. Proc. of the Technical Program.

62. Weber, M., Principles of Hydraulic and Pneumatic Conveying in Pipes, Bulk Solids Handling, Vol. 1, No. 1, February, 1981, pp. 57-63.

63. Weber, M., Correlation Analyses in the Design of Pneumatic Transport Plant, Bulk Solids Handling, Vol. 2, No. 2, June, 1982, pp. 231-233.

64. Weber, M., Friction of the Air and Air/Solid Mixture in Pneumatic Conveying, Bulk Solids Handling, Vol. 11, No. 1, March, 1991, pp. 99-102.

65. Weidner, G., Grundsätzliche Untersuchung über den pneumatischen Fördervorgang, insbesondere über die Verhaltnisse bei Beschleunigung und Umlenkung, Forsch. Ing.-Wes. 21-5, 1955, 145.

66. Westman, M. A., Michaelides, E. E. and Thomson, F. M., Pressure Losses due to Bends in Pneumatic Conveying, Journal of Pipelines, 7, 1987, pp 15-20.

67. Wirth, K. E.and Molerus, O., Prediction of Pressure Drop with Pneumatic Conveying of Solids in Horizontal Pipes, Journal of Powder & Bulk Solids Technology, Vol. 7, No. 2, 1983, pp. 17-20.

68. Wypych, P.W. & Arnold, P.C., On Improving Scale-up Procedures for Pneumatic Conveying Design, Powder Technology, Vol. 50, No. 3, 1987, pp. 281-294.

69. Wypych, P. W., Arnold, P. C. and Armitage, W. R., Developing New Methods for the Pneumatic Transport of Bulk Solids through Pipelines, Chemeca 88, Int. Conf. for the Process Industries, Sydney, N.S.W., 28-31 August, 1988. Organised by the Institution of Engineers, Australia, pp. 652-656.

70. Wypych, P. W., Pneumatic Conveying of Bulk Solids, Thesis (PhD), The University of Wollongong, N.S.W., Australia, 1989.

71. Wypych, P. W. and Arnold, P. C., Demands of Long-Distance and Large-Throughput Pneumatic Conveying Applications in Australia, 6th Int. Symp. on Freight Pipelines, Columbia, U.S.A., May, 1989.

72. Wypych, P. W., Kennedy, O. C. and Arnold, P. C., Pneumatic Conveying of Pulverised and Crushed R.O.M. Coal, Pneumatech 4, Int. Conf. on Pneumatic Conveying Technology, Glasgow, Scotland, 26-28 June, 1990. Organised by the Powder Advisory Centre, London, England. Proc. of the Technical Program, pp. 159-173.

73. Yang, W., Keairns, D. L. and Archer, D. H., Estimating the Solid Particle Velocity in Horizontal Pneumatic Conveying Lines, Can. J. Chem. Eng., Vol. 51, 1973, p. 779.

74. Yang, W., Estimating the Solid Particle Velocity in Vertical Pneumatic Conveying Lines, Ind. Eng. Chem. Fundamentals, Vol. 12, 1973, p. 349.

75. Yang, W., Correlations for Solid Friction Factors in Vertical And Horizontal Pneumatic Conveyings, 77th AIChE National Meeting, Pittsburgh, June, 1974.

76. Yang, W., A Verified Theory on Dilute Phase Pneumatic Transport, Journal of Powder & Bulk Solids Technology, Vol. 1, No. 1, 1977, pp. 89-95.

77. Yang, W., Flow Characteristics of Solid/Gas Transportation Systems, U.S. Department of Interior, Bureau of Mines, PA, IC8314, pp. 62-72.

78. Yang, W., Pneumatic Transport in a 10-cm Pipe Horizontal Loop, Powder Technology, Vol. 49, 1987, pp. 207-216.

79. Hetsroni, G., Handbook of Multiphase Systems, McGraw Hill, 1982, Chapter 7.

80. Rose, H. E. and Duckworth, R. A., Transport of Solid Particle in Liquids and Gases, The Engineer, March, 1969, pp. 192, 430, 478.

APPENDIX A

EXPERIMENTAL DATA FOR ALL TEST BENDS AND PIPELINES

Table A.1 Experimental values of pressure for R=100 mm bend.

No.	p1 (kPag)	p2 (kPag)	p3 (kPag)	p4 (kPag)	p5 (kPag)	p6 (kPag)	p7 (kPag)	p8 (kPag)	p9 (kPag)	p10 (kPag)	m_s (kg s^{-1})	m_f (kg s^{-1})
1	79.5	79.4	74.9	73.5	71.4	64.6	64.0	63.4	62.6	61.5	0.895	0.0797
2	77.0	76.6	72.5	71.1	70.0	63.9	62.4	62.0	61.1	60.1	1.012	0.0714
3	71.9	71.6	68.5	67.3	66.5	59.2	58.8	58.5	57.6	55.2	1.238	0.0583
4	67.7	67.5	65.2	63.3	61.7	55.6	54.8	53.6	51.8	50.0	1.455	0.0456
5	64.6	63.9	59.8	57.8	55.7	50.2	49.4	48.0	45.9	43.4	1.663	0.0339
6	59.6	56.9	53.0	50.3	47.8	42.9	41.0	38.0	35.9	33.7	1.780	0.0204
7	88.8	88.7	83.4	82.3	80.5	73.7	72.3	72.0	71.0	70.3	1.121	0.0782
8	85.8	85.3	81.2	79.8	78.9	72.2	70.9	70.2	69.3	67.8	1.282	0.0702
9	81.1	81.2	77.2	76.0	74.8	67.3	66.4	66.3	65.3	62.9	1.504	0.0588
10	75.9	75.7	72.5	70.8	69.2	62.3	61.5	60.5	58.4	56.3	1.768	0.0465
11	71.9	71.6	66.7	65.0	62.7	56.3	55.4	53.5	51.3	48.8	1.993	0.0350
12	67.6	64.6	60.9	58.5	55.4	50.1	48.0	45.3	42.5	39.6	2.120	0.0217
13	100.9	100.3	95.4	94.1	93.2	84.8	83.7	83.2	82.4	80.7	1.460	0.0779
14	97.5	97.2	92.5	91.3	90.4	81.8	80.9	80.6	79.8	77.6	1.582	0.0710
15	92.4	92.0	88.4	87.0	86.0	77.6	76.7	76.0	74.5	71.7	1.827	0.0596
16	85.4	85.5	81.5	79.3	78.0	69.6	69.3	68.0	66.0	63.8	2.082	0.0479
17	80.6	80.1	74.8	72.9	70.7	62.9	62.0	60.1	58.0	55.0	2.315	0.0367
18	75.8	72.3	68.3	65.8	63.1	57.0	55.1	51.8	48.9	45.9	2.475	0.0233
19	110.9	110.4	105.4	103.8	103.1	94.1	93.0	92.0	91.1	89.5	1.700	0.0783
20	107.8	107.2	103.0	101.3	100.7	91.3	90.4	89.7	88.6	86.1	1.859	0.0716
21	101.5	101.3	96.5	95.0	93.9	84.4	83.8	83.0	81.3	78.7	2.115	0.0603
22	94.5	94.3	89.4	87.6	86.0	77.2	76.6	75.3	73.1	70.7	2.375	0.0492
23	88.0	87.4	81.5	79.5	77.3	69.0	68.2	65.8	63.7	60.5	2.620	0.0375
24	81.9	79.3	74.3	72.0	69.0	62.4	60.4	57.1	53.8	51.0	2.835	0.0249
25	120.7	120.6	115.2	113.7	112.6	103.2	101.6	101.3	99.7	98.1	1.980	0.0786

Continuation of Table A.1

No.	p1 (kPag)	p2 (kPag)	p3 (kPag)	p4 (kPag)	p5 (kPag)	p6 (kPag)	p7 (kPag)	p8 (kPag)	p9 (kPag)	p10 (kPag)	m_s (kg s^{-1})	m_f (kg s^{-1})
26	117.1	116.6	111.7	110.2	109.5	99.2	98.5	97.6	96.5	93.6	2.109	0.0725
27	109.8	109.8	104.5	103.0	102.1	91.8	91.2	90.2	88.6	85.7	2.340	0.0616
28	100.9	100.9	95.5	93.6	92.1	82.8	82.1	80.6	78.2	75.6	2.635	0.0499
29	93.6	92.9	86.9	84.8	82.5	74.3	73.5	71.2	68.5	65.1	2.833	0.0394
30	87.4	84.5	79.7	77.1	74.3	67.4	65.3	62.0	58.9	55.3	3.079	0.0265
31	129.2	129.1	123.7	122.3	121.2	110.4	109.6	108.6	107.6	105.2	2.167	0.0797
32	124.0	123.7	118.3	116.8	116.1	105.0	104.4	103.3	102.1	99.0	2.260	0.0732
33	117.8	118.0	112.5	111.2	109.3	98.6	98.1	96.7	94.9	92.1	2.534	0.0623
34	110.1	109.9	103.7	101.8	99.9	90.1	89.3	87.5	85.0	82.2	2.866	0.0505
35	105.0	104.5	97.4	95.2	92.5	83.7	82.5	79.9	76.7	73.2	3.167	0.0396
36	94.8	91.9	86.4	83.6	80.7	73.0	70.6	67.1	64.0	60.5	3.323	0.0271
37	138.2	137.9	131.9	130.4	129.9	118.2	116.9	115.8	114.8	112.0	2.393	0.0804
38	133.7	133.5	127.4	125.7	125.1	113.3	112.4	111.4	110.0	106.8	2.504	0.0736
39	125.3	125.4	119.0	117.2	116.5	104.6	104.1	102.9	100.9	98.1	2.815	0.0628
40	115.9	116.0	109.0	106.8	105.1	94.3	93.8	91.8	89.4	86.3	3.032	0.0515
41	107.8	107.0	100.1	98.0	95.7	86.0	85.2	82.2	79.2	75.6	3.366	0.0406
42	99.2	96.6	90.8	88.3	85.3	77.0	74.9	71.1	68.1	64.4	3.571	0.0280
43	143.4	143.4	137.0	135.2	134.7	122.4	121.5	120.3	118.9	116.0	2.530	0.0804
44	139.0	139.1	132.8	131.0	130.6	118.1	117.2	116.2	114.6	111.4	2.677	0.0740
45	130.0	130.3	123.5	121.5	121.1	108.8	108.1	106.9	104.7	101.7	2.971	0.0631
46	119.7	119.7	112.7	110.7	109.4	98.0	97.4	95.4	93.0	89.9	3.147	0.0524
47	114.0	113.7	105.9	103.7	101.3	91.1	90.2	87.0	84.1	80.5	3.565	0.0411
48	150.4	150.4	143.8	141.9	141.7	128.2	127.3	126.1	124.6	121.5	2.782	0.0804
49	143.7	144.1	137.2	135.3	135.1	121.9	121.1	120.0	118.2	115.0	2.870	0.0741
50	136.3	136.8	129.7	127.8	126.7	114.0	113.5	111.9	109.8	106.6	3.142	0.0633

Table A.2 Experimental values of pressure for R=254 mm bend.

No.	p1 (kPag)	p2 (kPag)	p3 (kPag)	p4 (kPag)	p5 (kPag)	p6 (kPag)	p7 (kPag)	p8 (kPag)	p9 (kPag)	p10 (kPag)	m_s (kg s^{-1})	m_f (kg s^{-1})
1	79.3	78.8	75.1	73.3	70.9	64.4	63.6	62.5	62.3	61.4	0.869	0.0805
2	76.4	75.9	72.3	70.6	69.0	61.8	61.9	60.9	60.6	59.6	1.001	0.0708
3	72.1	71.9	69.0	67.8	65.7	59.5	59.2	58.1	57.2	55.2	1.233	0.0574
4	68.7	68.2	65.8	63.8	61.4	55.9	55.0	53.9	52.1	49.8	1.428	0.0455
5	64.5	64.1	59.6	57.9	55.2	49.7	49.2	46.9	44.7	42.6	1.573	0.0335
6	61.3	58.3	54.4	51.7	48.7	44.3	42.2	38.4	36.9	34.8	1.738	0.0201
7	86.4	85.9	82.0	80.7	78.8	71.7	71.0	70.1	69.3	68.2	1.160	0.0733
8	85.7	85.1	81.6	80.1	78.7	70.8	70.7	70.2	69.4	68.2	1.261	0.0686
9	82.4	82.1	78.8	77.5	75.1	68.2	68.1	67.1	66.2	64.3	1.512	0.0580
10	76.6	76.5	73.2	71.5	69.0	62.2	62.0	60.9	59.0	56.8	1.701	0.0464
11	73.0	72.5	67.5	65.7	63.0	57.2	56.4	54.5	51.9	49.9	1.933	0.0350
12	66.7	63.6	59.7	57.5	54.5	49.8	47.9	44.7	42.3	39.7	2.032	0.0217
13	99.7	99.3	94.9	93.2	91.5	82.9	82.7	81.7	81.0	79.9	1.443	0.0743
14	99.0	98.8	94.8	93.1	91.3	82.4	82.6	81.5	80.9	79.7	1.548	0.0699
15	92.4	92.4	88.3	87.2	85.4	76.7	76.5	75.4	74.6	72.3	1.776	0.0591
16	86.5	86.5	82.3	80.5	78.1	70.6	70.4	69.2	67.0	64.7	2.037	0.0474
17	81.7	80.8	75.6	73.3	70.5	64.1	63.4	61.4	58.6	56.2	2.275	0.0362
18	75.6	73.0	68.8	66.1	63.1	57.3	55.8	52.4	49.8	47.1	2.455	0.0236
19	111.8	110.7	106.5	104.0	102.7	93.1	92.8	91.8	91.2	89.9	1.652	0.0767
20	108.0	107.8	103.1	101.1	99.3	89.1	89.8	88.5	88.1	87.8	1.796	0.0705
21	101.8	101.9	97.8	95.9	94.2	85.3	84.7	83.5	82.4	79.8	2.036	0.0598
22	96.8	96.8	91.3	89.2	87.0	78.5	78.2	76.3	74.4	71.9	2.382	0.0486
23	89.3	88.8	82.7	80.6	77.7	70.5	70.0	66.6	64.0	61.4	2.594	0.0376
24	83.6	80.6	76.0	73.2	69.8	64.3	62.1	58.3	55.5	52.5	2.768	0.0247
25	121.1	120.4	115.5	113.7	112.0	101.5	101.4	99.8	99.4	98.0	1.938	0.0782

Continuation of Table A.2

No.	p1 (kPag)	p2 (kPag)	p3 (kPag)	p4 (kPag)	p5 (kPag)	p6 (kPag)	p7 (kPag)	p8 (kPag)	p9 (kPag)	p10 (kPag)	m_s (kg s^{-1})	m_f (kg s^{-1})
26	116.7	116.6	111.4	109.5	107.9	97.4	97.0	96.1	95.4	93.5	2.069	0.0721
27	109.8	109.7	104.5	102.7	101.0	91.0	90.7	89.4	88.1	85.5	2.330	0.0610
28	96.1	95.8	89.4	87.2	84.3	76.5	75.8	72.8	70.0	67.2	2.846	0.0388
29	87.5	84.9	80.0	77.3	74.0	67.7	65.9	62.3	59.4	56.3	3.048	0.0263
30	129.0	128.6	123.3	121.5	119.8	108.4	108.3	107.0	106.2	104.8	2.142	0.0788
31	124.9	124.8	119.1	117.4	115.6	105.6	103.9	103.0	102.2	100.0	2.280	0.0725
32	117.9	117.8	112.0	110.0	108.0	97.7	97.3	96.1	94.6	92.0	2.522	0.0618
33	110.5	110.3	104.5	102.4	99.9	90.5	90.2	87.8	85.6	82.8	2.841	0.0506
34	102.8	102.4	95.7	93.5	90.6	82.5	81.9	78.7	75.7	72.9	3.097	0.0398
35	93.7	91.0	85.6	83.1	79.7	73.2	71.3	67.7	64.6	61.3	3.369	0.0274
36	133.1	133.0	126.7	124.6	123.0	111.9	111.3	109.9	108.9	106.9	2.496	0.0724
37	126.3	126.8	120.1	118.0	116.0	105.1	104.9	103.3	101.4	98.8	2.776	0.0618
38	116.4	116.7	109.7	107.6	105.1	95.6	95.0	92.9	90.2	87.2	3.016	0.0511
39	111.4	110.9	103.9	101.7	98.5	89.7	89.0	85.3	82.3	79.3	3.432	0.0405
40	99.3	96.6	90.6	87.9	84.3	77.7	75.8	72.1	68.9	65.6	3.597	0.0279
41	144.2	144.1	137.9	135.8	134.1	121.9	121.0	119.7	118.9	117.0	2.538	0.0790
42	139.7	139.7	133.3	131.1	129.6	117.5	116.5	115.2	114.2	111.7	2.659	0.0730
43	130.8	131.0	124.2	122.1	120.3	108.6	107.9	106.5	104.6	101.7	2.957	0.0623
44	124.1	124.3	116.9	114.3	112.1	101.5	100.9	98.2	95.4	92.3	3.223	0.0512
45	115.2	114.9	107.0	104.7	102.0	92.9	91.7	87.7	85.1	82.0	3.538	0.0409
46	151.1	151.1	144.8	142.7	141.3	127.9	127.5	125.7	125.0	122.8	2.771	0.0796
47	145.0	145.4	138.7	136.6	134.9	122.1	121.5	120.0	118.9	116.3	2.884	0.0733
48	135.8	136.3	129.2	127.0	125.4	112.9	112.6	110.8	108.6	105.7	3.052	0.0627

Table A.3 Experimental values of pressure for R=450 mm bend.

No.	p1 (kPag)	p2 (kPag)	p3 (kPag)	p4 (kPag)	p5 (kPag)	p6 (kPag)	p7 (kPag)	p8 (kPag)	p9 (kPag)	p10 (kPag)	m_s (kg s^{-1})	m_f (kg s^{-1})
1	79.1	78.7	74.1	72.1	70.9	65.5	63.8	63.2	62.3	61.2	0.909	0.0801
2	76.8	76.5	72.3	71.4	69.9	64.6	62.7	61.8	61.1	59.8	1.008	0.0724
3	71.5	71.4	67.7	66.6	66.0	61.4	59.4	58.4	57.2	55.6	1.238	0.0598
4	67.3	67.1	64.3	62.9	61.2	56.4	54.4	53.7	51.7	49.7	1.499	0.0454
5	63.1	62.8	58.8	56.9	55.2	50.7	48.7	47.1	45.1	43.0	1.743	0.0333
6	59.1	56.2	52.9	50.8	48.2	44.0	41.5	39.7	37.1	34.8	1.932	0.0205
7	88.9	88.3	84.3	83.0	81.1	75.0	72.8	72.2	71.2	69.9	1.110	0.0792
8	86.4	85.9	81.6	80.2	79.1	74.0	71.7	70.9	69.9	68.7	1.229	0.0725
9	80.6	80.3	76.7	75.5	74.7	69.8	67.5	66.6	65.3	63.3	1.519	0.0596
10	75.4	75.2	71.8	70.7	69.0	63.5	61.6	60.4	58.5	56.2	1.789	0.0464
11	70.9	70.7	66.3	64.4	62.4	57.1	55.1	53.4	51.3	49.0	2.039	0.0355
12	65.2	62.4	58.7	56.4	54.1	49.2	46.9	44.8	42.3	39.6	2.237	0.0225
13	99.8	99.3	94.6	93.0	92.0	85.2	82.8	82.1	81.3	80.0	1.393	0.0800
14	97.5	97.0	92.7	91.1	90.4	85.0	82.2	81.2	80.1	78.5	1.587	0.0722
15	91.4	91.2	87.0	85.7	84.7	78.9	76.4	75.3	74.1	71.8	1.844	0.0605
16	85.9	85.8	81.6	80.1	78.4	72.1	70.3	69.0	66.8	64.4	2.185	0.0477
17	80.3	79.8	74.6	72.6	70.7	64.6	62.8	60.7	58.4	55.7	2.435	0.0361
18	74.5	71.7	67.4	65.3	62.6	57.5	55.0	52.7	49.9	46.8	2.655	0.0240
19	111.4	111.2	106.0	104.3	103.3	95.8	93.5	92.5	92.1	90.6	1.700	0.0810
20	108.6	108.3	103.3	102.1	100.6	94.4	91.0	90.4	89.3	87.7	1.866	0.0734
21	102.7	102.6	97.9	96.4	95.3	88.7	86.3	85.1	83.6	80.7	2.190	0.0612
22	94.9	94.8	89.8	88.1	86.9	79.8	78.0	76.6	74.0	71.4	2.448	0.0494
23	88.4	88.0	82.1	80.4	78.5	71.3	69.5	67.0	64.8	61.9	2.738	0.0373
24	82.4	79.3	74.8	72.3	69.7	64.3	61.9	59.0	55.9	52.7	2.964	0.0253
25	122.0	121.6	116.2	114.2	113.8	106.3	103.4	102.3	101.4	99.7	1.972	0.0817

Continuation of Table A.3

No.	p1 (kPag)	p2 (kPag)	p3 (kPag)	p4 (kPag)	p5 (kPag)	p6 (kPag)	p7 (kPag)	p8 (kPag)	p9 (kPag)	p10 (kPag)	m_s (kg s^{-1})	m_f (kg s^{-1})
26	117.5	117.1	112.2	110.6	109.8	102.4	100.0	98.5	97.4	95.3	2.149	0.0737
27	109.7	109.6	104.3	102.8	102.0	94.1	92.1	90.9	89.3	86.3	2.410	0.0621
28	102.2	102.2	96.6	94.5	93.3	85.7	83.8	82.1	79.8	76.8	2.697	0.0505
29	93.0	92.1	86.5	84.7	82.5	75.4	73.4	71.2	68.6	65.5	2.928	0.0391
30	87.5	84.5	79.5	77.5	74.8	68.7	66.3	63.4	60.5	57.0	3.309	0.0270
31	125.2	124.9	119.5	117.7	117.5	109.1	106.1	104.8	104.0	102.3	2.060	0.0820
32	123.7	123.6	118.1	116.5	115.8	107.5	104.9	103.5	102.4	100.0	2.302	0.0744
33	116.4	116.3	110.3	109.3	108.0	99.8	97.8	96.5	94.7	91.6	2.568	0.0632
34	108.3	108.1	102.4	100.3	99.1	90.7	89.0	87.1	84.4	81.4	2.830	0.0515
35	101.7	101.1	94.6	92.5	91.0	83.0	81.1	78.4	75.7	72.5	3.189	0.0408
36	91.4	88.7	83.1	80.9	78.6	71.9	69.8	66.5	63.7	60.3	3.516	0.0273
37	137.3	136.9	130.9	128.8	128.6	119.8	116.6	115.4	114.3	112.3	2.390	0.0826
38	130.8	130.7	125.0	123.2	122.5	113.7	110.9	109.6	108.3	105.6	2.521	0.0746
39	123.4	123.5	117.6	115.6	114.9	106.0	103.9	102.4	100.5	97.3	2.822	0.0635
40	115.3	115.4	110.3	106.4	105.5	96.4	94.6	92.5	89.9	86.6	3.127	0.0521
41	108.0	107.7	100.6	98.4	96.8	88.4	86.7	83.4	80.7	77.5	3.428	0.0415
42	95.9	93.3	87.2	84.9	82.8	75.9	73.5	70.3	67.4	64.0	3.757	0.0282
43	142.4	142.3	136.0	134.1	133.6	124.0	120.9	119.5	118.3	116.1	2.564	0.0822
44	136.6	136.6	130.3	128.7	127.9	118.5	115.9	114.4	113.0	110.1	2.717	0.0746
45	128.0	128.2	121.5	119.5	119.1	109.4	107.4	105.8	103.5	100.3	2.996	0.0633
46	120.9	121.2	114.0	111.9	110.9	101.5	99.7	97.2	94.5	91.2	3.314	0.0526
47	114.1	114.0	105.9	103.7	101.8	93.2	91.2	87.8	85.2	81.8	3.774	0.0407
48	149.3	149.3	142.8	140.8	140.3	130.3	127.2	125.6	124.4	122.1	2.762	0.0824
49	141.5	141.5	135.0	133.2	132.6	123.0	120.2	118.5	117.0	114.1	2.866	0.0756
50	131.8	132.0	125.1	123.2	122.6	112.6	110.7	108.7	106.5	103.1	3.141	0.0635

Table A.4 Experimental values of pressure for R=1000 mm bend.

No.	p1 (kPag)	p2 (kPag)	p3 (kPag)	p4 (kPag)	p5 (kPag)	p6 (kPag)	p7 (kPag)	p8 (kPag)	p9 (kPag)	p10 (kPag)	m_s (kg s^{-1})	m_f (kg s^{-1})
1	82.0	81.3	78.3	72.5	69.7	64.5	63.5	62.8	62.2	61.1	1.033	0.0741
2	81.4	80.2	77.5	71.3	68.9	63.6	62.7	62.3	61.6	60.6	1.113	0.0699
3	76.7	76.0	73.1	67.5	65.4	60.2	59.8	59.4	58.7	56.9	1.299	0.0594
4	74.1	73.3	69.8	65.1	62.8	58.6	57.3	56.2	54.1	51.9	1.487	0.0460
5	70.6	69.3	64.5	61.3	58.3	53.9	51.5	49.7	47.4	45.1	1.593	0.0345
6	67.0	63.0	59.3	55.8	52.0	47.7	45.1	42.5	39.6	36.9	1.608	0.0210
7	93.0	91.9	88.8	82.0	78.8	73.6	72.4	71.6	71.0	69.9	1.211	0.0756
8	91.7	90.5	87.5	80.7	78.1	72.1	71.3	70.5	70.1	68.9	1.311	0.0713
9	86.5	85.6	82.9	76.7	74.2	68.9	68.0	67.5	66.5	64.4	1.545	0.0598
10	80.9	80.3	76.6	71.5	69.1	64.8	63.6	62.6	60.2	57.9	1.773	0.0472
11	76.4	75.3	70.6	66.6	63.4	59.2	57.3	55.0	52.3	50.2	1.916	0.0356
12	73.2	69.4	65.5	61.9	58.3	54.2	51.1	48.0	45.1	41.8	1.951	0.0222
13	106.9	105.6	102.1	94.5	91.2	85.6	83.7	83.4	82.3	81.3	1.440	0.0791
14	103.2	102.0	98.7	91.5	88.6	82.4	81.3	80.8	80.1	78.9	1.566	0.0723
15	97.9	96.6	93.5	86.8	84.0	78.3	77.6	77.0	75.8	73.5	1.833	0.0606
16	91.7	91.2	86.9	81.1	78.6	73.8	72.4	71.1	68.4	65.4	2.051	0.0481
17	87.2	87.4	80.9	76.4	73.1	68.3	66.2	63.6	60.9	58.4	2.221	0.0368
18	83.1	79.9	75.5	71.1	66.8	62.3	58.8	55.8	52.6	49.1	2.346	0.0235
19	118.6	114.6	113.2	104.9	101.5	95.7	93.6	93.7	92.6	91.5	1.668	0.0786
20	107.7	107.0	102.8	95.3	92.7	86.3	85.7	85.2	84.1	81.6	2.046	0.0609
21	99.9	99.3	94.5	88.3	85.5	80.6	79.4	78.2	75.2	72.3	2.333	0.0488
22	95.1	93.4	88.3	82.6	79.0	74.3	72.7	69.4	66.6	63.6	2.620	0.0375
23	89.1	85.6	81.5	77.0	73.0	68.5	65.5	61.8	58.3	54.8	2.771	0.0247
24	128.9	127.4	123.8	114.9	111.6	104.7	103.4	102.2	101.3	100.1	1.907	0.0796
25	123.3	122.6	118.3	110.1	106.7	99.8	99.1	98.0	97.2	95.6	2.059	0.0726

Continuation of Table A.4

No.	p1 (kPag)	p2 (kPag)	p3 (kPag)	p4 (kPag)	p5 (kPag)	p6 (kPag)	p7 (kPag)	p8 (kPag)	p9 (kPag)	p10 (kPag)	m_s (kg s^{-1})	mf (kg s^{-1})
26	116.4	115.4	111.5	103.8	100.6	94.2	93.6	92.6	91.2	88.5	2.339	0.0615
27	108.6	107.6	103.2	96.1	92.7	87.5	86.5	84.6	81.9	78.8	2.623	0.0495
28	102.1	100.3	94.8	89.1	85.0	80.3	78.6	75.0	72.4	69.3	2.8294	0.0387
29	101.4	96.7	92.2	87.0	82.1	76.5	72.7	68.8	64.8	60.7	2.498	0.0251
30	130.7	128.9	125.4	116.0	112.4	104.7	104.0	103.3	102.4	100.7	2.029	0.0793
31	125.8	124.3	120.7	111.9	109.9	101.2	100.9	100.1	98.8	96.6	2.131	0.0738
32	120.9	120.0	115.7	108.0	104.2	97.6	97.7	96.7	94.0	90.4	2.415	0.0624
33	114.7	113.7	108.0	101.5	97.7	91.4	91.3	88.7	84.5	81.4	2.646	0.0506
34	110.0	107.4	101.8	95.8	91.3	85.8	84.1	80.1	77.0	73.4	2.865	0.0397
35	103.9	99.5	94.6	89.2	84.3	79.1	75.4	71.4	67.4	63.2	2.935	0.0268
36	139.2	137.5	133.5	123.9	120.7	112.3	111.9	111.0	110.1	108.3	2.215	0.0803
37	135.8	134.5	130.6	120.9	117.4	109.1	109.9	108.9	107.5	104.8	2.386	0.0737
38	127.2	126.2	121.9	113.2	109.5	102.8	102.7	101.8	99.1	95.7	2.627	0.0628
39	118.9	118.1	112.9	105.5	101.3	95.0	95.2	92.6	89.0	85.6	2.876	0.0511
40	113.7	111.2	106.0	99.3	94.9	90.9	88.0	84.1	80.5	77.2	3.052	0.0407
41	145.8	144.7	140.8	130.4	126.4	118.1	118.1	116.9	115.9	113.9	2.411	0.0798
42	142.6	141.1	137.7	128.1	123.8	116.2	115.9	114.5	113.1	110.1	2.571	0.0737
43	134.4	133.2	128.3	119.7	115.9	110.3	108.8	107.4	104.8	101.6	2.815	0.0631
44	125.5	124.5	118.7	110.5	106.3	99.4	100.5	98.1	94.4	91.1	3.137	0.0517
45	153.2	151.9	148.0	136.9	132.8	125.2	124.9	123.1	121.9	119.6	2.628	0.0796
46	149.2	147.6	142.7	133.1	129.4	122.5	121.3	119.6	117.8	114.9	2.765	0.0735
47	139.7	138.5	134.4	125.2	120.7	113.5	113.3	111.6	109.1	105.8	3.039	0.0633

Table A.5 Experimental values of pressure for Blinded-tee bend.

No.	p1 (kPag)	p2 (kPag)	p3 (kPag)	p4 (kPag)	p5 (kPag)	p6 (kPag)	p7 (kPag)	p8 (kPag)	p9 (kPag)	p10 (kPag)	m_s (kg s^{-1})	m_f (kg s^{-1})
1	81.4	80.4	77.8	72.0	69.8	60.0	57.6	56.8	56.1	54.9	0.884	0.0743
2	79.4	78.7	76.1	70.4	68.2	57.9	56.6	56.1	55.3	53.9	0.954	0.0692
3	75.9	75.4	72.7	67.3	65.5	54.6	54.1	53.8	52.6	51.5	1.138	0.0584
4	71.3	70.5	67.6	63.2	61.1	51.6	51.5	50.3	49.0	47.2	1.383	0.0454
5	67.0	66.2	61.5	58.1	56.1	47.4	46.8	45.5	43.2	40.9	1.529	0.0335
6	62.3	59.0	55.6	51.5	48.7	41.3	39.9	37.6	34.9	32.4	1.622	0.0204
7	91.9	90.9	87.8	81.6	79.0	66.7	65.6	64.4	61.2	63.2	1.034	0.0750
8	89.9	89.0	86.2	80.1	77.5	63.6	64.0	63.4	62.8	61.5	1.125	0.0700
9	85.0	84.4	81.7	75.7	73.7	60.2	61.0	60.6	59.4	58.3	1.313	0.0589
10	78.4	77.8	75.0	70.1	68.0	57.2	56.9	55.6	54.4	52.5	1.565	0.0461
11	74.1	73.5	70.2	65.2	62.5	51.4	52.5	51.2	49.1	46.7	1.783	0.0348
12	68.5	65.4	62.5	58.7	55.2	47.8	46.0	43.2	40.3	37.7	1.923	0.0216
13	103.9	103.3	100.4	93.5	90.7	75.6	75.3	74.7	73.6	72.4	1.231	0.0755
14	102.5	101.9	99.2	91.5	88.8	74.6	73.5	72.9	71.9	70.6	1.346	0.0707
15	97.2	96.4	93.7	86.6	84.1	70.8	69.5	69.2	67.7	66.5	1.566	0.0596
16	90.4	89.7	85.7	80.2	77.7	67.3	64.8	63.8	62.2	60.4	1.904	0.0472
17	84.9	83.7	79.6	74.9	71.8	60.5	59.2	57.6	55.2	52.9	2.155	0.0361
18	79.0	75.4	72.0	68.3	64.0	54.7	53.5	50.7	47.5	44.5	2.378	0.0230
19	116.1	115.0	111.9	104.3	101.1	84.4	83.6	83.2	81.9	80.5	1.604	0.0716
20	112.4	111.6	108.3	100.8	98.2	81.6	81.0	80.2	79.2	77.5	1.668	0.0671
21	109.0	108.2	104.7	97.6	94.8	79.0	78.4	77.9	76.1	74.5	1.856	0.0594
22	101.8	100.9	97.3	90.9	88.1	73.2	72.8	71.8	69.8	67.7	2.065	0.0494
23	95.2	93.9	88.9	84.1	80.5	67.9	67.2	65.0	63.0	60.3	2.388	0.0382
24	88.9	85.4	82.2	77.0	72.9	62.8	61.0	57.3	54.1	51.0	2.636	0.0243
25	131.4	130.3	126.8	118.2	114.7	96.1	95.1	95.3	93.6	92.3	1.634	0.0809

Continuation of Table A5

No.	p1 (kPag)	p2 (kPag)	p3 (kPag)	p4 (kPag)	p5 (kPag)	p6 (kPag)	p7 (kPag)	p8 (kPag)	p9 (kPag)	p10 (kPag)	m_s (kg s^{-1})	m_f (kg s^{-1})
26	127.7	126.6	123.3	114.7	112.0	93.2	92.7	91.7	90.7	88.8	1.920	0.0707
27	118.1	117.3	113.9	106.5	103.5	85.5	85.3	84.5	82.9	80.7	2.125	0.0598
28	111.8	110.6	106.2	99.5	96.2	79.6	79.7	78.3	76.0	73.5	2.435	0.0482
29	103.4	101.8	96.8	91.6	88.1	73.7	72.8	70.6	67.5	64.4	2.715	0.0380
30	94.0	90.3	86.4	81.5	77.2	65.9	64.5	61.1	57.7	54.2	2.878	0.0255
31	141.2	140.0	136.5	127.7	124.3	104.3	102.7	102.2	100.9	99.4	1.808	0.0838
32	136.9	135.8	132.1	123.3	120.3	99.9	99.0	98.0	96.7	94.8	2.141	0.0716
33	127.4	126.3	122.1	114.8	112.1	92.3	92.1	91.3	89.4	86.8	2.365	0.0604
34	118.8	117.6	112.8	106.2	103.5	85.0	84.8	83.6	80.9	78.3	2.662	0.0493
35	109.8	108.0	102.7	96.7	93.3	77.5	76.9	74.6	71.7	68.5	2.913	0.0392
36	101.1	97.2	92.9	87.4	83.7	70.7	69.2	65.5	62.3	58.6	3.218	0.0267
37	149.5	148.5	144.7	135.3	132.7	109.9	109.1	107.9	106.9	104.9	2.172	0.0787
38	135.9	135.0	130.3	122.7	120.1	98.3	98.3	97.1	95.3	92.6	2.572	0.0618
39	117.0	115.5	109.8	103.6	100.3	82.2	81.9	79.8	76.5	73.2	3.090	0.0403
40	156.5	155.6	151.3	141.3	138.9	115.4	113.9	112.8	111.6	109.5	2.354	0.0788
41	150.8	150.2	145.4	136.3	133.9	110.6	109.7	108.6	107.3	105.0	2.462	0.0729
42	140.5	139.8	134.8	126.9	124.4	101.5	101.5	100.1	97.9	95.3	2.786	0.0606
43	130.6	129.6	123.9	116.6	113.7	93.5	93.1	91.4	88.7	85.7	3.014	0.0512
44	164.1	163.0	158.0	148.5	146.2	120.8	119.5	118.4	117.2	115.1	2.551	0.0796
45	157.5	157.2	151.7	142.2	139.7	114.6	114.3	112.9	111.4	109.1	2.694	0.0727
46	145.9	145.0	139.4	131.6	128.9	105.4	105.4	104.1	101.9	99.1	2.834	0.0625

Table A.6 Experimental values of pressure along Pipeline I.

No.	p_p (kPag)	p_{Ta} (kPag)	p_{Tb} (kPag)	p_{Tc} (kPag)	p_{Td} (kPag)	p_{Te} (kPag)	p_{Tf} (kPag)	m_s (kg s^{-1})	m_f (kg s^{-1})
1	61.2	43.6	41.8	34.0	31.9	20.7	11.4	1.120	0.0325
2	60.0	36.4	34.6	25.9	24.2	14.2	5.5	1.275	0.0191
3	70.4	36.9	34.5	25.3	23.0	11.5	1.8	0.868	0.0087
4	63.9	48.7	46.7	39.3	37.3	26.5	16.2	0.969	0.0459
5	49.5	35.6	34.1	27.5	26.3	16.7	8.6	0.821	0.0318
6	46.8	27.8	25.9	19.6	18.2	10.2	4.0	0.925	0.0182
7	77.8	59.3	57.6	48.9	46.6	33.0	21.1	1.325	0.0464
8	77.0	55.0	53.2	43.4	41.4	27.6	15.5	1.583	0.0340
9	79.0	50.4	47.9	36.9	34.7	21.0	8.3	1.819	0.0206
10	84.8	48.6	46.1	34.3	31.5	16.0	2.5	1.413	0.0103
11	106.1	80.5	78.7	67.3	64.8	46.0	30.5	2.065	0.0484
12	104.0	75.0	72.3	59.7	56.9	38.0	22.0	2.436	0.363
13	102.8	67.0	64.2	50.5	47.4	29.2	12.7	2.739	0.0227
14	102.6	60.7	57.9	44.5	41.3	22.0	5.0	2.309	0.0136
15	127.2	96.7	94.9	80.8	78.1	55.9	36.4	2.600	0.0505
16	119.5	88.1	84.9	70.6	67.7	46.4	28.0	2.924	0.0394
17	117.0	79.1	76.3	61.2	57.9	37.1	18.7	3.256	0.0264
18	117.5	71.0	68.2	53.0	49.7	28.1	9.4	3.145	0.0173
19	143.6	109.6	107.7	92.1	88.9	64.5	42.8	3.064	0.0521
20	136.3	102.0	99.2	82.4	79.5	55.0	34.4	3.382	0.0409
21	129.6	88.7	86.1	70.1	66.7	44.1	23.7	3.704	0.0286
22	125.2	76.5	73.4	57.8	54.9	32.0	12.5	3.629	0.0194
23	156.5	120.5	118.6	101.1	98.2	71.1	46.3	3.423	0.0525
24	145.7	109.1	106.3	89.0	85.9	60.0	37.3	3.689	0.0416
25	138.3	95.4	92.7	75.9	73.0	48.1	26.8	4.074	0.0292
26	132.8	82.3	79.1	63.1	60.1	36.1	15.7	4.043	0.0203
27	71.6	56.4	54.1	47.4	46.4	32.7	21.8	0.625	0.0758
28	91.3	71.4	69.1	60.8	59.7	43.3	30.5	0.904	0.0760
29	87.5	68.0	66.4	58.0	56.1	40.6	28.4	1.223	0.0600
30	117.2	92.7	91.2	80.4	79.0	57.9	42.2	1.429	0.0764
31	112.6	88.4	87.1	76.3	74.0	53.9	38.1	1.815	0.0615
32	141.6	113.6	112.3	99.4	97.7	72.1	53.3	1.997	0.0769
33	136.9	107.3	105.7	92.5	89.5	65.7	46.6	2.281	0.0620

Table A.7 Experimental values of pressure along Pipeline II.

No.	p_p (kPag)	p_{Ta} (kPag)	p_{Tb} (kPag)	p_{Tc} (kPag)	p_{Td} (kPag)	p_{Te} (kPag)	p_{Tf} (kPag)	m_s (kg s^{-1})	m_f (kg s^{-1})
1	64.9	53.8	50.2	42.6	37.4	22.3	13.3	0.790	0.0445
2	62.2	50.2	46.9	38.7	33.1	17.6	8.7	0.893	0.0324
3	61.9	43.0	38.6	30.1	24.7	13.9	4.0	1.000	0.0189
4	70.1	45.4	41.0	31.5	24.6	11.5	1.2	0.609	0.0083
5	85.3	70.4	65.8	56.5	49.2	30.1	18.3	1.188	0.0458
6	84.6	65.3	61.3	51.4	43.7	24.3	12.6	1.358	0.0337
7	83.3	60.2	54.2	43.1	35.0	18.0	5.6	1.492	0.0202
8	94.3	63.1	57.1	44.4	35.1	12.7	1.9	1.000	0.0101
9	112.1	91.2	86.5	74.4	65.8	39.3	25.2	1.774	0.0473
10	108.1	85.4	80.0	67.2	57.3	29.8	16.5	1.893	0.0359
11	107.0	79.5	73.6	59.5	49.7	23.5	9.9	2.046	0.0226
12	115.5	80.2	73.9	58.9	48.1	18.9	3.3	1.846	0.0123
13	135.8	110.4	105.4	91.5	81.0	48.6	30.5	2.314	0.0489
14	129.0	102.1	96.6	82.3	71.0	38.9	22.5	2.455	0.0384
15	128.5	96.3	90.1	74.6	62.8	30.7	14.4	2.710	0.0256
16	132.3	91.6	84.5	68.5	57.0	23.0	6.1	2.349	0.0162
17	148.5	120.8	115.5	100.2	88.1	52.7	31.0	2.637	0.0504
18	143.6	114.6	108.5	93.1	79.6	44.6	26.7	2.843	0.0401
19	140.4	105.3	99.0	83.2	70.0	35.7	18.2	3.087	0.0276
20	142.7	98.1	90.4	74.1	60.4	25.9	8.9	2.524	0.0183
21	162.3	132.6	126.3	110.4	98.1	58.8	36.9	2.962	0.0510
22	155.9	124.1	117.9	101.0	87.7	49.8	30.6	3.140	0.0409
23	148.1	111.2	104.5	87.9	75.1	38.5	19.7	3.293	0.0284
24	146.4	102.8	95.0	78.1	64.1	28.4	10.9	2.788	0.0195
25	73.7	61.3	57.6	51.0	45.2	28.5	18.1	0.529	0.0770
26	70.4	58.3	55.9	49.4	44.7	27.2	18.9	0.681	0.0599
27	94.6	78.9	74.5	66.6	59.6	39.3	26.5	0.782	0.0771
28	90.7	75.0	72.3	63.6	58.1	36.8	26.3	1.020	0.0605
29	120.8	101.1	97.0	87.2	79.6	53.9	38.5	1.192	0.0771
30	117.4	97.7	93.9	83.1	75.6	49.0	35.1	1.547	0.0610
31	148.8	125.1	121.3	109.2	100.5	68.0	50.3	1.736	0.0774
32	141.9	118.2	113.6	100.8	91.8	60.1	42.4	2.049	0.0624
33	163.3	137.5	133.3	119.9	110.0	74.6	55.0	2.054	0.0771
34	156.1	130.4	125.5	111.5	100.7	66.0	46.6	2.376	0.0631
35	176.4	149.0	144.1	129.3	118.8	80.7	59.2	2.320	0.0774
36	169.9	141.1	136.1	121.2	109.7	72.1	50.3	2.677	0.0637

Table A.8 Experimental values of pressure along Pipeline III.

No.	p_p (kPag)	p_{Ta} (kPag)	p_{Tb} (kPag)	p_{Tc} (kPag)	p_{Td} (kPag)	p_{Te} (kPag)	p_{Tf} (kPag)	m_s (kg s^{-1})	m_f (kg s^{-1})
1	45.0	30.3	27.8	21.7	16.5	7.1	3.0	1.817	0.0462
2	47.4	30.3	27.7	22.1	17.7	7.5	2.5	1.896	0.0337
3	63.3	46.3	42.7	34.1	26.9	11.5	4.8	2.601	0.0475
4	62.3	41.2	37.3	29.7	23.4	10.0	3.2	2.515	0.0345
5	45.5	35.4	32.9	27.3	23.3	12.6	7.3	1.477	0.0784
6	46.4	35.7	33.2	27.7	23.2	12.3	6.7	1.628	0.0706
7	46.0	34.0	31.4	25.5	21.1	9.9	5.1	1.745	0.0594
8	45.8	31.9	29.2	23.4	19.2	8.3	3.6	1.879	0.0489
9	61.3	47.7	44.7	37.7	32.1	18.0	10.8	1.979	0.0796
10	58.1	45.2	42.7	35.4	29.5	16.0	9.2	2.361	0.0721
11	60.7	45.3	42.2	34.7	28.6	13.8	6.9	2.517	0.0595
12	59.9	43.4	40.1	32.8	26.8	12.4	5.6	2.877	0.0507
13	72.9	58.1	54.5	46.0	39.3	22.5	13.4	3.095	0.0812
14	72.5	56.9	53.3	44.8	35.0	20.2	11.3	3.228	0.0737
15	72.0	54.6	51.2	42.5	35.7	17.5	8.5	3.232	0.0621
16	70.0	51.4	47.7	39.1	32.4	15.1	6.3	3.470	0.0537
17	80.5	63.9	60.0	51.2	43.1	24.2	14.2	3.533	0.0822
18	74.3	58.2	54.8	46.5	39.5	20.2	11.1	3.198	0.0749
19	76.9	58.0	54.1	44.8	37.2	18.6	8.6	3.389	0.0637
20	79.5	59.4	55.7	46.4	38.5	18.5	8.1	4.113	0.0571
21	89.9	71.3	67.1	57.3	48.6	28.3	16.2	3.495	0.0828
22	86.1	66.6	63.7	53.8	45.5	24.8	14.6	3.872	0.0758
23	86.3	64.9	61.1	50.8	42.3	21.8	10.7	3.901	0.0645
24	47.1	38.6	36.0	30.0	25.9	15.1	9.7	1.547	0.0920
25	48.3	40.1	37.5	31.2	27.4	16.8	11.5	1.440	0.1027
26	48.2	39.6	37.1	31.5	28.3	17.1	11.9	1.318	0.1130
27	48.6	40.4	38.2	32.4	28.8	17.7	13.3	1.278	0.1204
28	50.0	40.9	39.0	33.2	29.7	18.2	13.5	1.269	0.1276
29	49.9	41.0	39.0	32.9	29.7	18.7	13.6	1.303	0.1174
30	48.8	40.0	37.5	32.3	28.0	17.8	12.2	1.466	0.0996
31	59.8	48.4	46.0	39.1	34.2	21.1	14.7	2.190	0.0940
32	61.6	49.6	47.7	41.1	36.7	23.3	17.3	1.781	0.1274
33	70.9	57.2	54.3	46.2	40.4	24.6	17.3	3.004	0.0941
34	70.7	57.1	55.2	48.3	43.0	27.7	20.5	2.264	0.1270
35	77.7	62.6	59.3	51.1	45.0	27.6	18.7	3.487	0.0942
36	76.2	61.6	59.9	52.0	46.5	29.9	22.6	2.594	0.1267
37	84.5	67.5	64.0	55.2	49.1	30.0	20.4	3.780	0.0966
38	81.9	66.3	64.0	56.0	50.1	32.4	24.3	2.943	0.1262
39	88.8	71.8	69.4	61.0	54.6	35.9	26.7	3.265	0.1263

Table A.9 Experimental values of pressure along Pipeline IV.

No.	p_p (kPag)	p_{v1} (kPag)	p_{v2} (kPag)	p_{v3} (kPag)	p_{v4} (kPag)	p_{v5} (kPag)	m_s (kg s^{-1})	m_f (kg s^{-1})
1	63.9	60.2	58.0	57.5	55.8	54.3	0.909	0.0444
2	60.8	58.0	54.9	54.1	52.1	50.2	1.029	0.0322
3	59.6	55.6	52.7	48.9	46.7	43.4	1.150	0.0191
4	68.1	61.5	57.0	50.3	47.8	42.6	0.756	0.0087
5	82.1	77.7	75.2	73.6	71.2	69.2	1.306	0.0457
6	80.2	75.5	72.7	70.1	67.9	65.3	1.505	0.0339
7	79.3	74.1	70.5	66.1	62.6	58.2	1.668	0.0208
8	86.7	79.1	73.2	67.2	62.3	57.3	1.294	0.0104
9	106.8	101.5	98.2	96.5	93.0	90.7	1.899	0.0478
10	103.7	98.6	95.3	92.0	88.8	85.0	2.191	0.0363
11	102.2	95.8	91.2	86.3	81.6	75.9	2.358	0.0232
12	105.4	96.5	89.9	82.0	76.9	69.2	2.029	0.0137
13	128.4	121.9	118.4	114.9	111.8	107.9	2.463	0.0493
14	123.9	117.8	114.0	110.5	106.1	101.2	2.762	0.0385
15	120.1	113.0	107.8	102.0	96.8	90.2	2.996	0.0258
16	121.7	111.3	104.0	97.4	89.8	81.6	3.029	0.0171
17	141.7	135.1	131.2	126.8	123.8	119.2	2.843	0.0507
18	135.0	128.6	124.6	119.9	115.8	110.3	3.063	0.0406
19	132.9	124.6	119.4	113.0	107.4	99.4	3.528	0.0274
20	131.3	119.4	111.6	103.8	96.6	87.5	3.266	0.0187
21	152.9	145.8	142.0	138.0	134.3	129.2	3.124	0.0512
22	144.9	138.3	132.0	128.5	124.6	118.3	3.260	0.0413
23	138.4	130.3	123.9	118.2	112.5	105.2	3.582	0.0287
24	137.0	125.2	117.1	109.3	101.6	92.2	3.550	0.0196
25	71.3	67.5	66.2	65.6	65.0	64.3	0.595	0.0769
26	67.9	63.9	62.2	61.0	60.1	59.0	0.749	0.0607
27	92.1	86.5	85.1	84.0	83.0	81.7	0.875	0.0770
28	88.3	82.5	80.8	79.1	77.8	76.3	1.141	0.0612
29	120.7	113.0	111.3	109.9	108.2	106.1	1.365	0.0773
30	114.6	108.1	105.8	103.8	101.8	99.5	1.692	0.0623
31	145.3	137.3	134.9	132.8	130.9	128.3	1.851	0.0776
32	137.5	130.7	127.3	124.0	121.9	118.4	2.182	0.0634
33	159.4	151.1	148.5	145.8	143.7	140.5	2.174	0.0781
34	152.9	146.0	142.0	138.1	135.6	132.0	2.605	0.0642
35	172.2	163.6	160.6	157.0	154.5	151.4	2.465	0.0785
36	161.5	154.2	150.1	145.3	142.7	139.0	2.767	0.0648

APPENDIX B

DIFFERENT CONFIGURATIONS OF PIPELINE

Appendix B-1: Schematic Layout of Pipelines

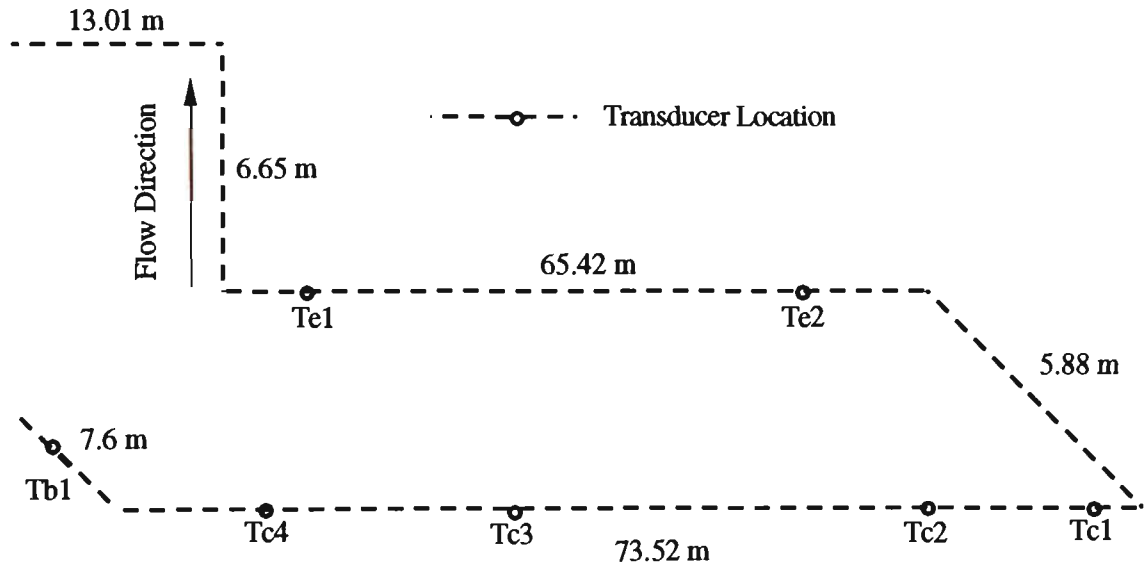

Figure B.1 Schematic layout of Pipeline A1 (L=172 m, D=69 mm).

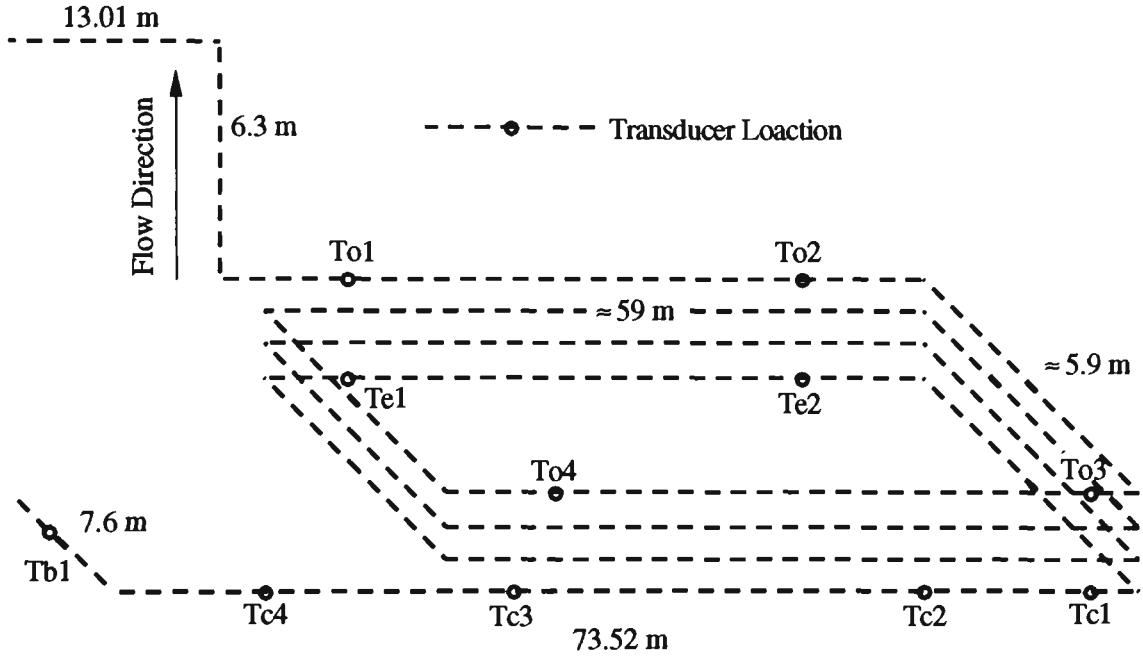

Figure B.2 Schematic layout of Pipeline A2 (L=553 m, D=69 mm).

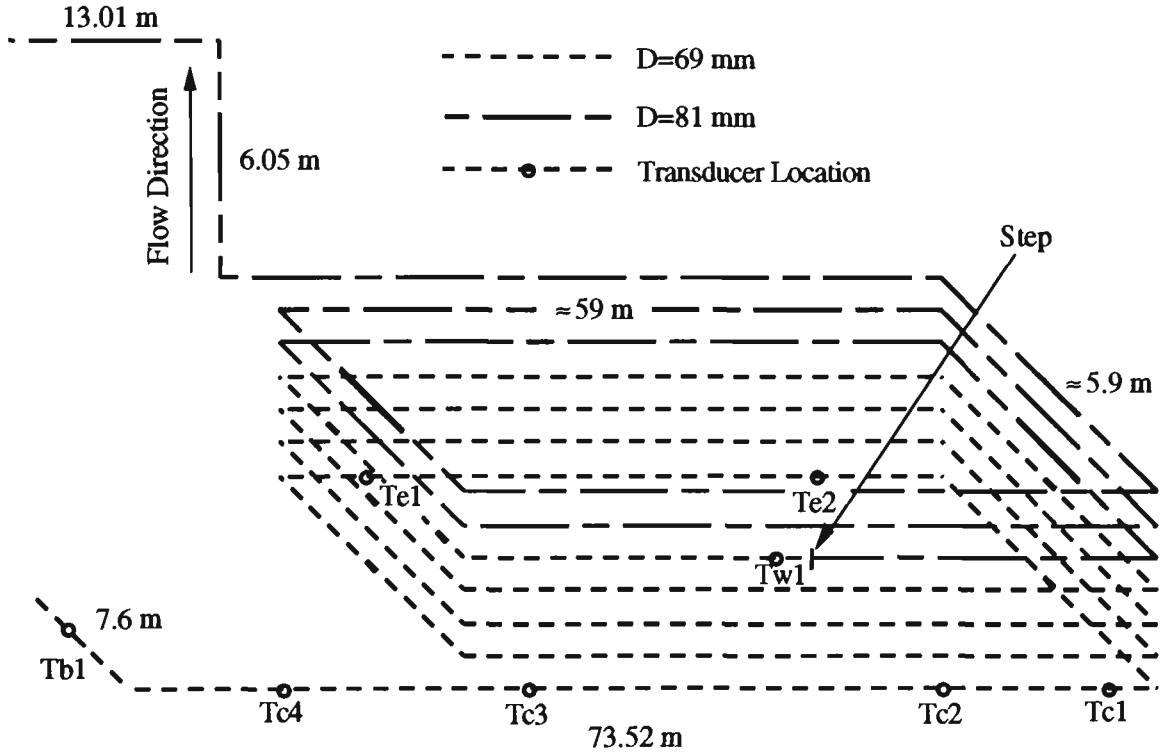

Figure B.3 Schematic layout of Pipeline A3 (L=945 m, D=69/81 mm).

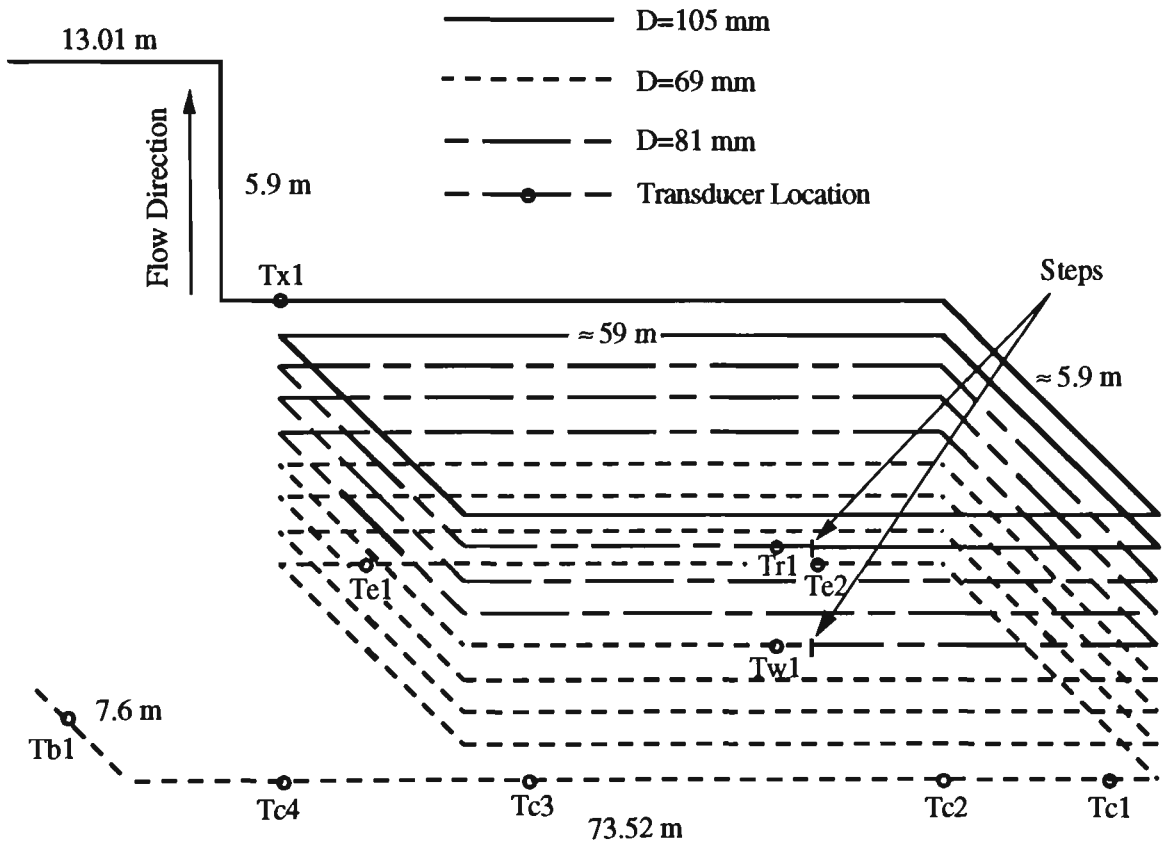

Figure B.4 Schematic layout of Pipeline A4 (L=1208 m, D=69/81/105 mm).

Appendix B-2: Pipeline Details and Transducer Locations

Table B.1 Pipeline details.

Pipeline	D (m)	Tot. Effec. Length (m)	R (m)	No. of Bends	No. of Straights
A1	0.069	172	1.0	5	6
A2	0.069	553	1.0	17	18
A3	0.069	564	1.0	17	13
	0.081	391	1.0	12	18
A4	0.069	564	1.0	17	18
	0.081	391	1.0	12	13
	0.105	253	1.0	8	9

Table B.2 Transducer location (effective distance from the blow tank).

	Location of transducer (m)						
Pipeline	Tb1	Tc4	Tc3	Tc2	Tc1	Te2	Te1
A1	2.2	25.5	39.2	65.0	78.0	97.7	146.4
A2	2.2	25.5	39.2	65.0	78.0	97.7	137.7
A3	2.2	25.5	39.2	65.0	78.0	97.7	137.7
A4	2.2	25.5	39.2	65.0	78.0	97.7	137.7

Continuation of Table B.2

	Location of transducer (m)						
Pipeline	To4	To3	To2	To1	Tw1	Tr1	Tx1
A1	-	-	-	-	-	-	-
A2	429.6	466.1	494.0	525.6	-	-	-
A3	-	-	-	-	563.4	-	-
A4	-	-	-	-	563.4	954.6	1182.6

APPENDIX C

PUBLICATIONS WHILE PhD CANDIDATE

1. Wypych, P. W. and Pan, R., Determination of Air-only Pressure Drop in Pneumatic Conveying Systems, Powder Handling & Processing, Vol. 3, No. 4, 1991, pp 303-309.

2. Pan, R. and Wypych, P. W., Scale-up Procedures for Pneumatic Conveying Design, To Be Published in Powder Handling & Processing, Vol. 4, No. 2, 1992.

3. Pan, R. and Wypych, P. W., Bend Pressure Drop in Pneumatic Conveying of Fly Ash, Powder & Bulk Solids Conference/Exhibition, Rosemont, Illinois, U.S.A., 11-14 May, 1992.

4. Pan, R. and Wypych, P. W., Pressure Drop due to Solid-Air Mixture in Horizontal and Vertical Pipes, To Be Presented at 4th Int. Conf. on Bulk Materials Storage, Handling and Transportation, Wollongong, N.S.W., Australia, 6-8 July, 1992.